DATA MINING AND VISUALIZATION OF EARTH HISTORY
DATASETS FROM GEOLOGICAL TIMESCALE CREATOR PROJECT

by
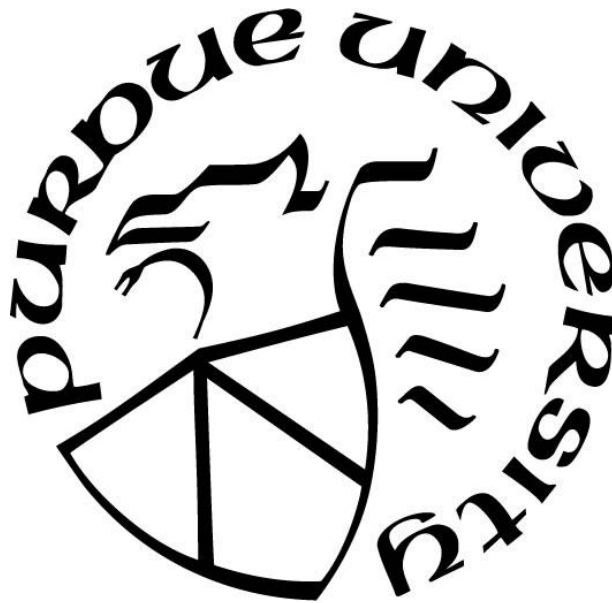
Abdullah Khan Zehady

A Dissertation

Submitted to the Faculty of Purdue University

In Partial Fulfillment of the Requirements for the degree of

Doctor of Philosophy

Department of Earth, Atmospheric, and Planetary Sciences

West Lafayette, Indiana

May 2020

THE PURDUE UNIVERSITY GRADUATE SCHOOL
STATEMENT OF COMMITTEE APPROVAL

Dr. Wen-wen Tung, Chair

Department of Earth, Atmospheric, and Planetary Science

Dr. James Ogg, Research Adviser

Department of Earth, Atmospheric, and Planetary Science

Dr. Robert Nowack, Academic Adviser

Department of Earth, Atmospheric, and Planetary Science

Dr. William S. Cleveland

Department of Statistics

Dr. Ananth Grama

Department of Computer Science

Approved by:

Dr. Daniel J. Cziczo

Dedicated to my dear mother who always inspired me to pursue higher education.

ACKNOWLEDGMENTS

TABLE OF CONTENTS

LIST OF TABLES

LIST OF FIGURES

connecting branches, a user selects the "Node" tool on the left and then draws from the beginning/base node to the end/top node. The ages for the range endpoints are automatically computed according to their proportion within the time guidelines. When the user selects a red-dot node on a Parent range, the branch node is automatically recognized and drawn as yellow, then the user extends its end point into a new child range. Options including zooming, panning, changing the initial image dimensions, and adding branch information. (b) This window opens when clicking on the base node of each range to enter information (e.g., for the range of the extinct *Parahippus* relative of modern horse). (c) View of the text-version of the datapack created in the graphical interface prior to exporting window. 40

Figure 2.11 A portion of the dataset for the dinoflagellate range chart of Figure 2.2 in Excel sheet format; see text for description of header (green shaded) and data (tan shaded) fields. The name "*Dracodinium varielongitudum*" (column **B**) will display vertically along its range (leftmost range line in Figure 2.2). That displayed name can include an embedded image using an HTML image tag that provides the alignment, scaling and image file name. In this example, the thumbnail picture was pre-rotated 90° so it will look upright when the range label is plotted vertically (see Figure 2.2). Values in Column **C** are ages in Ma for the beginning of each line style within the range line (Column **D**) with optional pop-up information (Column **E**). To insert a URL link within the pop-up text, one uses HTML anchor tag format – e.g., including "[Click Adnatosp haeridium_multispinosum for details]" will result in an active web link from "*Adnatosphaeridium_multispinosum*". If Excel is used to enter the dataset, then the sheet needs to be exported as a tab-delimited text file and merged with referenced .PNG or .JPG images into a zipped file, for loading into the *TSCreator* program. 43

Figure 2.12 Sample dataset for the schematic evolution of horses (Figure 2.4): in Excel sheet format. Green-shaded rows are header information, tan-shaded rows are range data, and gray-shaded rows are the evolutionary-branch statements. The upper panel is a brief explanation of the fields in the lower panel. See text for details. 45

Figure 3.1 Paleontological and molecular approaches to infraspecific terminology: planktonic foraminifer *Globorotalia*/*Truncorotalia truncatulinoides*. (**a,b**) A paleontological approach. Portions (after Figure 5E of Aze, T. et al., 2011) of trees of morphospecies [evolutionarily overlapping morphotaxa] (**a**) and lineages [paleobiological species] (**b**): living Lineage N64-T66 (**T. truncatulinoides* in b) includes three living morphospecies (in a), *Truncorotalia truncatulinoides*, *T. excelsa*, and *T. pachytheca* (*T. cavernula* originated in this lineage, but budded into its own living Lineage T65); for comparison with the outgroup in (**c**), these portions of the trees embrace living Lineage N48-T50 (**H. hirsuta* in **b**) which includes living morphospecies *Hirsutella hirsuta*; arrows indicate still living. (**c**) A molecular approach. Consensus molecular tree for the morphospecies [cryptic-species complex] *Globorotalia truncatulinoides*, using morphospecies *G. hirsuta* as the outgroup (after Figure 4b of Ujiie, Y. & Lipps, J. H., 2009): two major clades 1 ("1 = I ~ IV") and 2 ("2 = V") comprising five genotypes [cryptic species] I – IV and V, respectively. Note: *Globorotalia* versus *Truncorotalia*, *Hirsutella*, etc., are alternative nominal genera, the former preferred for molecular workers' broader less-settled sweep across living species, the latter for those paleontologists keen to emphasize temporally deep but taxonomically confined lines of descent. 60

13

ABSTRACT

The Geologic *TimeScale Creator* (TSCreator) project has compiled a range of paleo-environmental and bio-diversity data which provides the opportunity to explore origination, speciation and extinction events. My PhD research has four major interconnected themes which include the visualization methods of evolutionary tree and the impacts of climate change on the evolution of life in longer and shorter timeframes: **(1)** Evolutionary range data of planktonic foraminifera and nannofossils over the Cenozoic era have been updated with our latest geological timescale. These evolutionary ranges can be visualized in the form of interactive, extensible evolutionary trees and can be compared with other geologic data columns. **(2)** A novel approach of integrating morphospecies and lineage trees is proposed to expand the scope of exploration of the evolutionary history of microfossils. It is now possible to visualize morphological changes and ancestor-descendant lineage relationships on TSCreator charts which helps mutual learning of these species based on genetic and bio-stratigraphic studies. **(3)** These evolutionary datasets have been used to analyze semi-periodic cycles in the past bio-diversity and characteristic rates of turnover. Well-known Milankovitch cycles have been found as the drivers of fluctuations in the speciation and extinction processes. **(4)** Within a shorter 2000-year time period, global cooling events might have been a factor of human civilization turnover. Using our regional and global cultural turnover time series data, the effect of climate change on human culture has been proposed. The enhancement of the evolutionary visualization system accomplished by this research will hopefully allow academic and non-academic users across the world to research and easily explore Earth history data through publicly available TSCreator program and websites.

CHAPTER 1.   INTRODUCTION

1.1   Background and motivation

The true origin of the universe is still a mystery and even though science has helped us to know a great deal about the cosmic, geologic and biologic events in the past that eventually shaped planet Earth into a life-bearing, burgeoning planet, we still have many unsolved questions to answer. The age of the Earth has been estimated to be about 4.54 billion years whereas our species appeared only a few millions of years ago. The theory of evolution gave us an understanding of how life emerged and flourished from a single-celled organism to multicellular complex life like us on our loving pale blue planet. However, for millions and billions of years, there was no intelligent observer to observe how our planet has gone through the transformation to bring an optimal environment for life to exist. It's only a few hundred years of human history and modern science when we started gathering the data from across the globe and began to understand the driving forces and underlying mechanisms behind the evolution of Earth and life. For our ongoing survival and progress as a species on Earth, it is very crucial to investigate and thoroughly understand the physical, chemical, geologic and ecologic processes and also the biological transitions in the history of evolution using empirical evidence. To predict "what" may happen in the future or to infer about the "how" questions of the Earth history, we need strong evidence and distinguish between facts and falsifiable assumptions. Therefore, we need more and more reliable data to statistically test our hypothesis and to draw our conclusion from.

Geologic *Timescale Creator* Project (TSCreator) has been the frontier of collecting Earth historical data for over a decade. There are about 30 intensive datapack files (Table 1.1) to be visualized on TSCreator program which include detailed birth and extinction information of the evolution of modern life (from Archaea microbes to primates, spanning 4 billion years), vertebrate evolution (from earliest fist to primates with extended sections on dinosaurs), Foraminifera evolution, human evolution (main Homo and Australopithecus ranges and major events in primate evolution), human cultural and dynastic transitions. Our dataset also includes regional tectonic plate data, biostratigraphic and lithostratigraphic record for regional basins located in Arctic and Central Canada, USA-Alaska, Gulf of Mexico, South America, Great Britain, Belgium, Middle East, Africa, Russia, China, Malaysia, Australia and New Zealand. These bio-stratigraphic data

are companioned with geomagnetic polarity scale, sea level curves, Large Igneous Province (LIP) volume (260 Ma to present) data, stable isotope (strontium, carbon, sulfur, phosphorus and oxygen) record, events of global impacts, volcanism. This huge collection of data now can allow us to investigate the correlation and causal links between major evolutionary and geologic events using the TSCreator program and further perform statistical analysis.

A great amount of research effort went into the improvement of TSCreator Java program to enhance our visualization system. In CHAPTER 2 and CHAPTER 3, we discuss our visualization algorithms and the features added to the program for evolutionary tree data exploration. CHAPTER 4 and CHAPTER 5 concern data mining and cycle analysis to test some of the hypothesis described below.

1.2 Testable hypothesis and methods

Many researchers of Earth history have suggested that there are major upheavals in the past with uncertain cause-effects (asteroid impacts, massive volcanic eruptions, mass extinctions, swings in global climate and sea-level, disruptions of the planetary carbon cycle, etc.). What is needed is a "mining" and realistic statistical evaluation of Earth history data to see when there are synchronous anomalies, when there are long-term oscillations, what are the main trends, and what are statistically significant changes in rates.

1. "The Earth has had semi-periodic episodes of unusual surface/biological change."

How many events are occurring in each 100-thousand-year or 1-million-year window for the past 60 (Cenozoic Era) or even 600 million (Phanerozoic) years? This will be a fascinating output: (a) Are there suggestions of the postulated long-term (ca. 2 to 5 myr) astronomical cycles, and (b) which peaks in events correlate with peaks in global temperature proxy, volcanic activity, continental collisions and/or major asteroid impacts? What happens if we run 2 or 5 million year sliding windows instead? What would be the projected main changes for the next million years (our own future) based on any periodicities and trends?

2. "**Rates of evolution are correlated with rates of geochemical and sea-level change.**"

Rates of change in Earth's geochemical cycles: We have compiled and re-scaled records for temperature, sea level (long/short trends), carbon cycle, and strontium (a measure of spreading rates of oceans and continental erosion). No one has really examined whether rates of change of

these are interconnected, but only a visual comparison of main trends and "excursions". Is there any correlation between such rate changes and the frequency of volcanic eruptions, continental collisions, evolutionary pulses? What would this imply about the response of Earth's processes (rates) to our current human interference?

3. "**A major factor in the rise and fall of human civilization in different continents is climate change.**"

Human history: One of our data sets is the record of all major civilizations, dynasties and other cultural shifts for all continents for the past 10,000 years. Are there any "times of high frequency of events" in these datasets? We also have ice-core records of temperature and carbon-dioxide levels, plus volcanic eruption histories. Can one identify whether natural processes and climate change (and rates of these changes, not just shifts) are playing an important role in human-civilization upheavals and trends? For example, anomalous global cooling events have been implicated in both the rise and the collapse of the Egyptian pyramid building dynasty; but are there other trends/features that are subtle but above the noise level?

Table 1.1 List of some TSCreator datasets

Dataset	Description
Marine genera ranges	18,000 genera ranges through Phanerozoic.
Regional biostratigraphy and basin lithostratigraphy	Regions include Australia, New Zealand, China, India, Malaysia, Africa, Britain, Belgium, South America, USA-Alaska, Canada, Mexico, Russia.
Phanerozoic(0~541 Ma) sea level curve	Computed as mid-point of coastal onlaps for Cenozoic era and some portion of Triassic period.
Carbon-13 curve for Phanerozoic	Carbon-13 isotopic data collected from various sources for different geologic periods.
Strontium 87/86 ratio	Reflects the rate of oceanic spreading and continental erosion.
Global trends, Impacts, Volcanism, Tectonics	Carbonate trends, global and regional impact events, super, major and regional LIP(Large Igneous Province) events etc.
Other geochemical data: P, Si, S, F_{org}	Phosphorus, silicon, sulfur data. F_{org} represents the fraction of carbon buried as organic carbon.

CHAPTER 2.   VISUALIZATION OF EVOLUTIONARY RELATIONSHIP THROUGH GEOLOGIC TIME IN TIMESCALE CREATOR

Abstract

Evolutionary trees showing interpretations of the divergences, lineages, extinctions and relative abundances of life forms through geologic time provide a very useful visualization for both public audiences and research communities. The Java-based *TimeScale Creator* platform was originally designed to present graphics of Earth history with a streamlined interface. We have added an evolutionary tree display column in addition to the array of other geo-history columns for chart making and on-screen exploration through any interval of geologic time. Enhancements include on-screen images of life forms, single-click on/off control of color-coded family branches, pop-up windows giving additional details, embedded evolution charts of morphotypes that developed within genotypes, an option to make more-compact charts by allowing new evolutionary branches to reposition over earlier extinct branches, and export/import of some common evolution-data sharing formats. A suite of current public datapacks include major vertebrate groups (including dinosaurs), marine plankton through the past ca. 70 million years, and the Tree of Life of extant organisms. Students and researchers can upload their own datasets using a simple tabular-data format from Excel-type spreadsheets. The package and external datapacks are freely available at *www.timescalecreator.org*. The intended audiences range from Earth-science classes in schools to paleontologists and evolutionary biologists who wish to compare their phylogenies to other geologic events and trends of Earth history.

2.1   Introduction

The developments of the diversity of life on Earth are routinely illustrated by evolutionary trees. Even though an evolutionary tree is an interpretation based on biological or paleontological evidence subjected to continual revision, it does provide a vivid diagram and a model that can be correlated to other events in Earth history in order to gain insights on environmental and other feedbacks. The *TimeScale Creator* visualization software displays from an extensive suite of detailed Earth-history information (regional stratigraphy, geomagnetic polarity, marine macro-

and micro-fossil evolution, vertebrate and hominid evolution, stable isotopic and sea-level curves, global reconstruction images, etc.) that have been migrated to standardized geologic time scales for comparative analysis. We were motivated to design a system for both educational and research audiences that would incorporate an automated production of phylogenetic trees for ancient fossil branches and extant life forms that would provide other features requested by users, such as images, pop-up windows displaying additional information on organisms and details of the age calibrations, and simplification of large trees by collapsing subtrees and growing new branches over extinct ones (Figure 2.1).
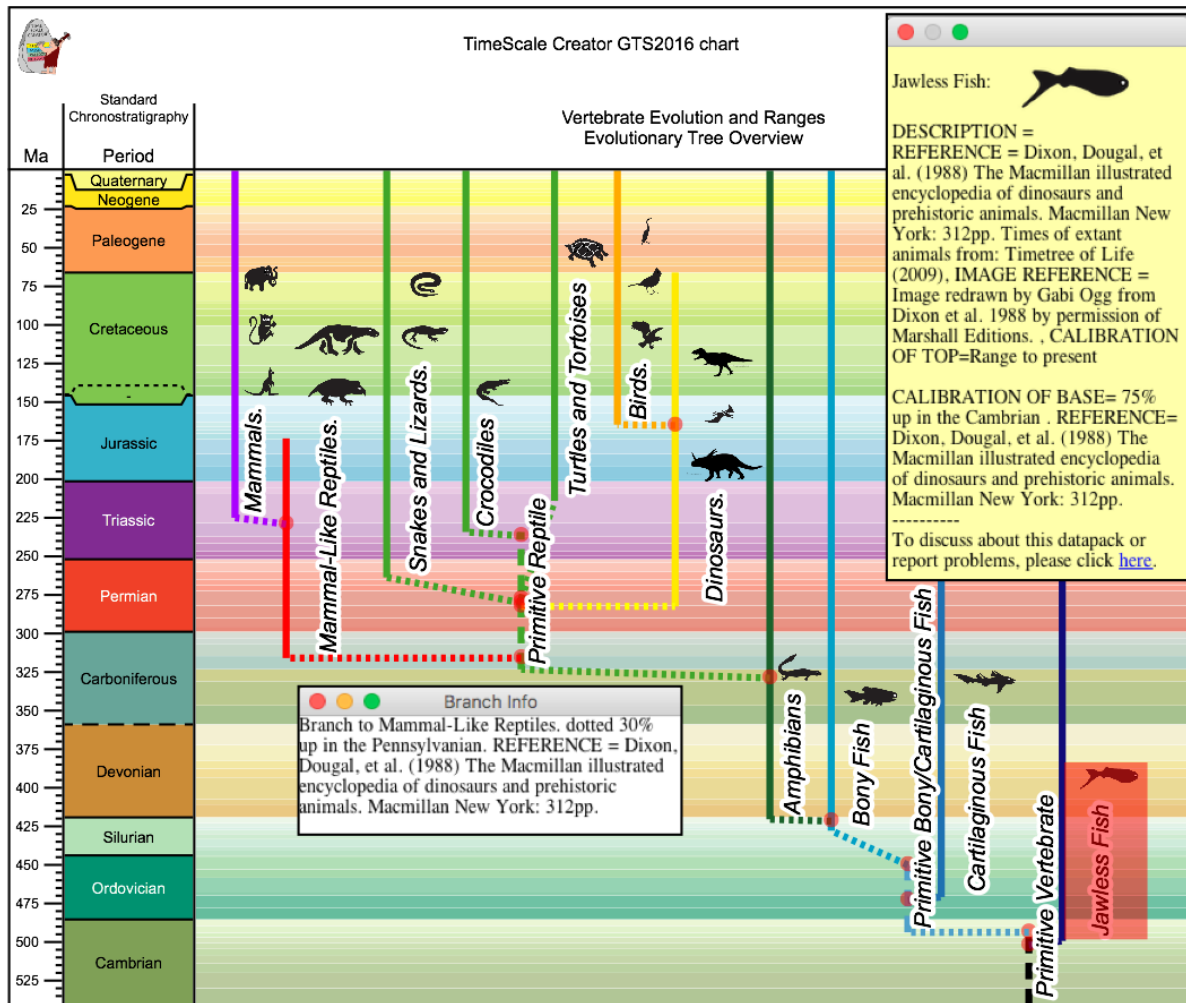
Figure 2.1 Example of evolutionary tree display within the TimeScale Creator system using a subset from a generalized vertebrate datapack (fish, dinosaurs, birds, mammals, etc.). The loaded datapack contains ancestor–descendant relationships and ranges, a library of images, details on each group, and instructions for color coding. When the mouse hovers over a range, a left-click on the activated red-shaded highlight (e.g., Jawless Fish in this example) then triggers a pop-up window (yellow rectangle) containing details, images, and URL links. This pop-up window can be moved and rescaled as desired. Right-clicking on an evolutionary node (red dots on ranges) activates a pop-up window with details about that ancestor–descendant relationship. This chart has used the option to display a background of pastel colors (international standard set from the Commission for the Geological Map of the World, 2012) for the stages that comprise each geologic period of the Phanerozoic.

2.2   Selected related phylogenetic software

The dynamic field of phylogenetic research had led to a huge and growing array of software tools (e.g., one website posting in 2014 gave annotated descriptions of 392 phylogeny packages

and 54 free web-based systems (Felsenstein, 2014). Tree reconstruction is performed by mathematical modeling based on the evolutionary data in some software packages, and model selection is necessary to identify the best model that can generate the most accurate tree. Some of the leading software, such as MrBayes (Huelsenbeck and Ronquist, 2001), BEAST (Drummond and Rambaut, 2007), BayesTraits (Meade and Pagel, 2019), BATWING (Wilson et al., 2003), BAli-Phy (Suchard and Redelings, 2006), PAML (Yang 1997), and TOPALi (Milne et al., 2008), take a probabilistic approach by using Bayesian inference method. Others, such as MetaPIGA2 (Helaers et al., 2010), PAUP (Swofford et al., 2001), phyclust (Chen, 2019), PHYLIP (Felsenstein, 2019) and PhyML (Guindon et al., 2005), include tools for estimating the likelihood of generated trees using maximum likelihood or use AIC (Akaike Information Criterion) or BIC(Bayesian Information Criterion) for model selection. Tree reconstruction procedures using distance matrixes are used in other software, such as BioNumerics (Applied Maths, 2020), ClustalW (Higgins et al., 1997) and phangorn (Schliep, 2010). However, most of these lacks the capability to display these evolutionary trees using geologic time. Mesquite (Maddison et al., 2018) is one of the few software packages besides *TimeScale Creator* that can be used to draw an evolutionary tree with an adjacent geologic timescale, but it is designed to emphasize phylogenetic analysis rather than a detailed visualization of lineages of organisms.

The current packages use a variety of programming languages and libraries. Phybase (Liu and Yu, 2010), Rphylip (Revel and Chamberlain, 2014), phangorn (Schliep, 2010), ape (Paradis et al., 2004), phytools (Revell, 2012), GGTREE (Yu, 2019) are packages written in R programming language to reconstruct, visualize and perform statistical analysis with the tree data. Some Javascript libraries (Javascript InfoVis toolkit (Fekete, 2004), jsPhyloSVG (Smits and Ouverney, 2010), PhyD3 (Kreft, 2017), phylotree.js (Shank et al., 2018)) are developed to create websites for phylogenetic tree visualization of publishable quality. There are also some existing online tools such as AQUAPONY (Cazaux, 2019), ETE Toolkit tree viewer (Huerta-Cepas et al., 2010), EvolView (Zhang et al., 2012), IcyTree (Vaughan, 2017), iTOL- interactive Tree Of Life (Letunic and Bork, 2006), Phylo.io (Robinson et al., 2016), T-REX (Alix et al., 2012), TreeDraw (Luo, 1993), TreeViz (Johnson, 1992) which can be accessed via modern web browsers, and user-formatted tree-files can be uploaded for visualization in some of these on-line systems. Examples of some desktop software packages which provide integrated environments for interactive tree visualization and annotation for different operating systems are TreeGraph2 (Stöver and Müller,

2010), macclade (Maddison, 1989), ARB (Ludwig et al., 20004), Dendroscope (Huson et al., 2007), Tree View (Page, 1996), UGENE (Okonechnikov, 2012), PHYLOVIZ (Francisco et al., 2012), Treevolution (Santamaria and Therón, 2009), TreeDyn (Chevenet et al., 2006). There has been a trend to partly standardize the uploading of tree data for use in these varied systems using formats called Newick, Nexus, FASTA, etc.

Many of these software packages are dedicated for specific purposes, especially with strengths in static visualization of particular tasks (e.g. compatibility analysis, tree-based sequence alignment, gene duplication, biogeographic analysis, tree simulation, geologic dating etc.). In contrast, the new tree feature developed for the *TSCreator* software focuses on deep-time tree visualization alongside extensive Earth historical data.

2.3   TimeScale Creator platform for Earth history

TimeScale Creator (TSCreator) is a free Java package for depicting Earth history and deriving custom charts of any portion of the geologic time scale. The visualization interfaces and extensive datapacks were developed and progressively enhanced in conjunction with academic and industrial stratigraphers and paleontologists, with the International Commission on Stratigraphy, and with several geological surveys (e.g., Ogg and Gradstein, 2006; Ogg and Przybylski, 2009; Smith et al., 2015; Bobick et al., 2016). The *TSCreator* internal database suite now contains over 300 columns with over 50,000 events or data points on sea level, stable isotope, biologic, geomagnetic, and other aspects of Earth history (plus the Moon and Mars). In addition to this internal dataset, users can download and incorporate any of about twenty specialized datapacks (e.g., biostratigraphic and geologic history of all Australian basins as compiled by Geoscience Australia (Smith et al., 2015)). In addition to screen displays that have interactive pop-up windows, the *TSCreator* can export charts in PDF, SVG, PNG or JPEG format.

The pre-2008 versions had focused on a convenient user-friendly way to generate charts. A series of *TSCreator* updates progressively added features, such as: pop-up windows with images for fossils; map interfaces to access regional stratigraphic columns and transects; an age-slider option to display regional rock types with time; depth-to-age conversions; gradient backgrounds; search tools that also allow access to pop-up information; and web-accessed datapack makers. All datapacks are based on tab-delimited text, because the detailed event compilations with

explanatory notes and underlying age relationships were initially exported suites of spreadsheet (Microsoft Excel) workbooks, in which the interrelationship equations embedded within these spreadsheets was a flexible method to automatically recalculate the ages of all events to new calibrations or to new published age models. Many data-column types (e.g., zones, first/last occurrence arrows, geochemical curves, lithology patterns, etc.) can be combined in a single text file separated by headers to instruct the visualization software on the type of column for displaying each individual dataset. *TSCreator* version 7 and the extensive array of external datapacks are currently standardized to the published age models of *Concise Geologic Time Scale 2016* (Ogg et al., 2016), and are now being recalibrated during 2020 to the in-press *The Geologic Time Scale 2020* (Gradstein et al., 2012).

2.4   Methods

2.4.1   Implementation of the tree visualization in TimeScale Creator

The earlier *TSCreator* versions had the capability to display the stratigraphic ranges of organisms against the geologic time scale but lacked a means to show postulated evolutionary relationships among those organisms. The basic range diagram is a set of labeled vertical lines that begin and end at designated ages and have line styles denoting relative abundances (Figure 2.2; see Appendix 2.A for this datapack format).
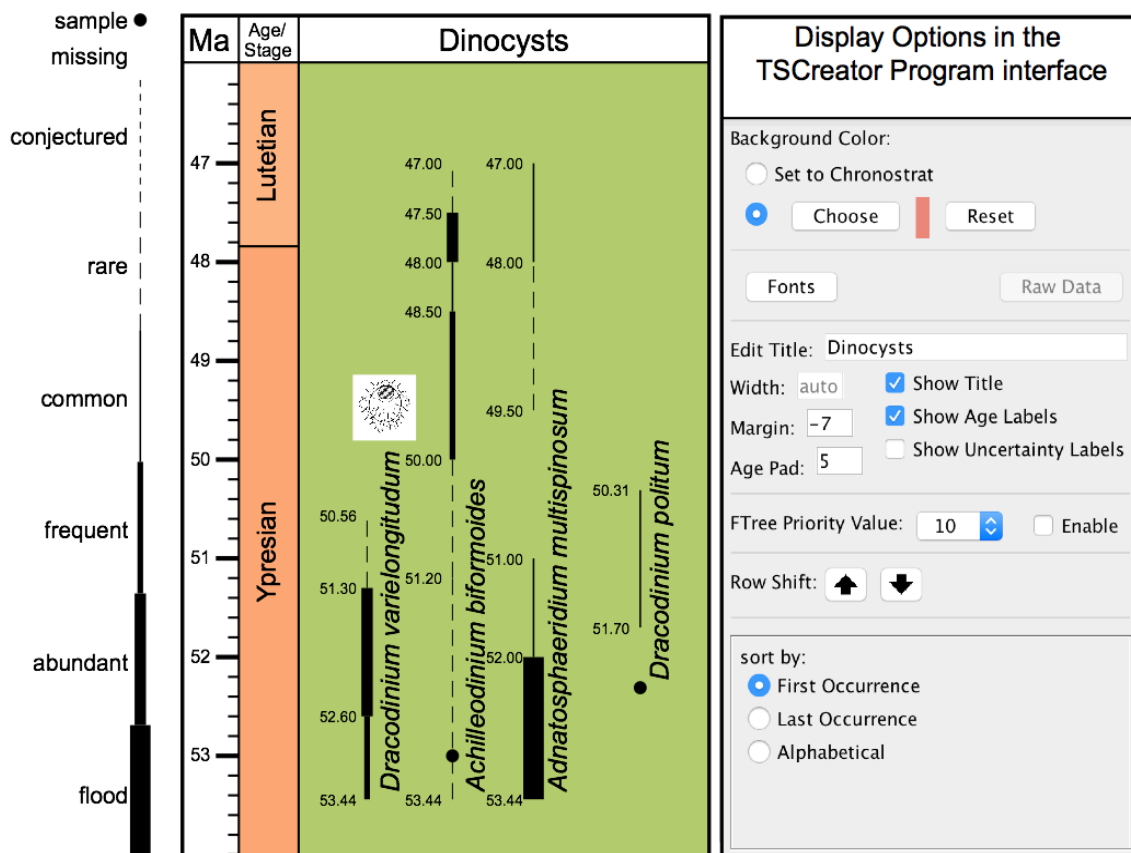
Figure 2.2 Stratigraphic range chart in TSCreator using a schematic set of dinoflagellates from 54 to 46 million years ago (Ma). A portion of the underlying dataset array is given in Appendix 2.A. Options for line styles are shown to the left of the TSCreator chart. The program auto-adjusts the horizontal spacing between ranges displayed on-screen or in exported charts according to whether their names include images of different sizes. In this chart activation of "Show Age Labels" renders display of numerical ages for each line style interval within the dinoflagellate ranges. The menu on the right side of the chart provides considerable flexibility for visualization, including: choosing background color, font size and color; editing the title for a column and options to display that title; age labels (activated here), width/margin and age-padding for changing positions of labels next to range lines; display of only those ranges that exceed an assigned priority (useful when a chart has hundreds of ranges); and arrangement of the ranges by first/last occurrence or alphabetically.

The basic concept in an evolutionary tree is that a "Parent" (ancestor) produces a "Child" (descendant). Parents can have multiple Childs. The initial approach to adding an evolutionary tree to *TSCreator* was merely to add a "*branch*" option to the existing range display format as a flag to draw a line from a point at any position along the range of the Parent to connect to the base of the range of the named Child. Once implemented, other display enhancements were made in response to user recommendations. We wished to be able to employ alternative tree styles to represent a

26

variety of approaches to phylogeny reconstruction, including trees of only relationships, such as cladograms; and relationships with an implied chronology through deep time (Figure 2.3). We also wished the flexibility to display either species-level taxa or higher taxonomic groups.
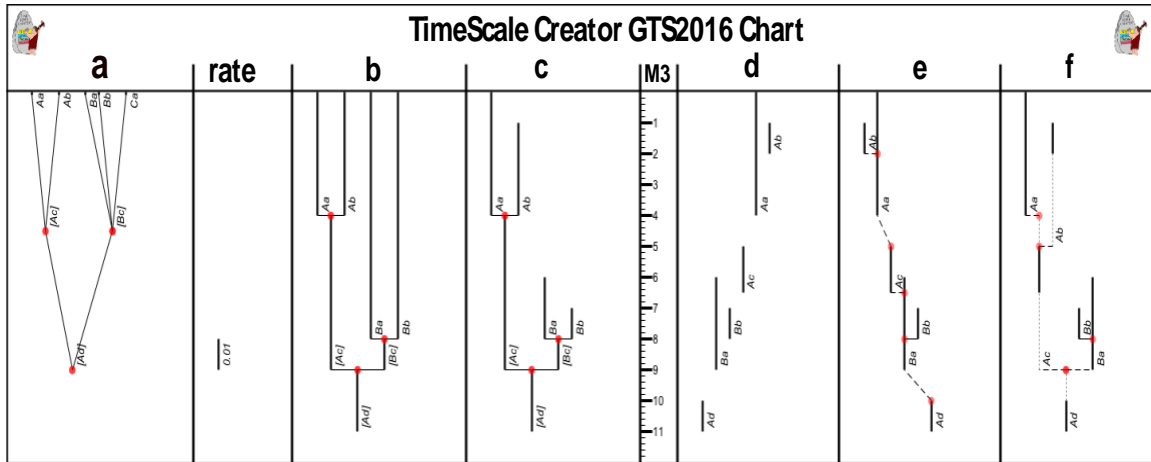
Figure 2.3 Schematic examples of some of the tree styles available in TSCreator. a: phylogeny of living operational taxonomic units (Aa, Ab, Ba, Bb, Ca), with implied ancestral nodes ([Ac], [Ad], [Bc]) and an unresolved polytomy; leaves are slanted. b, c: example a without Ca, with a chronology or a rate of evolution implied (e.g., substitutions per sequence site); leaves are rectilinear and unscaled (b) or scaled (c). d–f: operational taxonomic units (Aa–Ad, Ba, Bb): d: with recorded stratigraphic ranges against Ma scale; e: phylogeny of ranges and branches, strongly influenced by stratigraphic succession but with undefined evidential support (branches with broken line styles, slanted or horizontal depending on relative stratigraphic positions of ancestor and descendant), except for the strongly supported budding of Bb from Ba (rectilinear branch with unbroken line style); f: revised phylogeny with specific dates proposed for branches, requiring both upward and downward extensions ("conjectured" line style, dotted) to recorded stratigraphic ranges, and with implied bifurcating (Ad–Ac/Ba), succession (Ac–Aa), and budding (Ac–Ab, Ba–Bb).

2.4.2   Data structure for evolutionary tree

The addition of a "*branch*" flag is all that was required to augment the pre-existing format coding of range data to add connections between ranges to produce an evolutionary tree display in *TSCreator*. For example, to show the evolution of Birds from Dinosaurs, a branch line in the Late Jurassic (160 Ma) is added to connect a point at 160 Ma from the Dinosaur range (indicated by a "red-dot") to the base of the fossil record of Birds at 150 Ma (Figure 2.1). The addition of this

branch flag was been exploited to offer enhancements including: branch labels to highlight subtrees (clades) of interest, colors applied to these labels and the range lines within the subtrees, as well as priorities for subtrees to allow on-screen pruning within large charts; three levels of branch line styles to differentiate categories of branches (e.g., levels of confidence for ancestor–descendant proposals); and pop-up windows attachable to any taxon (range line) which can include any amount of text, images, and URL links to provide on-screen access to relevant information (e.g., Figure 2.4).
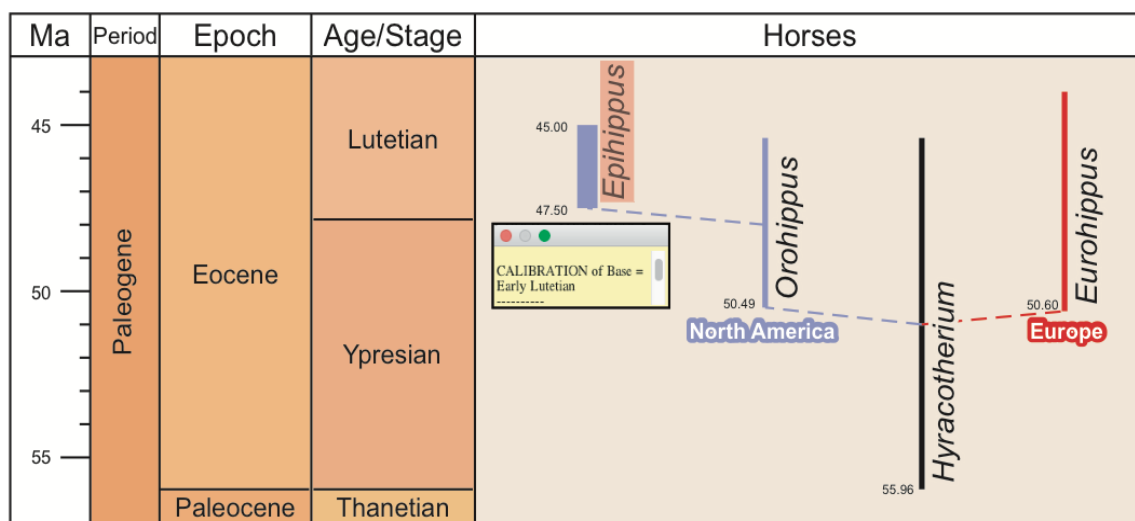
Figure 2.4 A portion of a schematic evolution of horses generated from the sample datapack of Appendix 2.B. In the display, a mouse has hovered over "Epihippus" range to activate the orange background and then clicked to open the yellow-shaded pop-up window with information on the calibration (item in column E in the dataset in the Figure 2.11 example). Connecting branch lines have been set as "dashed". Labels for subtrees (North America, Europe) have background colors that are also inherited by the component range lines. The display of the numerical ages for base of each range has been turned on from the user-control menu (see Figure 2.2).

2.4.3 Algorithm and programming the tree display

The display of evolutionary trees required several steps.

- **Input:** Evolutionary tree datapack in text format.

28

- **Output:** SVG chart with the desired evolutionary tree in a data column generated by *TSCreator* program.

- **Steps:**

1. Data extraction. Extract evolutionary-range and branch point data according to the tree data structure from the input datapack using JavaCC (Java Compiler Compiler) parser. The parser essentially parses each of the data point from a tab-delimited text file (Figure 2.12 of Appendix 2.B) and stores the information in various Java data objects.

2. Array of ranges. Calculate the total number of unique range lines from the parsed data.

3. Tree structure parameters. Deduce the Parent–Child relationships for each of the range lines to construct the evolutionary-tree data structure. For example, in the horse evolutionary tree (Figure 2.12 of Appendix 2.B), the program can parse the information that the *Hyracotherium* parent is branching out to the *Orohippus* child. A typical tree data structure consists of nodes and edges/links from parent nodes to children nodes. In the *TSCreator* evolutionary-tree data structure, a vertical range line refers to a node, and the branch line from a parent range to a child range refers to an edge/link. Each parent range technically can have as many children as required depending on the evolutionary history. A parent range is programmed to keep track of information of its children to determine spacing, coloring, and other attributes in order of geological time. Our evolutionary tree creates a subtree rooted at each child range branching out from the parent range and gradually expands the tree (within the temporal scope of chart, assigned by the Top and Base Interval within Settings).

4. Range lines. Each range line consists of multiple range data points which together convey a number of flags. For each range line:

a. Range point information (each item in a single row in the dataset) is extracted. For example, the starting horse range line of North America named "*Orohippus*" has three range points (lower panel in REF _Ref39236284 \h Figure 2.12of Appendix 2.B)

b. We then determine the type of each point such as TOP (end of the line), BASE (start of the line), or intermediate branch points shown as "red-dots". Information for branch labels and branch colors are assigned for every branch point at the same time.

c. Drawing style, such as the line width and color for each range point is assigned. Special flags are set for situations such as whether a point (red dots) will be blinking if the branch and subtrees are visible or not.

d. Priority flags are set when branch priorities are enabled. Priority values are passed down the branches of the trees depending on the value.

5. Branching structure. This was the most complex suite of algorithms. A left–right branching algorithm partly enables the *TSCreator* evolutionary tree to look visually balanced and semi-symmetric. In the *TSCreator* tree data structure, a range line acts as a parent node, from which left or right child ranges branch. To avoid or minimize possible collisions, the algorithm carefully places child ranges either left or right such that vertical range lines minimally interferes with the horizontal branch lines coming from the parent range. The centering of the parent range and the left/right positioning of each child range follow these simple rules:

a. Single child — If there is only a single child, then its range is positioned to the left side of its parent range.

b. Multiple children — If there is an odd number of children, then the earliest (stratigraphically lowest) child is positioned to the left side of the parent, then the next later child to the right, and then this left/right alternation is continued. If there is an even number of children, then the earliest child is positioned to the right side of the parent, then the next child to the left, and so on. This rule also logically matches with the previous rule, because a single child is an odd number.

c. Coeval descent — If two or more children arise from the parent simultaneously, then the left/right positioning of each child range depends on the order that each child appeared in the text dataset.

The tree branching algorithm then calculates the line height and width of each subtree branching out from a parent range. It keeps track of three main variables: (a) y coordinate of the TOP (LAD: Last Appearance Datum) range point, (b) y coordinate of the BASE (FAD: First Appearance Datum) range point, (c) x coordinate or the horizontal location of the range line. When the parent–child relationship of each range line is established, the x coordinates of a parent and its children are determined programmatically based on the number of children and required widths. All of their widths are calculated simultaneously using recursive function calls (from child to parent). The width of a tree rooted on the parent range is the accumulation of widths of all the subtrees created by its child ranges from both left and right sides. The width determination function takes into account the width of range lines depending on their line styles

(e.g., frequent, common, rare, abundant etc.), range labels, pop-up rectangles containing images, and global margin and range padding values provided in the settings window. Width of range-label names again depends on the font size and associated image dimension. All the ranges are finally stored in a single array before drawing where they are, by default, sorted according to the increasing y coordinate value of the BASE range point, i.e. the earlier organisms occur before the later ones. The algorithm first draws the range lines in that sorted order and therefore, the range lines of earlier organisms are drawn on the SVG chart before those which appeared later. The algorithm follows an iterative process (from parent to child) according to the rules a, b, and c to determine the x coordinate of each range line in the evolutionary tree. After drawing the vertical range lines, the algorithm finally connects the child ranges to the parent by drawing the horizontal branch lines using the BASE age, branch point age, and the x coordinate information.

6. Color inheritance. The branch color is specified in the input dataset in the "*BranchColor*" field, which the algorithm combines with the branch line-style information to ultimately determine the drawing style for a horizontal or left/right-inclined branch. Because the algorithm already established the parent–child relationship between the ranges, it can also allow the color inheritance from branch to subsequent child ranges.

7. Space conservation is a feature in which new evolutionary branches extend into the blank spaces above extinct branches (Figure 2.5). This is similar to "new higher branches growing over older lower ones" in a tree and reduces empty space on the chart. Because the ages in the range line interval are already extracted and our algorithm calculates the width of every subtree, then keeping track of empty space above extinct branches is just an extra step. This "*Conserve Chart Space in Family Tree Plotting*" option is available in the main setting menu in *TSCreator*.
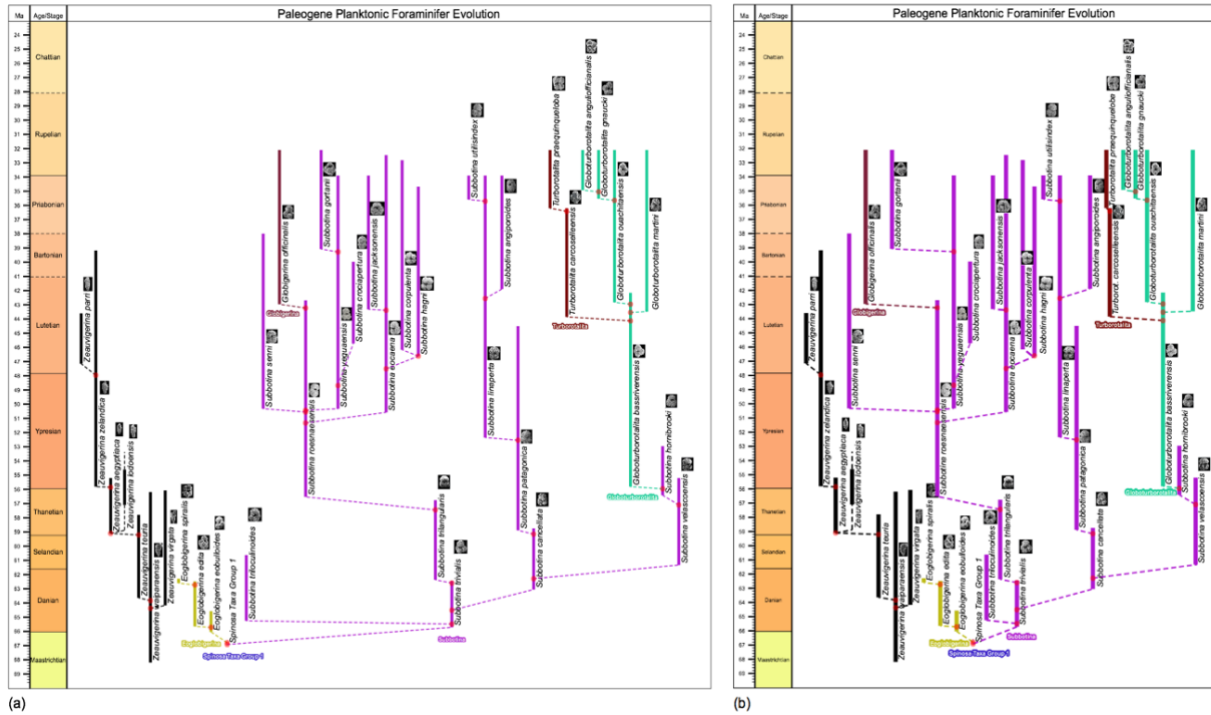
Figure 2.5 Conserve chart space option. (a) An extract from the Paleogene Planktonic Foraminifer datapack without the space conservation feature. There is empty space above earlier branches due to the extinction of some families, such as the *Eoglobigerina* (yellow range lines in the Danian Stage). (b) Activating the "Conserve Chart Space" option reduces the needed display space. Some *Subbotina* clades (pink range lines) are now shifted above the extinct *Eoglobigerina* set to enable a more compact chart.

8. Age labels and spacing. The tree-drawing algorithm simultaneously determines the locations of numerical-age labels while determining the range line positions (e.g., the numerical ages on the ranges of horses in Figure 2.4). The user can choose to hide (which is the default) or show these labels. Age labels are located in the left side of the ranges and are set to display only 2 decimal places. Users can adjust the placement and other paddings using the settings-menu window for desired visualization (Figure 2.2).

9. Priority. With this feature certain branches can be prioritized over others when on-screen diagrams become unwieldy large (Figure 2.6). For instance, high priority could be assigned to organisms that evolve into other major groups, and progressively lesser priority to meager branches. With this feature and the ability by users to turn on/off branch nodes (§ Turning branches on/off, below) in the onscreen display, our *TSCreator* program has become highly scalable.
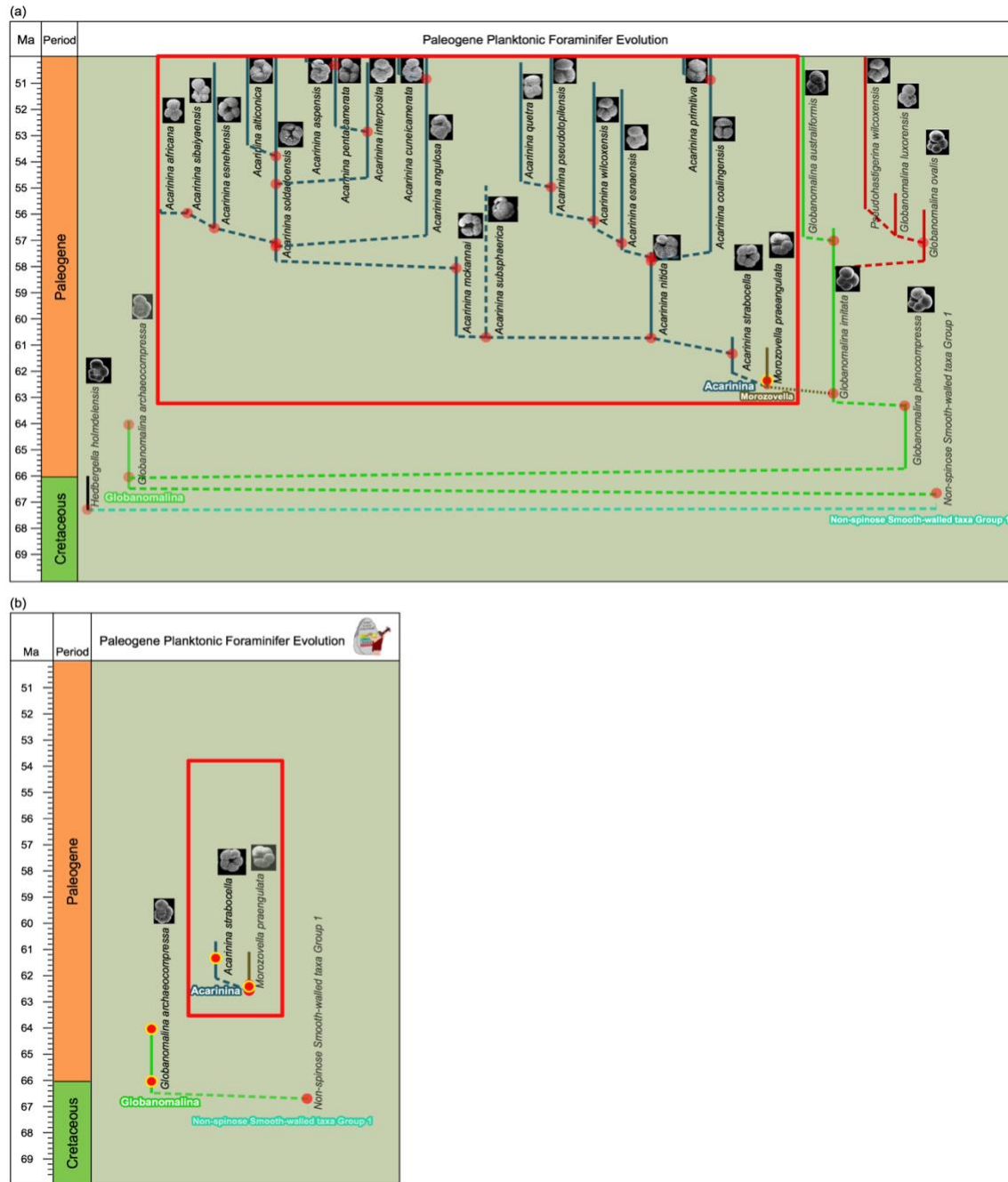
Figure 2.6 Using "Priority" assignments in a complex evolutionary tree. (a) A portion of the evolutionary tree of Paleogene Planktonic Foraminifer focused on the *Acarinina* clade (within red rectangle along with ancestor, *M. praeangulata*; the two *Morozovella* clades descending from *M. praeangulata* are turned off, indicated by hidden nodes with yellow borders). This was generated without enabling "FTree Priority Value". (b) The same portion of the evolutionary tree, in which FTree Priority Value is enabled and the value has been set to 10, thereby displaying only subtrees with priority values of 10. The *Acarinina* clade is now shrunk down to its initial *A. strabocella* because the remaining *Acarinina* morphospecies have been assigned lower priorities and so are now represented by hidden nodes (with yellow borders).

10. Turning branches on/off. Another powerful feature that increases the scalability of *TSCreator* program to explore large trees is the option to toggle branch nodes on/off in order to show or hide specific tree branches (Figure 2.7). Left-clicking on a "red-dot" node turns off the connected branch. That "red-dot" blinks on-screen to notify the user that it is turned off and can be activated again by a left-click. The algorithm knows from the pre-established parent–child relationship to change the visibility flag to be false for all the subsequent child ranges (e.g., in Figure 2.7, dinosaurs and crocodiles are descendants of *Proterosuchians*, therefore the algorithm recalculates the width of *Proterosuchians* without these ranges). The algorithm recalculates the position/location attribute of the ranges in the all other subtrees to redraw the chart. We also provide "Hide Ancestors" option from the tree column option panel in the settings window and you can hide all the parent ranges of any range simply clicking on any "red-dot" of a range after enabling this option. You can also revert back to the full tree and unhide all the branches by selecting "Show All Branches" option.
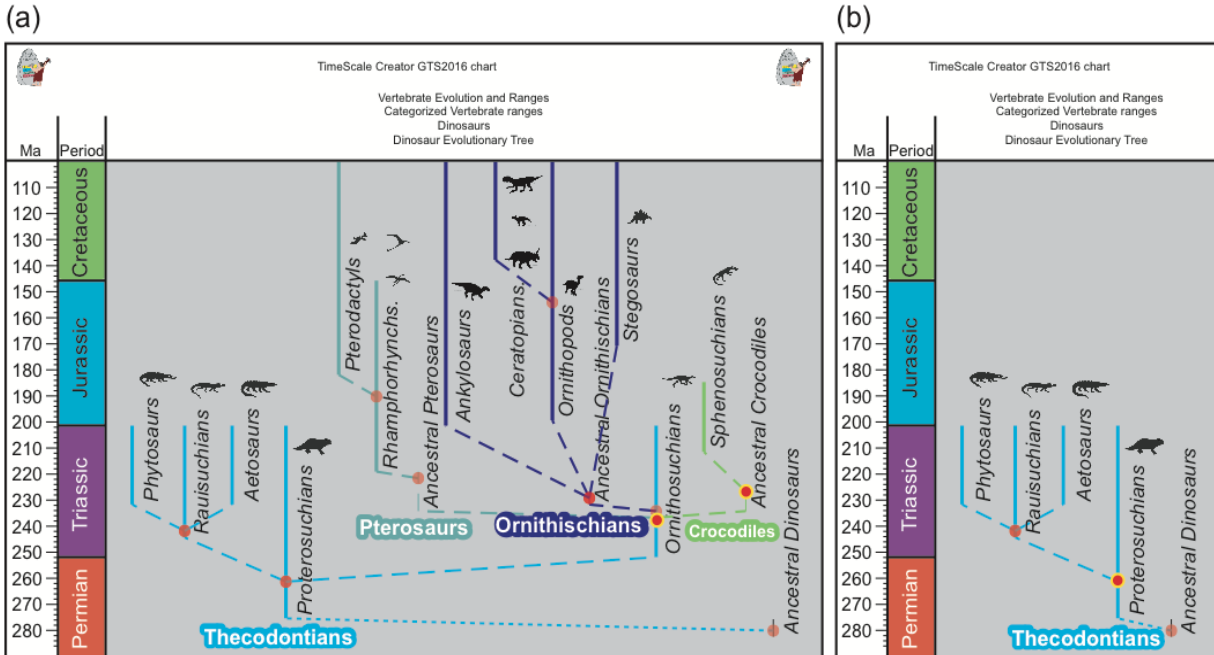
Figure 2.7 Turning branches on/off. (a) Evolution of early land reptiles and their dinosaur and crocodile descendants. The "red-dot" nodes (without yellow borders) on range lines are at the beginning of evolutionary branches and can be left-clicked on/off. (b) The dinosaur branch (Pterosaurs, Ornithischians) and crocodile branch are not displayed after left-clicking the red-dot on the Proterosuchians range, and the red-dot continues blinking (indicated here by a yellow-border to the red dot) to indicate the invisibility of that subtree. The branch can be turned back on by left-clicking on that blinking red dot.

11. **Display evolutionary path history and common ancestor.** It's possible now to display the evolutionary history of any organism instead of visualizing the entire evolutionary tree. The tree column option in the settings window provides textbox to input the name of the organism and upon clicking the button "Show evolutionary history", a user can easily transform the full evolutionary tree into a partial tree showing the evolutionary past of that organism. The interface allows input for two organisms for which you can also draw the subtree rooted at the common ancestor of them. The easiest way to input the organism name is to open the popup box by clicking the red rectangles and copy the organism name and then paste into the textbox.

2.5   Additional features and applications of *TSCreator* evolutionary tree display

Installing evolutionary-tree displays within the *TSCreator* visualization framework provides an accessible way to explore evolution and the history of life on Earth in an interactive environment (Figure 2.8).
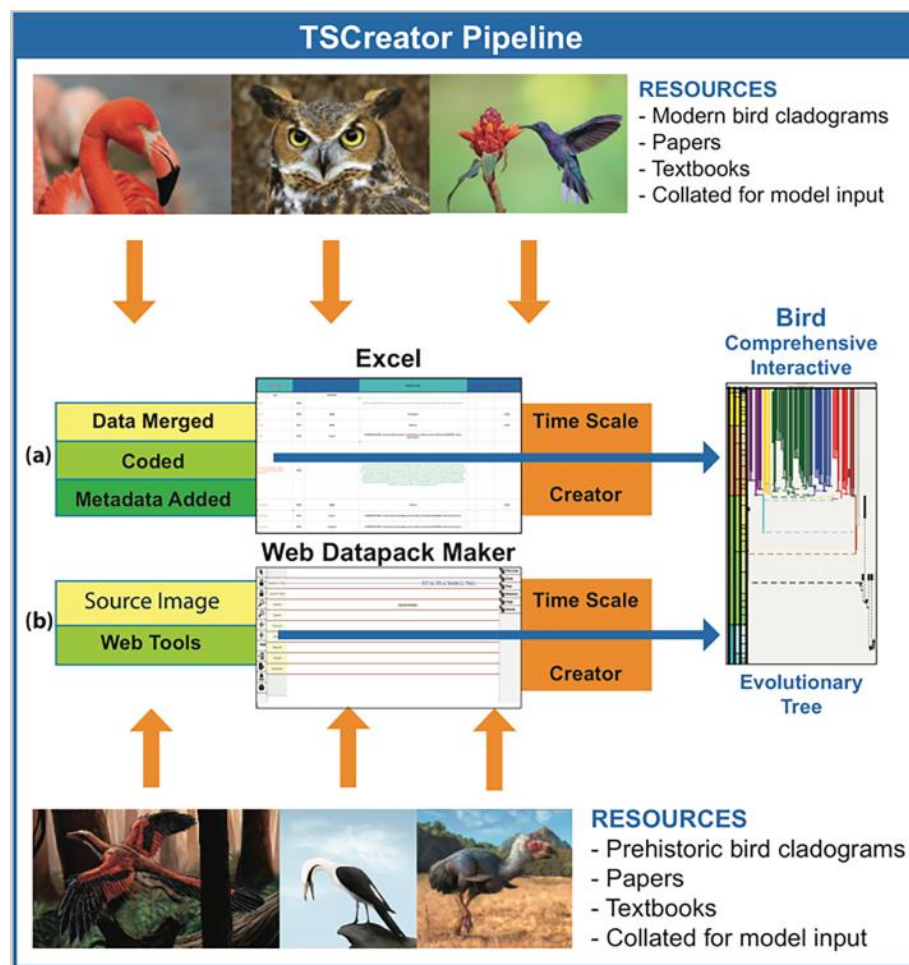
Figure 2.8 Workflow from data collection and synthesis to chart visualization in the TSCreator software suite using bird evolution as an example. Users can construct datapacks using Excel or our web-based datapack maker (see section 2.5.4. Web interface for creating evolutionary tree datapacks, below) and then visualize the evolutionary tree alongside other geologic timescale columns.

2.5.1 Coding Groups by a Group Label and inherited color

In *TSCreator*, we can specify "*BranchColor*", which is by default inherited by the child ranges and we can also give a "*BranchLabel*". For example, Figure 2.9 uses this label/color option to highlight that Ancestral mammals branch into Marsupial (yellow solid range line) and Placental mammals (black dotted range line) during middle of the Jurassic Period. This feature helps highlight origins and emergence of groups or distinctive taxonomic character sets.
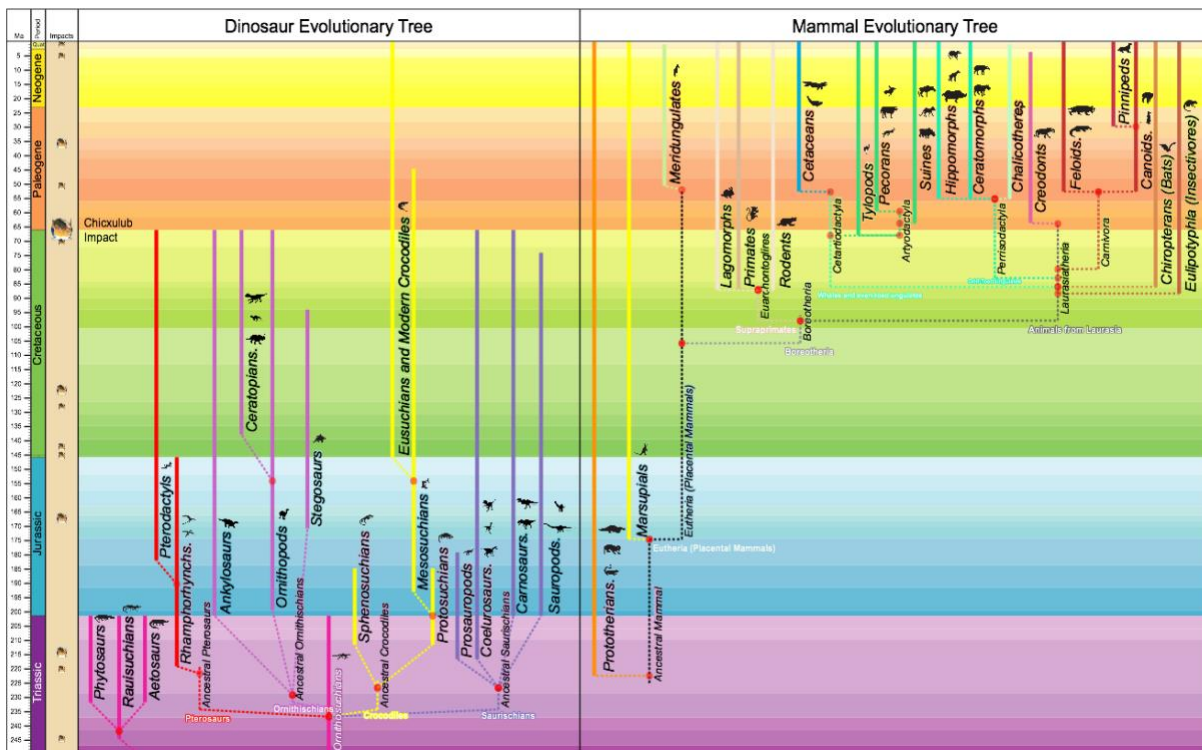
Figure 2.9 Using multiple evolutionary and geologic event columns within TSCreator. The datapack on vertebrate evolution was loaded as "add datapack" into TSCreator, and then the Dinosaur and Mammal evolutionary trees were activated in addition to the geologic time scale and major-bolide-impact column from the regular internal dataset. The background option of "geologic stage colors" was turned on to highlight the time intervals across the evolutionary tree columns. The Dinosaurs (without birds and crocodiles) are extinguished at the boundary of the Cretaceous and Paleogene (boundary between green and the upper orange colors), followed by the rapid evolutionary divergence of Mammal groups. This major change in the dominant vertebrates on land coincides with the Chicxulub impact (the fireball in the left tan-shaded column).

2.5.2   Display of multiple evolution and data columns

A single evolutionary tree can often become quite large and complex. A large complex tree chart does provide the opportunity to scan clusters and patterns, but it can quickly become too complicated visually to extract information for specific ranges. It is easy to create a datapack with both a mega evolutionary tree and individual partial evolutionary trees (e.g., our Tree of Life datapack). *TSCreator* allows drawing of multiple evolutionary trees as multiple columns side by side (Figure 2.9). Multiple evolutionary trees can be displayed for any time period against as many other columns as desired. This provides an elegant means by which to explore other potential factors relevant to evolution (e.g., Figure 2.9).

2.5.3   Exporting of charts

2.5.3.1   Graphic export formats

Once charts are constructed with the chosen options (fonts, background colors, display of age labels, etc.), they can be exported to established image formats (PDF, SVG, PNG, JPEG). The SVG exported charts can be enhanced within other graphic-design programs.

2.5.3.2   Exporting and importing of other Tree data formats

The *TSCreator* tree control panel on the settings window provides an option to export a loaded tree using standard Newick and Nexus tree formats. This provides a way to transfer our *TSCreator* tree data and load into existing software like Mesquite (Maddison and Maddison, 2018) and its fore-runner MacClade (Maddison and Maddison, 1989) or with R package like Ape and further perform rigorous statistical analysis. If the tree data was encrypted by another provider before visualization, then this export option is disabled because we respect the interest of the datapack maker to keep their data confidential. It is now also possible to load the exported Newick/Nexus tree directly to the *TSCreator* using the "*Add Datapack*" option under the "File" menu of the user interface. As *TSCreator* is designed to visualize tree associated with geologic timescale, an arbitrary Newick tree without a deep-time distance measure can be misinterpreted after being loaded alongside the default timescale. However, users can still load any Newick tree,

and we suggest disabling all other columns including the ruler column (named as "Ma") to just visualize the tree topology and explore the tree branches and use other tree features like vertical scaling and exporting in various image formats.

2.5.4   Web interface for creating evolutionary tree datapacks

As part of the *TSCreator* research program, with especially the general user in mind, an online web datapack[1] maker using a graphical interface has been developed. This then serves as an alternative to the manually generated spreadsheet method for compiling datapacks. Typically, one would like to draw an evolutionary tree using a source tree image that was published in a research paper. The online system enables a user to underlay that image below a "canvas", then graphically sketch the ranges and branches within time-control scaling guidelines (Figure 2.10). Menu windows allow adding the options for range name, color, branch label, branch color and other attributes. One saves the entire project as a JSON file that can be re-uploaded for revisions and as an exported text file for uploading into *TSCreator*. Because an existing project can be re-loaded, it can also be used to easily make alternative trees. The online system with its user manual is hosted alongside our other *TSCreator* column datapack makers on our TSCreator website. We believe our online datapack-maker is a game changer for those users who wish to easily generate evolutionary trees.

---

[1] https://timescalecreator.org/tscmaker-dev/evtree_maker/html
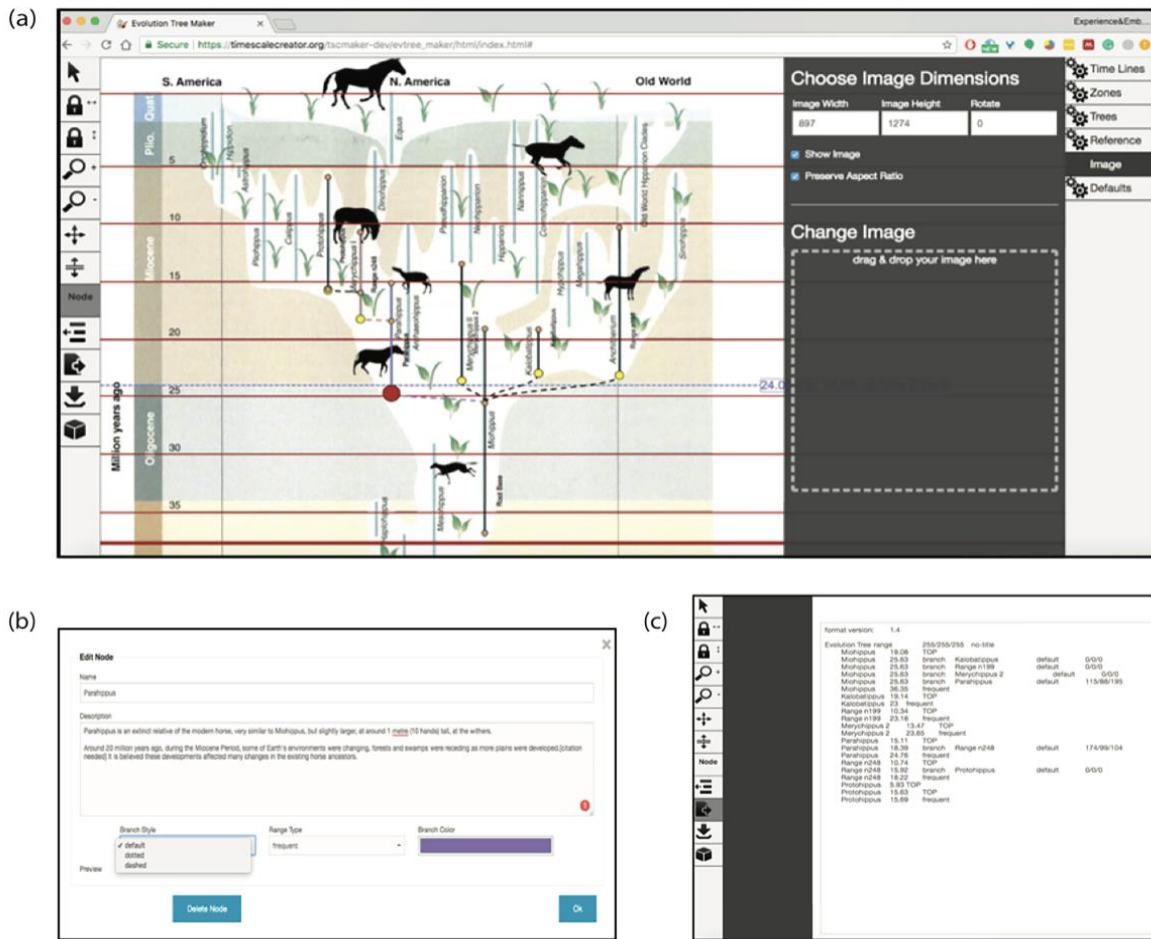
Figure 2.10 Interactive web-based graphical interface for making evolutionary tree datapacks. (a) A published image for horse evolution being prepared for conversion. The user drags the diagram into the "*Change Image*" panel on the right, then adds time-control guidelines onto the drawing canvas by selecting the timeline tool (highlighted in gray on left) and dragging to match the geological intervals on the diagram, then adding their numerical ages. To draw range intervals and connecting branches, a user selects the "Node" tool on the left and then draws from the beginning/base node to the end/top node. The ages for the range endpoints are automatically computed according to their proportion within the time guidelines. When the user selects a red-dot node on a Parent range, the branch node is automatically recognized and drawn as yellow, then the user extends its end point into a new child range. Options including zooming, panning, changing the initial image dimensions, and adding branch information. (b) This window opens when clicking on the base node of each range to enter information (e.g., for the range of the extinct *Parahippus* relative of modern horse). (c) View of the text-version of the datapack created in the graphical interface prior to exporting window.

2.6   Selected examples of current evolutionary tree datapacks

For public use in TSCreator, go to TSCreator website[2] , then click "datapacks" tab.

Evolution of Modern life: This datapack includes evolutionary history from Archea microbes to primates throughout 4 billion years of Earth history (Hedges et al., 2009)).

Vertebrate evolution: This datapack contains an example of evolutionary relationships from the earliest fish to dinosaurs to primates accompanied by schematic images and external links.

Human evolution: Although not a phylogeny, included are tool intervals, main Homo and Australopithecus ranges (ca. 5 Ma, includes images), and major events in primate evolution (ca. 50 Ma).

Planktonic Foraminifer Evolution through the Paleocene–Eocene: Dataset and images are from Chenglie Liu et al. (ExxonMobil Exploration) to TSCreator for general release (includes images of 200 taxa).

Cenozoic Macroperforate Planktonic Foraminifera: Phylogenetic tree data (Aze et al., 2011), with updated databases and images (Fordham et al., 2018) which enables detailed morphospecies evolution to be shown alongside macroevolutionary lineage trees.

2.7   Conclusion

Most current evolutionary-tree graphical packages lacked the capability to display trees against other time-scaled geologic or geochemical data, or they do not enable click-access to the underlying data through pop-up windows.

The embedding of an evolutionary-tree display with an array of special features within the *TimeScale Creator* platform enables paleontologists and other geoscientists, biologists and science students to visually compare the evolutionary events to other biologic, lithologic, magnetic, sea level, chemical and tectonic records from different regions to investigate potential relationships.

Our addition of evolutionary-tree graphics to the *TimeScale Creator* visualization software for Earth history provides a powerful and flexible method to display and study development of life through deep time.

---

2 https://timescalecreator.org/

2.8 Computer code availability

TimeScale Creator evolutionary tree software module was developed by Abdullah Khan Zehady, Jason Bobick and Gangi Palem. The software can be launched in any modern computer with Windows, Macintosh or Linux operating systems installed. The proper instruction to run and generate charts using datapacks are provided in Supplementary file 1. Java programming language is used to write the code and Java 1.6, or higher version is recommended to execute the program. The code is freely available from a github repository3. The size of our code (only java files) is 524K. The repository also provides a downloadable 33Mb java jar file to directly run the program and generate charts. The software package and all datasets (encoded) are available free of charge from the downloads section of our project homepage4. A *TSCreator* Pro license is needed for non-academic use. For self-made datasets that exceed 3000 characters, a Pro license needs to be requested. However, if you are an academic or a researcher and are willing to make your dataset publicly available through our website, we will allow free version upon request.

2.9 Appendix 2.A TSCreator datapack format for ranges

In the range-column dataset, the initial tab-delimited header (green-shaded rows in Figure 2.11) includes the title for the display (column A) and the flag "range" (column B) to indicate the column type. Optional fields are a background color in R/G/B (column D), whether the title should be displayed (column E), whether the column should be automatically on or off (column F), and a comment field (column G) that is activated as a pop-up window when the column title is mouse-clicked.

This header is followed by the range data for each successive organism (tan-shaded rows in Figure 2.11). The entry consists of the name (column B), the (earliest) age to begin a line style (column C), the type of line style (column D; see left side of Figure 2.2 for the types), an optional comment field (column E), and an optional line color (Column F). The line types (column D) are merely flags to set a line thickness or style, except that "TOP" terminates a line, "missing" is a flag to insert a gap, and "sample" superimposes a dot on any portion of a range-line or outside of that range. During the loading of the dataset, the program looks for all data with the same name, and

3 https://github.com/brishtiteveja/TSCreator_Evolutionary_Tree_Visualization
4 https://timescalecreator.com

then draws the indicated line style upward (higher/later) until either an age for different line style is indicated, the word "TOP" is indicated in the line-style field, or the top of the selected age span is encountered.

Datapack Format for Range Columns with Abundances

A	B	C	D	E	F	G	H
<Title>	range	<blank>	<color>	notitle	on/off	<popup>	*Header Row*
<blank>	<label>	<age>	<abundance>	<popup>			*Data Row*

Example

A	B	C	D	E	F	G
Dino-cysts	range		175/201/108	notitle	off	fictitious dino abundances
	Dracodinium varielongitudum <img align="middle" width="30" src="Dracodinium_varielongitudum 90.png">	50.56	TOP	you could also add an URL link into this popup		
	Dracodinium varielongitudum	51.3	rare	poorly preserved		
	Dracodinium varielongitudum	52.6	abundant			
	Dracodinium varielongitudum	53.44	frequent			

Figure 2.11 A portion of the dataset for the dinoflagellate range chart of Figure 2.2 in Excel sheet format; see text for description of header (green shaded) and data (tan shaded) fields. The name "*Dracodinium varielongitudum*" (column **B**) will display vertically along its range (leftmost range line in Figure 2.2). That displayed name can include an embedded image using an HTML image tag that provides the alignment, scaling and image file name. In this example, the thumbnail picture was pre-rotated 90° so it will look upright when the range label is plotted vertically (see Figure 2.2). Values in Column **C** are ages in Ma for the beginning of each line style within the range line (Column **D**) with optional pop-up information (Column **E**). To insert a URL link within the pop-up text, one uses HTML anchor tag format – e.g., including "[Click Adnatosphaeridium_m ultispinosum for details]" will result in an active web link from "*Adnatosphaeridium_multispinosum*". If Excel is used to enter the dataset, then the sheet needs to be exported as a tab-delimited text file and merged with referenced .PNG or .JPG images into a zipped file, for loading into the *TSCreator* program.

2.10 Appendix 2.B TSCreator datapack format for evolutionary tree

A "branch" flag consisting of four items is all that is required to enhance the format coding of range data in order to display connections among ranges for an evolutionary tree display in *TSCreator*: the name of the Parent range (Column **B** in Figure 2.12), the age of branch from its range (**C**), the flag "branch" (**D**) and the name of the Child range (**E**). Other display options have been progressively added to that basic "branch" statement:

Parent-name (B) ⇒ Age (Ma) (C) ⇒ "branch" (D) ⇒ Child-name (column E)

⇒ "on/off" (column F) ⇒ BranchLabel (G) ⇒ Dashed/Dotted (H) ⇒ Pop-up (I)

⇒ BranchColor (J) ⇒ Priority (K)

(the "⇒" between the items below indicates a [TAB], and the letters inside brackets indicate the column in the Excel sheet of Figure 2.12).

Datapack Format for Evolutionary Tree Columns

	A	B	C	D	E	F	G	H	I	J	K	L
	<Title>	range	<blank>	<color>	notitle	on/off	<popup>					*Header Row*
	<blank>	<label>	<age>	<abundance>	<popup>							*Data Row for range*
	<blank>	<parent name>	<age>	branch	<child name>	on/off	<branch label>	dashed/ dotted	<popup>	<branch color>	<priority>	*Data Row for branch*

Example

	A	B	C	D	E	F	G	H	I	J	K
	Horses	range		245/232/ 217		on	the data is not real				
		Hyracotherium	45.39		popup for Hyracotherium						
		Hyracotherium	51	branch	Orohippus		North America	dashed	70% up in Ypresian	144/139/ 250	10
		Hyracotherium	55.96	frequent	Base = Ypresian						
		Orohippus	45.39		only few fossils						
		Orohippus	48	branch	Epihippus			dashed	Base Lutetian		10
		Orohippus	50.49	frequent	Base = 2/3 up in Ypresian						
		Epihippus	45	TOP	Base = Early Lutetian						
		Epihippus	47.5	flood							
		Hyracotherium	51	branch	Eurohippus		Europe	dashed	70% up in Ypresian	250/0/0	10
		Eurohippus	44								
		Eurohippus	50.6		Base = 70% up in Ypresian						

Figure 2.12 Sample dataset for the schematic evolution of horses (Figure 2.4): in Excel sheet format. Green-shaded rows are header information, tan-shaded rows are range data, and gray-shaded rows are the evolutionary-branch statements. The upper panel is a brief explanation of the fields in the lower panel. See text for details.

The field "*Child-name*" (**E**) must be identical to the range-name of the Child (but *TSCreator* ignores an image entry appended to the name). The branch age must be within the age range of the "Parent"; and, obviously, cannot be older than the base of the "Child" range.

The "**on/off**" (**F**) option denotes whether the child and its subtree (clade) is to be automatically displayed. If this field is blank, then the default is "on".

BranchLabel (**G**) is a horizontal label in larger font for the new subtree and is printed under the branch line coming from the parent range (e.g., "North America" and "Europe" in the Figure 2.4). **Dashed/dotted** (**H**) provide alternative options to the default solid branch line style.

Pop-up (I) is the content that will be displayed in a pop-up when one left-clicks the selected red-shaded rectangles on range labels or right clicks the red-dot node (Figure 2.1). It is our practice to always try to include the calibration of the geologic age and the source of the information. Those pop-ups can also include images and URL links to external websites (Figure 2.11).

BranchColor (**J**) is an RGB value that will be applied to the "BranchLabel" font and to the range lines of the subtree. For example, in Figure 2.4 the branch label "North America" is given bluish-gray color and the child range lines of *Orohippus* and *Epihippus* inherit that color. That color will be overwritten if another color is specified for a subsequent branch (and its subtree).

Priority (K) provides the ability to prioritize certain branches over others when on-screen diagrams become unwieldly large (see § Programming the Evolutionary tree display, Priority).

2.11   References

Alix, B., Boubacar, D.A., Vladimir, M., 2012. T-REX: a web server for inferring, validating and visualizing phylogenetic trees and networks. Nucleic Acids Research 40(W1), pp. W573-W579. https://doi.org/10.1093/nar/gks485.

Applied Maths, 2020. BioNumerics SEVEN: a unique software platform. Software for analysis of electrophoresis patterns, phenotype arrays, sequences and much more. http://www.applied-maths.com/bionumerics.

Aze, T., Ezard, T.H., Purvis, A., Coxall, H.K., Stewart, D.R., Wade, B.S., Pearson, P.N., 2011. A phylogeny of Cenozoic macroperforate planktonic foraminifera from fossil data. Biological Reviews 86(4), pp. 900-927. https::/doe.org/10.1111/j.1469-185X.2011.00178.x.

Bobick, R., Ogg, J.G., Salgado Jauregui, E., Santos Filho, M.A.B, Ault, A., and students of Purdue University, 2016. Earth history visualization system for Gondwana basins. 35th International Geological Congress (27 Aug – 4 Sept, 2016, Cape Town, South Africa) abstracts. American Geoscience Institute. https://www.americangeosciences.org/igc/16592, https://www.americangeosciences.org/sites/default/files/igc/5196.pdf.

Cazaux, B., Castel, G., Rivals, E., 2019. AQUAPONY: visualization and interpretation of phylogeographic information on phylogenetic trees. Bioinformatics 35(17), pp. 3163-3165. https://doi.org/10.1093/bioinformatics/btz011.

Chen, W.C., 2019. phyclust: Phylogenetic Clustering (Phyloclustering. Ames, IA, USA: Iowa State University. https://cran.r-project.org/web/packages/phyclust/.

Chevenet, F., Brun, C., Bañuls, A.L., Jacq, B., Christen, R., 2006. TreeDyn: towards dynamic graphics and annotations for analyses of trees. BMC Bioinformatics, 7, article #439. https://doi.org/10.1186/1471-2105-7-439.

Commission for the Geological Map of the World, 2012. Stratigraphic Chart: Paris [cited 2018, https://ccgm.org/en/27-stratigraphic-chart]. [color codes provided for various products, see also appendix in Gradstein et al., 2012].

Drummond, A.J., Rambaut, A., 2007. BEAST: Bayesian evolutionary analysis by sampling trees. BMC Evolutionary Biology, 7, article #214. https://doi.org/10.1186/1471-2148-7-214.

Fekete, J.D., 2004, October. The InfoVis toolkit. In IEEE Symposium on Information Visualization, Austin, TX167-174). https://ieeexplore.ieee.org/document/1382905.

Felsenstein, J., 2014. Phylogeny Programs, http://evolution.genetics.washington.edu/phylip/software.html; last update was 2014; Accessed 20 Feb 2020.

Felsenstein, J., 2019. PHYLIP (phylogeny inference package), version 3.698 c. Joseph Felsenstein. http://evolution.genetics.washington.edu/phylip.html; last update was 2014; Accessed 20 Feb 2020.

Fordham, B.G., Aze, T., Haller, C., Zehady, A.K., Pearson, P.N., Ogg, J.G., Wade, B.S., 2018. Future-proofing the Cenozoic macroperforate planktonic foraminifera phylogeny of Aze & others (2011). PLOS One, 13(10): e0204625. https://doi.org/10.1371/journal.pone.0204625.

Francisco, A.P., Vaz, C., Monteiro, P.T., Melo-Cristino, J., Ramirez, M., Carriço, J.A., 2012. PHYLOViZ: phylogenetic inference and data visualization for sequence based typing methods. BMC Bioinformatics, 13, article #87. https://doi.org/10.1186/1471-2105-13-87.

Gradstein, F.M, Ogg, J.G., Schmitz, M.D., Ogg, G.M. (coordinators), 2012. The Geologic Time Scale 2012. Elsevier, 2 volumes plus chart, pp. 1176. https://www.elsevier.com/books/the-geologic-time-scale-2012/gradstein/978-0-444-59425-9.

Gradstein, F.M, Ogg, J.G., Schmitz, M.D., Ogg, G.M. (coordinators), in press. The Geologic Time Scale 2020. Elsevier, pp. 1300. https://www.elsevier.com/books/geologic-time-scale-2020/gradstein/978-0-444-63798-7.

Gradstein, F.M., Ogg, J.G., 2006. Chronostratigraphic database and visualization; Cenozoic-Mesozoic-Paleozoic integrated stratigraphy and user-generated time scale graphics and charts. GeoArabia, 11(3), pp. 181-184. https://doi.org/10.6084/m9.figshare.11872155.

Guindon, S., Lethiec, F., Duroux, P., Gascuel, O., 2005. PHYML Online—a web server for fast maximum likelihood-based phylogenetic inference. Nucleic Acids Research, 33(suppl_2), pp. W557-W559. https://doi.org/10.1093/nar/gki352.

Hedges, S.B., Kumar, S., [Eds.], 2009. The TimeTree of Life. Oxford University Press, pp. 551. http://timetree.org/book.

Helaers, R., Milinkovitch, M.C., 2010. MetaPIGA v2. 0: maximum likelihood large phylogeny estimation using the metapopulation genetic algorithm and other stochastic heuristics. BMC Bioinformatics, 11, article #379. https://doi.org/10.1186/1471-2105-11-379.

Huelsenbeck, J.P., Ronquist, F., 2001. MRBAYES: Bayesian inference of phylogenetic trees. Bioinformatics, 17(8), pp. 754-755. https://doi.org/10.1093/bioinformatics/17.8.754.

Huerta-Cepas, J., Dopazo, J., Gabaldón, T., 2010. ETE: a python environment for tree exploration. BMC Bioinformatics, 11, article #24. https://doi.org/10.1186/1471-2105-11-24.

Huson, D.H., Richter, D.C., Rausch, C., Dezulian, T., Franz, M., Rupp, R., 2007. Dendroscope: An interactive viewer for large phylogenetic trees. BMC Bioinformatics, 8(1), article #460. https://doi.org/10.1186/1471-2105-8-460.

Johnson, B., 1992. TreeViz: treemap visualization of hierarchically structured information. In Proceedings of the SIGCHI Conference on Human Factors in Computing Systems, June 1992, pp. 369-370. https://doi.org/10.1145/142750.142833.

Kreft, L., Botzki, A., Coppens, F., Vandepoele, K., Van Bel, M., 2017. PhyD3: a phylogenetic tree viewer with extended phyloXML support for functional genomics data visualization. Bioinformatics, 33(18), pp. 2946-2947. https://doi.org/10.1093/bioinformatics/btx324.

Letunic, I., Bork, P., 2006. Interactive Tree Of Life (iTOL): an online tool for phylogenetic tree display and annotation. Bioinformatics, 23(1), pp. 127-128. https://doi.org/10.1093/bioinformatics/btl529.

Liu, L., Yu, L., 2010. Phybase: an R package for species tree analysis. Bioinformatics, 26(7), pp. 962-963. https://doi.org/10.1093/bioinformatics/btq062.

Ludwig, W., Strunk, O., Westram, R., et al. (32 authors), 2004. ARB: a software environment for sequence data. Nucleic Acids Research, 32(4), pp. 1363-1371. https://doi.org/10.1093/nar/gkh293.

Luo, T., 1993. TreeDraw: a tree-drawing system. Department of Computer Science, University of Western Ontario. TreeDraw: a tree-drawing system. [documentation at http://citeseerx.ist.psu.edu/viewdoc/summary?doi=10.1.1.39.7837].

Maddison, W.P., Maddison, D.R., 1989. Interactive analysis of phylogeny and character evolution using the computer program MacClade. Folia Primatologica, 53(1-4), pp. 190-202.

Maddison, W.P., Maddison, D.R., 2018. Mesquite: A modular system for evolutionary analysis. Current release 3.61. http://www.mesquiteproject.org.

Meade, A., Pagel, M., 2019. BayesTraits v3.0.2. Computer program and documentation. 1-81. http://www.evolution.rdg.ac.uk/BayesTraitsV3.0.2/BayesTraitsV3.0.2.html http://www.evolution.rdg.ac.uk/BayesTraitsV3.0.2/Files/BayesTraitsV3.0.2Manual.pdf.

Milne, I., Lindner, D., Bayer, M., Husmeier, D., McGuire, G., Marshall, D.F. and Wright, F., 2009. TOPALi v2: a rich graphical interface for evolutionary analyses of multiple alignments on HPC clusters and multi-core desktops. Bioinformatics, 25(1), pp. 126-127. https://doi.org/10.1093/bioinformatics/btn575.

Ogg, J., Lugowski, A., Gradstein, F., 2010. Earth History databases and visualization – the TimeScale Creator system. In: EGU General Assembly Conference Abstracts (2-7 May 2010, Vienna). Available at https://ui.adsabs.harvard.edu/abs/2010EGUGA.12.7039O/abstract.

Ogg, J., Przybylski, P., 2009. Jurassic chronostratigraphic database and the *TimeScale Creator* visualization system. Volumina Jurassica, 7, pp. 175-179. https://vjs.pgi.gov.pl/article/view/26548/18252.

Ogg, J.G., Ogg, G.M., Gradstein, F.M., 2016. Concise Geologic Time Scale 2016. Elsevier Publ., 234 pages. https://doi.org/10.1016/c2009-0-64442-1.

Okonechnikov, K., Golosova, O., Fursov, M. the UGENE team, 2012. Unipro UGENE: a unified bioinformatics toolkit. Bioinformatics, 28(8), pp. 1166-1167.

Page, R.D., 1996. Tree View: An application to display phylogenetic trees on personal computers. Bioinformatics, 12(4), pp. 357-358. https://doi.org/10.1093/bioinformatics/12.4.357.

Paradis, E., Claude, J., Strimmer, K., 2004. APE: Analyses of phylogenetics and evolution in R language. Bioinformatics, 20(2), pp. 289-290.

Revell, L.J., 2012. phytools: an R package for phylogenetic comparative biology (and other things). Methods in Ecology and Evolution, 3(2), pp. 217-223. https://doi.org/10.1111/j.2041-210X.2011.00169.x.

Revell, L.J., Chamberlain, S.A., 2014. Rphylip: an R interface for PHYLIP. Methods in Ecology and Evolution, 5(9), pp. 976-981. https://doi.org/10.1111/2041-210x.12233.

Robinson, O., Dylus, D., Dessimoz, C., 2016. Phylo.io: Interactive viewing and comparison of large phylogenetic trees on the web. Molecular Biology and Evolution, 33(8), pp. 2163-2166. https://doi.org/10.1093/molbev/msw080.

Santamaría, R., Therón, R., 2009. Treevolution: visual analysis of phylogenetic trees. Bioinformatics, 25(15), pp. 1970-1971. https://doi.org/10.1093/bioinformatics/btp333.

Schliep, K.P., 2010. phangorn: phylogenetic analysis in R. Bioinformatics, 27(4), pp. 592-593. https://doi.org/10.1093/bioinformatics/btq706.

Shank, S.D., Weaver, S., Koskovsky Pond, S.L., 2018. phylotree.js - a JavaScript library for application development and interactive data visualization in phylogenetics. BMC Bioinformatics, 19, article #276. https://doi.org/10.1186/s12859-018-2283-2.

Smith, T., Ogg, J.G., Kelman, A., Abbott, S., Bernecker, T., 2015. Toward updated stratigraphic frameworks for Australia's offshore hydrocarbon provinces. The Australian Petroleum Production & Exploration (APPEA) Journal, 55(1), pp. 105-111. https://doi.org/10.1071/AJ14008.

Smits, S.A., Ouverney, C.C., 2010. jsPhyloSVG: A javascript library for visualizing interactive and vector-based phylogenetic trees on the web. PloS one, 5(8), e12267. https://doi.org/10.1371/journal.pone.0012267.

Stöver, B.C., Müller, K.F., 2010. TreeGraph 2: Combining and visualizing evidence from different phylogenetic analyses. BMC Bioinformatics, 11(1), article #7. https://doi.org/10.1186/1471-2105-11-7.

Suchard, M.A., Redelings, B.D., 2006. BAli-Phy: simultaneous Bayesian inference of alignment and phylogeny. Bioinformatics, 22(16), pp. 2047-2048. https://doi.org/10.1093/bioinformatics/btl175.

Swofford, D.L., 2017. Paup* (Phylogenetic analysis using PAUP). http://paup.phylosolutions.com.

Thompson, J.D., Higgins, D.G., Gibson, T.J., 1994. CLUSTAL W: Improving the sensitivity of progressive multiple sequence alignment through sequence weighting, position-specific gap penalties and weight matrix choice. Nucleic Acids Research, 22(22), pp. 4673-4680. https://doi.org/10.1093/nar/22.22.4673.

Vaughan, T.G., 2017. IcyTree: rapid browser-based visualization for phylogenetic trees and networks. Bioinformatics, 33(15), pp. 2392-2394. https://doi.org/10.1093/bioinformatics/btx155.

Wilson, I.J., Weale, M.E., Balding, D.J., 2003. Inferences from DNA data: population histories, evolutionary processes and forensic match probabilities. Journal of the Royal Statistical Society: Series A (Statistics in Society), 166(2), pp. 155-188. https://doi.org/10.1111/1467-985X.00264.

Yang, Z.H., 1997. PAML: a program package for phylogenetic analysis by maximum likelihood. Bioinformatics, 13(5), 555-556.

Yu, G.C., Smith, D.K., Zhu, H.C., Guan, Y., Lam, T.T.Y., 2017. GGTREE: an R package for visualization and annotation of phylogenetic trees with their covariates and other associated data. Methods in Ecology and Evolution, 8(1), pp. 28-36. https://doi.org/10.1111/2041-210X.12628.

Zhang, H.K., Gao, S.H., Lercher, M.J., Hu, S.N., Chen, W.H., 2012. EvolView, an online tool for visualizing, annotating and managing phylogenetic trees. Nucleic Acids Research, 40(W1), pp. W569-W572. https://doi.org/10.1093/nar/gks576

CHAPTER 3.   INTEGRATED SPECIES–PHENON TREES: VISUALIZING INFRASPECIFIC DIVERSITY WITHIN LINEAGES

Abstract

The unprecedented detail with which contemporary molecular phylogenetics are visualizing infraspecific relationships within living species and species complexes cannot as yet be reliably extended into deep time. Yet paleontological systematics has routinely dealt in (mainly) morphotaxa envisaged in various ways to have been components of past species lineages. Bridging these perspectives can only enrich both. Our integrated species–phenon tree merges ancestor–descendant proposals for fossil morphotaxa (phena) with reconstructed phylogenies of lineages (species), to digitally visualize infraspecific diversity within species through deep time. Aze & others' important macroevolutionary dataset provides a case example to encourage mutual learnings between paleontological and molecular approaches

3.1   Introduction

Recent advances in molecular systematics are not only building a tree of life but are also allowing the evolutionary structure within a species to be investigated more finely than ever. It is now quite commonplace for species to be revealed as a rich array of clades at multiple taxonomic levels, of difficult-to-assign infraspecific groupings, of cryptic or pseudocryptic species, or of variously fragmented haplotype-phylogeographic populations (follow-up statements in later sections will provide references).

Less well known is that in paleontology an analogous morphotaxonomic granularity within species lineages, long expressed as formal or informal infraspecific morphotypes and the like, is now being portrayed phylogenetically and on a large taxonomic scale — at least in one fossil group. This group is the Cenozoic macroperforate planktonic foraminifera: Aze, T. et al., 2011 have proposed for it a species-lineage evolutionary tree comprising 210 lineages, each explicitly incorporating (usually multiple) component morphotaxa.

The macroevolutionary properties of Aze & others' lineage phylogeny have attracted considerable interest (e.g. Etienne, R. S. et al., 2012). However, this is not so when it comes to the phylogeny's microevolutionary ramifications, which in fact do include a granularity within their

species lineages implied by the morphotaxa. We contend that this microevolutionary aspect of Aze & others' phylogeny also deserves attention by evolutionary researchers, especially as most of those species lineages which have survived to the present have now been subjected to molecular analyses, placing planktonic foraminifera in quite a unique position to compare in detail infraspecific diversity from both living and fossil perspectives.

One could nominate important reasons why the focus on Aze & others' phylogeny has been macro- rather than micro-evolutionary. However, we suggest that there has also been a merely practical hindrance to looking into the content within these lineages — Aze & others' visuals were simply too complicated to employ for this purpose. This is because they provided the morphotaxonomic content for their species lineages indirectly via a separate evolutionary tree for their morphotaxa, and because the internal timing and the topology of both lineage and morphotaxic trees do not match (deliberately so, but more on that later). So, for the reader to appreciate that content, considerable dexterity is required when comparing corresponding parts of each tree: visual dexterity for their tree figures, arithmetic dexterity for their spreadsheet listings (which date and decode their lineages with regard to morphotaxa).

Given the special research potential provided by planktonic foraminifera, we seek to remedy the brain teaser presented by the trees of Aze & others by providing a visualization tool which combines both into a single graphic. In fact, as we will demonstrate, not only does the new integrated tree capture all relevant aspects of each component tree, its additional visual aids delineate when and from where morphological changes are implied to arise both within the species lineage and across proposed speciation events. So it encourages a critical appraisal of the dynamics of morphological evolution in relation to speciation (cladogenesis) and lineage continuity (anagenesis).

Below, we briefly introduce the case study of Aze & others (2011) and we explain why their terminology needs to be adjusted for our tool to bridge both paleontological and living research practices in planktonic foraminifera. We then show that the tool is needed in order to merge two trees (of species lineages and of phena) that are decoupled from each other. In Results section, the tool is introduced and applied to the case study, followed by a discussion highlighting mutual learnings it can help broker between paleontological and living research perspectives, as well as other potential applications. § Methods deals with the programming behind the tool and its

challenges. But firstly, below we seek to briefly contextualize where visualization within species is at.

3.2 Visualizing infraspecific relationships

Graphically depicting evolutionary relationships within species—and specifically between entities or taxa below the species level — has been on the agenda even since Darwin. Darwin did so with his tree-like diagram in the Origin of Species (Darwin, C., 1859) (between pp. 116 and 117) where he envisaged lineal continuity between forms, varieties, subspecies, and species (Bouzat, J. L., 2014). However, in our contemporary evolutionary lexicon of species as metapopulation lineages (de Queiroz, K., 2005), one might presume much of infraspecific usage to be outdated, and so visualizing them to be largely superfluous. That is, until you look a little further. Depictions of varieties and subspecies, for instance, are not hard to find within state-of-the-art taxonomic studies drawn from across the organic world — be they about pathogenic bacteria (Gulla, S., Lund et al., 2016), reed grasses (Hardion, L. et al., 2017), endangered crayfish (Bernini, G. et al., 2016), or titi monkeys (Serrano-Villavicencio, J. E. et al., 2017). One could in fact get the impression that even the phenon has an assured place in current molecular microbial studies (Fujimoto, T. et al., 2018).

A key incentive in recent times to visualize relationships within species has been the discrimination increasingly afforded by molecular systematics. Earlier, in both established systematic traditions as well as initial molecular-systematic studies, the focus was and continues to be on superspecific relationships: from specialist research within, say, a family to collaborative ventures aimed at the tree of life. For this context, species are inputs to the study (as such, or as representatives of higher taxa) and their validity is a given. However, the subsequent blossoming of molecular-phylogenetic studies has for the first time allowed in-depth examination of evolution from the gene up. A key component of this research centres around and below the species, with much of the focus in case studies now reframed as the "species complex" (Belfiore, N. M. et al., 2008; Weir, B.S. et al., 2012; Barrett, R.A. et al., 2015; Wen, D. et al., 2016; Sota, T. et al., 2016; Han, T., Lee et al., 2016; Bogarín, D. et al., 2018; Mizuyama, M. et al., 2018; Cuezzo, M. G. et al., 2018). And exciting challenges now involve rethinking of once-given species, including their

genetic discrimination (Luo, A. et al., 2018) as well as delineation of their putative evolutionary components.

In this contemporary research environment, a variety of approaches to recognizing and visualizing evolutionary entities around and within the species are being tried. Often, gene trees for species complexes or, say, closely related genera are fully subdivided into clades recognized as species — though the choice and extent of clades is usually manual and pragmatic, influenced by prior systematics (Weir, B. S. et al., 2012), and the genetic complexity within and among prior species may raise the level needed to recognize reliable groupings to, say, nominal subgenera (Belfiore, N. M. et al., 2008). In other cases, for example: molecular support for prior species may prove poor (Barrett, R. A. et al., 2015); geographic variants may cut across prior species (Sota, T. et al., 2016); or a formal–informal hierarchy of genera, infrageneric clades, species, and unlabeled infraspecific groupings may be viable for most prior species, but there may also be a desiderata of cryptic and pseudocryptic species and species with ambiguous genetic distances (Han, T. et al., 2016). For the geographic–genetic differentiation of populations within species or species complexes gained from haplotype phylogeography, mitochondrial-DNA trees are often complemented by annotated networks and ordination of haplogroups (Gaubert, P., 2005; Charruau, P. et al., 2011; Lancaster, M. L. et al., 2010; Emami-Khoyi, A. et al., 2016). Given the many considerations needed to evaluate gene trees, enhanced visualization approaches have been developed, including embedded display of database information, gene sequences, and phylogeographic maps (Allende, C. et al., 2015; Benavente, E. D. et al., 2015).

Another layer of interpretative and visualization complexity comes from addressing incongruence between gene and species trees arising from incomplete lineage sorting (deep coalescence), horizontal gene transfer, or gene duplication or loss/extinction events (Nei, M., 1987; Doyle, J. J., 1992; Maddison, W. P., 1997). This applies in particular to very recent speciations or, more generally throughout deep time, when successive speciations are rapid relative to effective population sizes (Avise, J. C. & Robinson, T. J., 2008). So this is especially pertinent for visualizing genetic dynamics within the species, particularly when associated with speciation, potential or eventual. Computational inference of species trees from gene trees (Goodman, M. et al., 1979) can now employ a rapidly growing array of methods (Szöllősi, G. J. et al., 2014). When applied to multigene studies, the challenge of visualizing many gene trees (Belfiore, N. M. et al., 2008; Bogarín, D. et al., 2018) may be best guided by the image of a "cloudigram" (Maddison, W.

P., 1997) rather than simple lineal trees and, apart from networks and ordination (Wen, D., 2016), visualizations such as rotatable three-dimensional trees (Kim, N., 2007) and tanglegrams (Scornavacca, C., 2011) become relevant.

Despite the sophistication which molecular phylogenetics can now bring to differentiation within the species, translating that into phylogenies against deep time has almost always been confined to a simple, and so usually simplistic, projection employing fossil or paleogeographic evidence to date and calibrate selected nodes (Singh, S. P. et al., 2017; Hofmeyr, M. D. et al., 2017). So the deep-time history of the molecularly detected infraspecific entities remains largely illusory. Studies which do attempt to detail this history — on groups considered to have an instructive fossil record (Hills, S. F. K. et al., 2012; Vitek, N. S., 2018) — will usually need to raise their taxonomic focus for deep time to that of the encompassing species or species groups, providing only a qualitative context to their enhanced depiction of living infraspecific diversity.

3.2.1   The opportunity now afforded by planktonic foraminifera

A taxonomic area which does offer hope for detailing evolution of molecularly or otherwise delineated entities within species through deep time is that of microfossils (Armstrong, H. A. & Brasier, M. D., 2005). These phylogenetically diverse groups are united by typically highly rich fossil records from which abundant assemblages can be recovered from tiny samples. Where their fossilisable microscopic parts appear to preserve evolutionary change along stratigraphic sequences, biostratigraphers have typically captured those changes taxonomically, often using a variety of infraspecific labels, formal or informal (Knappertsbusch, M., 2007). So for those microfossil groups that include living representatives, contemporary molecular studies are now providing the potential to compare living infraspecific diversity with that implied through deep time.

A notable example of this opportunity is given by foraminifera, especially the fifty or so living species that are planktonic (Schiebel, R. & Hemleben, C., 2017). A growing body of molecular studies on planktonic foraminifera are not merely applying stratigraphic evidence to calibrate their genetic trees against geologic time, but are explicitly exploring a deep-time context for their molecularly detected infraspecific entities (Huber, B. T. et al., 2017; de Vargas, C. & Pawlowski, J., 1998; Darling, K. F. et al., 1999; de Vargas, C. et al., 2001; de Vargas, C. et al.,

2002; Darling, K. F. et al., 2004; Sexton, P. F. & Norris, R. D., 2008; Aurahs, R. et al., 2011; Weiner, A. K. M. et al., 2014; Weiner, A. K. M. et al., 2015; Ujiié, Y. & Ishitani, Y., 2016). And added to this, their biostratigrapher colleagues have quite recently provided a key macroevolutionary framework for infraspecific diversity through the Cenozoic. For the largest living group of planktonic foraminifera, the macroperforates, Aze & others (Aze, T. et al., 2011) have proposed phylogenies not just of the usual biostratigraphic taxa but also one which integrates these taxa within whole-species paleobiological lineages, and so depicting deep-time polytypic species directly comparable to living species.

It is Aze & others' conceptualization which we consider adds an exciting input into the interchange between living and fossil research, and which forms the case study for our visualization tool. But before introducing the tool, we need to explain why we have avoided their term, morphospecies, and then explain why the tool is needed.

3.2.2 Avoiding "morphospecies"

As already alluded to, Aze & others1 presented two parallel evolutionary trees for Cenozoic macroperforate planktonic foraminifera: one of biostratigraphic taxa, traditional for micropaleontology, accorded Genus species binomina, and termed morphospecies; and another of newly introduced biological-species lineages constructed of mostly multiple morphospecies and given codes. These morphospecies are not chronospecies, they do not subdivide lineages into temporal chunks but rather into segments in morphological space (see p. 195, Text-Figure 2 in Pearson, P. N., 1993; pp. 903–905, Figure 1b in Aze, T. et al., 2011; pp. 6–7 in Fordham, B. G. et al., 2018). Despite the pragmatic role that this kind of morphospecies plays in paleontology, in the context of informing and interacting with research into living planktonic foraminifera and its conventions, this usage of "morphospecies" becomes problematic, as seen in the following example.

Aze & others portrayed the later phylogeny of the well-studied living Truncorotalia (or Globorotalia) truncatulinoides as two successive Pliocene–Quaternary lineages comprising six morphospecies (Figure 3.1a,b; Lineages N62-T63 and N64-T66; morphospecies series beginning with T. tenuitheca). As a result, the living T. truncatulinoides comprised one lineage but three morphospecies, T. truncatulinoides, T. excelsa, and T. pachytheca. On the other hand, molecular

researchers (de Vargas, C. & Pawlowski, J., 1998; de Vargas, C. et al., 2001; de Vargas, C. et al., 1997; Darling, K. F. & Wade, C. M., 2008; Ujiie, Y. & Lipps, J. H., 2009; Ujiie, Y. et al., 2010; Quillévéré, F. et al., 2013) have consistently considered living T./G. truncatulinoides a single "morphological species". This characterization references an earlier taxonomic tradition which actually included most micro paleontologists whereby only one nominal species, T./G. truncatulinoides, was recognized for the entire Quaternary lineage (and so also for the present day), whether infraspecific taxa were also delineated (Blow, W. H., 1969; Sprovieri, A. et al., 1980; Bolli, H. M. & Saunders, J. B., 1985; Fordham, B. G., 1986; Stewart, D. R. M., 2003) or not (Saito, T., Breger, D. & Thompson, P. R., 1981; Kennett, J. P. & Srinivasan, M. S., 1983; Cifelli, R. & Scott, G. H., 1986; Lazarus, D. et al., 1995; Chaisson, W. P. & Pearson, P. N., 1997).

This disjunct between the terminology of Aze & others and molecular researchers has been further underlined by the latter's practice of using "morphospecies" as a shorthand for their "morphological species". So, in current parlance, the living *T./G. truncatulinoides* contains three morphospecies in one part of the literature but one morphospecies in another. It is somewhat ironical then that the above-quoted molecular research on *T./G. truncatulinoides* has delineated five genotypes, possibly indicative of two genetic lineages, one with four putative species (Figure 4.1c). And, though the relationship between these genotypes and the three morphospecies recognized by Aze & others is apparently yet to be addressed, the potential for a coming together of paleontological and molecular concepts for a one-to-one genotype–morphospecies correspondence for these taxa appears poor. Rather, the apparently exclusively subtropical extent (Caribbean, Mediterranean and Canary Islands, west Pacific) (Blow, W. H., 1969; Sprovieri, A., Ruggieri, G. & Untl, M., 1980) of the two ancillary morphospecies, *T. excelsa* and *T. pachytheca*, suggests both might be subsumed within only a single genotype which would also include the nominate *T. truncatulinoides* (see the distribution of genotype Type II in Figure 7 of Darling, K. F. & Wade, C. M., 2008). So, without much more investigation, these three paleontological morphospecies seem unlikely to contribute much to a deep-time context for the five genotypes.

Figure 3.1 Paleontological and molecular approaches to infraspecific terminology: planktonic foraminifer *Globorotalia*/*Truncorotalia truncatulinoides*. (**a,b**) A paleontological approach. Portions (after Figure 5E of Aze, T. et al., 2011) of trees of morphospecies [evolutionarily overlapping morphotaxa] (**a**) and lineages [paleobiological species] (**b**): living Lineage N64-T66 (**T. truncatulinoides* in b) includes three living morphospecies (in a), *Truncorotalia truncatulinoides*, *T. excelsa*, and *T. pachytheca* (*T. cavernula* originated in this lineage, but budded into its own living Lineage T65); for comparison with the outgroup in (**c**), these portions of the trees embrace living Lineage N48-T50 (**H. hirsuta* in **b**) which includes living morphospecies *Hirsutella hirsuta*; arrows indicate still living. (**c**) A molecular approach. Consensus molecular tree for the morphospecies [cryptic-species complex] *Globorotalia truncatulinoides*, using morphospecies *G. hirsuta* as the outgroup (after Figure 4b of Ujiie, Y. & Lipps, J. H., 2009): two major clades 1 ("1 = I ~ IV") and 2 ("2 = V") comprising five genotypes [cryptic species] I – IV and V, respectively. Note: *Globorotalia* versus *Truncorotalia*, *Hirsutella*, etc., are alternative nominal genera, the former preferred for molecular workers' broader less-settled sweep across living species, the latter for those paleontologists keen to emphasize temporally deep but taxonomically confined lines of descent.

Examples other than *T.*/*G. truncatulinoides* would point to similar problems with the "morphospecies" but for different reasons. This is because in molecular studies of living planktonic foraminifera the relationship between the nominal species, usually labeled "morphospecies", and genetic species is a complicated one(Darling, K. F. & Wade, C. M., 2008;

Morard, R. et al., 2016): about half of the nominal species analyzed each have a one-to-one relationship between nominal and genetic species (though high genetic diversity can nonetheless occur at low genetic levels, as in *Pulleniatina obliquiloculata* in Morard, R. et al., 2016); in another half of the nominal species, each contain multiple genotypes suggestive of multiple putative species or, in fact, genetic lineages; the reverse situation of multiple nominal species containing a single genotype is rarer but represented by *Trilobatus*, (Figure 3 in Morard, R. et al., 2016) apart from the somewhat contrived case of *T./G. truncatulinoides*; and finally in some cases a nominal–genetic hierarchy (in either direction) may break down because multiple nominal species are phylogenetically interwoven between multiple genotypes (as in *Globigerinella* and *Globigerinoides ruber* sensu lato in Morard, R. et al., 2016).

This discussion suffices to demonstrate the ambiguity and ineffectiveness of "morphospecies" as a term applied to planktonic foraminifera when wanting to integrate current living and paleontological research. Seeking an alternative taxonomic category, the only other option in zoology would be the subspecies, but it would suffer analogous inconsistencies, especially given its important conceptual role in evolutionary practice. So, in applying the case study of Aze & others to our visualization tool, we have retreated to informal practice and replaced Aze & others' "morphospecies" with Mayr's use of phena (Mayr, E., 1969; Mayr, E., 1982), as applied previously to biostratigraphic taxa in planktonic foraminifer (Fordham, B. G., 1986) , more generally (Smith, A. B. , 1994; Wurst, E. & Frank, B., 1998), and of course to prokaryotes (Wieland, B. et al., 2006). This informal paleontological taxonomy then mirrors the emerging informal, though rules-based, system of molecular nomenclature intended to parallel and link to formal nomenclature for planktonic foraminifera and other organisms (Morard, R. et al., 2016). And for Aze & others' other tree, we simply refer to their biological-species lineages as species. Overall, these two adjustments to the terminology employed by Aze & others allow us to avoid the very confusing "morphospecies" but otherwise run with the emerging language of molecular research, and comfortably discuss species in an uncontroversial and broadly applicable way.

3.2.3   Why our visualization tool is needed

The above-discussed developments in the study of planktonic foraminifera, from both the living and fossil research communities, can provide a much clearer rationale for extending the

living infraspecific diversity of planktonic foraminifera into deep time. There is, however, a practical issue in applying Aze & others' phylogenies to this purpose. Their separate trees of species (biological-species lineages) and phena (biostratigraphic "morphospecies") have topologies which do not correspond in a straightforward way. This is because the timing they interpreted for the emergence of species in deep time, though influenced by the stratigraphic ranges of related phena, was based on different evidence — the tracing of morphological clusters of collections of specimens (not taxa, formal or informal) along stratigraphic sequences (p. 195, Text-fig 3 in Pearson, P. N., 1993; Fig 2 in Aze, T. et al., 2011; § Ancestor–descendant relationships in Fordham, B. G. et al., 2018). This methodology disarticulates the origins of species from those of phena, and so allows phenon ranges to pass unbroken from an ancestral species to one of its descendant species (see morphospecies m3 in Figure 1b of Aze, T. et al., 2011; note also in Figure 3.1a, b herein that, for instance, phenon T. truncatulinoides appears in the uppermost Pliocene so, when Lineage N64-T66 buds of from its ancestral Lineage N62-T63 in the early Quaternary, that phenon would carry over from its membership of the latter to that of the former). This breakdown in the simple species–phenon hierarchy also underlines the inappropriateness of employing, for example, nominal subspecies for these biostratigraphic taxa.

Making sense of these biostratigraphers' out-of-synch evolutionary trees of species and phena turns out to be a visual brain-teaser. In this paper our visualization tool provides a graphical solution to this. Our integrated species–phenon tree takes the species tree and widens each species range line into a "species box" within which is displayed that species' algorithmically determined portion of the tree of phena. Within a species box, symbols attached to the range lines of the phenon tree provide guides to both the origins of the phenon phylogeny from ancestral species and its continuance into descendant species. And all this is accomplished programmatically from a single extra data link between the two trees' datasets.

We now describe the integrated species–phenon tree, apply it to this case example of Cenozoic macroperforate planktonic foraminifera, and then suggest how these trees might enhance broader research into infraspecific diversity, especially that which we seek to detail through deep time.

3.3 Results

3.3.1 The software tool

Our integrated species–phenon tree, part of the *TimeScale Creator* software package (§ Methods), is a species tree drawn as an SVG chart against geologic time but with the species expanded into boxes in which is projected an underlying infraspecific (phenon) tree (Figure 3.2i). Those infraspecifics could be taxa (subspecies, botanical varieties or forms, prokaryotic infrasubspecifics, etc.) or other entities of interest (molecular OTUs, gene sequences/loci, biostratigraphic taxa, etc.).

The key incentive for a software tool to bring together both species and phenon trees is that, though the trees refer to the same organisms, they have different topologies, in terms of both the nature and number of entities recognized and the timing of their evolution. Even in our simple improvised example of just a few taxa (Figure 4.2i), observing which species (column b of Figure 4.2i) contain which parts of the phenon tree (column a) is not easy. So our tool does that for you (column c). It also provides range guides (Figure 4.2ii) to better appreciate the context of the now broken-up parts of the phenon tree; these make clear the full durations of phena and easily distinguish these from transfers of the phena between species. So now the integrated tree can provide not only all the information contained in the individual species and phenon trees, but also enhance understanding of the morphologic/genetic/etc. variability within species, as well as the timing of evolutionary change within and between species, including what morphological change taxa capture within and across speciation events. In so doing it encourages an examination of the dynamics of morphological evolution in relation to speciation (cladogenesis) and lineage continuity (anagenesis).
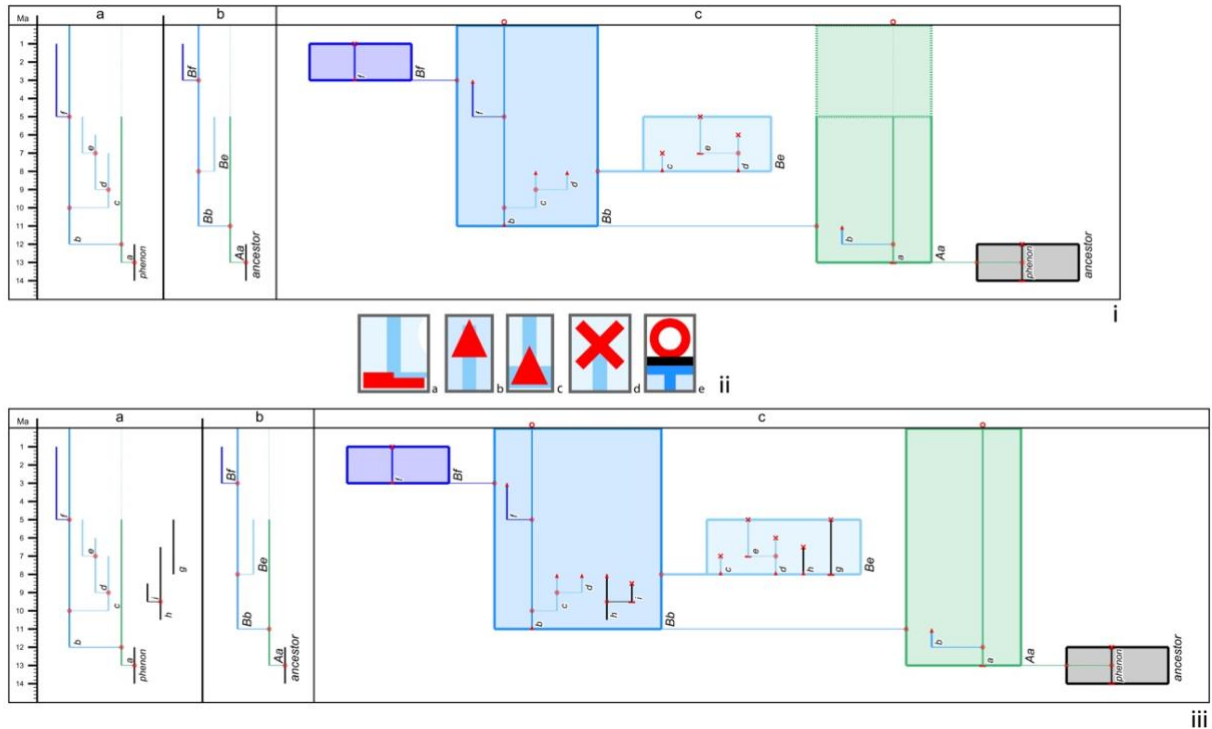
Figure 3.2 Sample derivation of an integrated species–phenon tree. (i) Improvised example of evolutionary trees against geologic time scale (Ma), depicting a "black" ancestor giving rise to a "green" descendant, in turn to a "blue" group ("medium blue", ancestral to "light blue" and "dark blue" descendants); all range lines effected in the same line style ("frequent"), except for the upper/later portion of phenon a and species Aa ("conjectured"; for TimeScale Creator line styles, see pp. 48–49 of Ogg, J. G. & Ogg, G. M., 2019); drawn by TimeScale Creator datapacks (§ Data availability). Column a = phenon tree. Column b = species tree. Column c = integrated species–phenon tree. (ii) Enlarged view of guide symbols attached to phenon range lines in column c to provide stratigraphic or phylogenetic context, including their parts broken between species boxes: (a) range origin; (b) top of broken part of range, to transfer to the next descendant species box; (c) bottom of broken part of range, to transfer from the immediate ancestral species box; (d) range extinction; (e) still living. (iii) Incorporation of disconnected phenon trees and ranges (see § Methods); evolutionary-tree series of (i), with added phenon range and phenon tree in black. Column a: the original coloured phenon tree, additional phenon tree (h–i), and additional phenon range (g), all displayed in the same column, from left to right in order of First Occurrence (the default option). Column b: as in (i); the additional black phena, (g–i), from column a have been assigned to the Bb–Be lineage series, but their ancestor–descendant relationships with the original coloured phena are considered poorly known. Column c: integrated species–phenon tree, with the disconnected phenon tree (h–i) and range (g) positioned in their corresponding species boxes.

64

3.4   Case example

The practical viability of our tool finds a ready check in Aze & others' (Aze, T. et al., 2011) jointly published species and phenon trees for Cenozoic macroperforate planktonic foraminifera, especially apposite as they were recently transferred onto the *TimeScale Creator* platform (Fordham, B.G. et al., 2018). As already alluded to above (§ Avoiding "morphospecies"), their trees constitute a major dataset of large and complex trees comprising 210 species (their biological-species lineages) and 339 phena (their "morphospecies") over a time interval of 66 Myr. To systematically recognize, let alone name, species lineages is unusual in micropaleontology; Aze & others introduced codes for their lineages, e.g., N133-T135, by concatenating numerical codes given to their included lineage-tree leaves, prefixed with N if internodal, T if terminal. Their "morphospecies", given as *Genus species* binomina, followed a convention in their field to employ distinctive, especially biostratigraphically useful, morphologies as formal taxa. Moves are underway to revise the trees of Aze & others to incorporate the recently published major changes to Oligocene taxonomy and phylogeny[76] and analogous but longer-term updates expected from a fledgling Neogene Planktonic Foraminifera Working Group.

Within Aze & others' trees the rate and content of macroevolutionary change in terms of species and infraspecific taxa is highly variable (Figure 7 in Fordham et al., 2018). The relationship between species and phenon trees, constructed stratophenetically (Figure 2 in Aze et al., 2011), is similarly variable: for example, though origins for about 40% of the species lineages coincide with one of their contained phena (see "morphospecies" in pdf p. 18 in Fordham, B. G. et al., 2018), many phena originate within species lineages and a substantial number cross from ancestral to descendant lineages. So envisaging, for example, the phenon content of species lineages from the trees figured in the original paper is just too difficult for the average observer (compare in Allende et al., 2015 the top and bottom parts of Figures 5, 5A–5J, or the separately drawn "morphospecies" and lineage trees in Appendices S2 and S3). And this visual challenge is only partially alleviated by enhanced displays (§ Linkages between morphospecies and lineage trees in Fordham et al., 2018) introduced to assist with this.

Applying the new integrated species–phenon tree to bring these trees together results in an even wider tree (Figure 3.3c); nonetheless the new chart still draws quickly, a testament to the scalability built into the Java code of *TimeScale Creator* software (Ogg & Gradstein, 2006). Closer inspection demonstrates that the phenon range lines (Figure 3.3a, inset) have indeed separated at

species lineage origins (Figure 3.3b, inset) to transform into their respective species boxes (Figure 3.3c, inset). The much easier access to species–phenon relationships afforded by the integrated tree is underlined by comparison of these species boxes with our earlier attempt (Figure 7f in Fordham et al., 2018) at a similar effect by manually overlaying lineage outlines onto the phenon ("morphospecies") tree. The integrated tree also features range guides (Figure 3.3d; legend in Figure 3.3ii) to help the viewer appreciate the stratigraphic and phylogenetic context for any phenon range, and especially to follow the trajectory of those that cross species boxes (note the phenon highlighted). In addition, as already stated, the integrated tree brings with it all the information from the individual species and phenon trees. Viewed interactively on the *TimeScale Creator* platform, this includes the mouse-over pop-ups which, in this case example, include a wealth of taxonomic, morphologic, ecologic, and biostratigraphic detail from the back-end database (including the lineage–morphospecies linkages already mentioned) (Fordham et al., 2018).

Figure 3.3 Derivation of an integrated species–phenon tree for the case study of Cenozoic macroperforate planktonic foraminifera (Aze, T. et al., 2011) . Evolutionary-tree charts drawn by *TimeScale Creator* datapacks, (**a–c**) against entire Cenozoic time scale (the last 66 Myr), with insets of a Ypresian–Bartonian (Eocene) clade which begins with a phenon (morphospecies *Acarinina pseudotopilensis*, **a**), or with its corresponding species (Lineage N130-N131-N136-N142-N144-T148*, **b,c**); clade shown within Figure 5C of Aze, T. et al., 2011 and Figures 7f and 20 of Fordham et al., 2018; tree colours and groupings by morphogroup; background coloured by stages ("Chronostrat" option). (**a,b**) Entire phenon (morphospecies) and species (lineage) trees Fordham et al., 2018, respectively, each with inset (below). (**c**) Entire integrated species–phenon tree, with inset (above); this tree introduced herein (§ Data availability); images (Haller & Ogg, 2013) for morphospecies added as heuristics to help appreciate the break-up of the phenon tree within the species tree, but these images are not authoritative. (**d**) Detail (upper right) from inset of (**c**); red range guides on phenon range lines as in Figure 3.2ii; time interval is late Ypresian–Bartonian (Eocene). Note the breaking graphically of the range line of the highlighted phenon (morphospecies *Acarinina bullbrooki*) between the ancestral species box (Lineage N130-N131-N136-N142-N144-T148, far left) and its descendant species box (Lineage N133-T135, far right). *With regard to species-lineage labels in (**c,d**), note that, in order to make it easier to follow the lineage codes of Aze & others, as part of the transfer to *TimeScale Creator* (Fordham et al., 2018) these labels were programmatically appended with a list of included phena. This label then becomes "N130-N131-N136-N142-N144-T148: A. pseudotopilensis > A. quetra > A. boudreauxi > A. mcgowrani > A. bullbrooki > A. praetopilensis > M. bandyi > M. crassatus > M. coronatus > A. topilensis > A. rohri": this lineage happens to be one of their more inclusive!

3.5 Discussion

We have already alluded to the many approaches to visualizing infraspecific content of species through time, so our integrated species–phenon tree has a rich heritage. It could, for instance, be traced back to the then newly enthused evolutionary paleontologists of the late nineteenth century (Archibald, J.D., 2014). More specifically, our formulation was anticipated by predigital species–phenon boxes employed to document stratigraphic distributions (Figure 3.4b) within the context of a species tree (Figure 3.4a). Also, within the context of documenting infraspecific content, there is the "phenon group", an informal category uniting homologous phena in multielement fossils (Fordham, B. G., 1991; Fordham, B. G., 1995). Interestingly, if trees of phenon groups were constructed, given that both descendants at speciation would often retain the same phena for some phenon groups, the relationship of phenon-group trees with their species trees should bear similarities to relationships between gene trees and their species trees — bringing us back to some topics we raised above.

Coming forward to contemporary research related to our case example of planktonic foraminifera, parallels can be made, especially with regard to living representatives, between the perspective the integrated tree brings and that coming from molecular studies. For instance, the integrated tree explicitly visualizes species as dynamically evolving polytypic lineages, presenting them in terms of a two-level species–phenon hierarchy (Figure 4.5a). Meanwhile, some molecular studies are not only genetically circumscribing nominal species and separating out misunderstood cryptic look-a-likes, they are also laying the basis for an informal (but rules-based) multilayered infraspecific taxonomy: a visualization that recognizes the complexity of species lineages and their phylo-geography/ecology/oceanography in terms of genetic lineages, putative species, and populations (Morard, R. et al., 2016) (Figure 4.5b). Given that deep-time (for example paleoceanographic) applications of planktonic foraminfera depend on developing analogous levels of understanding, one wonders if the species–phenon depiction will continue to be adequate into the future, in regard to either its mere two-level hierarchy or the way phena (as species-group taxa) are currently employed. However, compared to other phylogenetic schemes currently employed for deep time, the species–phenon tree does provide both a comprehensive and specific set of proposals and timings, in terms of both species and phena (Figure 4.5c). And some of these could potentially be amenable to, for example, molecular dating and phylogenetics. And, despite the rich

fossil record of planktonic foraminifera, taking the results of molecular phylogenetics into deep time can usefully suggest parts of this record needing reexamination for stratophenetic phylogenetics (Figure 4.5d, e: the case of *Globigerinoides elongata*).
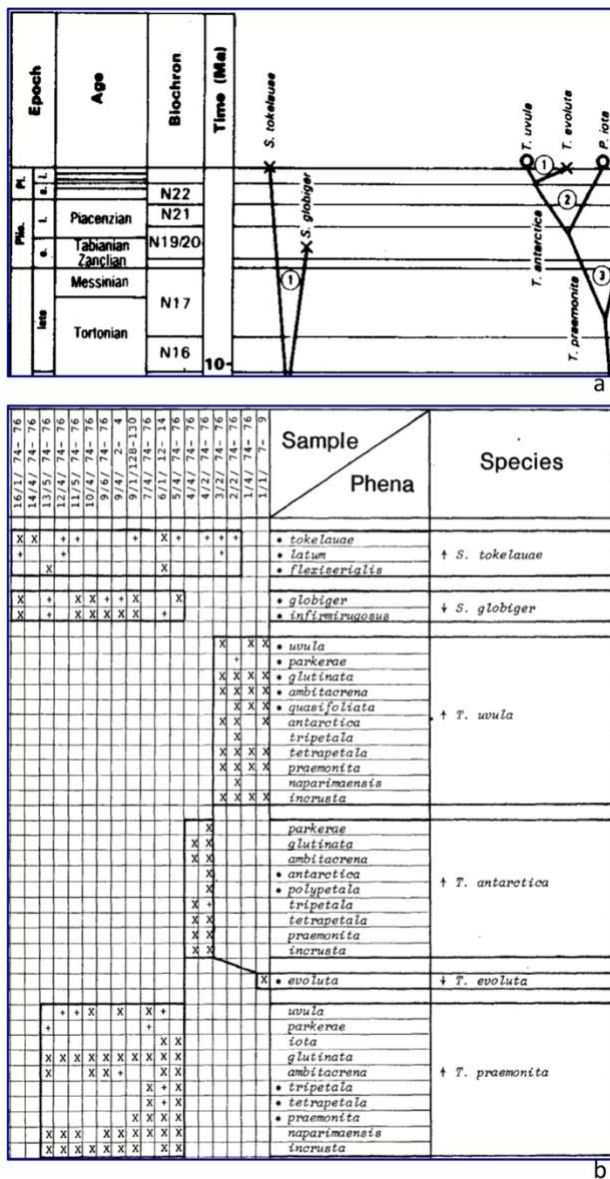
Figure 3.4 Earlier thinking towards species–phenon trees. A small portion of the phylogeny and stratigraphic charts from a study (Fordham, 1986; Fordham, 1979) of Cenozoic planktonic foraminifera: a window limited to the last 10 Myr, focusing in on *Streptochilus* and *Tinophodella praemonita* and descendants (see original for details). (**a**) Portion of species tree (Text-Figure 2b of Fordham, 1986, upper-left). (**b**) Corresponding stratigraphic-distribution chart for Deep Sea Drilling Site 208 (Table 3a of Fordham, 1986, portion): species boxes arranged and linked according to the species tree, with occurrences of included phena listed by stratigraphic order of primary types.

Figure 3.5 Mutual learnings between integrated species–phenon trees and molecular trees. (**a, b**) Living species of planktonic-foraminifer genera, *Orbulina* and *Trilobatus*, and their evolution during the Neogene. (**a**) Portion with these two genera from the integrated species–phenon tree of the case study of Cenozoic macroperforate planktonic foraminifera (see Figure 3.3c). (**b**) A molecular phylogeny of those two genera and related groups (Figure 3 of Morard, R. et al., 2016). *Orbulina* (grey boxes): rather than a single species lineage (T338) with two phena that are still living, the genetics point to the need for stratophenetic studies to check for progressive speciation through the Miocene–Pleistocene which resulted in three living species. *Trilobatus* (green boxes): stratophenetic studies have already placed the four genetically almost identical nominal species employed by molecular studies into a single species lineage (N337-N339-T341; with two of those nominal species portrayed as intergradational phena, two synonymized). (**c–e**) Phylogenies since the late Oligocene of planktonic foraminifera related to *Globigerinoides*. (**c**) An annotated portion from the integrated species–phenon tree of the case study of Cenozoic macroperforate planktonic foraminifera (see Figure 3.3c); coloured by ecogroups; species binomina are not authoritative (genus epithets after Spezzaferri, S. et al., 2015); details of phena within species, etc. are viewable interactively when the datapack is loaded onto the *TimeScale Creator* platform (§Data availability). (**d**) A stratophenetic scheme influenced by molecular phylogenetics (Figure 5 of Spezzaferri, S. et al., 2015; see for details). (**e**) A molecular–stratigraphic scheme (Figure 6 of Aurahs, R. et al., 2011; see for details). The molecular study (**e**) suggested species *G. elongata* (green ellipse) is a living descendant of *G. conglobate* and as-yet unrecognized by the stratophenetic approaches [see green ellipse in (**c**)] as it is a homeomorph of *G. rubra* (though this would be a relatively minor convergence as both share quite a close common ancestor, *G. subquadrata*
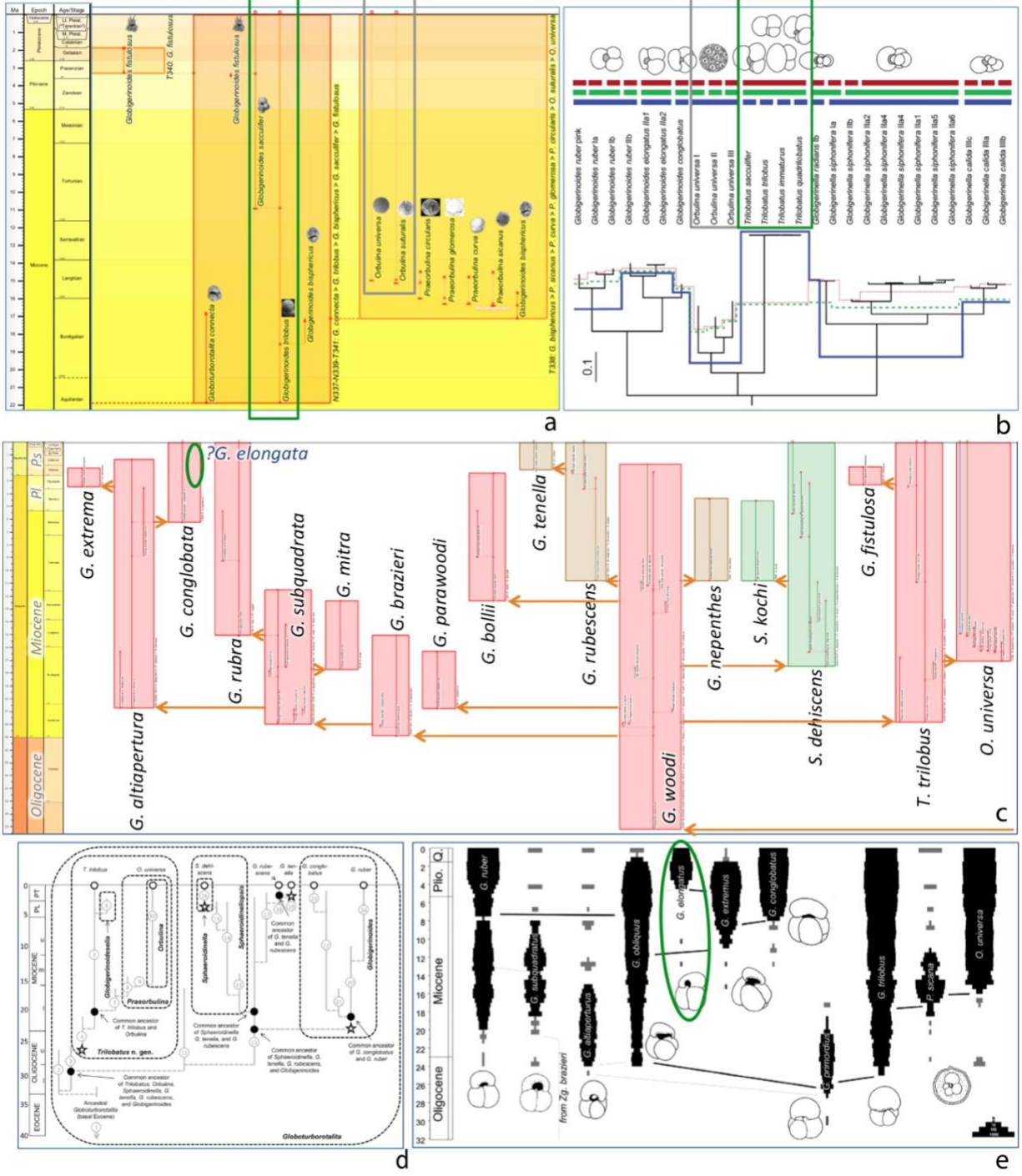
Beyond Aze & others' phylogeny of planktonic foraminifera, our integrated tree should have immediate application for similar cases where the fossil record is rich enough to motivate the proposal of phylogenetic trees of not just fossil morphotaxa but paleobiologic species. And, if those organisms have living representatives, a similarly fruitful interchange with molecular and other living research would be expected. But we would also encourage researchers with other kinds of temporal infraspecific information to consider placing that within the expandable graphic provided by our tool in order to visualize the phylogenetic context and detail of that information. This information need not be in tree form. For instance, the graphic could be used to display, say, the temporal positions and proposed species memberships of specimens, especially when at the working stage of a phylogenetic study. More generally in a more purely graphical context, a visualization tool which can bring together two nested trees that can nonetheless remain loosely coupled may have broader application.

3.6   Methods

3.6.1   Introduction and rationale

Our integrated species–phenon tree takes a species tree (Figure 3.2i, column b) and phenon tree (column a) for the same organisms, both set against geologic time, and combines the two (column c). This is accomplished by allowing the species time ranges (leaves) of the species tree to expand laterally into rectangles ("boxes"), breaking up the ranges of the phenon tree at the branch points of the species containing them, and then placing the broken-up parts of the phenon tree into their corresponding species boxes. Guide symbols (Figure 3.2ii) are added to the extremities of each of the broken phenon ranges so as to indicate their context (their origin, their extinction or still-living presence, or transfer from their ancestral species or to their descendant species).

The new integrated tree is drawn within the Java-based *TimeScale Creator* (*TSCreator*, *TSC*) visualization software package, as were its component species and phenon trees. The integration is achieved with minimal additional data input — a single extra entry for each phenon, denoting the species in which its range ends — the tool does the rest. This minimal indication of links between the two component trees avoids the introduction of errors from manual tree compilation,

likely with even the most meticulous effort when the dataset is large (e.g., for our case example (Aze, T. et al., 2011), the original listings in Appendix S5 of the 339 morphospecies in the 210 lineages contained a small % of such errors, understandably).

Visualization of the integrated tree on the same platform as its component trees makes it easy to transfer all of the latters' graphical features as well: line styles, colours, thumbnail images, pop-ups, and, most importantly, the exact dimensions of the tree topologies. An additional flexibility built into the integrated-tree tool allows the inclusion of phenon ranges within species boxes for any phena not connected into the original phenon tree. Similarly, any phenon trees/subtrees disconnected from the main phenon tree will also be drawn within their species boxes; this could be employed for depiction of additional infraspecific categories. A further feature allows the user to provide alternative labels for phena; this could be employed, for example, to label phena with only a single species epithet (*species*, of *Genus species*) which is then easily visually distinguished from the binomen of its enveloping species (*Genus species*).

Programming the new integrated tree presented significant challenges. The key issue for the previously coded evolutionary tree for *TimeScale Creator* concerned collation and coordination of widths of diverse graphical components, quite a task in itself. The integrated tree adds further complications arising from the lack of a simple overall parent–child hierarchy, with the result that, for example, the number of breaks within phenon ranges is not easily determined up-front, requiring greater preemptive space complexity and concomitant memory. A key solution has been the computation of a species–phenon relationship map, which is progressively populated by tracking down the phenon tree from top to bottom. With the resulting extended tree data structure, the internal dimensions for species boxes can then be determined and so the graphical footprint of the overarching species tree put in place.

3.6.2   Evolutionary trees in *TimeScale Creator*

TimeScale Creator is a Java-based visualization software package which lets users draw interactive charts to explore and compare Earth-history events of any portion of geologic time. Evolutionary trees are now available for these charts (pp. 50–51 of Ogg, J. G. & Ogg, G. M., 2018). These trees can be displayed in columns alongside other columns such as regional lithostratigraphy, biostratigraphic zonations, isotopic curves, trends, sequences, or global and regional event time-

series data. The tool to draw the new integrated species–phenon tree (pp. 52–53 of Ogg, J. G. & Ogg, G. M., 2018) has been included in this evolutionary-tree feature.

An evolutionary tree is inputted into our software package via a datapack containing a tab-delimited text file. Each row in this file contains text or numeric data within equivalent spreadsheet columns B–K to represent the evolutionary relationship and attributes of a time-range point. The specific format is (pp. 50–51 of Ogg, J. G. & Ogg, G. M., 2018):

Data row for range.
Label [Parent-name] (column B) ⇒ Age (Ma) (C) ⇒ Abundance (D) ⇒ Pop-up(E).
Data row for branch.
Parent-name (column B) ⇒ Age (Ma) (C) ⇒ "branch" (D) ⇒ Child-name (E) ⇒ "on/off" (F) ⇒ BranchLabel (G) ⇒ Dashed/Dotted (H) ⇒ Pop-up (I) ⇒ BranchColor (J) ⇒ Priority (K).

A general tree data structure is a connected network between nodes where a unique path from any ancestor to any descendant is maintained; a reverse path (from descendant to an ancestor) is not allowed. Because we are also positioning evolutionary events against standard geologic time in the evolutionary-tree column, each node in the tree corresponds to an evolutionary range (pp. 48–49 of Ogg, J. G. & Ogg, G. M., 2019), informing the first-appearance datum (FAD or BASE point of the range) and the last-appearance datum (LAD or TOP point of the range) for an organism. The left–right branching and spacing of descendant ranges starting at the branch point of its parent range is deduced by calculating the number of children (p. 51 of Ogg, J. G. & Ogg, G. M., 2019) and positioning them on the drawing canvas. Our evolutionary-tree algorithm receives only range data with point and line attributes and then generates the tree data structure determining the branch connections among parent and child ranges and hierarchies among subtrees.

The main challenge in drawing an evolutionary tree is the determination of the left–right horizontal and up–down vertical positioning of the range lines in order to avoid collisions between branches and subtrees and so generate a visually balanced tree. Our algorithm determines the width of left and right subtrees branching out from the parent ranges to recursively calculate the total width of the final tree. It draws the vertical range lines on the drawing canvas first, followed by the horizontal branch lines.

3.6.3   Integrated species–phenon tree

3.6.3.1   Additional programming

Drawing of the integrated tree adds a further layer of programming to that of the evolutionary tree. In particular, the width determination and positioning algorithm now needs to accommodate the breaking up of phenon range lines into parts which are then transferred across multiple rectangular species range boxes. For example, in Figure 3.2i we can see that the phenon range *b* is broken into two range-line segments, the first in the species range box *Aa* and the second in *Bb*. Similarly, parts of the phenon ranges *c* and *d* are transferred from the species range box *Bb* to *Be*. This latter instance more obviously demonstrates that this breaking-up and transfer process disrupts the phenon tree structure and gives rise to disconnected subtrees within descendant species range boxes in the integrated tree. There are two new subtrees inside the species box *Be* in Figure 3.2i (column c), the first one contains only the partial range line *c* and the second one is a subtree rooted at the range line *d* inside the species box *Be*. The integrated-tree algorithm needs to address the additional spacing and information transfer for these new partial ranges forming these segregated subtrees.

Programming for the integrated tree also needs to handle the possibility of phenon ranges split between several species boxes forming a successive series of ancestors and descendants. A single phenon range may be transferred to more than two species boxes depending on its first and last appearance point. The transferring of the same contents of a phenon range to its broken-up parts across multiple species boxes adds to the complications. It requires more sophisticated data structure, higher space complexity, and greater memory consumption, because there is not a fixed limit on the number of breaks in phenon range lines which may be needed. The simple counting of children per parent range under each subtree and subsequent width determination in the existing tree-drawing algorithm are not sufficient. Besides the widths of range lines and subtrees, the widths of the rectangular species range boxes need to be precisely calculated after the extended set of range lines are created. For this reason, the algorithm needs to map species–phenon relationships between an individual species range and its occupant group of phenon ranges (Table 3.1).

Table 3.1 Species–phenon relationship map for the integrated tree of Figure 3.2(i)

Relationship ID in the map	Name of Species Range	Size of phenon range group	Name of grouped Phenon ranges	One-to-many relationship map
1-1	ancestor	1	phenon	ancestor <- phenon
2-1	*Aa*	2	*a*	*Aa <- a*
2-2			*b*	*Aa <- b*
3-1	*Bb*	4	*b*	*Bb <- b*
3-2			*c*	*Bb <- c*
3-3			*d*	*Bb <- d*
3-2			*f*	*Bb <- f*
4-1	*Be*	3	*c*	*Be <- c*
4-2			*d*	*Be <- d*
4-3			*e*	*Be <- e*
5-1	*Bf*	1	*f*	*Bf <- f*

3.6.3.2 Additional data to link phena and species

In order to link and combine the species and phenon trees, additional information needs to be provided in the datapack. However, our program minimizes this additional input by exploiting the convenient but somewhat surprising graphical fact that only one linking item is needed to accomplish this: for each phenon we need only provide the species in which its range ends. Once the top of a phenon time range is positioned in its corresponding species box, the earlier parts of its tree can be progressively transferred onto the species tree algorithmically (see previous subsection). This insight is especially handy for the user as it minimizes not only the effort needed to gather the additional data required but also the potential for errors to creep in if additional lists of mutual species–phenon memberships are compiled by other means (see § Introduction and rationale, above).

To generate an extended tree data structure the format of the input dataset of the datapack needs to be modified. The TOP range point of each phenon range line is employed to distinguish between species and phenon range lines; the tree algorithm uses this to separately create species and phenon trees. Only two entries are added to the TOP range point of an individual phenon range: (a) column G now contains the flag "phenon" and (b) column H contains the name of the

species range box in which this TOP range point of the current phenon range will be positioned (see also dataset TSCEvolTree_IntTree2019Fig2ic.txt, § Data availability):

Data row for TOP range point.

Label (column B) ⇒ Age (Ma) (C) ⇒ TOP (D) ⇒ Pop-up(E) ⇒ blank (F) ⇒ "phenon" (G) ⇒ Species-name (H)

3.6.3.3   Programming implementation

Given two side-by-side trees, the first one a species tree and the second one a phenon tree, we can establish the species–phenon mapping relationship by simply knowing which species range box will include the last appearance datum (LAD or TOP) of a phenon range. The new algorithm starts from the LAD or TOP point of a phenon range, associates this TOP point with its occupying species range line using the "phenon" flag (column H in the new format) and maps the first relationship, then continues comparing subsequent earlier (geologically past) range point ages of the phenon range line with the points of the mapped species range line. Every time it finds a younger branch connection age in the species tree than the phenon range (FAD point of the current species range greater than the phenon range points), it ends the current phenon range line under consideration by adding a new first appearance datum (FAD or BASE point). It simultaneously transfers the rest of the phenon range line to the parent species box of the current box after adding a new last appearance datum (LAD or TOP point) to the phenon range. Similarly, it continually adds new TOP and BASE points for the broken-up phenon range lines and populates the species– phenon relationship maps (Table 3.1) until it reaches the BASE point of the starting phenon range. This same process is applied to all the phenon range lines and, in the end, the algorithm acquires the new extended set of range lines with new range points for the phenon range lines and branch connections for further resolution of width, new symbols, and colour inheritance.

Each species range from the species tree expands horizontally to a box in the integrated tree (Figure 3.2i). Each box has the exact time range (i.e., vertical extent) as on the species tree, and the branches adopted from the species tree are extended horizontally. Species boxes are basically the same species ranges with a rectangular shape and varied widths. Therefore, the boxed species tree maintains the same topology as the species tree before integration and phenon-range transfer.

The species box is filled with colour that matches the colour of the inherited branch label, but with some added transparency (in the example from Figure 3.2i, species box *Aa* is green but with a RGBA alpha value chosen to enable the phenon range lines, labels, and images to be visible and readable). When a colour is assigned to a branch in the datapack dataset, the ranges of its descendants inherit that colour until a new colour is assigned to a later descendant.

The choice of line styles for the range (see Figure 3.2) of the species is exactly transferred to the box. In the example in Figure 3.2i, all ranges except one are "frequent", so all boxes except one have all sides with a "frequent" thickness. The exception is *Aa*, which is "frequent" from 13 to 5 Ma and "conjectured" from 5 Ma to the present. So the box is drawn with a "frequent" thickness along its base and 8 Myr up its sides from the base, and with a "conjectured" top and then 5 Myr down the sides from the top. Ranges can be assigned any of several abundance settings for any part of a range, so the equivalent species box will need to reflect this.

The width of each species box is dependent on the number of phenon ranges inside it. Using the species–phenon relationship map, the algorithm quickly resolves the group of phenon ranges to be drawn inside each species box. It takes consideration of the width of both the range label and image for each phenon range. It is also possible that there may exist a species box without phenon ranges; these are given a minimum width to handle such exceptions.

Each instance of the phenon range retains its core features. When phenon splits are required, all the features of the phenon ranges are duplicated and attached to each broken-up portion, e.g., the thumbnail image and pop-ups. However, the line style of the phenon ranges strongly follows the parent phenon tree because line styles are directly associated with the abundance details (line styles) for the phenon range. Visual distinction between species and phena is accomplished by employing different settings for the "default" line styles (frequent vs. common, respectively). The species range box boundaries are therefore thicker than the phenon range line (Figure 3.2i, column c).

In order to make it easier to appreciate the context of phenon range lines, especially to distinguish between their ranges and their parts broken between species boxes, guide symbols are added to the extremities of each of their parts (Figure 3.2ii).

3.6.3.4 Disconnected trees and phenon ranges

Our integrated-tree tool can manage multiple phenon trees (Figure 3.2iii: original coloured tree, with additional phenon tree *h–i* in black). If the datapack contains more than one mutually unconnected tree, the preexisting evolutionary-tree algorithm has been retained to draw all trees within the same *TimeScale Creator* column, positioning them side by side based on "First occurrence", "Last occurrence" or "Alphabetic order" (p. 49 of Ogg, J. G. & Ogg, G. M., 2019).

Our integrated tree can also handle disconnected phenon ranges: not all of the phenon ranges need to be part of a tree structure (Figure 3.2iii: additional phenon *g* in black). The algorithm orders the phenon ranges using the "First Occurrence" by default. But three options: (a) First Occurrence (b) Last Occurrence (c) Alphabetic Order are provided to the user from the settings window of the software. Ordering of the phenon ranges inside the species box can thus be freed from the topology of the unified phenon tree.

3.6.3.5 Short phenon labels

The integrated tree allows alternative labels for phena, usually to conserve space. Another application for this could be to apply a particular nomenclatural format for phenon labels. For instance, if a study conferred scientific names on phena, one could opt for phena to be given only a single species epithet (*species*, of *Genus species*), and so distinguish them from binomina (*Genus species*) of their enveloping species boxes. This feature is implemented by placing "|" within the phenon range name in the dataset, in which case the text after "|" is excluded; if the name does not contain "|", then the full name is used. (This option was effected in the back-end database of the case study via the table SpeciesGroupName, in which the original assignations of scientific names are rearranged to begin with the most trivial name — in order to provide an index invariant to later nomenclatural revisions; see links to details of the database in Table 2 and Figure 8 of Fordham, B. G. et al., 2018. For example, to take morphospecies *Acarinina bullbrooki*, featured in Figure 3.3d, its original assignation, "*Globorotalia bullbrooki* Bolli, 1957", rearranges to "*bullbrooki* Bolli, 1957; *Globorotalia*". If then the phenon range name in the dataset is given as "*bullbrooki* | Bolli, 1957; *Globorotalia*", the phenon range label displayed on the integrated tree will be reduced to "*bullbrooki*".) If the user's key concern is to more distinctly distinguish visually between species

and phenon labels, the fonts for each can be separately manipulated (*TimeScale Creator* settings: Choose Time Interval, select datapack column, Fonts).

3.7   Code availability

The source-code files for the Integrated Species–Phenon Tree feature are available at https://github.com/brishtiteveja/TSCreator_Integrated_Evolutionary_Tree.

Australian National University Data Commons collection anudc:5980, doi.org/[to be minted upon acceptance of article] (Zehady, A. K. et al., 2019). These repositories contain the source-code files constituting the core programming for the Integrated Species–Phenon Tree feature within the Evolutionary Tree column of the *TimeScale Creator* software platform.

RangeColumn.java: includes detailed data structures for evolutionary range points and ranges, and tree-drawing utility functions.

ImageGenerator.java: draws the evolutionary tree data column and generates the final chart.

Main.java: includes the main function which is the entry point to the software and spawns the Java process on a Java Virtual Machine.

Readme.txt.

The *TimeScale Creator* software platform is freely available at https://timescalecreator.org/download/download.php, from where it can be downloaded as a Java archive (jar) file or Windows executable (exe) file. Instructions to install *TimeScale Creator* and load datapacks are given in Instructions_for_TSCreator_datapacks.pdf, included in anudc:5980.

3.8   Data availability

The *TimeScale Creator* datapacks introduced herein for the integrated species–phenon tree from the case study of Cenozoic macroperforate planktonic foraminifera are available at Australian National University Data Commons collection anudc:5981, doi.org/[to be minted upon acceptance of article] (Zehady et al., 2019).

Datapacks.

Coloured by ecogroup.

With labels: TSCEvolTree_Aze&2011_CorrJul2018_ISPEco.dpk.

Without labels: TSCEvolTree_Aze&2011_CorrJul2018_ISPEcoNoLbl.dpk.

Coloured by morphogroup.

With labels: TSCEvolTree_Aze&2011_CorrJul2018_ISPMph.dpk.

Without labels: TSCEvolTree_Aze&2011_CorrJul2018_ISPMphNoLbl.dpk.

Settings: TSCEvolTree_Aze&2011_CorrJul2018_ISP_4dpks.tsc.

Note that these datapacks do not include the images of foraminifera featured in Figure 3.3, because authoritative images are not yet available for these datasets. These datapacks are also freely available from the *TimeScale Creator* website https://timescalecreator.org/datapack/datapack.php.

Other supplementary information for this article is available at Australian National University Data Commons collection anudc:5982, doi.org/[to be minted upon acceptance of article] (Zehady, A. K., 2019).

TimeScale Creator datapacks, the relational database, and related files for the previously published lineage and morphospecies trees from the case study are also available at Australian National University Data Commons collections (for details see Fordham, B. G. et al., 2018). These datapacks are also freely available from the *TimeScale Creator* website.

3.9 References

Allende, C., Sohn, E. & Little, C., 2015. Treelink: data integration, clustering and visualization of phylogenetic trees. BMC Bioinformatics, 16, pp. e414. https://doi.org/10.1186/s12859-015-0860-1.

Archibald, J. D., 2014. Aristotle's ladder, Darwin's tree: the evolution of visual metaphors for biological order. Columbia University Press.

Armstrong, H. A. & Brasier, M. D., 2005. Microfossils. (Blackwell).

Aurahs, R., Treis, Y., Darling, K. & Kucera, M., 2011. A revised taxonomic and phylogenetic concept for the planktonic foraminifer species *Globigerinoides ruber* based on molecular and morphometric evidence. Marine Micropaleontology, 9, pp. 1–14. https://doi.org/10.1016/j.marmicro.2010.12.001.

Avise, J. C. & Robinson, T. J., 2008. Hemiplasy: a new term in the lexicon of phylogenetics. Systematic Biology, 57, pp. 503–507. https://doi.org/10.1080/10635150802164587. .

Aze, T. et al., 2011. A phylogeny of Cenozoic macroperforate planktonic foraminifera from
fossil data. Biological Reviews of the Cambridge Philosophical Society, 86, pp. 900–927.
https://doi.org/10.1111/j.1469-185X.2011.00178.x.

Barrett, R. A. et al., 2015. A chloroplast phylogeny of Zieria (Rutaceae) in Australia and New
Caledonia shows widespread incongruence with species-level taxonomy. Australian
Systematic Botany, 27, pp. 427–449. https://doi.org/10.1071/SB14033.

Belfiore, N. M., Liu, L. & Moritz, C., 2008. Multilocus phylogenetics of a rapid radiation in the
genus *Thomomys* (Rodentia: Geomyidae). Systematic Biology, 57, pp. 294–310.
https://doi.org/10.1080/10635150802044011.

Benavente, E. D. et al., 2015. PhyTB: phylogenetic tree visualisation and sample positioning for
M. tuberculosis. BMC Bioinformatics, 16, pp. e155. https://doi.org/10.1186/s12859-015-
0603-3.

Bernini, G. et al., 2016. Complexity of biogeographic pattern in the endangered
crayfish Austropotamobius italicus in northern Italy: molecular insights of conservation
concern. Conservation Genetics, 17, pp. 141–154. https://doi.org/10.1007/s10592-015-
0767-4.

Blow, W. H., 1969. Late middle Eocene to Recent planktonic foraminiferal biostratigraphy. In
Proceedings of the First International Conference on Planktonic Microfossils (eds
Bronnimann, P. & Renz, H. H.) Vol. 1, pp. 199–421. E. J. Brill.

Bogarín, D. et al., 2018. Anchored hybrid enrichment generated nuclear, plastid and
mitochondrial markers resolve the Lepanthes horrida (Orchidaceae: Pleurothallidinae)
species complex. Molecular Phylogenetics and Evolution, 129, pp. 27–47.
https://doi.org/10.1016/j.ympev.2018.07.014.

Bolli, H. M. & Saunders, J. B., 1985. Oligocene to Holocene low latitude planktic foraminifera.
In Plankton stratigraphy (eds Bolli, H. M., Saunders, J. B. & Perch-Nielsen, K.), Vol. 1,
pp. 155–262. Cambridge University Press.

Bouzat, J. L., 2014. Darwin's diagram of divergence of taxa as a causal model for the origin of
species. The Quarterly Review of Biology, 89, pp. 21–38.
https://doi.org/10.1086/674992.

Chaisson, W. P. & Pearson, P. N., 1997. Planktonic foraminifer biostratigraphy at Site 925: middle Miocene–Pleistocene. In Proceedings of the Ocean Drilling Program. Scientific Results (eds Shackleton, N. J., Curry, W. B., Richter, C. & Bralower, T. J.), 154, pp. 3–32. http://www-odp.tamu.edu/publications/154_SR/01_CHAP.PDF.

Charruau, P. et al., 2011. Phylogeography, genetic structure and population divergence time of cheetahs in Africa and Asia: evidence for long-term geographic isolates. Molecular Ecology 20, pp. 706–724. https://doi.org/10.1111/j.1365-294X.2010.04986.x.

Cifelli, R. & Scott, G. H., 1986. Stratigraphic record of the Neogene globorotalid radiation (planktonic Foraminiferida), Smithsonian Contributions to Paleobiology, 58. https://doi.org/10.5479/si.00810266.58.1.

Cuezzo, M. G., Miranda, M. J., Vogler, R. E. & Beltramino, A. A., 2018. From morphology to molecules: a combined source approach to untangle the taxonomy of Clessinia (Gastropoda, Odontostomidae), endemic land snails from the Dry Chaco ecoregion. PeerJ, 6, pp. e5986. https://doi.org/10.7717/peerj.5986.

Darling, K. F. & Wade, C. M., 2008. The genetic diversity of planktic foraminifera and the global distribution of ribosomal RNA genotypes. Marine Micropaleontology, 67, pp. 216–238. https://doi.org/10.1016/j.marmicro.2008.01.009.

Darling, K. F., Kucera, M., Pudsey, C. J. & Wade, C. M., 2004. Molecular evidence links cryptic diversification in polar planktonic protists to Quaternary climate dynamics. Proceedings of the National Academy of Sciences of the United States of America, 101(20), pp. 7657–7662. https://doi.org/10.1073/pnas.0402401101.

Darling, K. F., Wade, C. M., Kroon, D., Brown, A. J. L. & Bijma, J., 1999. The diversity and distribution of modern planktic foraminiferal small subunit ribosomal RNA genotypes and their potential as tracers of present and past ocean circulations. Paleoceanography, 14, pp. 3–12. https://doi.org/10.1029/1998pa900002.

Darwin, C., 1859. On the origin of species by means of natural selection, or, the preservation of favoured races in the struggle for life. H. Milford; Oxford University Press. https://doi.org/10.1037/14088-004.

de Queiroz, K., 2005. Ernst Mayr and the modern concept of species. Proceedings of the National Acadamy of Sciences of the USA 102(Suppl 1), pp. 6600–6607. https://doi.org/10.1073/pnas.0502030102.

de Vargas, C. & Pawlowski, J., 1998. Molecular versus taxonomic rates of evolution in planktonic foraminifera. Molecular Phylogenetics and Evolution, 9, pp. 463–469. https://doi.org/10.1006/mpev.1998.0491 .

de Vargas, C., Bonzon, M., Rees, N. W., Pawlowski, J. & Zaninetti, L. A, 2002. A molecular approach to biodiversity and biogeography in the planktonic foraminifer *Globigerinella siphonifera* (d'Orbigny). Marine Micropaleontology, 45, pp. 101–116. https://doi.org/10.1016/s0377-8398(02)00037-3 .

de Vargas, C., Renaud, S., Hilbrecht, H. & Pawlowski, J., 2001. Pleistocene adaptive radiation in Globorotalia truncatulinoides: genetic, morphologic, and environmental evidence. Paleobiology, 27, pp. 104–125. http://dx.doi.org/10.1666/0094-8373(2001)027<0104:PARIGT>2.0.CO;2.

de Vargas, C., Zaninetti, L., Hilbrecht, H. & Pawlowski, J., 1997. Phylogeny and rates of molecular evolution of planktonic foraminifera: SSU rDNA sequences compared to the fossil record. Journal of Molecular Evolution, 45, pp. 285–294. https://doi.org/10.1007/pl00006232.

Doyle, J. J., 1992. Gene trees and species trees: molecular systematics as one-character taxonomy. Systematic Botany, 17, pp. 144–163. https://doi.org/10.2307/2419070.

Emami-Khoyi, A. et al., 2016. Mitochondrial DNA structure and colony expansion dynamics of New Zealand fur seals (*Arctocephalus forsteri*) around Banks Peninsula. New Zealand Journal of Zoology, 43, pp. 322–335. https://doi.org/10.1080/03014223.2016.1179649.

Etienne, R. S. et al., 2012. Diversity-dependence brings molecular phylogenies closer to agreement with the fossil record. Proceedings of the Royal Society. B, Biological Sciences, 279, pp. 1300–1309. https://doi.org/10.1098/rspb.2011.1439.

Fordham, B. G. et al., 2018. Future-proofing the Cenozoic macroperforate planktonic foraminifera phylogeny of Aze & others (2011). PLoS One, 13, e0204625. https://doi.org/10.1371/journal.pone.0204625.

Fordham, B. G., 1979. A chronocladogeny and corresponding classification of Neogene planktic foraminifera with a documentation of morphotypes from two Pacific deep sea stratigraphic sections. PhD thesis, University of Queensland. https://openresearch-repository.anu.edu.au/handle/1885/9007.

Fordham, B. G., 1986. Miocene–Pleistocene planktic foraminifers from D. S. D. P. Sites 208 and 77, and phylogeny and classification of Cenozoic species. 200 pp., 25 pls. Evolutionary Monographs, 6. https://www.mn.uio.no/cees/english/services/van-valen/evolutionary-monographs/.

Fordham, B. G., 1991. A literature-based phylogeny and classification of Silurian conodonts. Palaeontographica, Abteilung A 217, pp. 1–136.

Fordham, B. G., 1995. Advantages of comprehensive taxonomy for routine systematic documentation in conodont biostratigraphy. Boletín de la Academia Nacional de Ciencias, Córdoba [Argentina] 60, pp. 469–482.

Fujimoto, T. et al., 2018. Biochemical, physiological, and molecular characterization of Dickeya dianthicola (formerly named Erwinia chrysanthemi) causing potato blackleg disease in Japan. Journal of General Plant Pathology, 84, pp. 124–136. https://doi.org/10.1007/s10327-018-0772-9.

Gaubert, P., Taylor, P. J., Fernandes, C. A., Bruford, M. W. & Veron, G., 2005. Patterns of cryptic hybridization revealed using an integrative approach: a case study on genets (Carnivora, Viverridae, Genetta spp.) from the southern African subregion. Biological Journal of the Linnean Society, 86, pp. 11–33. https://doi.org/10.1111/j.1095-8312.2005.00518.x.

Goodman, M., Czelusniak, J., Moore, G. W., Romero-Herrera, A. E. & Matsuda, G., 1979. Fitting the gene lineage into its species lineage, a parsimony strategy illustrated by cladograms constructed from globin sequences. Systematic Zoology, 28, pp. 132–163. https://doi.org/10.2307/2412519.

Gulla, S., Lund, V., Kristoffersen, A. B., Sørum, H. & Colquhoun, D. J., 2016. vapA (A-layer) typing differentiates Aeromonas salmonicida subspecies and identifies a number of previously undescribed subtypes. Journal of Fish Diseases, 39, pp. 329–342. https://doi.org/10.1111/jfd.12367.

Haller, C. & Ogg, J. G., 2013. Cenozoic macroperforate planktonic foraminifera evolution [Poster]. Third Geological Problem Solving with Microfossils Conference (Microfossils III), 10-13 March, 2013, North American Micropaleontology Section (NAMS) of the Society for Sedimentary Geology (SEPM).

Han, T., Lee, W., Lee, S., Park, I. G. & Park, H., 2016. Reassessment of species diversity of the Subfamily Denticollinae (Coleoptera: Elateridae) through DNA barcoding. PLoS One, 11, pp. e0148602. https://doi.org/10.1371/journal.pone.0148602.

Hardion, L. et al., 2017. Does infraspecific taxonomy match species evolutionary history? A phylogeographic study of *Arundo formosana* (Poaceae). Botanical Journal of the Linnean Society, 183, pp. 236–249. https://doi.org/10.1093/botlinnean/bow006.

Hills, S. F. K., Crampton, J. S., Trewick, S. A. & Morgan-Richards, M., 2012. DNA and morphology unite two species and 10 million year old fossils. PLoS One, 7, pp. e52083. https://doi.org/10.1371/journal.pone.0052083.

Hofmeyr, M. D., Vamberger, M., Branch, W., Schleicher, A. & Daniels, S. R., 2017. Tortoise (Reptilia, Testudinidae) radiations in southern Africa from the Eocene to the present. Zoologica Scripta 46, pp. 389–400. https://doi.org/10.1111/zsc.12223. .

Huber, B. T., Bijma, J. & Darling, K., 1997. Cryptic speciation in the living planktonic foraminifer *Globigerinella siphonifera* (d'Orbigny). Paleobiology, 23, pp. 33–62. https://doi.org/10.1017/S0094837300016638.

Kennett, J. P. & Srinivasan, M. S., 1983. Neogene planktonic foraminifera: a phylogenetic atlas. Hutchinson Ross.

Kim, N. & Lee, C., 2007. Three-Dimensional Phylogeny Explorer: distinguishing paralogs, lateral transfer, and violation of "molecular clock" assumption with 3D visualization. BMC Bioinformatics, 8, p. e213. https://doi.org/10.1186/1471-2105-8-213.

Knappertsbusch, M., 2007. Morphological variability of Globorotalia menardii (planktonic foraminifera) in two DSDP cores from the Caribbean Sea and the eastern equatorial Pacific. Carnets de Géologie, Article 7. http://paleopolis.rediris.es/cg/CG2007_A04/index.html.

Lancaster, M. L., Arnould, J. P. Y. & Kirkwood, R., 2010. Genetic status of an endemic marine mammal, the Australian fur seal, following historical harvesting. Animal Conservation, 13, pp. 247–255. https://doi.org/10.1111/j.1469-1795.2009.00325.x.

Lazarus, D., Hilbrecht, H., Spencer-Cervato, C. & Thierstein, H., 1995. Sympatric speciation and phyletic change in *Globorotalia truncatulinoides*. Paleobiology, 21, pp. 28–51. https://doi.org/10.1017/S0094837300013063.

Luo, A., Zhu, C.-D., Ho, S. Y. W. & Ling, C., 2018. Comparison of methods for molecular species delimitation across a range of speciation scenarios. Systematic Biology, 67, pp. 830–846. https://doi.org/10.1093/sysbio/syy011.

Maddison, W. P., 1997. Gene trees in species trees. Systematic Biology, 46, pp. 523–536. https://doi.org/10.2307/2413694.

Mayr, E. , 1982. The growth of biological thought. Belknap Press.

Mayr, E., 1969. Principles of systematic zoology. McGraw-Hill.

Mizuyama, M., Masucci, G. D. & Reimer, J. D., 2018. Speciation among sympatric lineages in the genus *Palythoa* (Cnidaria: Anthozoa: Zoantharia) revealed by morphological comparison, phylogenetic analyses and investigation of spawning period. PeerJ, 6, p. e5132. https://doi.org/10.7717/peerj.5132.

Morard, R., et al., 2016. Nomenclature for the nameless: a proposal for an integrative molecular taxonomy of cryptic diversity exemplified by planktonic foraminifera. Systematic Biology, 65, pp. 925–940. https://doi.org/10.1093/sysbio/syw031.

Nei, M., 1987. Molecular evolutionary genetics. Columbia University Press.

Ogg, J. G. & Gradstein, F. M., 2006. TS-Creator©-chronostratigraphic data base and visualisation: Cenozoic–Mesozoic–Paleozoic integrated stratigraphy and user-generated time scale graphics and charts. Episodes 29, pp. 65–66. https://doi.org/10.18814/epiiugs/2006/v29i1/008.

Ogg, J. G. & Ogg, G. M., 2019. TimeScale Creator Manual. (Geologic TimeScale Foundation Inc., https://timescalecreator.org/download/TS-Creator%20Manual_July2019.zip.

Pearson, P. N., 1993. A lineage phylogeny for the Paleogene planktonic foraminifera. Micropaleontology, 39, pp. 193–232. https://doi.org/10.2307/1485898.

Quillévéré, F. et al., 2013. Global scale same-specimen morpho-genetic analysis of Truncorotalia truncatulinoides: a perspective on the morphological species concept in planktonic foraminifera. Palaeogeography, Palaeoclimatology, Palaeoecology, 391, pp. 2–12. https://doi.org/10.1016/j.palaeo.2011.03.013.

Saito, T., Breger, D. & Thompson, P. R., 1981. Systematic index of Recent and Pleistocene planktonic foraminifera. University of Tokyo Press.

Schiebel, R. & Hemleben, C., 2017. Planktic foraminifers in the modern ocean. Springer.

Scornavacca, C., Huson, D. H. & Zickmann, F., 2011. Tanglegrams for rooted phylogenetic trees and networks. Bioinformatics, 27(13), pp. i248–i256. https://doi.org/10.1093/bioinformatics/btr210.

Serrano-Villavicencio, J. E., Vendramel, R. L. & Siniciato Terra Garbino, G, 2017. Species, subspecies, or color morphs? Reconsidering the taxonomy of Callicebus Thomas, 1903 in the Purus–Madeira interfluvium. Primates, 58, pp. 159–167. https://doi.org/10.1007/s10329-016-0555-x.

Sexton, P. F. & Norris, R. D., 2008. Dispersal and biogeography of marine plankton: long-distance dispersal of the foraminifer Truncorotalia truncatulinoides. Geology, 36, pp. 899–902. https://doi.org/10.1130/G25232A.1.

Singh, S. P., Groeneveld, J. C., Al-Marzouqi, A. & Willows-Munro, S., 2017. A molecular phylogeny of the spiny lobster *Panulirus homarus* highlights a separately evolving lineage from the southwest Indian Ocean. PeerJ, 5, p. e3356. https://doi.org/10.7717/peerj.3356.

Smith, A. B., 1994. Systematics and the fossil record. Blackwell Scientific.

Sota, T., Kojima, T., Lee, Y. J. & Lin, C.-P., 2016. Phylogenetic relationships of Japanese Auritibicen species (Hemiptera: Cicadidae: Cryptotympanini) inferred from mitochondrial and nuclear gene sequences. Zoological Science, 33(4), pp. 401–406.

Spezzaferri, S. et al., 2015. Fossil and genetic evidence for the polyphyletic nature of the planktonic foraminifera "Globigerinoides", and description of the new genus Trilobatus. PLoS One 10, e0128108. https://doi.org/10.1371/journal.pone.0128108.

Sprovieri, A., Ruggieri, G. & Untl, M., 1980. Globorotalia truncatulinoides excelsa n. subsp., foraminifero planctonico guida per il Pleistocene inferiore. Bollettino della Societa Geologica ltaliana, 99, pp. 3–11.

Stewart, D. R. M., 2003. Evolution of Neogene globorotaliid foraminifera and Miocene climate change. (PhD thesis, University of Bristol, https://research-information.bristol.ac.uk/files/34489299/288306.pdf).

Szöllősi, G. J., Tannier, E., Daubin, V. & Boussau, B., 2014. The inference of gene trees with species trees. Systematic Biology, 64, e42–e62. https://doi.org/10.1093/sysbio/syu048.

Ujiié, Y. & Ishitani, Y., 2016. Evolution of a planktonic foraminifer during environmental changes in the tropical oceans. PLoS One, 11(2), pp. e0148847. https://doi.org/10.1371/journal.pone.0148847.

Ujiie, Y. & Lipps, J. H., 2009. Cryptic diversity in planktic foraminifera in the northwest Pacific Ocean. Journal of Foraminiferal Research, 39, pp. 145–154. https://doi.org/10.2113/gsjfr.39.3.145.

Ujiié, Y., de Garidel-Thoron, T., Watanabe, S., Wiebe, P. & de Vargas, C., 2010. Coiling dimorphism within a genetic type of the planktonic foraminifer *Globorotalia truncatulinoides*. Marine Micropaleontology, 77, pp. 145–153. https://doi.org/10.1016/j.marmicro.2010.09.001.

Vitek, N. S., 2018. Delineating modern variation from extinct morphology in the fossil record using shells of the Eastern Box Turtle (*Terrapene carolina*). PLoS One, 13, pp. e0193437. https://doi.org/10.1371/journal.pone.0193437.

Wade, B. S., Olsson, R. K., Pearson, P. N., Huber, B. T. & Berggren, W. A., 2018. Atlas of Oligocene planktonic foraminifera. Cushman Foundation for Foraminiferal Research Special Publication, vol. 46.

Weiner, A. K. M. et al., 2014. Phylogeography of the tropical planktonic foraminifera lineage Globigerinella reveals isolation inconsistent with passive dispersal by ocean currents. PLoS One, 9(3), pp. e92148. https://doi.org/10.1371/journal.pone.0092148.

Weiner, A. K. M., Weinkauf, M. F. G., Kurasawa, A., Darling, K. F. & Kucera, M., 2015. Genetic and morphometric evidence for parallel evolution of the *Globigerinella calida* morphotype. Marine Micropaleontology, 114, pp. 19–35. https://doi.org/10.1016/j.marmicro.2014.10.003.

Weir, B. S., Johnston, P. R. & Damm, U., 2012. The *Colletotrichum gloeosporioides* species complex. Studies in Mycology, 73, pp. 115–180. https://doi.org/10.3114/sim0011.

Wen, D., Yu, Y., Hahn, M. W. & Nakhleh, L., 2016. Reticulate evolutionary history and extensive introgression in mosquito species revealed by phylogenetic network analysis. Molecular Ecology, 25, pp. 2361–2372. https://doi.org/10.1111/mec.13544.

Wieland, B. et al., 2006. Phenon cluster analysis as a method to investigate epidemiological relatedness between sources of *Campylobacter jejuni*. Journal of Applied Microbiology, 100(2), pp. 316–324. https://doi.org/10.1111/j.1365-2672.2005.02788.x.

Wurst, E. & Frank, B., 1998. Contributions to a revision of the genus *Schwiebea* (Acari: Acaridae). I. Redescription of *Schwiebea talpa* and *Schwiebea nesbitti*. Stuttgarter Beiträge Zur Naturkunde, Serie A 579.

Zehady, A. K., 2019. Source code, Integrated Species–Phenon Tree feature, Evolutionary Tree column, TimeScale Creator visualization platform. Australian National University Data Commons Collection anudc:5980. https://doi.org/10.25911/5db66f7bc1935.

Zehady, A. K., Fordham, B. G. & Ogg, J. G., 2019. Cenozoic macroperforate planktonic foraminifera phylogeny of Aze & others (2011). TimeScale Creator Integrated Species–Phenon Tree. Corrected Version, July 2018. Four datapacks for Java software package. Australian National University Data Commons Collection anudc:5981. https://doi.org/10.25911/5db66faba683b.

Zehady, A. K., Fordham, B. G. & Ogg, J. G., 2019. Integrated species–phenon trees: visualizing infraspecific diversity within lineages. Data repository for published article. Australian National University Data Commons Collection anudc:5982. https://doi.org/10.25911/5db66fd8c5127.

CHAPTER 4.   PACING OF FORAMINIFER AND NANNOFOSSIL TURNOVER BY MILANKOVITCH GRAND CYCLES

Abstract

Pelagic foraminifers and calcareous nannofossils are the most widely preserved marine organisms in Cenozoic pelagic carbonates. We used the origination/speciation and extinction events to quantify organism lifespans and create evolutionary turnover time series data for entire Cenozoic for both foraminifer and nannofossil. We found ~1.2 Myr and ~2.4 Myr connection with Milankovitch cycles which have been shown to affect climatic events in a macroscale. Obliquity minima and eccentricity minima are linked with ice sheet expansion and cooling. The turnover peaks can be aligned with oxygen-18 events from Oligocene to Miocene and early Pleistocene which give us evidence for the climate-turnover hypothesis for marine microfossils.

4.1   Introduction

Long term astronomical cycles influence the atmosphere and ecology of our planet. The principal planetary rotations are eccentricity, obliquity and precession. Eccentricity determines the shape of the orbit. Obliquity is the tilt of our planet with respect to the solar plane. Precession refers to Earth's own rotation around the vertical axis. Variation in eccentricity changes the distance between sun and Earth's hemisphere and thus the received solar energy through sunlight is dependent on eccentricity cycle which has been measured to be 100 kyr (on the minor axis) and 410 kyr (on the major axis). These two cycles interact and show a longer 0.97 and 2.32 Myr cycles that cause amplitude modulation of precession or obliquity cycle. The long astronomical cycle (~2 Myr) has been found in many segments of geologic time in different sources (Table 4.1). Studies have shown that the Miocene cold events are forced by these very long-term Milankovitch cycles.

Table 4.1 Studies showing very-long astronomical cycles of 1.2 to 6 Myr duration

Age Interval	Cycle Duration	Proxy	Reference
0-24 Ma	~1.2-2.5 Myr	Rodent turnover	Van Dam et al., 2006
0-35 Ma	~1.8-2.4 Myr	Oxygen isotope of benthic foraminifera	De Vleeschouwer et al., 2017
0-80 Ma	~1.2-2.4 Myr	Carbon and oxygen isotope of benthic foraminifera	Cramer et al., 2009
11.5-15.2 Ma	~2.4 Myr	L* of lake sediments	Abels et al., 2010
14-36 Ma	~2.4 Myr	Sedimentary facies of lake sediment	Valero et al., 2014
47-53 Ma	~2.4 Myr	Fe intensity of pelagic marine succession	Westerhold et al., 2012
53-57 Ma	~2.25 Myr	Bulk carbonate d13C and magnetic susceptibility (MS) records across the Elmo horizon	Lourens et al., 2005
60-84 Ma	~2.5 Myr	Carbonate content of pelagic marine succession	Herbert et al., 1999
79-100 Ma	~1.6 Myr	Carbon isotope of bulk carbonate	Sprovieri et al., 2013
82-92 Ma	~1.2-2.4 Myr	Formation Micro-resistivity Imaging (proxy for carbonate content) of marine succession	Ma et el., 2017
100-125 Ma	~1.6 Myr	Color of limestone succession	Huang et al., 2010a
125-195 Ma	~1.6-3.5 Myr	Carbon isotope of belemnite carbonate.	Martinez & Dera, 2015
147-154Ma	~2.0 Myr	Color of limestone succession	Huang et al., 2010b
156-161 Ma	~2.0 Myr	Magnetic susceptibility of marine marl succession	Boulila et al., 2010
180-250 Ma	~1.2-3.3 Myr	Biogenic silica burial flux of pelagic deep-sea succession	Ikeda et al., 2017
198-230 Ma	~2.2-1.6 Myr	Sedimentary facies of lake succession	Kent et al., 2017
200-240 Ma	~1.2-3.5 Myr	Carbon isotope of bulk carbonate	Muttoni et al., 2004
411-486 Ma	~1.3, 2.6 Myr	Graptoloid diversity	Crampton et al., 2018

Microfossil appearance ages and diversity rate information are heavily informative in oil and gas reservoir exploration. Using benthic foraminifera, planktonic foraminifera and nannofossils, petroleum industries correlated time in deep wells and constructed global Cenozoic timescales.

We investigated the turnover of microfossils and the influence of Milankovitch cycles on their evolution. We focused on the evolution of planktonic foraminifera and calcareous nannofossils during the Cenozoic era (~65 Ma) and correlate to climatic events since Oligocene (~34 Ma). This paper contributes to the study of finding links between climatic events due to Earth's orbital oscillations and their effect on marine species and gives us insights to answering macroevolutionary questions. In particular, the analysis of the syntheses proves the climate-turnover hypothesis in the evolutionary data of foraminifer and nannofossil. Evolution of foraminifer and nannofossils show similar trends, the burst of the origination and extinction of

these species are highly correlated. We can see cyclic patterns in their turnover (speciation + extinction) time series.

4.2   Datasets

We focused on the macroevolutionary trends in the late Cenozoic era. To study evolutionary trends over millions of years, it is required to have access to a group of organisms which was prevalent throughout the entire time in almost all ecological habitat

Fossil records come with incompleteness due to (a) some taxa are not studied extensively (b) some geologic time period are under sampled.

4.2.1   Planktonic foraminifers

Foraminifera are the most thoroughly researched marine organisms because of their outstanding fossil record. They have great significance in the discovery of Earth history as they capture geochemical information about past ocean chemistry and can help us infer past Earth climate, geologic and ecologic environments. They are members of a phylum of single-celled eukaryotic organisms that can flourish in all marine environments. Foraminifera are classified into two main categories: a) Planktonic foraminifera which lack the ability to float against the current of a water body and b) Benthic foraminifera which belong to the community of organisms that live near marine or freshwater sedimentary environment (e.g. sands, muds, rocks) at the bottom of the sea, rivers and lakes. The ecological success of foraminifera can be attributed to their ability to move and capture food (small organism like bacteria, diatom) using thread-like pseudopods extended from the cell body. The most important feature of the foraminiferal cell is the shell, which can have diverse morphological shapes depending on the species. These shells are made of calcium carbonate and are fundamental components of many rocks. The morphological differences in test shells are used to classify pelagic foraminifers. Because the development of the outer shell depend on the environment they try to adapt, foraminifer test shells of extant species found in foraminifer samples provide us the information to reconstruct the ecological habitats and environment too. Foraminifer samples collected from sediments can be compared with similar living foraminifera and past environment can be de deduced. Diversity of extinct species, shell type ratio, shell chemistry can be used as powerful tools too. Scientists have used foraminifer to identify past global

temperature, measure sea level and ocean depth, study how the shorelines and tropical regions have changed over time. The outstanding fossil record of foraminifera can help us study the evolutionary history and establish connection between the external climatic events and the effect in the speciation and extinction process of these species.

Planktonic foraminifera have the most complete fossil record in the Cenozoic. Aze et al. (2011) have looked into multiple studies of foraminifer fossil records and compiled a dataset of evolutionary ranges of foraminifer fossils for the whole Cenozoic. The grouping mechanism of the organisms relied mainly on the morphological characteristics (Table A2) and further grouped by ecological information (Table A3). Genetic similarity or dissimilarity between organisms were not considered as it is difficult to obtain ancient DNA. The dataset provides two main evolutionary trees: one represents the lineage tree (Table A8) and the other is more elaborative morphospecies tree (Table A1).

The naming convention for each of the lineage is described in Aze et al., 2011. There are 212 lineages determined from the 340 morphospecies. They are also categorized by their morphogroup and ecogroup. The number of lineages and lifespan statistics for each of the groups are provided in Table A9 which shows the start, end and mean lifespan for all 19 morphogroup and 6 ecogroup for all lineages. The evolution of foraminifer lineages closely matches with the evolution of morphospecies (Figure 4.7B, Figure 4.7A).
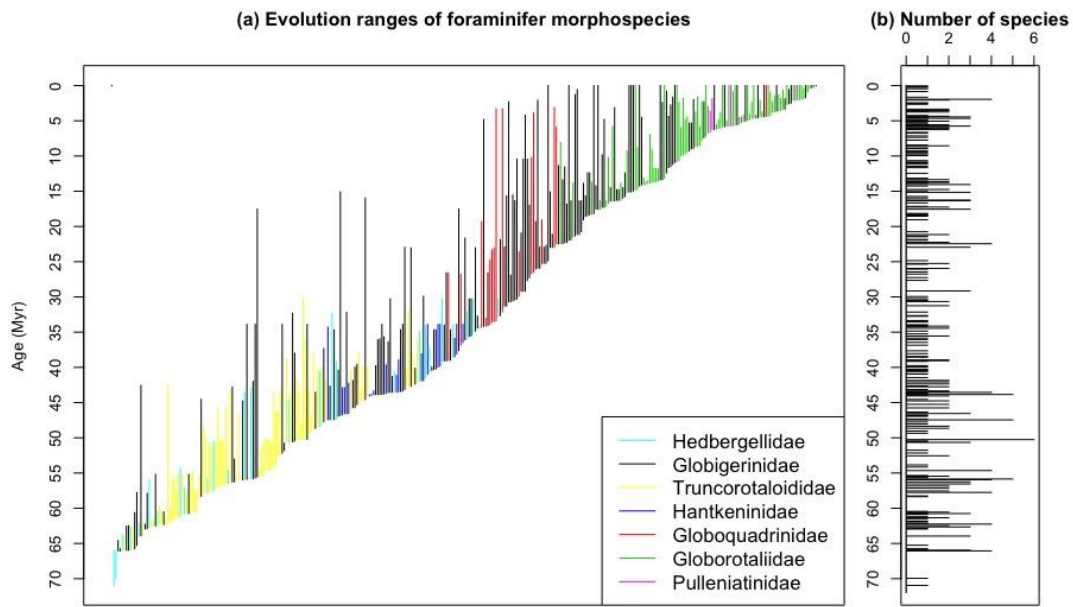
Figure 4.1(a) Evolution ranges of foraminifer morphospecies showing evolution of 7 distinct families. The ranges are sorted by their first appearance age throughout the Cenozoic Era. (b) Number of species by counting first appearance datums (FADs) at each pseudolevel (100 kyr intervals).
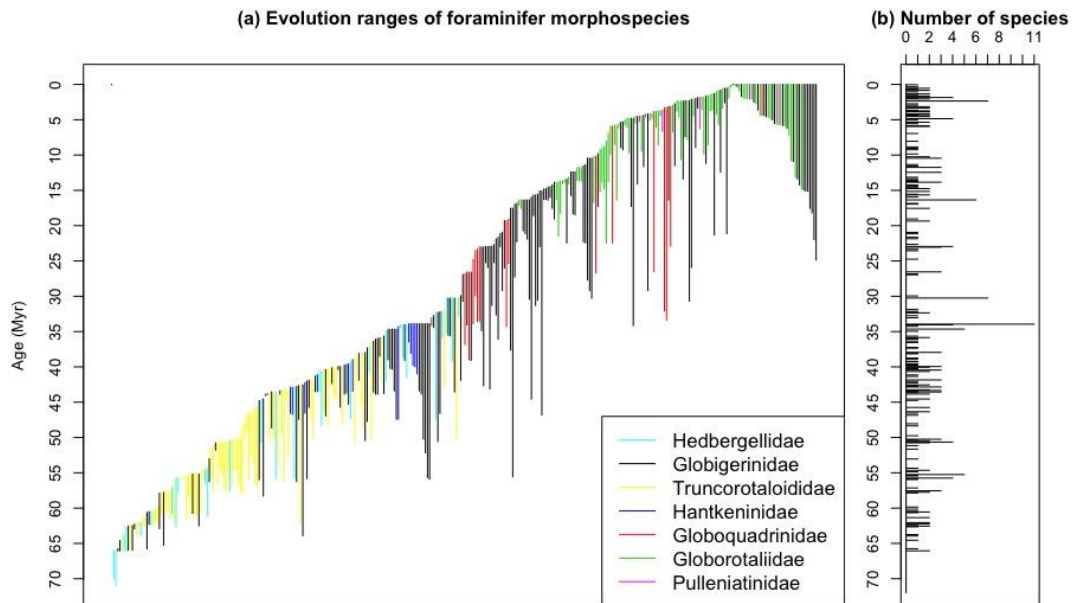
Figure 4.2(a) Evolution ranges of foraminifer morphospecies showing evolution of 7 distinct families. The ranges are sorted by their last appearance age throughout the Cenozoic Era. (b) Number of species by counting last appearance datums (LADs) at each pseudolevel (100 kyr intervals).

Divesity of foraminifer morphospecies by their families
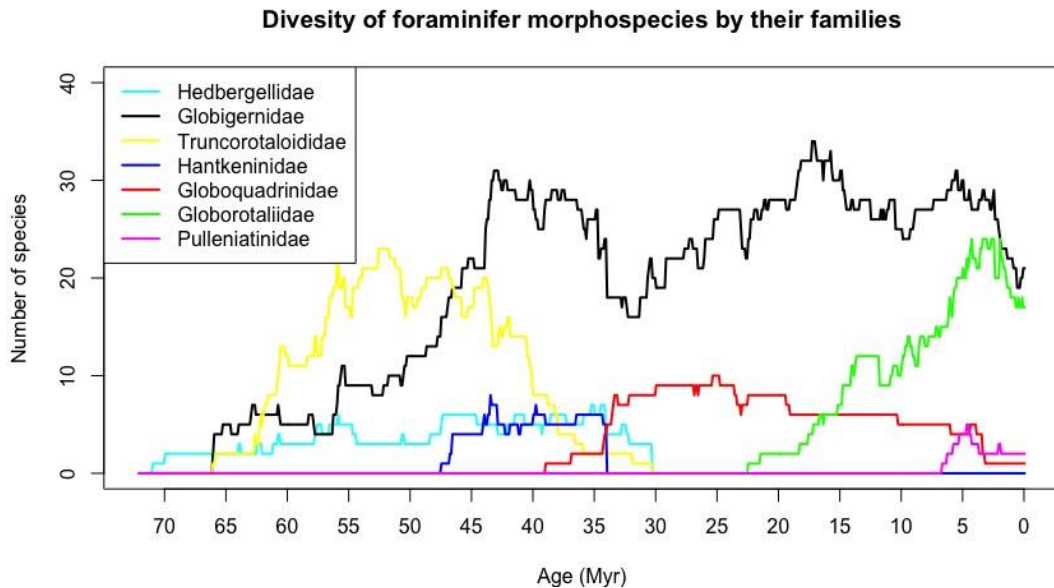
Figure 4.3 Standing diversity of foraminifer morphospecies throughout the Cenozoic colored by 7 foraminifer families.

4.2.2 Calcareous nannofossils

Calcareous nannofossils include coccolith and coccolithophores. Coccoliths are plates made of limestone (calcium carbonate) formed by single celled plant-like organism called coccolithophores. After death of these organisms, the coccolith plates get separated from the cosmosphere and preserved in sedimentary rocks. The skeletons of coccolithophores are vastly available in marine deposits and are one of the major rock components (e.g. chalk of island Rugen in Baltic sea). These nannofossils, due to their small size, are well distributed across all habitats and thus can be used similarly as foraminifer to study paleo climate and their abundance and diversity make them amazingly useful for macroevolution studies.

A Gulf of Mexico synthesis paper (Bergen et al., 2017) created a standard framework to detect the biozonation using nannofossils. For some genera, the family name is missing, and the class or phylum name was used. And in some case "-" is used. The nannofossils in our study are under the following families: "-", "Calcidiscaceae", "Ceratolithaceae", "Coccolithaceae", "Discoasteraceae", "Helicosphaeraceae", "Noelaerhabdaceae", "Pontosphaeraceae",

"Sphenolithaceae". Discosteraceae family has the highest (95) number of nannofossil species where as Pontosphaeraceae and Calcidiscaceae have only 2 or 3 species under them respectively (Table A12 Number of species and lifespan of nannofossils grouped by family). Figure 4.4, Figure 4.5 and Figure 4.6 show the evolutionary turnover of nannofossils.
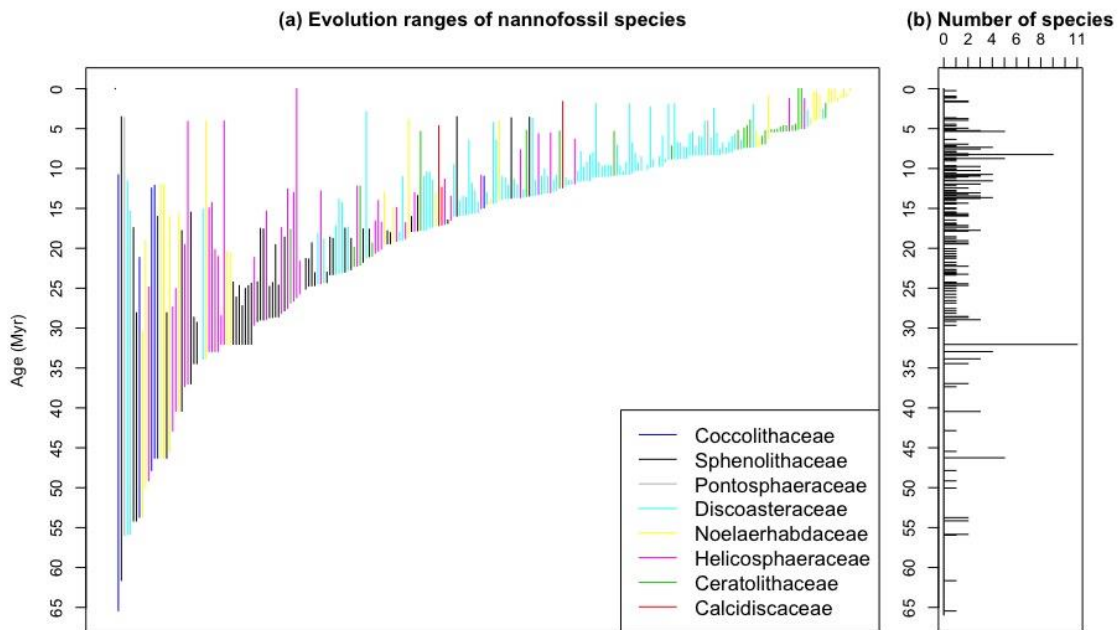
Figure 4.4(a) Evolution ranges of nannofossil species showing evolution of 8 distinct families. The ranges are sorted by their first appearance age throughout the Cenozoic Era. (b) Number of species by counting first appearance datums (FADs) at each pseudolevel (100 kyr intervals).
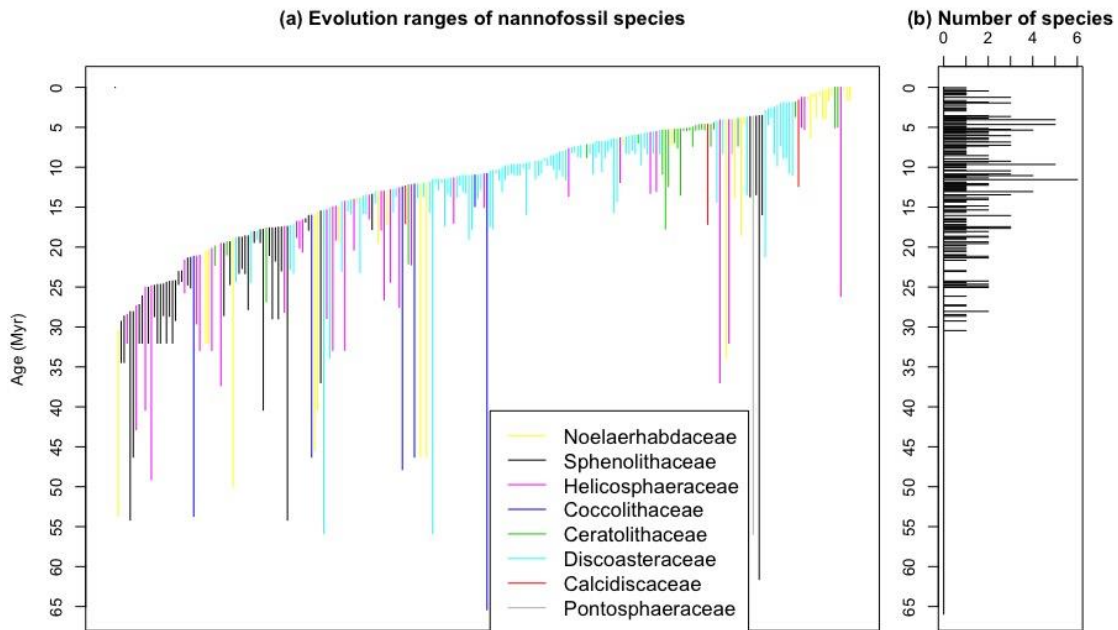
Figure 4.5(a) Evolution ranges of nannofossil species showing evolution of 8 distinct families. The ranges are sorted by their last appearance age throughout the Cenozoic Era. (b) Number of species by counting last appearance datums (LADs) at each pseudolevel (100 kyr intervals).
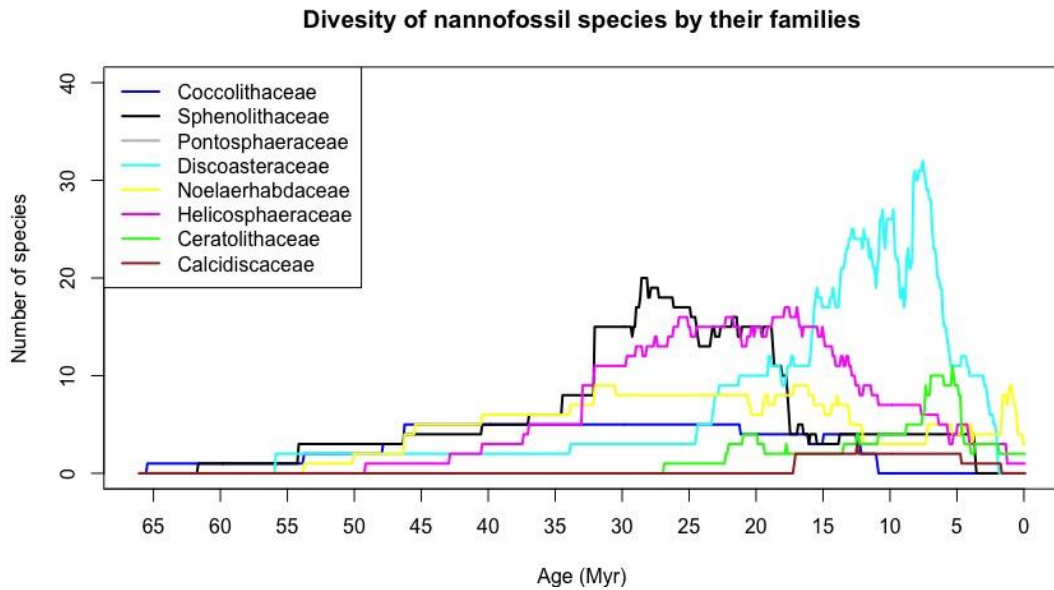
Figure 4.6 Diversity of nannofossil species throughout Cenozoic colored by 8 nannofossil families.

99

4.3   Methods

To get better granularity, we divide the whole Cenozoic era (65 Ma) into many pseudolevels each separated by 100 kyr (0.1 Myr). Our data mining algorithm parses through the times series of speciation (FAD) and extinction (LAD) and count them individually for each pseudolevel. The turnover time series is calculated by taking the sum of speciation and extinction (FAD + LAD) for each pseudolevel.

We visualized the foraminifer morphospecies evolution throughout the Cenozoic era by FAD and then LAD in Figure 4.1, Figure 4.2 and nannofossil species in Figure 4.4, Figure 4.5. When it is sorted by LAD, species which have same/close LAD values are grouped together. Similarly species which have same/close FAD values are grouped together in case of FAD sorting. The species are colored by their family which show interesting pattern. We can see that the nannofossil families sequentially evolved and died. On the other hand, morphospecies families evolved parallelly.

We have calculated the raw turnover probability using the following equations.

$$Es[i] = Es[i-1] + Ns[i] – Ne[i]$$

$$Ee[i] = Es[i-1] = Es[i-2] + Ns[i-1] – Ne[i-1]$$

$$Rs[i] = Ns[i] / Es[i]$$

$$Re[i] = Ne[i]/ Ee[i]$$

Where,

Es[i] : Number of existing species in pseudolevel i which includes the new species originated in the current pseudolevel**.**

Ee[i] : Number of species subjected to extinction in pseudolevel or number of existing species in previous pseudolevel (i-1).

Ns[i] : Number of speciation events in pseudolevel i.

Ne[i] : Number of extinction events in pseudolevel i**.**

Rs[i] : Raw speciation probability (New species originated out of existing species).

Re[i] : Raw extinction probability (How many species died out of the existing species from the last level?).

We have shown the speciation (green), extinction (red) and turnover (black) curve for foraminifer morphospecies (Figure 4.7A), lineages (Figure 4.7B) and nannofossils (Figure 4.7C). Mean-lifespan time series is calculated by taking the sum of lifespan till current pseudolevel for

all the living species in that lifespan. For each of our species collection, we have plotted the number of existing species, also known as standard diversity, and mean lifespan together. We can see small bulges which shows how increasing number of existing species drive the mean lifespan per pseudolevel down in most cases.

(A)
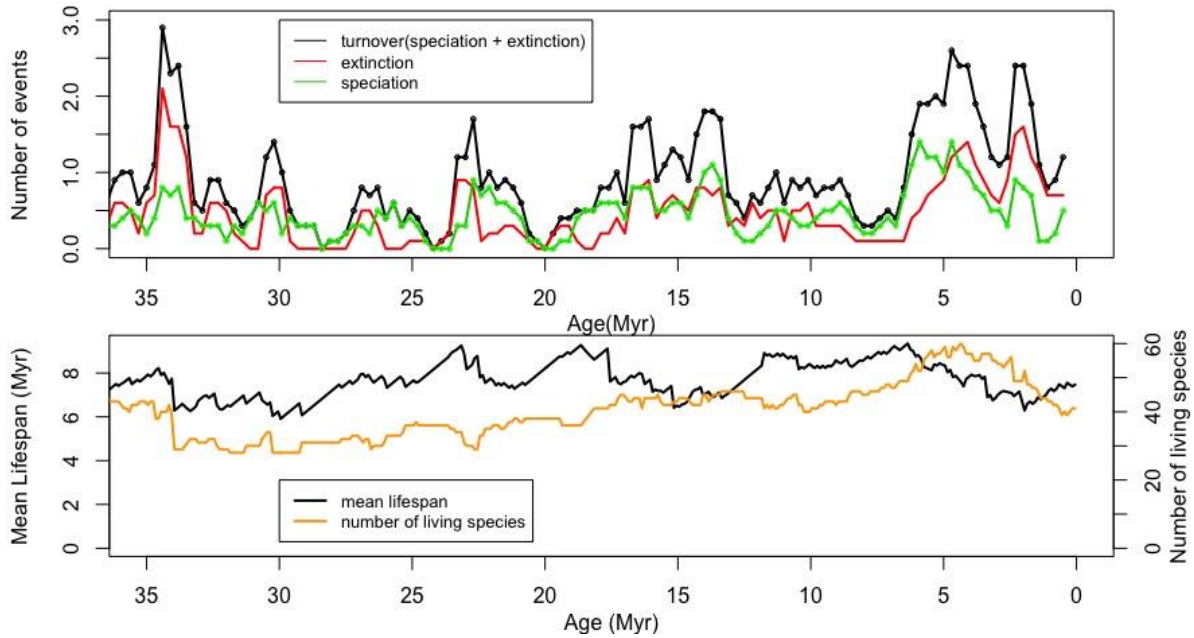
Figure 4.7 Speciation, extinction and turnover events per million years. Mean lifespan of standing species per pseudolevel and standing species diversity are also shown in each panel. (A) foraminifer morphospecies, (B) foraminifer lineages, (C) nannofossils.

Figure 4.7 continued

(B)
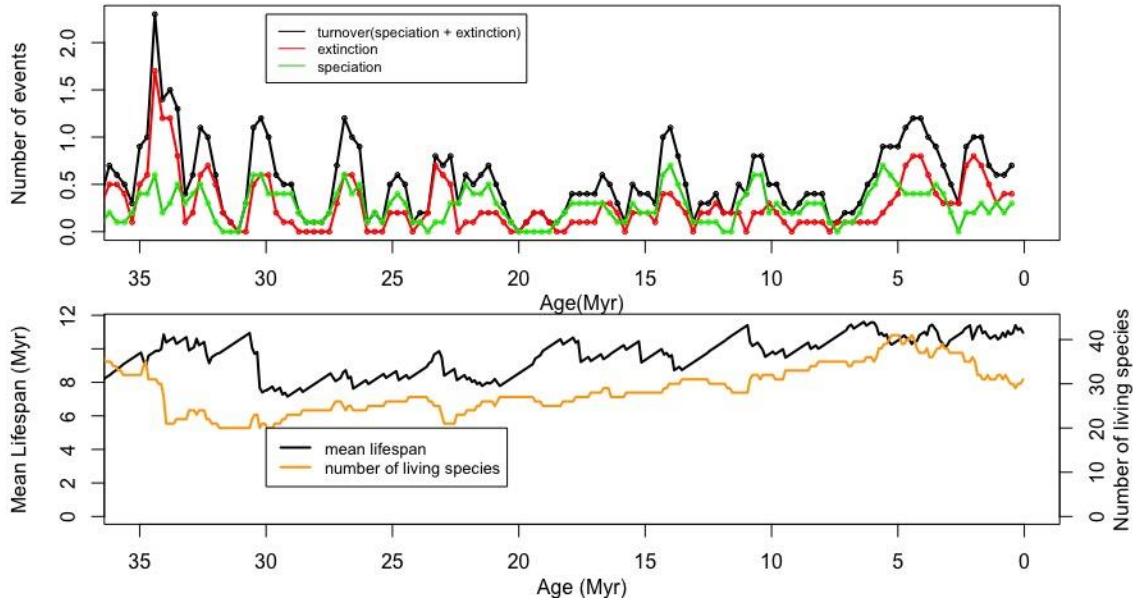
(C)
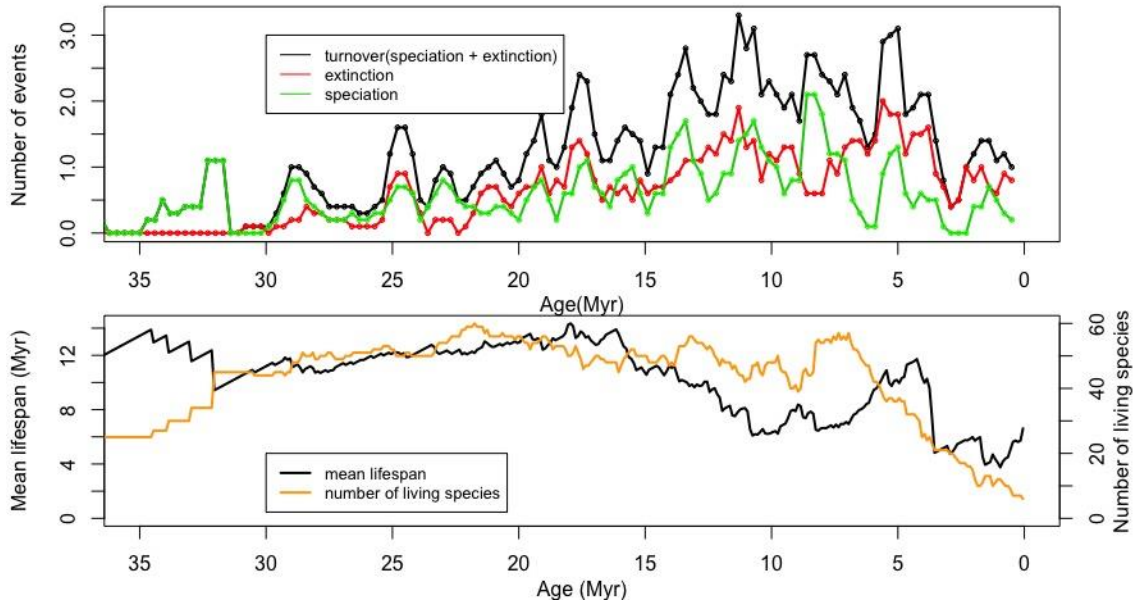
Spectral analysis was performed to find periodicity in the turnover record and the significance for certain periods is measured with confidence level estimates from autoregressive (AR-1) model and harmonic variance ratio F-test using the "Astrochron" package (Meyers, 2014) for the R programming language.

4.3.1 Fourier analysis

We performed Fourier spectral analysis on our time-series data. Any function can be expanded as a sum of harmonic functions (sines and cosines) and the resulting expression is known as Fourier series. Any function can also be expanded in terms of polynomials and the resulting expression is known as Taylor series. If the underlying forces are harmonic and there possibly exists some periodicity, then the use of harmonic series is more useful than using polynomials as it produces simpler equations. It is possible to discover a few dominating terms from such series expansion which may help identify the known natural forces with the same period.

4.3.2 Periodogram

Fourier transform gives us the complex numbers and the square of the absolute value of these numbers represent the periodogram. This is the first form of numerical spectral analysis and is used to estimate spectral power. Even though the data points are collected only at evenly spaced discrete time, it is possible to evaluate periodogram at any frequencies. Periodogram can provide higher frequency resolution but the signal to noise ratio cannot be increased.

4.3.3 Fast Fourier Transform (FFT)

We can calculate the Fourier transform very efficiently by using FFT. It requires data at equally-spaced time points and is most efficient when the number of points is an exact power of two. Interpolation is often used to produce the evenly-spaced data which may introduce additional bias and systematic error. For real data consisting of N data points y[j], each taken at time t[j], the power spectrum outputs a set of $N + 1$ data points. The value of the first data point equals the value of the last data point that represents the power at frequency zero. The second up to the $N/2 + 1$ data points represent the power at evenly-spaced frequencies up to the Nyquist frequency. The spectral power for a given frequency is distributed over several frequency bins, therefore an optimum determination of the power requires combining these information and proper 101 investigation of leakage. FFT calculates the amplitude for a set of frequencies. $N/2$ complex amplitudes are calculated at $N/2$ different frequencies. Because these may not be the true frequencies present in the record, we subtract the mean from the data and then pad it with zeros to overcome this challenge.

4.3.4   Tapers

We apply taper or data window to reduce the side lobes of the spectral lines. Basically we want to minimize the leakage of power from the strong peaks to other frequencies. In multitaper method, several different tapers are applied to the data before Fourier transform and the resulting powers are then averaged. Thomson (1982) chose the Slepian or discrete prolate spheroidal sequences as tapers since these vectors are mutually orthogonal and possess desirable spectral concentration properties. Multitaper method can suppress side-lobes but have higher resolution. If we use few tapers, the resolution won't be degraded, but then side-lobe reduction won't happen much. So, there is a trade-off, which is often misunderstood. We used the multitaper method provided in R "Astrochron" package (Meyers, 2014).

4.3.5   Multitaper Analysis

We apply taper or data window to reduce the side lobes of the spectral lines. Basically we want to minimize the leakage of power from the strong peaks to other frequencies. In multitaper method, several different tapers are applied to the data before Fourier transform and the resulting powers are then averaged. Each data taper is multiplied element-wise by the signal to provide a windowed trial from which the power at each component frequency is estimated. As each taper is pairwise orthogonal to all other tapers, the windowed signals provide statistically independent estimates of the underlying spectrum. The final spectrum is obtained by averaging over all the tapered spectra. Thomson (1982) chose the Slepian or discrete prolate spheroidal sequences as tapers since these vectors are mutually orthogonal and possess desirable spectral concentration properties. Multitaper method can suppress side-lobes but have higher resolution. If we use few tapers, the resolution won't be degraded, but then side-lobe reduction won't happen much. So, there is a trade-off, which is often misunderstood.

4.4   Results and Discussion

4.4.1   Mean species lifetimes

We first used the morphospecies tree to perform our macroevolutionary analysis as our primary concern is the rate of change in the speciation, extinction and turnover that can be

benefitted if we have more data points per million years. Every morphospecies in the tree has a First (FAD) and Last Appearance Datum (LAD) which creates the evolutionary range. There are 340 (339 without the super ancestor) unique morphospecies under 48 unique genera which are grouped by 7 families: "Hedbergellidae", "Globigerinidae", "Truncorotaloididae", "Hantkeninidae", "Globoquadrinidae", "Globorotaliidae", "Pulleniatinidae". Table A1 shows the full list of morphospecies with their binomial name, FAD, LAD, genus, family, morphogroup and ecogroup. Mean species lifespan for all the morphospecies is 6.5 Myr (Table A4). Globoquadrinidae family has the maximum mean life span (13.7 Myr) whereas the short-lived family is Pulleniatinidae with mean life span of 2.7 Myr. The full list of mean lifespan, mean start of lifespan and mean end of lifespan results are provided in Table A4.

The greatest number of morphospecies, total 140 species, are under the family Globigerinidae (black line in Figure 4.3) which shows the mean life span of 9.6 Myr. Before Oligocene epoch (~34 Ma), the most diverse family was Truncorotaloididae (yellow line in Figure 4.3) which became extinct during the Oligocene. Different families show different evolution patterns over time: Truncorotaloididae, Hantkeninidae and Hedbergellidae were abundant before Oligocene when Earth was much warmer whereas the abundance of Globorotaliidae started to increase after Miocene epoch. The longest living foraminifer morphospecies is the "*Catapsydrax unicavus*" under Globigerinidae family which had a lifespan of 38.0 Myr (FAD= 55.56 Myr, LAD= 17.54 Myr). On the other hand, the shortest living morphospecies *Globigerinella adamsi* is a living foraminifer which came into existence 10,000 years (FAD= 0.01 Myr, LAD= 0 Myr) ago. Aze et al., 2011 and later Barry et al., 2018 have successfully categorized the foraminifer morphospecies into 19 Morphogroups (based on their test shell structure difference) and 6 Ecogroups shown in Table A2 and Table A3 respectively.

We have collected stats by grouping the organisms by family, morphogroup and eco-group. We have tabulated number of morphospecies, mean lifespan, mean start and end of lifespan in in Table A4, Table A5, Table A6 respectively for all families, morphogroups and ecogroups. Morphogroup 2 and 7 have the highest number of morphospecies (80 and 52 respectively). Out of 19 Morphogroups, only 10 Morphogroup (M1-flat, M2-globular, M3-globular with supplementary apertures, M4-spherical, M5-clavate, M6-planispiral, M7-globluar, M14-globorotaliform, keeled, M15-globorotaliform, anguloconical, M16-globorotaliform, non-killed) still exist till the present age, whereas the rest of the 9 morphogroups got extinct (M8-globular, keeled, M9-planispiral,

M10-tubulospinate, M11-keeped spines, M12-turborotaliform, keeled, M13-turborotaliform, non-keeled, M17-muricate, acarininiform, M18-muricocarinate, keeled, M19-muricocarinate, anguloconical) ("End of Lifespan" column in Table A5). The extinct morphogroups belong to the 3 families Hedbergellidae, Truncorotaloididae, Hantkeninidae and the other five families are still present.

Ecogroup 1 and 3 have the highest number of morphospecies (110 and 107 respectively). Out of the 6 ecogroups, the sixth ecogroup E6-upwelling/high became extinct at 15.1 Myr ago (Table A6). The high latitude foraminifer group (E5-high-latitude) has the maximum mean lifespan (16.0 Myr), whereas the thermocline Ecogroup has the minimum lifespan of 6.8 Myr. The E1-With Symbionts ecogroup has the highest number of species (110); the E3-thermocline group also has almost equally abundant (107) species. There are only 3 species which live in high latitude and 9 species in upwelling/high habitat.

Speciation, extinction and turnover events of nannofossils are shown (Figure 4.7C-upper panel). The number of nannofossils and lifespan statistics (Figure 4.7C-lower panel) for each of the groups are also provided in Table A11. Median life span for nannofossils is 2.8 Myr.

4.4.2   Cyclicity in microfossil turnover

We intend to understand the evolutionary changes happened in foraminifer and nannofossils. We have produced time series for speciation (pseudospeciation) and extinction (pseudoextinction) of foraminifer morphospecies (Figure 4.7A), lineage (Figure 4.7B) and nannofossil species (Figure 4.7C). We can see patterns and cyclical occurrences of bursts of speciation or extinction (Figure 4.7). We restricted our turnover data from Oligocene epoch to current period to see whether we can find any environmental or climatic impact on the turnover events of foraminifer and nannofossils. Using *TSCreator* charting system, we plotted the speciation, extinction and turnover events against the eccentricity, precession, obliquity, Oxy-18 events in Figure 4.8.
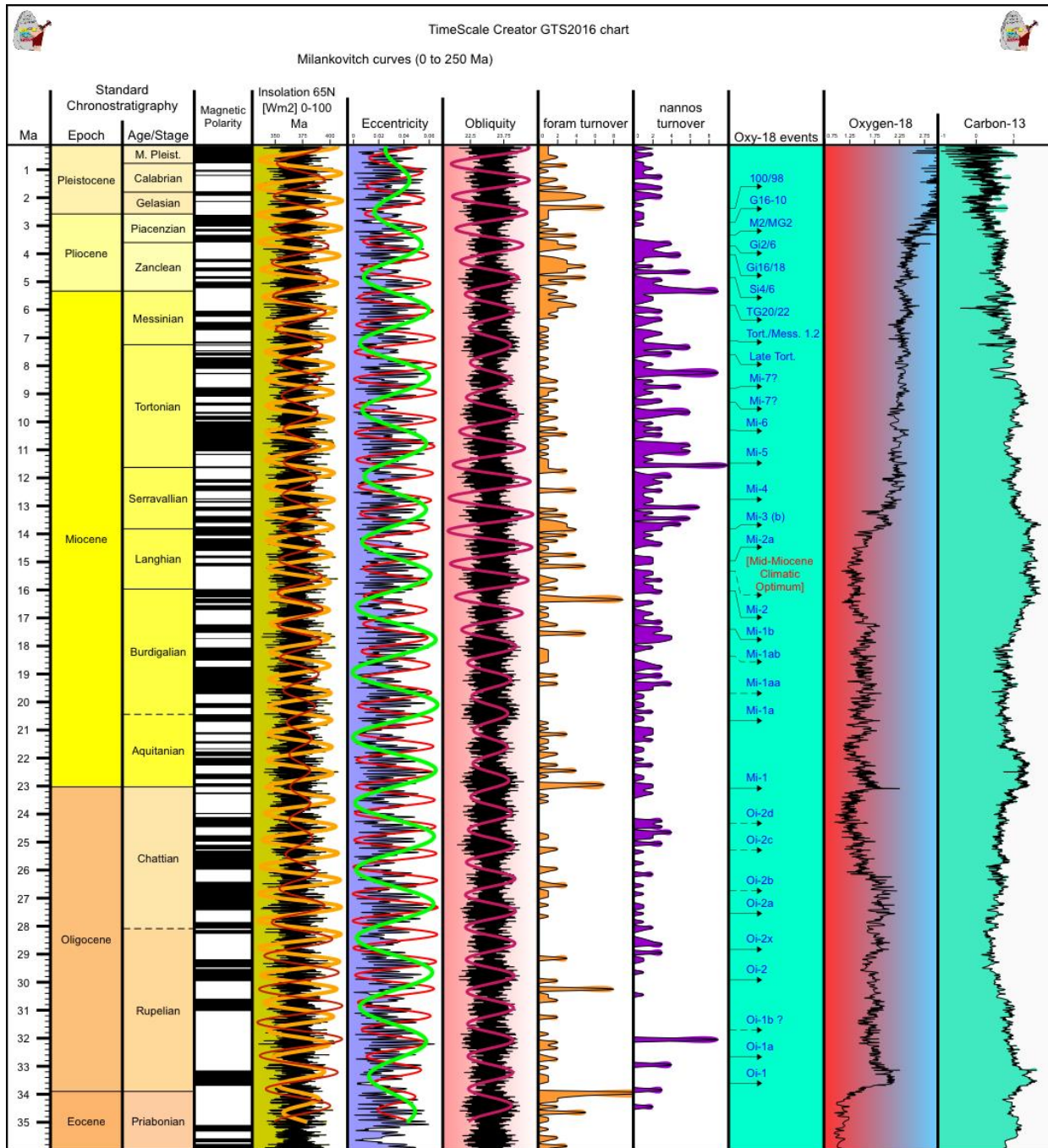
Figure 4.8 Speciation, extinction and turnover events compared to eccentricity, precession, obliquity, Oxy-18 and C-13 time series.

Studies have shown that the Miocene cold events are forced by above mentioned Milankovitch cycles. We have also found significant turnover events occurring in those zones of

cold events. In Table A7, we compared the morphospecies turnover events with the cold events and the nannofossils in Table A13.

We performed multitaper spectral analysis (Figure 4.9) to identify long-term astronomical cycles which might have induced the cold phase since Oligocene epoch impacting the turnover of foraminifera and nannofossils and to compare these to the long-term modulation cycles in Earth's eccentricity, obliquity and insolation.

A.
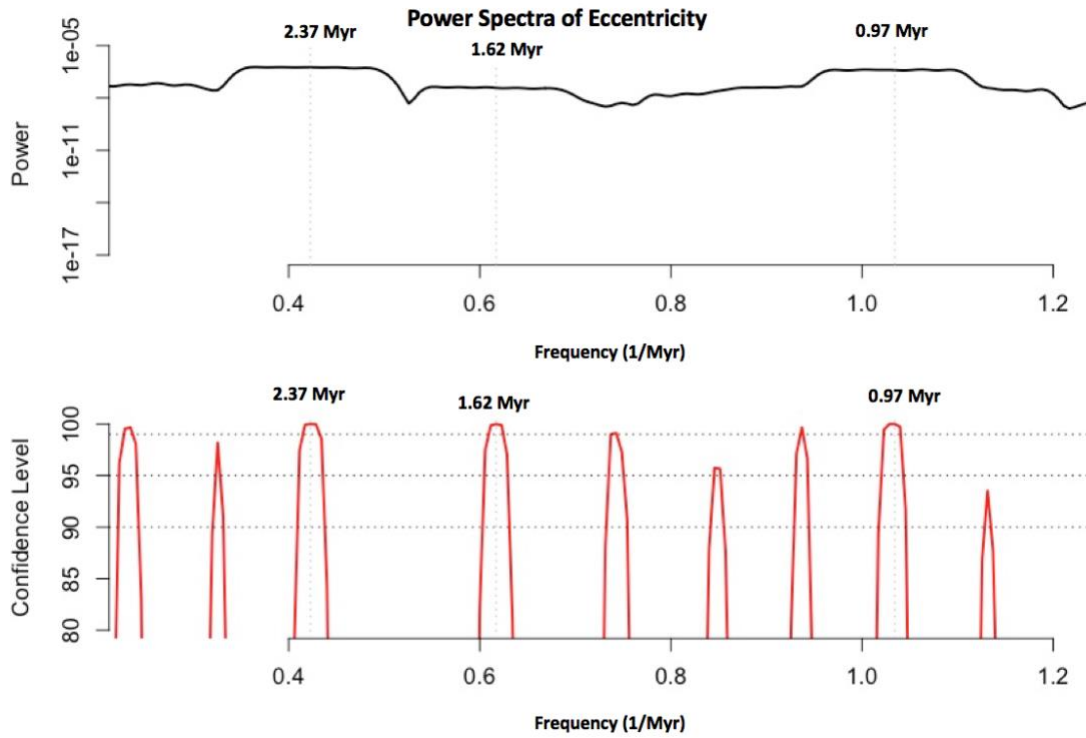
B.
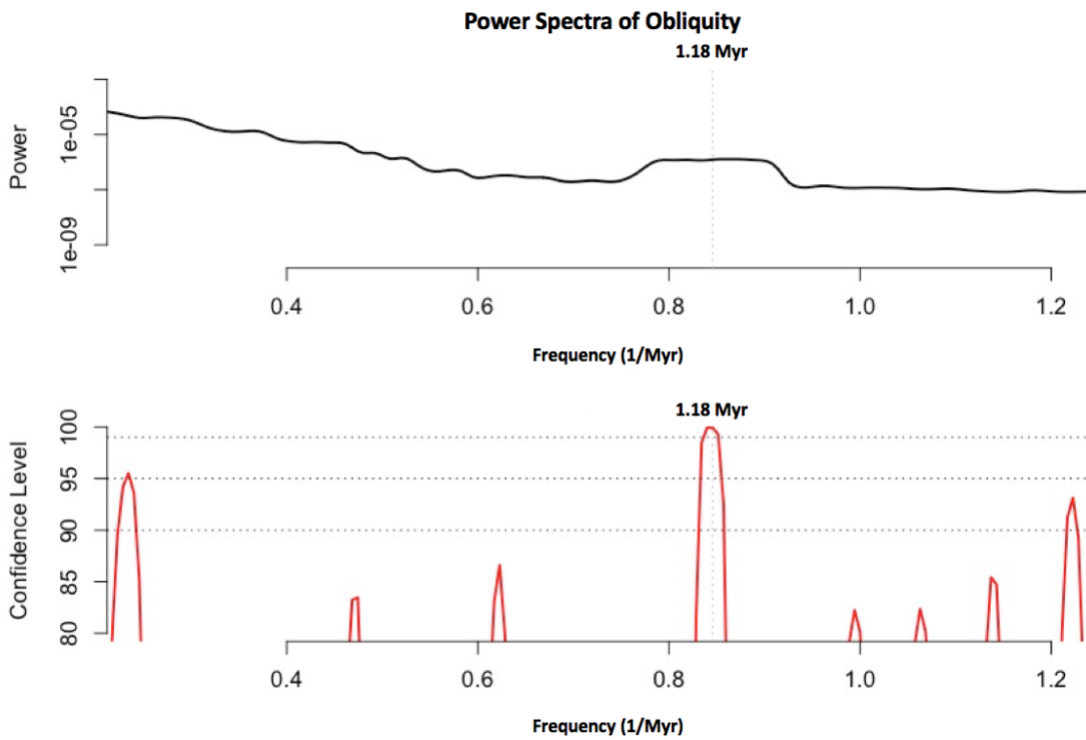
Figure 4.9 Long astronomical cycles in turnover time series using multitaper spectral analysis.

Figure 4.9 continued.

C.

Power Spectra of Insolation

D.

Power Spectra of Foraminifer Morphospecies Turnover

Figure 4.9 continued.

E.

Power Spectra of Foraminifer Lineage Turnover

F.

Power Spectra of Nannofossil species Turnover
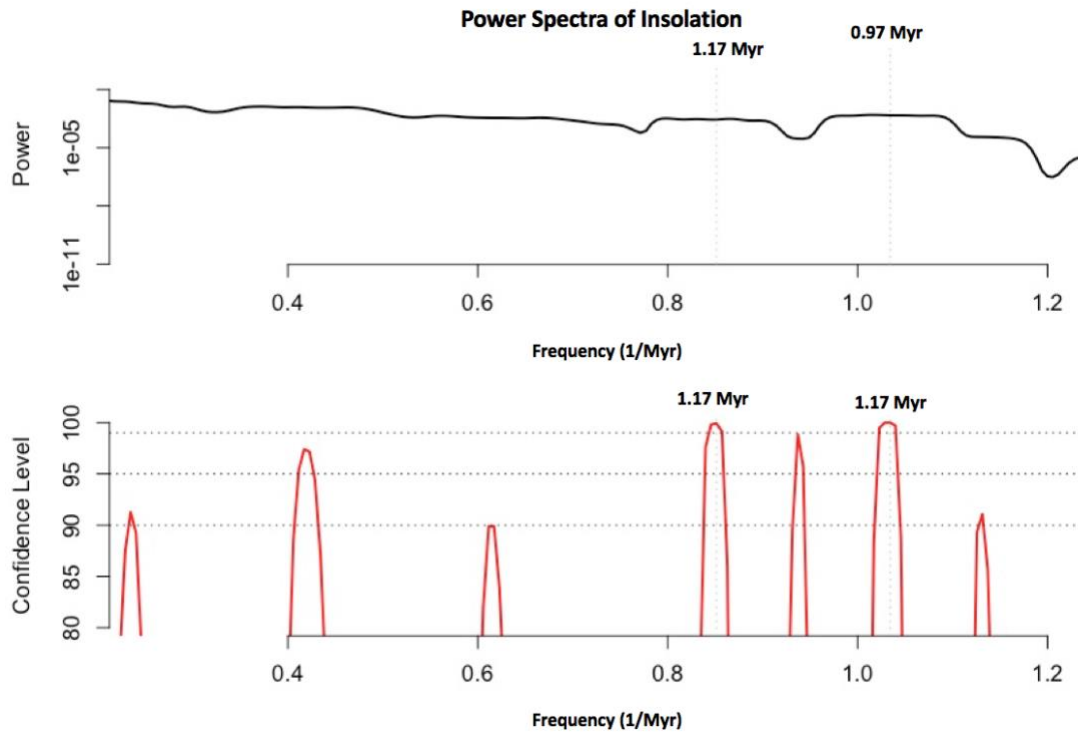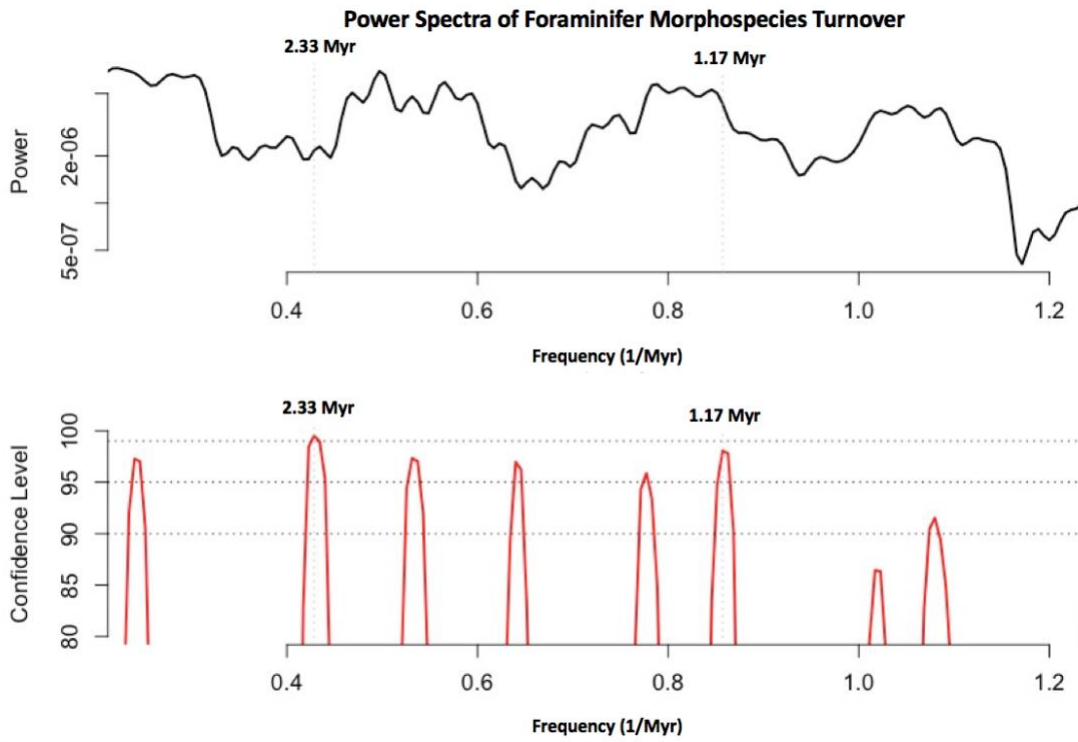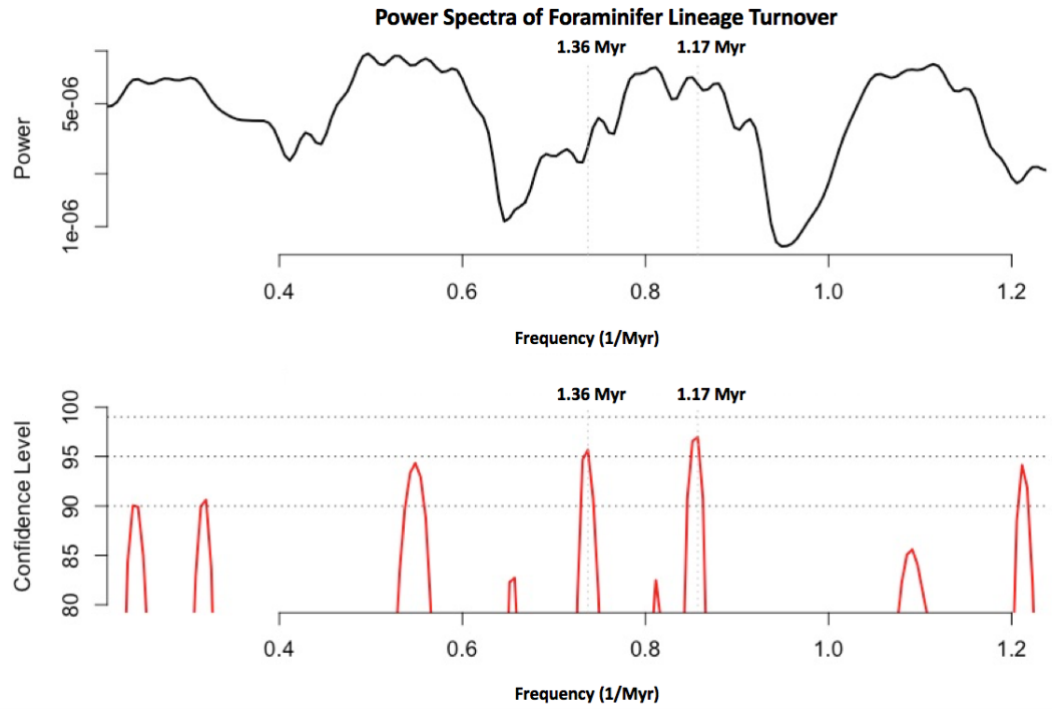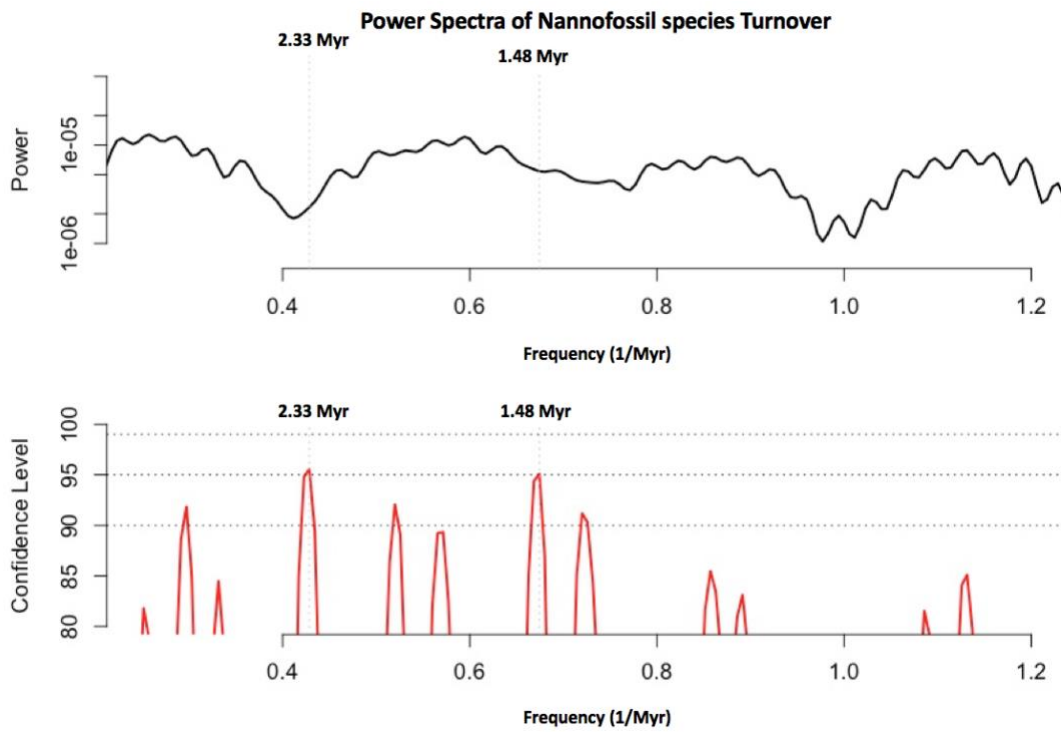
The spectral analyses indicate a ~1.17 Myr cycle in foraminifer morphospecies (Figure 4.9D) and lineage (Figure 4.9E) turnover that match with the well-studied ~1.2 Myr long astronomical cycle (Table 4.1). The 1.17 Myr cycle is possibly related to the 0.97 Myr cycle in modulation of eccentricity (Figure 4.9A), the 1.18 Myr cycle in modulation of obliquity (Figure 4.9B) and the 1.17 Myr cycle in insolation (Figure 4.9C). We also found a 2.33 Myr cycle in foraminifer morphospecies (Figure 4.9D) and nannofossil (Figure 4.9F) turnover data. The 2.33 Myr cycle is related to the 2.37 Myr cycle found in modulation of eccentricity. Therefore, we can conclude that evolutionary turnover of foraminifer and nannofossils are astronomically forced as these rotations cause climatic changes.

4.5 Conclusion

We compiled the evolutionary range of each of planktonic forams and nannofossil species and calculated the temporal speciation and extinction events. Interestingly, such speciation and extinction events also show similar periodicity which are believed to be produced by the amplitude modulation of various Milankovitch cycles.

The main contributions are:

 (a) Comprehensive tables (Table A1, Table A2, Table A3, Table A4, Table A5, Table A6) enlisting speciation, extinction and turnover events for every 100 kyr for Cenozoic macroperforate planktonic foraminifer morphospecies and lineages with their First Appearance Datum (FAD), Last Appearance Datum (LAD), lifespan grouped by family, genus, morphogroup end ecogroup.

(b) Speciation, extinction and turnover for every 100 kyr for foraminifer lineages (Table A8, Table A9, Table A10) with FAD, LAD, lifespan grouped by morphogroup end ecogroup.

(c) Speciation, extinction and turnover for every 100 kyr for nannofossils (Table A11, Table A12) with FAD, LAD, lifespan grouped by family, genus.

(d) Relationship of speciation, extinction, turnover of foraminiferal morphospecies (Table A7) and nannofossils (Table A13) with marine Oxy-18 cold events induced by Milankovitch cycles.

(e) Investigation of grand cycles in fossil turnover data and further evidence for climate-turnover hypothesis.

4.6 References

Abels, H.A., Aziz, H.A., Krijgsman, W., Smeets, S.J. and Hilgen, F.J., 2010. Long-period eccentricity control on sedimentary sequences in the continental Madrid Basin (middle Miocene, Spain). Earth and Planetary Science Letters, 289(1-2), pp. 220-231. https://doi.org/10.1016/j.epsl.2009.11.011.

Aze, T., Ezard, T.H., Purvis, A., Coxall, H.K., Stewart, D.R., Wade, B.S., et al., 2011. A phylogeny of Cenozoic macroperforate planktonic foraminifera from fossil data. Biological Reviews of the Cambridge Philosophical Society. 86(4), pp. 900-27. https://doi.org/10.1111/j.1469-185X.2011.00178.x.

Bergen, J.A., de Kaenel, E., Blair, S.A., Boesiger, T.M. and Browning, E., 2017. Oligocene-Pliocene taxonomy and stratigraphy of the genus Sphenolithus in the circum North Atlantic Basin: Gulf of Mexico and ODP Leg 154. Journal of Nannoplankton Research, 37(2-3), pp. 77-112.

Bergen, J.A., Truax, S., de Kaenel, E., Blair, S., Browning, E., Lundquist, J., Boesiger, T., Bolivar, M., Clark, K., 2019. BP Gulf of Mexico Neogene Astronomically-tuned Time Scale (BP GNATTS). Bulletin of the Geological Society of America, 131(11-12), pp.1871-1888. https://doi.org/10.1130/B35062.1.

Blair, S., Bergen, J., de Kaenel, E., Browning, E., and Boesiger, T., 2017, Upper Miocene-Lower Pliocene taxonomy and stratigraphy in the circum North Atlantic Basin: Radiation and extinction of Amauroliths, Ceratoliths, and the *D. quinqueramus* lineage: Journal of Nannoplankton Research, 37(2-3), pp. 113–144.

Boesiger, T., de Kaenel, E., Bergen, J., Browning, E., and Blair, S., 2017, Oligocene to Pleistocene taxonomy and stratigraphy of the genus *Helicosphaera* and other placolith taxa in the circum North Atlantic Basin. Journal of Nannoplankton Research, 37(2-3), pp. 145–175.

Boulila, S., Brange, C., Cruz, A.M., Laskar, J., Gorini, C., Reis, T. Dos, Silva, C.G., 2020 (in press). Astronomical pacing of Late Cretaceous third- and second-order sea-level sequences in the Foz do Amazonas Basin. Marine and Petroleum Geology. 117, article #104382 (in press). https://doi.org/10.1016/j.marpetgeo.2020.104382.

Boulila, S., Galbrun, B., Hinnov, L.A., Collin, P.Y., Ogg, J.G., Fortwengler, D. and Marchand, D., 2010. Milankovitch and sub-Milankovitch forcing of the Oxfordian (Late Jurassic) terres noires formation (SE France) and global implications. Basin Research, 22(5), pp. 717-732. https://doi.org/10.1111/j.1365-2117.2009.00429.x.

Boulila, S., Galbrun, B., Laskar, J., Pälike, H., 2012. A ~9myr cycle in Cenozoic δ 13C record and long-term orbital eccentricity modulation: Is there a link? Earth and Planetary Science Letters, 317, pp. 273-281. https://doi.org/10.1016/j.epsl.2011.11.017.

Boulila, S., Galbrun, B., Miller, K.G., Pekar, S.F., Browning, J. V., Laskar, J., Wright, J.D., 2011. On the origin of Cenozoic and Mesozoic "third-order" eustatic sequences. Earth-Science Reviews. 109, pp. 94–112. https://doi.org/10.1016/J.EARSCIREV.2011.09.003.

Browning, E., Bergen, J., Blair, S., Boesiger, T., and de Kaenel, E., 2017, Late Miocene to Late Pliocene taxonomy and stratigraphy of the genus *Discoaster* in the circum North Atlantic Basin: Gulf of Mexico and ODP Leg 154. Journal of Nannoplankton Research, 37(2-3), pp. 189–214.

Cramer, B.S., Toggweiler, J.R., Wright, J.D., Katz, M.E. and Miller, K.G., 2009. Ocean overturning since the Late Cretaceous: Inferences from a new benthic foraminiferal isotope compilation. Paleoceanography, 24(4), article #PA4216, pp. 14. https://doi.org/10.1029/2008PA001683.

Crampton, J.S., Meyers, S.R., Cooper, R.A., Sadler, P.M., Foote, M. and Harte, D., 2018. Pacing of Paleozoic macroevolutionary rates by Milankovitch grand cycles. Proceedings of the National Academy of Sciences, 115(22), pp. 5686-5691. https://doi.org/10.1073/pnas.1714342115.

De Vleeschouwer, D., Vahlenkamp, M., Crucifix, M. and Pälike, H., 2017. Alternating Southern and Northern Hemisphere climate response to astronomical forcing during the past 35 my. Geology, 45(4), pp. 375-378. https://doi.org/10.1130/g38663.1.

Fordham, B.G., Aze, T., Haller, C., Zehady, A.K., Pearson, P.N., Ogg, J.G., and Wade, B.S., 2018. Future-proofing the Cenozoic macroperforate planktonic foraminifera phylogeny of Aze & others (2011). PLOS One, 13(10), article #e0204625. https://doi.org/10.1371/journal.pone.0204625.

Grippo, A., Fischer, A.G., Hinnov, L.A., Herbert, T.D. and Silva, I.P., 2004. Cyclostratigraphy and chronology of the Albian stage (Piobbico core, Italy). In: D'Argenio (Ed.) Cyclostratigraphy: Approaches and Case Histories. SEPM Spec. Pub. 81: 57–81. https://doi.org/10.2110/pec.04.81.0057.

Hays, J.D., Imbrie, J., Shackleton, N.J., 1976. Variations in the earth's orbit: Pacemaker of the ice ages. *science*, *194*(4270), pp.1121-1132. https://doi.org/10.1126/science.194.4270.1121.

Herbert, T.D., 1999. Toward a composite orbital chronology for the Late Cretaceous and Early Palaeocene GPTS. Philosophical Transactions of the Royal Society of London. Series A: Mathematical, Physical and Engineering Sciences, 357(1757), pp. 1891-1905. https://doi.org/10.1098/rsta.1999.0406.

Huang, C., Hesselbo, S.P. and Hinnov, L., 2010. Astrochronology of the late Jurassic Kimmeridge Clay (Dorset, England) and implications for Earth system processes. Earth and Planetary Science Letters, 289(1-2), pp.242-255. https://doi.org/10.1016/j.epsl.2009.11.013.

Huang, C., Hinnov, L., Fischer, A.G., Grippo, A. and Herbert, T., 2010a. Astronomical tuning of the Aptian Stage from Italian reference sections. Geology, 38(10), pp. 899-902. https://doi.org/10.1130/g31177.1.

Ikeda, M., Tada, R. and Ozaki, K., 2017. Astronomical pacing of the global silica cycle recorded in Mesozoic bedded cherts. Nature Communications, 8(1), article #15532, 9 pp. https://doi.org/10.1038/ncomms15532.

Kent, D.V., Olsen, P.E. and Muttoni, G., 2017. Astrochronostratigraphic polarity time scale (APTS) for the Late Triassic and Early Jurassic from continental sediments and correlation with standard marine stages. Earth-Science Reviews, 166, pp. 153-180. https://doi.org/10.1016/j.earscirev.2016.12.014.

Kocken, I.J., Cramwinckel, M.J., Zeebe, R.E., Middelburg, J.J., Sluijs, A., 2019. The 405 kyr and 2.4 Myr eccentricity components in Cenozoic carbon isotope records. Climate of the Past, 15(1), pp. 91–104. https://doi.org/10.5194/cp-15-91-2019.

Laskar, J., Fienga, A., Gastineau, M., Manche, H., 2011. La2010: A new orbital solution for the long term motion of the Earth. *Astronomy & Astrophysics*, 532, article #A89, 15 pp. https://doi.org/10.1051/0004-6361/201116836.

Laskar, J., Robutel, P., Joutel, F., Gastineau, M., Correia, A.C.M., Levrard, B., 2004. A long-term numerical solution for the insolation quantities of the Earth. *Astronomy & Astrophysics*, *428*(1), pp.261-285. https://doi.org/10.1051/0004-6361:20041335.

Lourens, L.J., Sluijs, A., Kroon, D., Zachos, J.C., Thomas, E., Röhl, U., Bowles, J. and Raffi, I., 2005. Astronomical pacing of late Palaeocene to early Eocene global warming events. *Nature*, *435*(7045), pp.1083-1087. https://doi.org/10.1038/nature03814.

Ma, C., Meyers, S.R. and Sageman, B.B., 2017. Theory of chaotic orbital variations confirmed by Cretaceous geological evidence. Nature, 542(7642), pp.468-470. https://doi.org/10.1038/nature21402.

Martinez, M. and Dera, G., 2015. Orbital pacing of carbon fluxes by a~ 9-My eccentricity cycle during the Mesozoic. Proceedings of the National Academy of Sciences, 112(41), pp. 12604-12609. https://doi.org/10.1073/pnas.1419946112.

Meyers, S.R., 2014. Astrochron: An R package for astrochronology.

Muttoni, G., Kent, D.V., Olsen, P.E., Stefano, P.D., Lowrie, W., Bernasconi, S.M. and Hernández, F.M., 2004. Tethyan magnetostratigraphy from Pizzo Mondello (Sicily) and correlation to the Late Triassic Newark astrochronological polarity time scale. Geological Society of America Bulletin, 116(9-10), pp. 1043-1058. https://doi.org/10.1130/b25326.1.

Sprovieri, M., Sabatino, N., Pelosi, N., Batenburg, S.J., Coccioni, R., Iavarone, M. and Mazzola, S., 2013. Late Cretaceous orbitally-paced carbon isotope stratigraphy from the Bottaccione Gorge (Italy). Palaeogeography, Palaeoclimatology, Palaeoecology, 379, pp. 81-94. https://doi.org/10.1016/j.palaeo.2013.04.006.

Thomson, D.J. and Fitzgerald, W., 2000. Multitaper analysis of nonstationary and nonlinear timeseries data. Nonlinear and nonstationary signal processing, pp.317-394.

Thomson, D.J., 1982. Spectrum estimation and harmonic analysis. Proceedings of the IEEE, 70(9), pp.1055-1096.

Turco, E., Hilgen, F.J., Lourens, L.J., Shackleton, N.J., Zachariasse, W.J., 2001. Punctuated evolution of global climate cooling during the Late Middle to Early Late Miocene: High-resolution planktonic foraminiferal and oxygen isotope records from the Mediterranean. Paleoceanography 16, pp. 405–423. https://doi.org/10.1029/2000PA000509.

Valero, L., Garcés, M., Cabrera, L., Costa, E. and Sáez, A., 2014. 20 Myr of eccentricity paced lacustrine cycles in the Cenozoic Ebro Basin. Earth and Planetary Science Letters, 408, pp. 183-193. https://doi.org/10.1016/j.epsl.2014.10.007.

Van Dam, J.A., Aziz, H.A., Sierra, M.Á.Á., Hilgen, F.J., van den Hoek Ostende, L.W., Lourens, L.J., Mein, P., van Der Meulen, A.J. and Pelaez-Campomanes, P., 2006. Long-period astronomical forcing of mammal turnover. Nature, 443(7112), pp. 687-691. https://doi.org/10.1038/nature05163.

Westerhold, T., Röhl, U. and Laskar, J., 2012. Time scale controversy: Accurate orbital calibration of the early Paleogene. Geochemistry, Geophysics, Geosystems, 13(6). Article # Q06015, 19 pp. https://doi.org/10.1029/2012gc004096.

CHAPTER 5. EFFECT OF CLIMATE CHANGE ON CULTURAL TURNOVER

Abstract

Using a global cultural event dataset, we showed that climate cooling may have an indirect, negative effect on human civilization. We provide a global cultural turnover dataset which include cultural events from various regions across the world and can be visualized in TSCreator program. Extended cooling period might have led to social conflict and dynastic changes in various regions of the world throughout the past 2000 years. Global climate cooling has been shown to be driven by ~190 yr solar cycle and similar cyclicity appeared in the spectral analysis of our cultural turnover data corroborating climate-turnover hypothesis.

5.1   Introduction

Researchers have long tried to establish causal association between climate change and social conflict. A lot of studies have shown various causal pathways by which climatic variables can be linked to resource scarcity causing violence, armed conflict or war in decadal scale and even the collapse of civilization in centennial scale. Most societies across the continents are dependent on abundant agricultural production and we know from empirical research how climate change can negatively impact land fertility and bio-productivity and damage agricultural condition. Low standard of living due to lack of access to required resources can heighten resentment in the general populace and cause social unrest, chaos, political instability in a region. Gross domestic product (GDP) as an aggregate measure of production and per capita income and food supply per capita as a measure of individual economic condition and accessibility are generally used as critical index to reflect economic health of a region. Climatic variables like temperature, precipitation, monsoonal activity have strong correlation with productivity and income which are evidences of the negative effect of climate change in short or long term. Modern complex societies tend to have higher adaptation to the climatic change and social mechanism in place to tackle shortage and deficiency in resource and handle unrest or rebellions with military power. However, feudal, agro-based, less-educated and less-connected societies in pre-industrial eras were more prone to suffer from harsh climate change. Agriculturally unfavorable periods were the times when civilizations often collapsed due to climatic influence. There are various studies showing how politically

unstable societies can experience economic downfall, violence and social disturbance even in short period of time through climate influence. Climate change is not always the primary cause of social collapse and there may be other sociopolitical reasons behind civil conflict or nomadic conquests. But climate change caused by aggressive change in temperature and precipitation can still have major influence on the intermediate variables in a lengthy causal link towards aggression, violence and the uproot of social orders.

5.2   Literature review on the effect of climatic change

Climate change due to drought caused by lower rainfall, prolonged lower temperature, intense cooling period via solar activity degrade the environment for agricultural production and may cause unavailability of food, fresh water and energy insufficiency for the population in the region. Adaptation to such drastic changes requires social stability, co-operative framework for preparatory resource storage during hazardous time, efficient market mechanism, responsible governance with political goodwill to maintain good economic condition, active military effort to combat rebellions – all of which were hard to obtain in a preindustrial feudal society. Scarcity, extreme competition and discomfort induced by climatic change most often reduce the opportunity cost to join in rebellious insurgent groups and involve in criminal activities to attack and engage in violence and armed conflict to obtain resources via selfish forceful means. Interpersonal, intergroup conflict and nomadic conquests were very frequent in human history, which caused massive change in population size, dislocation via migration. Zhang et al., 2005 has found evidence of the connection between cold climatic phases and dynastic changes when they studied the rise and fall of Chinese dynasties. They argued that the reduced thermal energy input during cold climate negatively affected land productivity and livelihood resources from the late Tang to Qing Dynasties which resulted in high frequency of conflicts and wars. Wang et al. (2010) has also shown the link between climate and the collapse of Chinese dynasties. During the prolonged cold climate like during Little Ice Age, Chinese regions experienced weak summer Asian monsoon and therefore reduced rainfall. The degradation of vegetation through the cycles of desertification resulted in the lack of food resource and caused the decline in social harmony and collapse of dynasties in ancient china. Climatic fluctuations in the monsoonal Northern China caused the geo-political shifts via collapse of various dynasties over the past 2200 years. Climate variables such

119

as fossil based precipitation index, dry-wet index, drought index, extreme flood or drought years alongside economic variables such as famine index, grain price index and geo-political variables such as number of wars, peasantry uprising frequency, famine index (Li et al., 2017) have been used to reach the conclusion that the socio-economic change was triggered by climatic change. Zheng et al. (2014) have studied the collapse of Ming dynasty and associated the fiscal deterioration, food crisis, frequent unrest and peasantry uprising against an increasingly week military as an aftermath of intense droughts in 1627-1643 AD with extreme alteration in temperature, precipitation data. Climatic and dynastic data set (Chen, 2015) from China dating from 221 BCE were used to measure the likelihood of nomadic conquest as a result of low rainfall and drought. This result matches with the study on economic shock and civil conflict in Africa by Miguel et al. (2004). It was shown that there are negative effects of high temperature on economic development in poor countries throughout the last half-century in the climate change and economic growth study (Dell et al., 2008). They found no effect of precipitation whereas a causal link has been shown between China's mean precipitation and frequency of aggression, geo-political (Zhang et al., 2011; prior studies: Zhang et al., 2005, 2006, 2015). They also found that the short-term geopolitical changes are not caused by climate change. They investigated the periods of harmony and crisis in the northern hemisphere (NH) during the past millennium and associated European temperature anomaly, NH temperature anomaly with NH annual population growth rate and deadly epidemic events (malaria, plague, typhus, measles, smallpox, and dysentery) and the number of wars. Collier and Hoeffler (2004) argued that the difference between the earnings from joining armed rebellion relative to peaceful conventional employment such as farming can strongly indicate the probability of occurrence of civil wars and dynastic collapses. Therefore, climate change undeniably opens the intermediate causal channels that we will explore now.

5.3   Human culture and temperature datasets

Most studies focused on local regions or a short timeframe in the history due to the unavailability of reliable data on a global level collected from multiple regions in all the continents. However, in our study, we have used a global civilization dataset from our *TimeScale Creator* datapack suits which encompasses all the regions around the continents over last 2000 years to

emphasize the claim that climate change, specifically global cooling, directly or indirectly intrigue cultural and dynastic turnovers.

Global cultural turnover data for every 50 years (Figure 5.9) was extracted from the block and event column data of the Human Culture datapack for the entire Holocene epoch (0 to ~12 Ka) available from our *TimeScale Creator* datapack webpage[5]. This datapack contains "human culture" intervals (ca. 200 columns), plus climate signal from Greenland ice cores (Seierstad et al., 2014). Figure 5.1 through Figure 5.8 show the cultural intervals representing historical events on the SVG canvas of our *TimeScale Creator* visualization software. The event time series of Figure 5.9 was collected from all these regional event data and the methods section describe the procedure behind the event counting process. We tabulated the reconstructed temperature time series data in Table 5.1. Northern Hemisphere (NH) temperature anomaly (Figure 5.10) from 0 to 1973 AD is collected from Christiansen and Charpentier (2012). This is a multi-proxy temperature [°C] reconstruction time series, extracted from 91 records. About 30% of the proxy time series cover the entire timeframe with 1-year resolution. The second temperature reconstruction data (Figure 5.11) was extracted from over thousand tree-ring width series of central Europe (Büntgen et al., 2011). This covers the timeframe from -499 BC to 2003 AD with 1 year resolution. The third temperature reconstruction data (Figure 5.12) was generated from 59 proxy records from various Arctic (60°-90° N) regions (McKay and Kaufman, 2014). About 20% of them cover the whole period from 1 to 2000 AD with 1-year resolution. And lastly, the Human Culture datapack comes with the $\delta_{18}O$ temperature-proxy.

[5] https://timescalecreator.org/datapack/datapack.php

Table 5.1. List of temperature reconstruction data

	Dataset (source)	Duration	Resol.	Region
1.	Temperature Anomaly (Büntgen et al., 2011)	1-1990 AD	1 yr	Central Europe
2.	Stacked (91 proxies) Temperature Anomaly (Christiansen et al., 2012)	0-1973 AD	1 yr	Northern Hemisphere
3.	Tree-ring based temperature reconstruction using RCS (Regional Curve Standardization) method (D'Arrigo et al., 2006)	713-2004 AD	1 yr	Northern Hemisphere
4.	$\delta_{18}O$ temperature-proxy from ice core (Seierstad et al., 2014).	0 – 122 Ka. *(0-2000 AD used in this study)*	60 yr	Northern Greenland
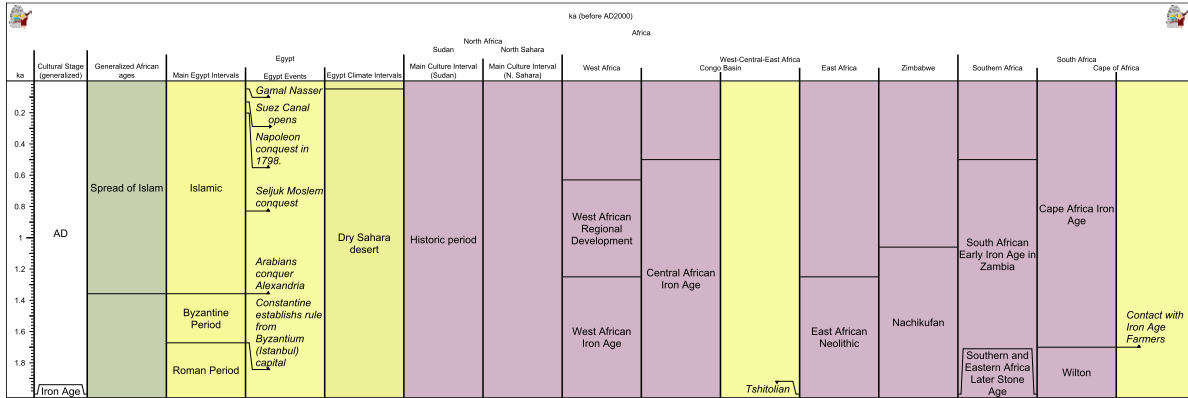
Figure 5.1. Events in Africa during the past 2 thousand years. This diagram is to show how African cultural event blocks can be visualized in TSCreator program and the texts inside are not meant to be read.
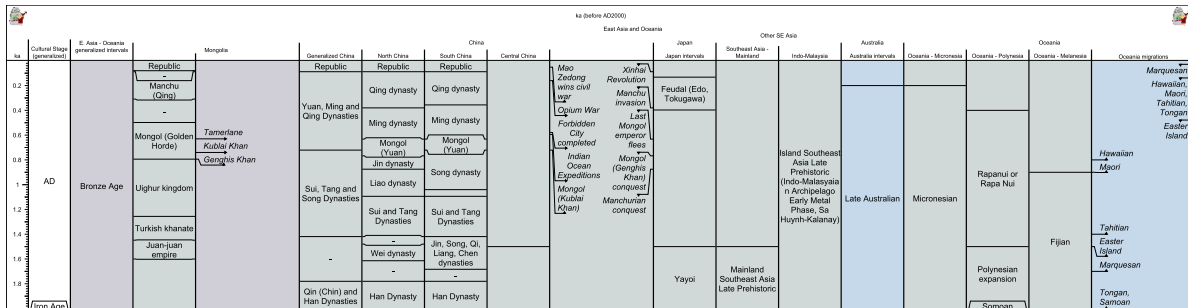
Figure 5.2. Events in the region of East Asia and Oceania during the past 2 thousand years. This diagram is to show how those event blocks can be visualized in TSCreator program and the texts inside are not meant to be read.
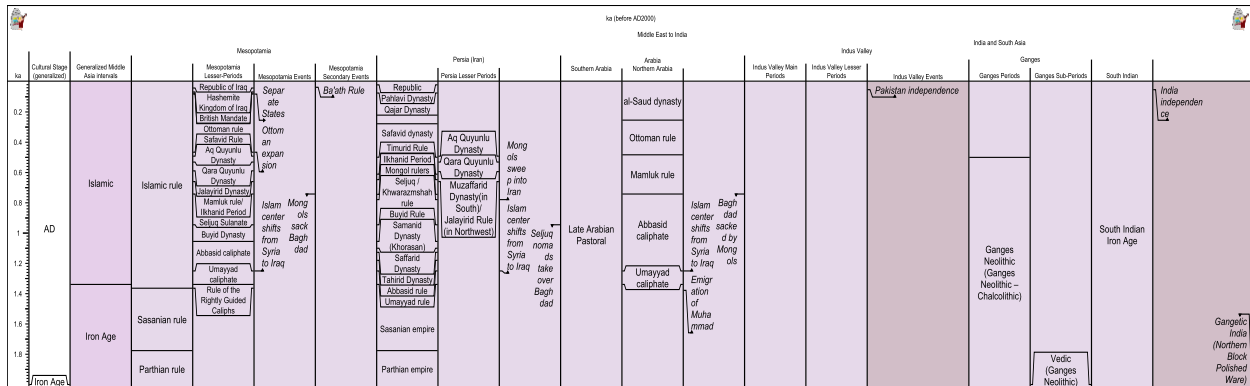
Figure 5.3. Events in Middle eastern and Indian region during the past 2 thousand years. The Indian region events are missing many details of the history of Indian subcontinent. This diagram is to show how those event blocks can be visualized in TSCreator program and the texts inside are not meant to be read.
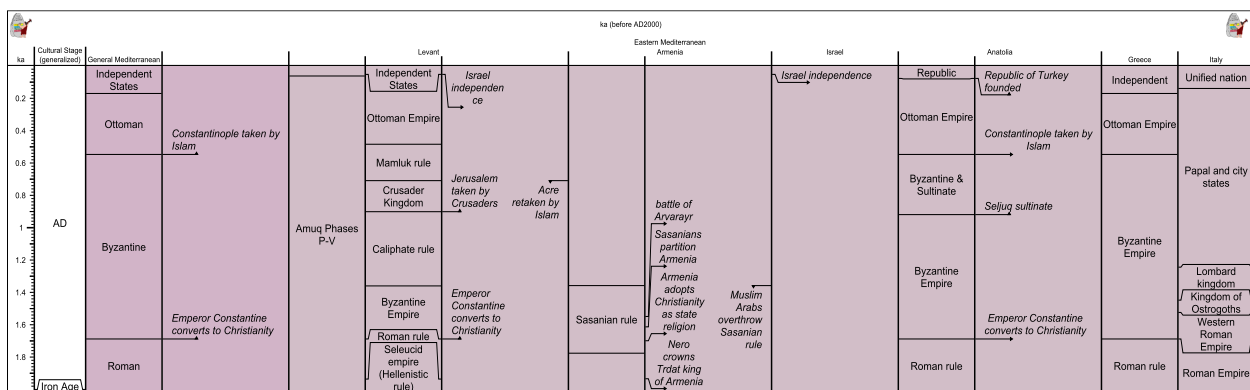
Figure 5.4. Events in European region during the past 2 thousand years. This diagram is to show how those event blocks can be visualized in TSCreator program and the texts inside are not meant to be read.

ka (before AD2000)

Arctic and Subarctic

| | | | Siberia-Baikal | Amur, Northeast Asia | | Alaska | | | |
ka	Cultural Stage (generalized)	Arctic overview	Siberia	Amur	Central Kamchatka	Alaska - North	Alaska - East	Alaska - South	Alaska - West
0.2							Eskimo, Athapaskan		
0.4									
0.6			Siberian Protohistoric						
0.8					Old Itel'men				Thule
1	AD	Thule						Norton	
1.2									
1.4									
1.6				Amur Neolithic and Bronze					
1.8			Siberian Neolithic and Bronze						
	Iron Age								
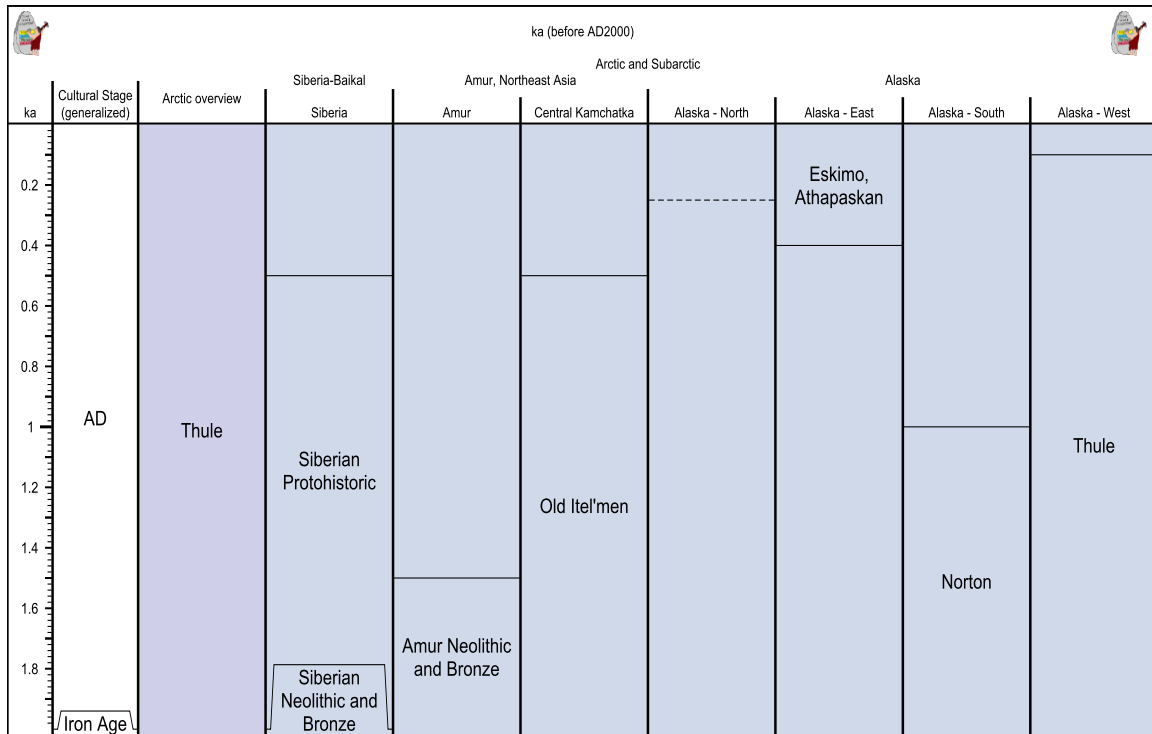
Figure 5.5. Events in Arctic and Sub-arctic regions during the past 2 thousand years.

ka (before AD2000)

Northwest and Canada

ka	Cultural Stage (generalized)	Northwest and Canada - Eastern Subarctic	Northwest and Canada - Coastal	Northwest and Canada - Western Subarctic	Northwest and Canada - Southern Subarctic
0.2		Inuit, Athapaskan			
0.4					
0.6			Late Northwest Coast (Developed Northwest Coast, Late Pacific, Late Prehistoric, Late Marine)	Proto-Athapaskan (Late Northern Archaic, Late Taltheilei in East, Athapaskan, Dene)	
0.8					
1	AD				Initial Shield Woodland
1.2					
1.4					
1.6			Middle Northwest Coast		
1.8					
	Iron Age			Northwest Microblade	

Figure 5.6. Events in Northwest and Canada during the past 2 thousand years.

124

Figure 5.7. Events in North American region during the past 2 thousand years. This diagram is to show how North American event blocks can be visualized in TSCreator program and the texts inside are not meant to be read.

Figure 5.8. Events in Middle and South American region during the past 2 thousand years. This diagram is to show how Middle and South American event blocks can be visualized in TSCreator program and the texts inside are not meant to be read.

Cultural turnover of 0-2 Ka

Figure 5.9. Cultural turnovers across continents during the past 2000 yr (0 to 2 Ka) .

Stack of different temperature of Northern Hemisphere
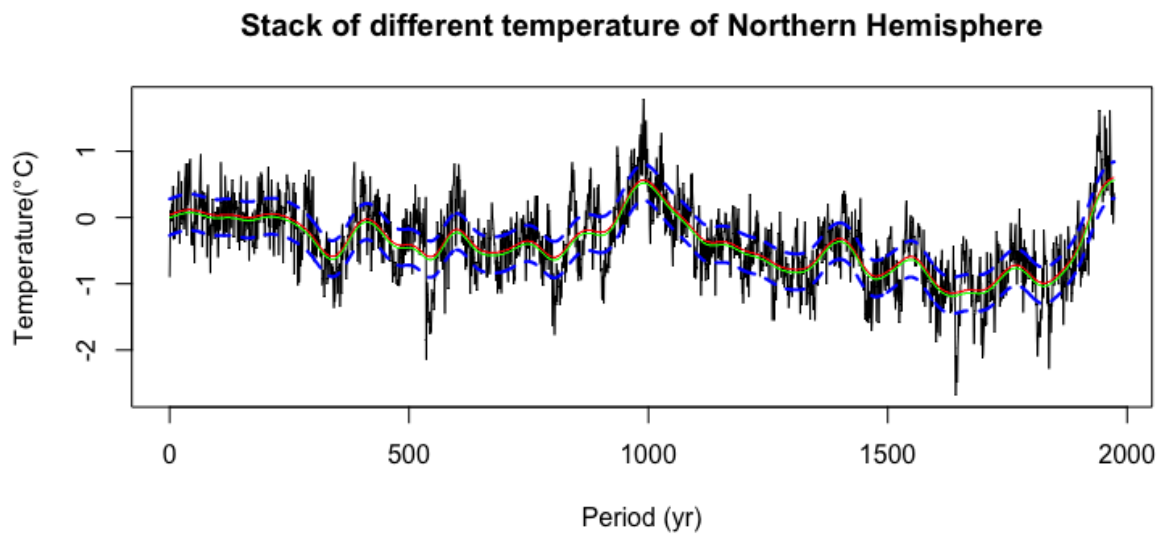
Figure 5.10. Northern hemisphere temperature reconstruction records (Christiansen et al., 2012) as anomalies around the mean in 0-2 Ka timeframe.

126

Büntgen et al.2017: temperature anomaly
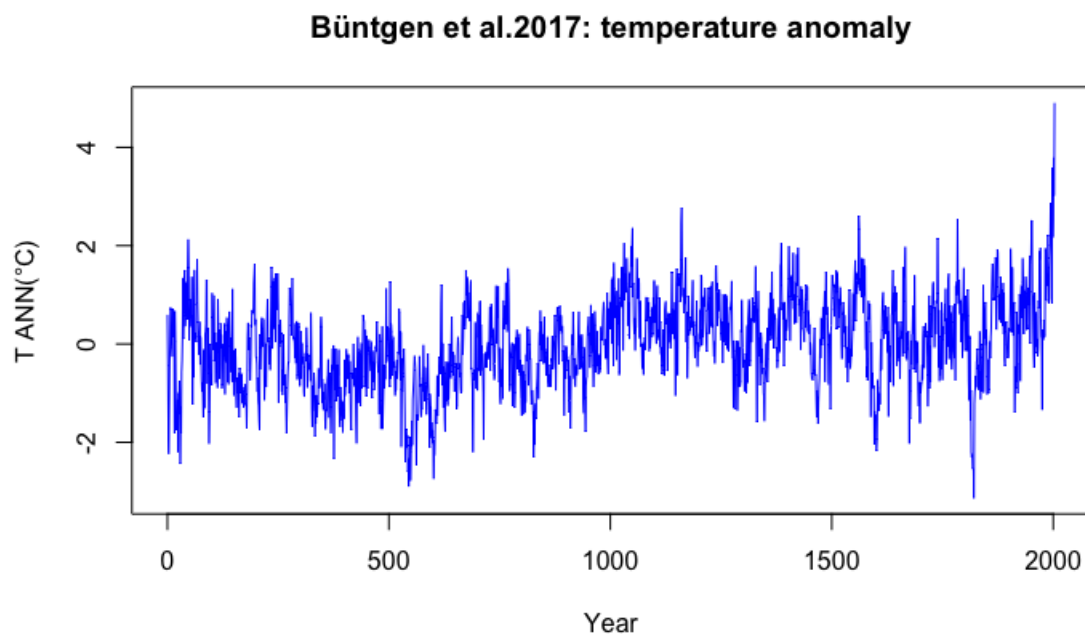
Figure 5.11. Tree-ring based Northern hemisphere temperature reconstruction records (D'Arrigo et al., 2006) as anomalies around the mean in 0-2 Ka timeframe.

Stack of different Arctic temperature proxies
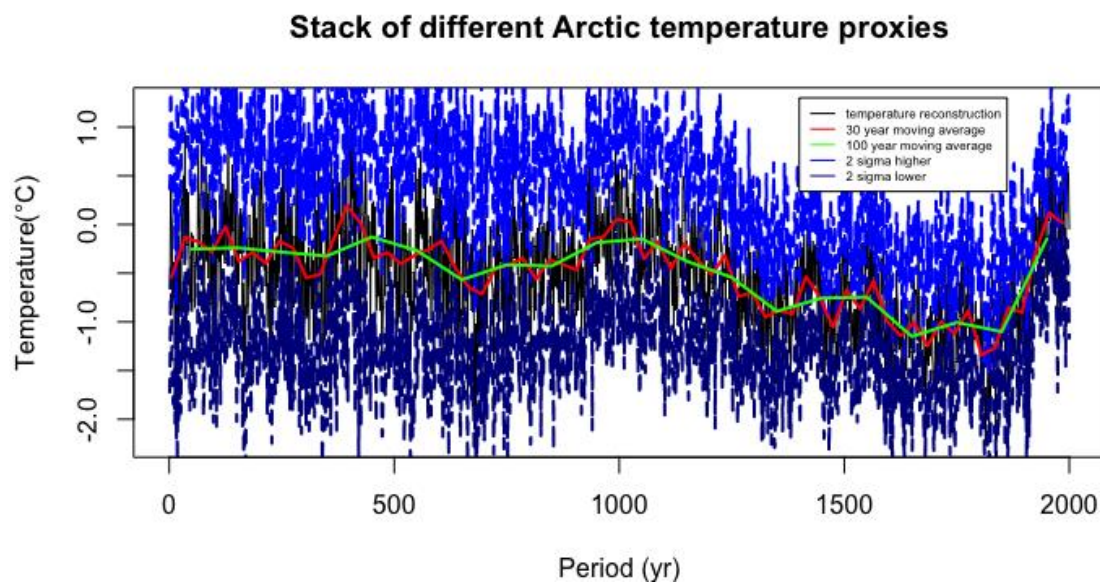
Figure 5.12. Arctic temperature reconstruction records (McKay, N.P., Kaufman, D.S., 2014) as anomalies around the mean in 0-2Ka timeframe. 30 year and 100 year moving averages are shown in red and green. The upper light blue and lower dark blue curve represents 2 standard deviation from the mean.
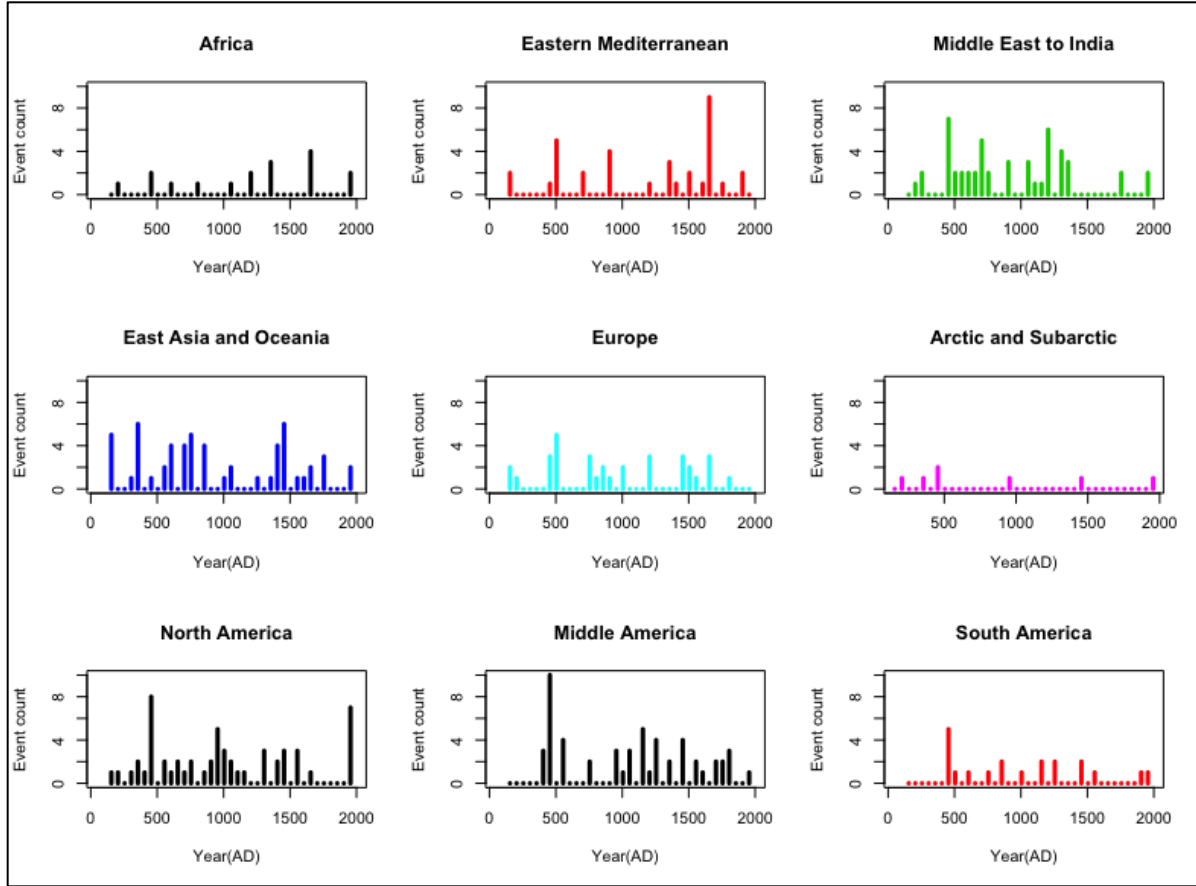
Figure 5.13. Number of cultural turnover events for nine geographical regions in 0-2Ka timeframe. Regional turnover events are calculated by sliding a 50 year time window throughout the entire timeframe for each regional event column shown in Figure 5.1-Figure 5.8. The bars are positioned at the center of every 50 year window showing the number of cultural events in that window for that region in each panel.

5.4 Methods

The goal of this project is to find correlation between global cultural turnover and reconstructed global temperature data for last 2000 years. We have decided to choose only the last 2000 years of reliable historical data even though our cultural datapack includes events for 10,000 years. We know that temperature fluctuates a lot region-by-region and it's hard to find accurate temperature reconstruction as we go back in time. However, a global temperature can be approximately estimated by taking average of regional temperatures and can tell us whether the Earth was going through a warmer or a cooler phase. An averaged Northern Hemispheric (NH) temperature or central European temperature anomaly can provide a general idea about cooler or

128

warmer global environment during certain periods of the recent Earth history. Therefore, we used the northern hemisphere temperature anomaly (Figure 5.10, Figure 5.11) and also arctic temperature reconstruction data (Figure 5.12). The Human Culture datapack also includes Oxygen-18 values (yellow line in Figure 5.14) that negatively correlate with temperature. It also comes with historic data columns, which places the historic event information under each of the regional columns. There are mainly two types of columns: (a) block column where a single block of event represents a historical zone with top and base age timeline, (b) event column where events are shown with arrows (Figure 5.1–Figure 5.8). The event column shows specific kind of arrows: (a) upward arrow for the beginning of an event alternatively called as First Appearance Data (FAD), (b) downward arrow for the end of an event alternatively called as Last Appearance Data (LAD), (c) regular arrow for events with short timeframe narrowed down by historians to a specific age. We determine the frequency of global events by counting the number of top or base age timelines or the occurrences of LAD, FAD or regular event arrows in every 50 years from the present (0 Ka) until 2 Ka (thousand years ago) for this study. Changes of civilization in a specific geologic region happen in a sequential way with the rise of the new dynasty after the uprooting the previous ones. Global cultural turnover (Figure 5.9) is thus defined as the number of historical events (count of base lines) from all the regional columns during a certain time period (50 years in this case). Regional and global cultural turnover event numbers are provided in Table A14. We also collected region wise cultural turnover data that we can see in Figure 5.13 to compare the differences in cultural turnover by regions. Our datapack definitely has limitations as we only include significant cultural and historical events. Some event ages are rounded to the nearest century causing precision loss in age values and therefore, certain time periods may include more data points than others. We notice that the frequencies of cultural turnover in different regions are different in different time periods (Figure 5.13), which possibly reflects migration and dispersion of human beings and many other possible historic events.

To perform Fourier analysis (See Methods in section 4.3) to detect periodicity in our data, we converted the non-stationary cultural turnover time series data into a weak stationary time series. Weak stationary time series has the property that the mean and autocovariance does not change with time. Therefore, each of the temperature anomaly record and cultural turnover time series was demeaned, detrended by subtracting residuals after performing linear regression and then filtered with Hanning moving average and tapered (10%) with cosine window to reduce the effect

of the terminations of data at both ends. Then we applied Fast Fourier Transform (Muller, R.A. and MacDonald, G.J., 2002) to get power spectra and obtain the periodogram using the frequency and period. We consider the frequency and the periods to be significant when they have high spectral power after smoothing the power spectra. We also used the "Astrochron" R package to perform the multi-taper spectral analysis to find statistically significant frequencies using their harmonic F-test. Astrochron provides multiple methods for robust background noise estimation and statistical significance of the peaks including lag-1 autocorrelation. REDFIT spectral analysis is also used from Past3[6] software which gives significance lines.

5.5   Results and Discussion

Our first approach was to measure correlation between cultural turnover and temperature. If we take correlation for the entire timeframe 0-2000 AD, we don't find any significant correlation. But then we have changed the length of the time series to observe the effect. If we take the first 500, 1000 or 1500 years, we can see clear negative correlation. However, adding the last 400 or 500 years reduce the correlation (Table 5.2). This possibly means that the modern societies have evolved to tackle better against climatic influences with the development of tools and technologies.

Table 5.2. Correlation between temperature anomaly and cultural turnover for timeframe with different length (500, 1000, 1500, 1900, 2000 years) starting from 0 AD

	0-500 AD	0-1000 AD	0-1500 AD	0-1900 AD	0-2000 AD
NH Temp Anomaly (°C)	-0.22	-0.29	-0.25	-0.13	-0.08
CE Temp Anomaly (°C)	-0.33	-0.27	-0.20	0.01	0.02
NGRIP Oxy 18	-0.35	-0.36	-0.30	-0.07	0.04

We also wanted to see whether there are any lag in the effect of global temperature variation. Table 5.3 shows lagged correlation with different lag values and again we find some significant negative correlation for 150 – 300 year lag. This also points towards cyclicity or periodicity that we explored later using Fourier spectral analysis.

[6] http://folk.uio.no/ohammer/past/

Table 5.3. Lagged correlation between temperature anomaly and cultural turnover.

Lag (year)	50	100	150	200	250	300	350	400	450	500
NH Temp Anomaly (°C)	0.04	-0.10	-0.16	-0.19	-0.17	-0.21	-0.08	0.13	0.37	0.07
CE Temp (°C)	0.07	0.00	-0.36	-0.05	0.06	-0.13	0.42	-0.07	-0.27	0.08
NGRIP Oxy 18	0.16	0.16	-0.08	-0.30	-0.09	-0.10	0.05	0.32	0.19	-0.04

We now take a look at specific periods when the cultural turnover frequency peaked. The rectangular boxes in Figure 5.14 indicate five global climate cooling phases when we can see clear spikes in cultural turnover data. The Current Warm Period (CWP) is easily detected by the high temperature value in the Figure 5.14 (bottom). Little Ice Age (LIA) occurred just after the Medieval Warming Period (MWP) extending from the 16th to the 19th century. Before that, human civilization experienced the wrath from the Dark Ages Cold Period (DACP). However, the LIA caused the greatest deal of problems for life.

Table 5.4. Years with high frequency of cultural turnover. Table is sorted by the turnover number in the second column.

Year (AD)	Cultural Turnover
1525	39
1925	21
525	20
325	19
25	18
1225	15
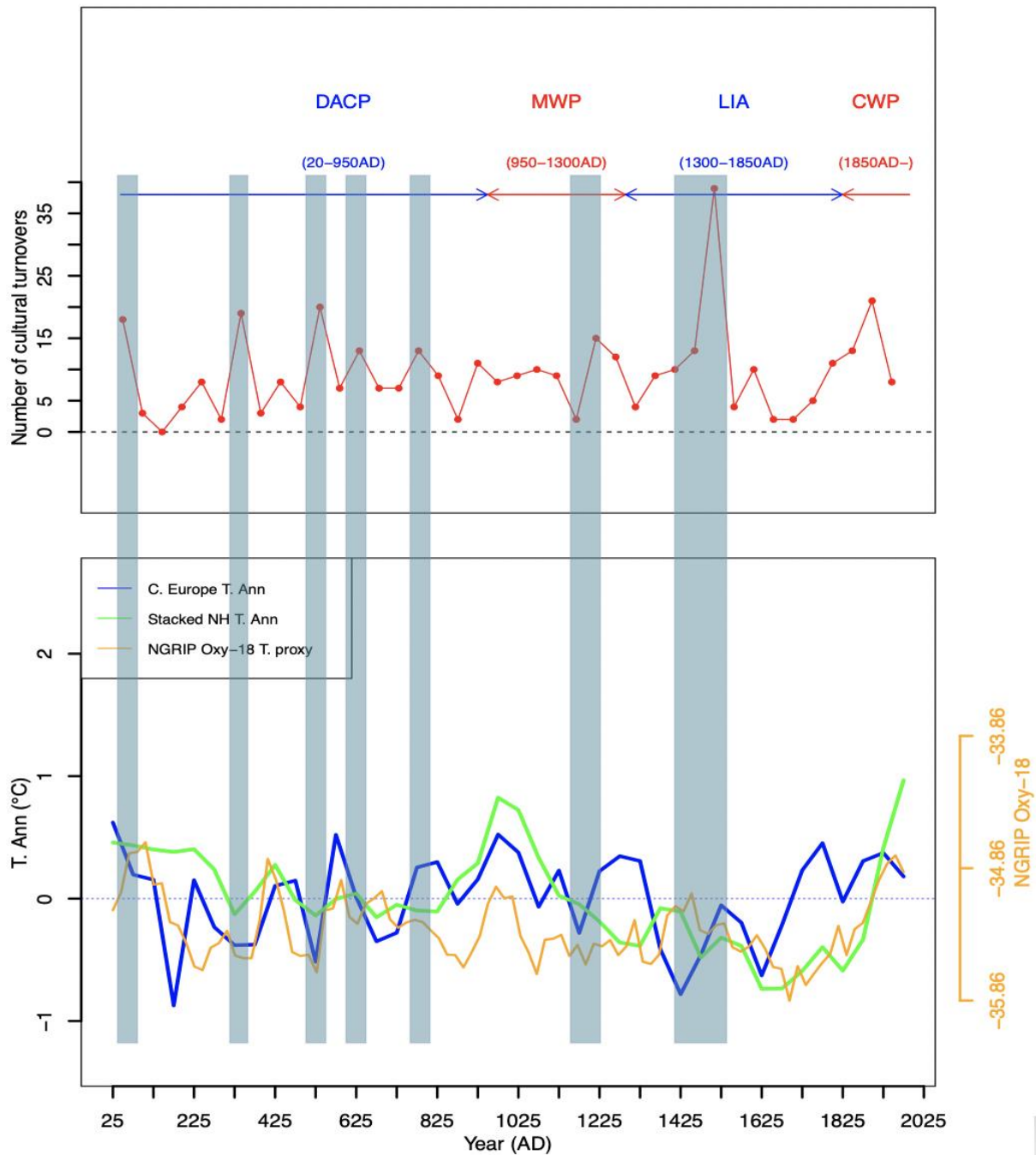
Figure 5.14. The cultural turnovers throughout the past 2000 years are plotted against the temperature data. The blueish grey rectangles show the periods when number of turnovers were higher dep illustrating a positive correlation with cooler temperature or high rate of change of temperature for cooling effect.

In Europe and North America, the Little Ice Age (LIA) caused colder winters, thereby increasing starvation leading towards famine. Many people struggled to find food due to unsuitable

environment for crop production and died because of cold. Table 5.4 shows the top 6 peaks in our data. Little Ice Age (LIA) has 39 cultural turnover events in the year 1925. It took a long time for people living during the Little Ice Age (LIA) to adapt to the environment. Farmers had to change their crops, but the lives of the people gradually improved over time. We find 20 and 19 cultural turnover events around the year 325 BP and 525 respectively during Dark Age Cold Period (DACP). Medieval warm period (MWP) has relatively low cultural turnovers indicating that human culture and civilization suffered more during the periods with cold temperature. The period 500-550 has experienced 20 cultural turnover events. The NH temperature (green line in Figure 5.14) shows that the temperature declined below zero degree around that time from a relatively high temperature in the recent past. The blue Central European temperature line in Figure 5.14 show a sharper decline in temperature. The period 1900-1950 (marked by year 1925 in Figure 5.14 and Table 5.4) in Current Warm Period (CWP) has also experienced high turnover as this is the period when the first and second world war took place. This aligns with a short span of temperature decline in the green Northern Hemispheric temperature line in Figure 5.14 (bottom). This indicates that geopolitical variables also play major role and we should not try to conclude a direct causation of global cooling behind high cultural turnover.

The sun has been shown to be a climate driver in different experiments. Earth's periodic rotation around sun determines the energy received in our planet which then dictate many factors crucial for life. The combined global temperature from temperature proxies have shown the strongest component as ~1000 yr, ~460 yr, and ~190 yr periods which are believed to have a solar origin (Lüdecke and Weiss, 2017). We have performed Fourier spectral analysis with periodogram, multitaper and evolutive harmonic analysis (EHA). R language provides spec.pgram and spec.taper, which are applied to produce the top 10 frequency, power and period shown in Table 5.5. The Fourier spectrum of our event data shows the strongest components as ~405 yr, ~150 yr, ~101 yr. This indicates some lag (~50 years) in the effect of temperature on the cultural turnover, also shown in the first column of Table 5.3. Figure 5.15 also shows the period calculated from the frequencies found in Fourier analysis. We found similar cycles, especially strong peaks around ~190 yr in the frequency/period analysis of all three reconstructed temperature data (Figure 5.16, Figure 5.17, Figure 5.18, Figure 5.19). We cross-checked our result by using PAST software tool (Figure 5.2) and multitaper methods provided in R Astrochron package (Figure 5.20). The multitaper method shows the three significant cycles of ~405 yr, ~150 yr and ~101 yr that clearly

133

matches our initial result in Table 5.5. Similar results are from Evolutive Harmonic Analysis (EHA) (Figure 5.21).

Table 5.5. Spectral analysis of cultural turnover data of 0-2 Ka

Frequency (cycle / 2Ka)	Power	Time/Period(Yr) Period = f_N * (1/Frequency)	True Frequency(1/Yr)
0.0632	45.40	400	0.0025
0.1645	31.09	154	0.0065
0.1012	29.57	250	0.004
0.0759	25.00	333.33	0.003
0.2531	19.45	100	0.01
0.1518	12.36	166.67	0.0059

*where frequency, $f_N = (2000 \text{ Yr}/ 40) / 2 = 25$

Spectral Power vs Period
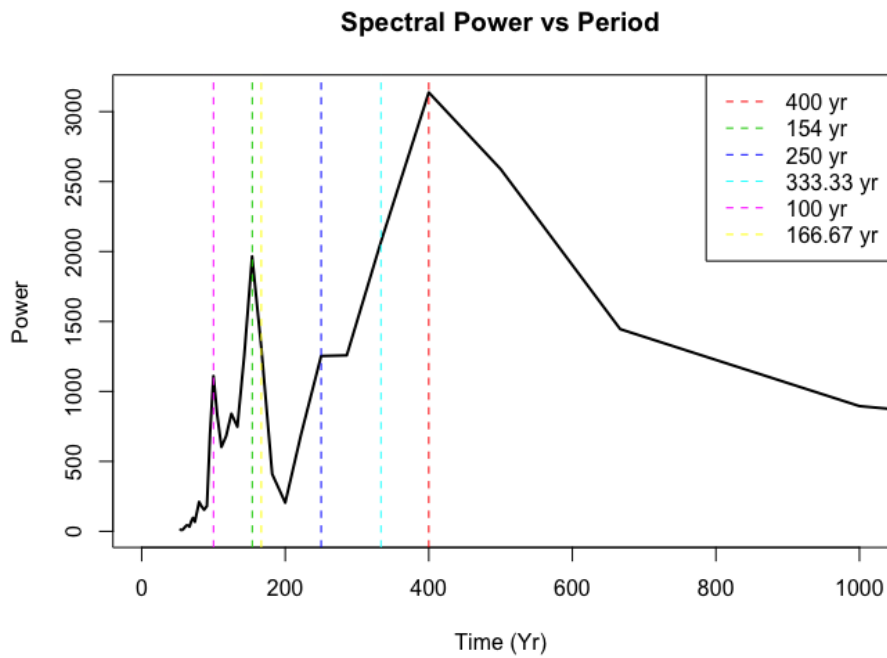
Figure 5.15 Harmonic periods found by Fourier spectral analysis on cultural turnover data. Here we show all the harmonic periods used to reconstruct the cultural turnover data in Figure 5.14, even though some frequencies don't show clear peaks in the power spectrum.
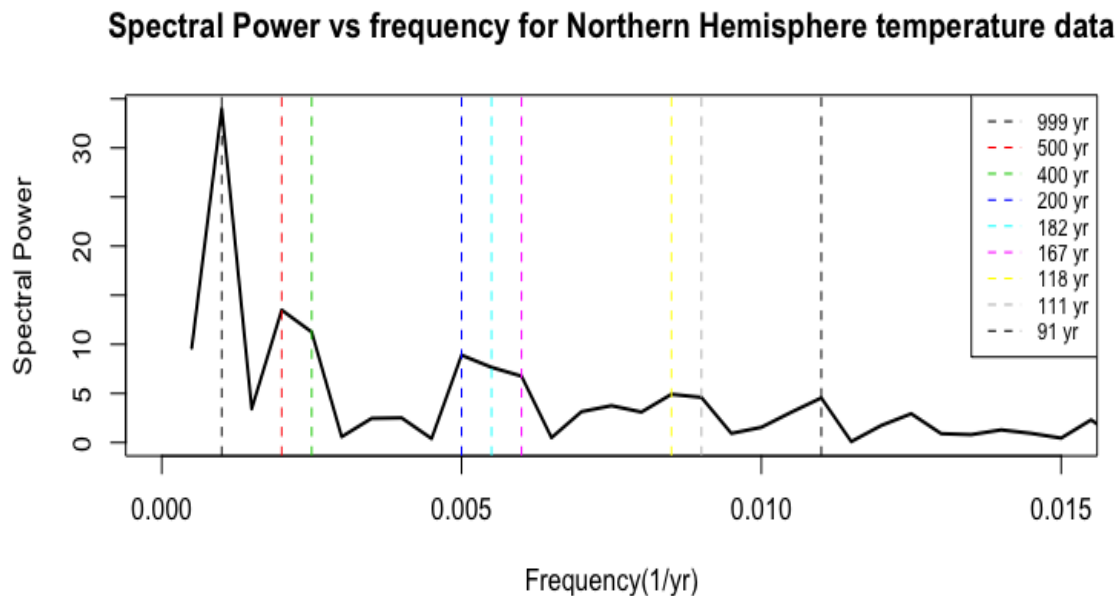
Figure 5.16 Frequency and period found in the Northern Hemisphere temperature data. We are showing 9 frequency/periods with significant power. The ~200 yr cycle (blue dotted line) is possibly related to the solar induced ~190 yr cycle that drive climate change.
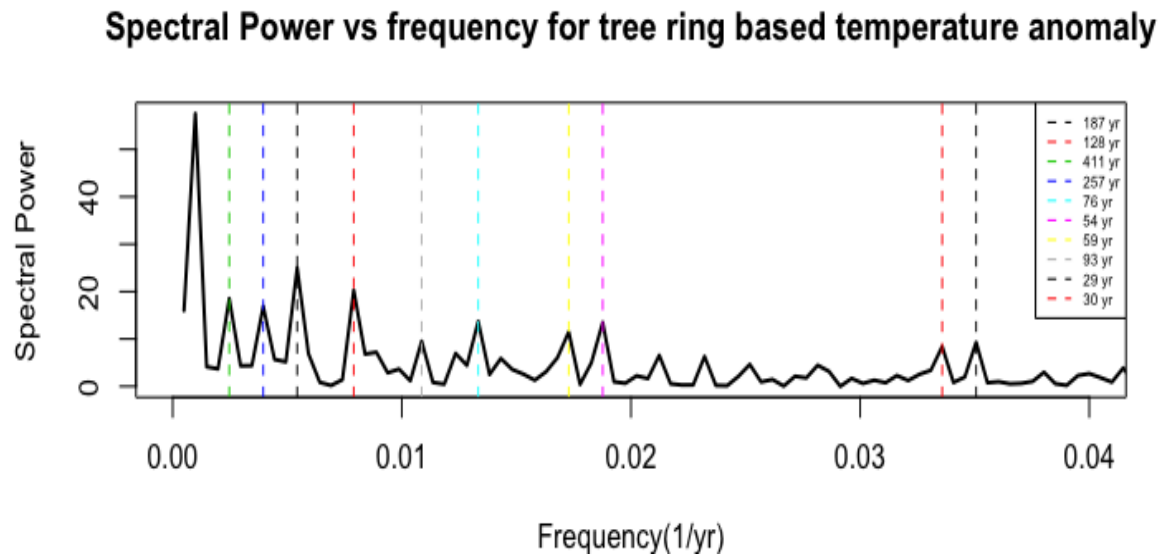
Figure 5.17 Frequency and period found in the tree-ring based Northern Hemisphere temperature data. We are showing 10 frequency/periods with significant power. The 187 yr cycle (black dotted line) is possibly related to the solar induced ~190 yr cycle that drive climate change.
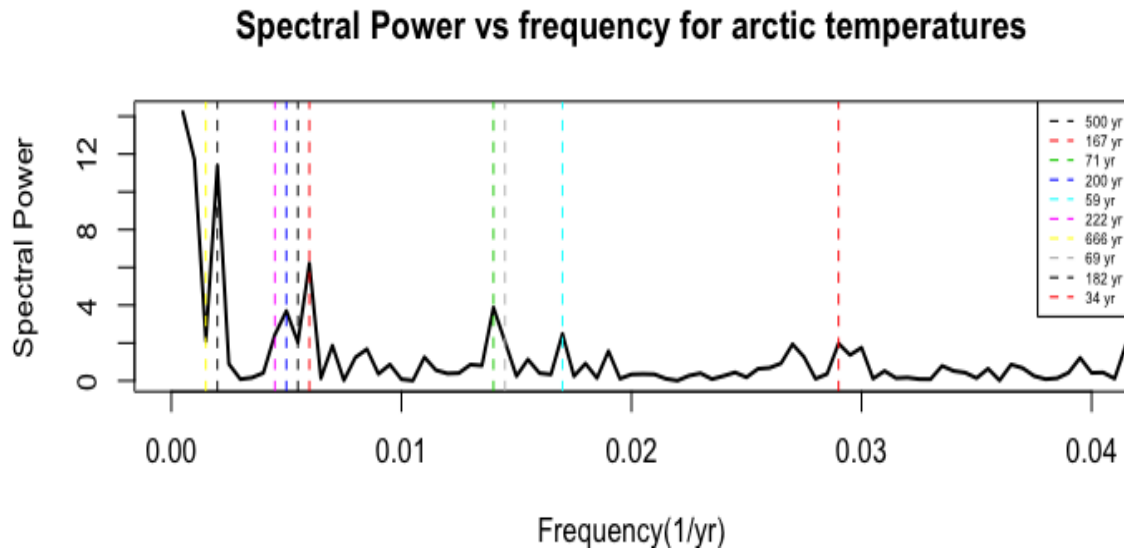
Figure 5.18 Frequency and period found in the arctic temperature data. We are showing 10 frequency/periods with significant power. The 200 yr cycle (blue dotted line) is possibly related to the solar induced ~190 yr cycle that drive climate change.
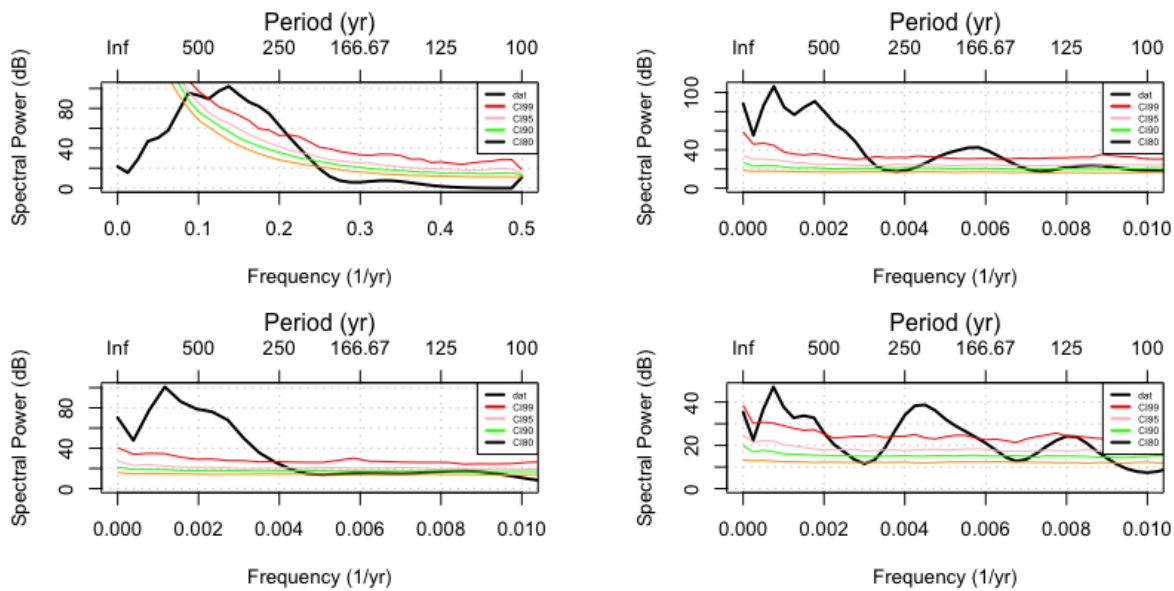
Figure 5.19 Spectral power (solid black curve) versus frequency/period of global cultural turnover of 0-2Ka (top left), stacked Northern Hemisphere (NH) temperature anomaly (top right), tree ring based NH temperature anomaly (bottom left) and central European temperature anomaly (bottom right) using REDFIT spectral method provided in PAST3 software tool. The red, light red, green, orange curve shows 99%, 95%, 90%, 80% confidence interval of numerous ar1 process based on red-noise model.

Table 5.6. Spectral analysis result of cultural turnover time series with multi-taper method using R "Astrochron" package

#cycle	Frequency (1/yr)	Period (yr)	F-test confidence level
1	0.00246	**405.06**	0.98
2	0.00663	**150.72**	0.99
3	0.00987	**101.27**	0.97
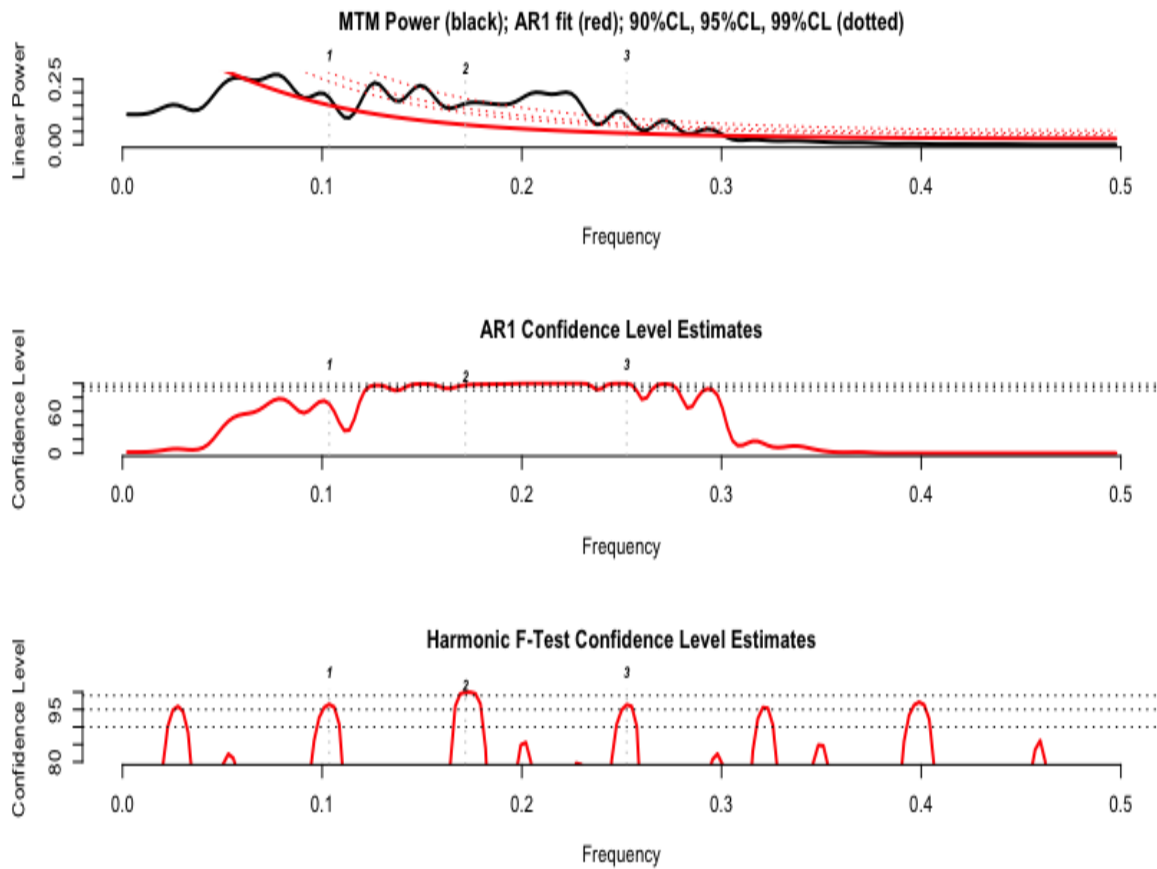
Figure 5.20 Spectral power versus frequency(unit: 1/yr) using multi-taper method provided in R Astrochron package. Confidence level is calculated using lag-1 autoregressive (AR1) background noise and also with F-test. The red dotted line shows three confidence levels(90%, 95%, 99%) in each panel to separate the significant peaks in the power spectra.
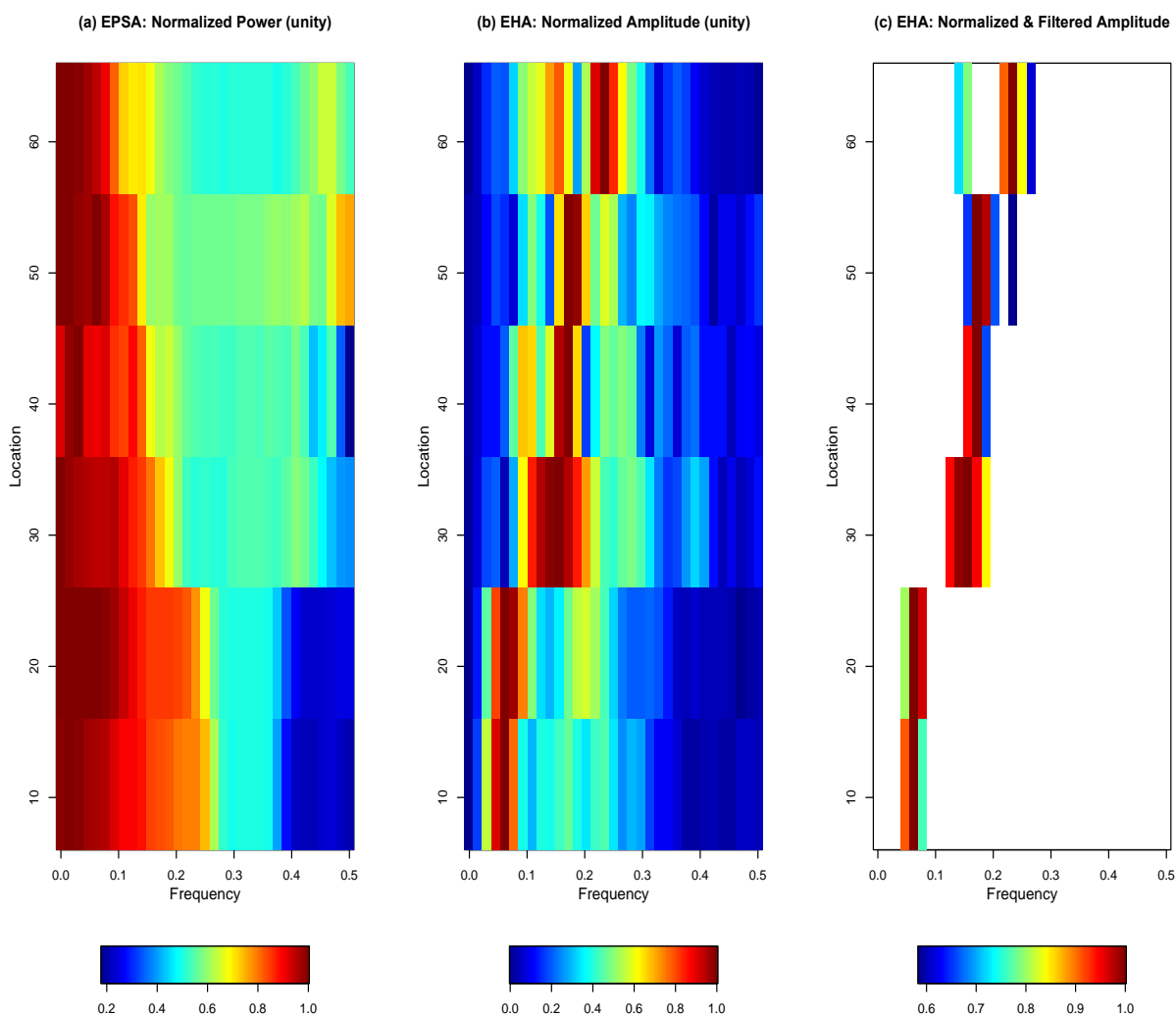
Figure 5.21 Power spectra using EPSA and EHA provide in R "Astrochron" package. Normalized and filtered amplitude from EHA clearly identifies (red bands in panel (b)) significant frequencies (unit: 1/Yr) around 0.06, 0.17 and 0.25 in various time periods of 2000 years (Location in y axis corresponds to time in Ka) .
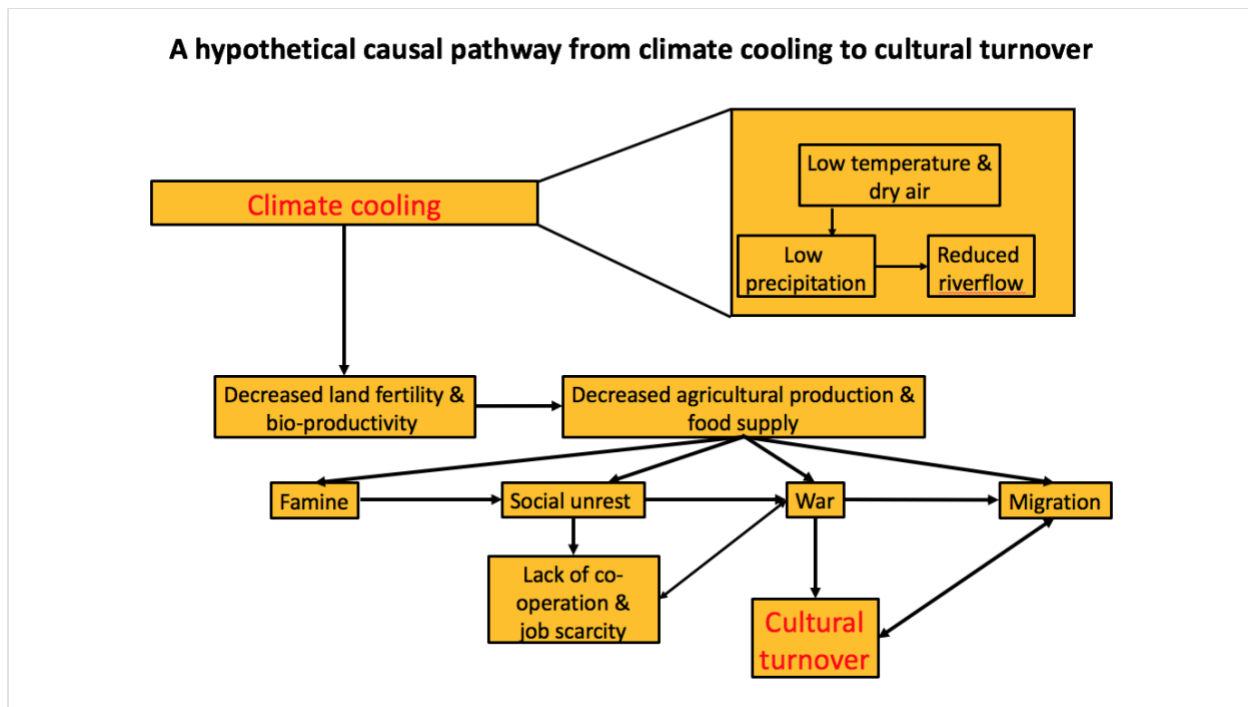
Figure 5.22 A causal pathway from cold climate to cultural turnover through war and social unrest.

5.6   Conclusion

We found evidence from our TSCreator data that a global cooling effect exists in the history of human cultural turnover. During the period of decreasing global temperature, the number of cultural turnovers increased in the last 2000 years of human history. Global change induced by solar cycles (~190 yr Suess cycle in Lüdecke et al., 2015) can cause the changes in human activities through decreased agricultural productivity and economic growth and also can force people to migrate from one region to another leading to social unrest and power struggle. A hypothetical causal pathway from climate cooling to cultural turnover is shown in Figure 5.22.

5.7   References

Chen, Q., 2015. Climate shocks, dynastic cycles and nomadic conquests: Evidence from historical China. Oxford Economic Papers, 67, pp. 185–204. https://doi.org/10.1093/oep/gpu032.

Collier, P., Hoeffler, A., 2004. Greed and grievance in civil war. Oxford Economic Papers, 56(4), pp. 563-595. https://doi.org/10.1093/oep/gpf064.

Dell, M., Jones, B.F. and Olken, B.A., 2008. Climate Change and Economic Growth: Evidence from the Last Half Century. National Bureau of Economic Research. NBER Working Paper Series, paper no. w14132. https://doi.org/10.3386/w14132.

Li, J., Dodson, J., Yan, H., Zhang, D.D., Zhang, X., Xu, Q., Lee, H.F., Pei, Q., Cheng, B., Li, C., Ni, J., Sun, A., Lu, F., Zong, Y., 2017. Chinese Dynasty - Quantifying climatic variability in monsoonal northern China over the last 2200 years and its role in driving Chinese dynastic changes. Quaternary Science Reviews, 159, pp. 35–46. https://doi.org/10.1016/j.quascirev.2017.01.009.

Lüdecke, H.J., Weiss, C.O. and Hempelmann, A., 2015. Paleoclimate forcing by the solar De Vries/Suess cycle. Climate of the Past Discussions, 11(1), pp.279-305. https://doi.org/10.5194/cpd-11-279-2015 .

McKay, N.P., Kaufman, D.S., 2014. An extended Arctic proxy temperature database for the past 2,000 years. Scientific Data, 1, 140026. https://doi.org/10.1038/sdata.2014.26.

Meyers, S.R., 2014. Astrochron: An R Package for Astrochronology. https://cran.r-project.org/web/packages/astrochron/index.html.

Miguel, E., Satyanath, S., Sergenti, E., 2004. Economic shocks and civil conflict: An instrumental variables approach. Journal of political Economy, 112(4), pp. 725-753. https://doi.org/10.1086/421174.

Muller, R.A. and MacDonald, G.J., 2002. Ice ages and astronomical causes: data, spectral analysis and mechanisms. Springer Science & Business Media. https://doi.org/10.5860/choice.38-3341.

Thomson, D.J., 1990. Time series analysis of Holocene climate data. Philosophical Transactions of the Royal Society of London. Series A, Mathematical and Physical Sciences, 330(1615), pp. 601-616.

Wang, X., Chen, F., Zhang, J., Yang, Y., Li, J., Hasi, E., Zhang, C., Xia, D., 2010. Climate, desertification, and the rise and collapse of China's historical dynasties. Human Ecology, 38(1), pp. 157-172. https://doi.org/10.1007/s10745-009-9298-2.

Zhang, D.D., Jim, C., Lin, C., He, Y., Lee, F., 2005. Climate change, social unrest and dynastic transition in ancient China. Chinese Science Bulletin, 50(2), pp. 137-144. https://doi.org/10.1360/03wd0641.

Zhang, D.D., Jim, C.Y., Lin, G.C.S., He, Y.Q., Wang, J.J., Lee, H.F., 2006. Climatic change, wars and dynastic cycles in China over the last millennium. Climatic Change, 76(3-4), pp. 459-477. https://doi.org/10.1007/s10584-005-9024-z.

Zhang, D.D., Lee, H.F., Wang, C., Li, B., Pei, Q., Zhang, J., An, Y., 2011. The causality analysis of climate change and large-scale human crisis. Proceedings of the National Academy of Sciences, pp. 108(42), 17296-17301. https://doi.org/10.1073/pnas.1104268108.

Zhang, D.D., Pei, Q., Lee, H.F., Zhang, J., Chang, C.Q., Li, B., Li, J., Zhang, X., 2015. The pulse of imperial China: A quantitative analysis of long-term geopolitical and climatic cycles. Global Ecology and Biogeography, 24(1), pp. 87-96. https://doi.org/10.1111/geb.12247.

Zheng, J., Xiao, L., Fang, X., Hao, Z., Ge, Q., Li, B., 2014. How climate change impacted the collapse of the Ming dynasty. Climatic Change, 127(2), pp. 169–182. https://doi.org/10.1007/s10584-014-1244-7.

APPENDIX A

Table A1 FAD, LAD, lifespan, family and groups of planktonic foraminifera morphospecies

Morphospecies name	FAD	LAD	Lifespan	Genus	Family	Morphogroup	Ecogroup
Acarinina africana	22.92	3.13	19.79	Acarinina	Globoquadrinidae	M7-globular	E1-With Symbionts
Acarinina alticonica	17.54	16.38	1.16	Acarinina	Globorotaliidae	M16-globorotaliform, non-keeled	E1-With Symbionts
Acarinina angulosa	16.28	14.79	1.49	Acarinina	Globigerinidae	M4-spherical	E1-With Symbionts
Acarinina aspensis	22.44	13.39	9.05	Acarinina	Globigerinidae	M2-globular	E1-With Symbionts
Acarinina boudreauxi	18.57	15.67	2.90	Acarinina	Globigerinidae	M3-globular with supplementary apertures	E1-With Symbionts
Acarinina bullbrooki	17.27	9.83	7.44	Acarinina	Globigerinidae	M2-globular	E1-With Symbionts
Acarinina coalingensis	17.27	4.81	12.46	Acarinina	Globigerinidae	M2-globular	E1-With Symbionts
Acarinina collactea	15.96	14.49	1.47	Acarinina	Globigerinidae	M4-spherical	E1-With Symbionts
Acarinina cuneicamerata	17.54	14.24	3.30	Acarinina	Globigerinidae	M3-globular with supplementary apertures	E1-With Symbionts
Acarinina echinata	16.27	14.79	1.48	Acarinina	Globigerinidae	M4-spherical	E1-With Symbionts
Acarinina esnaensis	18.26	13.73	4.53	Acarinina	Globorotaliidae	M16-globorotaliform, non-keeled	E1-With Symbionts
Acarinina esnehensis	18.18	0.00	18.18	Acarinina	Globigerinidae	M2-globular	E1-With Symbionts
Acarinina interposita	21.32	1.30	20.02	Acarinina	Globigerinidae	M3-globular with supplementary apertures	E1-With Symbionts
Acarinina mcgowrani	16.38	5.83	10.55	Acarinina	Globorotaliidae	M14-globorotaliform, keeled	E1-With Symbionts
Acarinina mckannai	22.28	11.54	10.74	Acarinina	Globigerinidae	M3-globular with supplementary apertures	E1-With Symbionts
Acarinina medizzai	18.45	12.40	6.04	Acarinina	Globigerinidae	M7-globular	E1-With Symbionts
Acarinina nitida	22.28	16.84	5.45	Acarinina	Globigerinidae	M2-globular	E1-With Symbionts
Acarinina pentacamerata	18.32	12.40	5.92	Acarinina	Globigerinidae	M3-globular with supplementary apertures	E1-With Symbionts
Acarinina praetopilensis	17.13	16.38	0.75	Acarinina	Globorotaliidae	M13-turborotaliform, non-keeled	E1-With Symbionts
Acarinina primitiva	16.26	13.87	2.39	Acarinina	Globorotaliidae	M14-globorotaliform, keeled	E1-With Symbionts
Acarinina pseudosubsphaerica	16.69	10.21	6.48	Acarinina	Globorotaliidae	M14-globorotaliform, keeled	E1-With Symbionts
Acarinina pseudotopilensis	16.38	3.16	13.22	Acarinina	Globigerinidae	M7-globular	E1-With Symbionts
Acarinina punctocarinata	19.05	13.88	5.17	Acarinina	Globigerinidae	M2-globular	E1-With Symbionts
Acarinina quetra	21.48	13.84	7.65	Acarinina	Globorotaliidae	M13-turborotaliform, non-keeled	E1-With Symbionts
Acarinina rohri	21.88	16.38	5.50	Acarinina	Globigerinidae	M3-globular with supplementary apertures	E1-With Symbionts
Acarinina sibaiyaensis	22.44	8.07	14.37	Acarinina	Globorotaliidae	M7-globular	E1-With Symbionts
Acarinina soldadoensis	16.38	14.53	1.85	Acarinina	Globigerinidae	M4-spherical	E1-With Symbionts
Acarinina strabocella	22.44	5.92	16.52	Acarinina	Globoquadrinidae	M7-globular	E1-With Symbionts

Acarinina subsphaerica	21.12	0.56	20.56	Acarinina	Globigerinidae	M2-globular	E1-With Symbionts
Acarinina topilensis	22.44	11.36	11.08	Acarinina	Globigerinidae	M2-globular	E1-With Symbionts
Acarinina wilcoxensis	20.72	16.38	4.34	Acarinina	Globigerinidae	M2-globular	E1-With Symbionts
Astrorotalia palmerae	3.59	1.35	2.24	Astrorotalia	Globorotaliidae	M15-globorotaliform, anguloconical	E1-With Symbionts
Beella digitata	55.43	51.67	3.76	Beella	Truncorotaloididae	M18-muricocarinate, keeled	E4-sub-thermocline
Beella megastoma	55.56	17.54	38.02	Beella	Globigerinidae	M2-globular	E4-sub-thermocline
Beella praedigitata	55.39	50.67	4.72	Beella	Truncorotaloididae	M18-muricocarinate, keeled	E4-sub-thermocline
Catapsydrax africanus	45.72	39.97	5.75	Catapsydrax	Globigerinidae	M2-globular	E4-sub-thermocline
Catapsydrax dissimilis	43.81	33.90	9.91	Catapsydrax	Globigerinidae	M2-globular	E4-sub-thermocline
Catapsydrax globiformis	54.61	50.67	3.94	Catapsydrax	Truncorotaloididae	M19-muricocarinate, anguloconical	E4-sub-thermocline
Catapsydrax howei	44.78	40.06	4.73	Catapsydrax	Truncorotaloididae	M19-muricocarinate, anguloconical	E4-sub-thermocline
Catapsydrax parvulus	44.78	43.23	1.55	Catapsydrax	Truncorotaloididae	M7-globular	E4-sub-thermocline
Catapsydrax stainforthi	44.55	15.96	28.59	Catapsydrax	Globigerinidae	M2-globular	E4-sub-thermocline
Catapsydrax unicavus	43.54	30.28	13.26	Catapsydrax	Globigerinidae	M2-globular	E4-sub-thermocline
Clavatorella bermudezi	55.49	54.61	0.88	Clavatorella	Truncorotaloididae	M19-muricocarinate, anguloconical	E4-sub-thermocline
Clavigerinella akersi	55.89	33.90	21.99	Clavigerinella	Globigerinidae	M2-globular	E4-sub-thermocline
Clavigerinella caucasica	55.96	55.75	0.21	Clavigerinella	Truncorotaloididae	M17-muricate, acarininiform	E4-sub-thermocline
Clavigerinella colombiana	55.89	43.54	12.35	Clavigerinella	Hedbergellidae	M13-turborotaliform, non-keeled	E4-sub-thermocline
Clavigerinella eocanica	55.81	42.90	12.92	Clavigerinella	Hedbergellidae	M9-planispiral	E4-sub-thermocline
Clavigerinella jarvisi	55.96	46.57	9.39	Clavigerinella	Truncorotaloididae	M17-muricate, acarininiform	E4-sub-thermocline
Cribrohantkenina inflata	2.04	0.00	2.04	Cribrohantkenina	Pulleniatinidae	M7-globular	E2-Without Symbionts
Dentoglobigerina altispira	56.25	43.31	12.94	Dentoglobigerina	Truncorotaloididae	M7-globular	E1-With Symbionts
Dentoglobigerina baroemoenensis	58.40	55.35	3.04	Dentoglobigerina	Truncorotaloididae	M18-muricocarinate, keeled	E3-thermocline
Dentoglobigerina binaiensis	65.96	62.49	3.46	Dentoglobigerina	Globigerinidae	M2-globular	E4-sub-thermocline
Dentoglobigerina galavisi	60.73	55.20	5.53	Dentoglobigerina	Globigerinidae	M2-globular	E3-thermocline
Dentoglobigerina globosa	60.42	57.56	2.86	Dentoglobigerina	Truncorotaloididae	M17-muricate, acarininiform	E3-thermocline
Dentoglobigerina globularis	60.68	55.20	5.48	Dentoglobigerina	Truncorotaloididae	M18-muricocarinate, keeled	E3-thermocline
Dentoglobigerina larmeui	60.52	57.56	2.96	Dentoglobigerina	Truncorotaloididae	M17-muricate, acarininiform	E3-thermocline
Dentoglobigerina prasaepis	63.90	62.29	1.61	Dentoglobigerina	Truncorotaloididae	M7-globular	E4-sub-thermocline
Dentoglobigerina pseudovenezuelana	60.83	55.20	5.63	Dentoglobigerina	Truncorotaloididae	M18-muricocarinate, keeled	E3-thermocline
Dentoglobigerina rohri	65.90	62.67	3.23	Dentoglobigerina	Hedbergellidae	M13-turborotaliform, non-keeled	E4-sub-thermocline
Dentoglobigerina sellii	65.25	57.79	7.46	Dentoglobigerina	Globigerinidae	M2-globular	E4-sub-thermocline
Dentoglobigerina sp	62.89	57.89	5.00	Dentoglobigerina	Globigerinidae	M2-globular	E3-thermocline

Dentoglobigerina tapuriensis	65.77	60.63	5.15	Dentoglobigerina	Globigerinidae	M2-globular	E4-sub-thermocline
Dentoglobigerina venezuelana	63.90	42.56	21.34	Dentoglobigerina	Globigerinidae	M2-globular	E4-sub-thermocline
Eoglobigerina edita	43.39	33.90	9.49	Eoglobigerina	Globigerinidae	M2-globular	E3-thermocline
Eoglobigerina eobulloides	43.50	41.31	2.19	Eoglobigerina	Globigerinidae	M3-globular with supplementary apertures	E3-thermocline
Eoglobigerina spiralis	43.50	40.65	2.85	Eoglobigerina	Hedbergellidae	M7-globular	E3-thermocline
Fohsella birnageae	5.70	0.00	5.70	Fohsella	Pulleniatinidae	M7-globular	E3-thermocline
Fohsella fohsi	4.35	0.00	4.35	Fohsella	Globorotaliidae	M15-globorotaliform, anguloconical	E3-thermocline
Fohsella lenguaensis	4.91	0.00	4.91	Fohsella	Globorotaliidae	M14-globorotaliform, keeled	E3-thermocline
Fohsella lobata	4.37	0.00	4.37	Fohsella	Globoquadrinidae	M7-globular	E3-thermocline
Fohsella paralenguaensis	5.22	4.49	0.73	Fohsella	Pulleniatinidae	M7-globular	E3-thermocline
Fohsella peripheroacuta	5.72	0.00	5.72	Fohsella	Globorotaliidae	M14-globorotaliform, keeled	E3-thermocline
Fohsella peripheroronda	4.61	4.21	0.40	Fohsella	Pulleniatinidae	M8-globular, keeled	E3-thermocline
Fohsella praefohsi	4.43	3.73	0.70	Fohsella	Globorotaliidae	M15-globorotaliform, anguloconical	E3-thermocline
Fohsella robusta	4.40	0.00	4.40	Fohsella	Globigerinidae	M2-globular	E3-thermocline
Globanomalina archeocompressa	5.53	0.00	5.53	Globanomalina	Globigerinidae	M7-globular	E3-thermocline
Globanomalina australiformis	4.61	2.39	2.22	Globanomalina	Globorotaliidae	M7-globular	E3-thermocline
Globanomalina chapmani	5.02	0.00	5.02	Globanomalina	Globigerinidae	M5-clavate	E3-thermocline
Globanomalina compressa	5.66	0.89	4.76	Globanomalina	Globorotaliidae	M15-globorotaliform, anguloconical	E3-thermocline
Globanomalina ehrenbergi	5.59	0.00	5.59	Globanomalina	Globorotaliidae	M15-globorotaliform, anguloconical	E3-thermocline
Globanomalina imitata	5.07	4.18	0.89	Globanomalina	Globorotaliidae	M15-globorotaliform, anguloconical	E3-thermocline
Globanomalina luxorensis	4.61	0.00	4.61	Globanomalina	Globorotaliidae	M14-globorotaliform, keeled	E2-Without Symbionts
Globanomalina ovalis	4.55	0.00	4.55	Globanomalina	Globigerinidae	M1-flat	E2-Without Symbionts
Globanomalina planocompressa	5.46	4.55	0.91	Globanomalina	Globorotaliidae	M7-globular	E3-thermocline
Globanomalina planoconica	4.81	4.12	0.69	Globanomalina	Globorotaliidae	M16-globorotaliform, non-keeled	E3-thermocline
Globanomalina pseudomenardii	4.20	1.01	3.20	Globanomalina	Globorotaliidae	M15-globorotaliform, anguloconical	E3-thermocline
Globigerina angulisuturalis	34.03	26.59	7.44	Globigerina	Globigerinidae	M2-globular	E1-With Symbionts
Globigerina bulloides	34.42	34.03	0.39	Globigerina	Hedbergellidae	M12-turborotaliform, keeled	E2-Without Symbionts
Globigerina ciperoensis	35.89	32.10	3.79	Globigerina	Hedbergellidae	M9-planispiral	E2-Without Symbionts
Globigerina druryi	32.79	30.22	2.57	Globigerina	Hedbergellidae	M7-globular	E1-With Symbionts
Globigerina eamesi	32.63	21.88	10.75	Globigerina	Globigerinidae	M2-globular	E1-With Symbionts
Globigerina falconensis	33.58	23.34	10.24	Globigerina	Globoquadrinidae	M7-globular	E1-With Symbionts
Globigerina officinalis	33.37	3.30	30.07	Globigerina	Globoquadrinidae	M7-globular	E1-With Symbionts
Globigerina praebulloides	31.29	15.67	15.62	Globigerina	Globigerinidae	M2-globular	E1-With Symbionts

Globigerina umbilicata	34.29	19.30	14.99	Globigerina	Globoquadrinidae	M7-globular	E1-With Symbionts
Globigerinatheka barri	48.31	40.40	7.91	Globigerinatheka	Truncorotaloididae	M17-muricate, acarininiform	E1-With Symbionts
Globigerinatheka curryi	50.67	44.60	6.07	Globigerinatheka	Hedbergellidae	M9-planispiral	E1-With Symbionts
Globigerinatheka euganea	52.17	33.90	18.27	Globigerinatheka	Globigerinidae	M2-globular	E1-With Symbionts
Globigerinatheka index	47.41	32.31	15.10	Globigerinatheka	Hedbergellidae	M9-planispiral	E1-With Symbionts
Globigerinatheka korotkovi	47.71	37.32	10.39	Globigerinatheka	Globigerinidae	M2-globular	E1-With Symbionts
Globigerinatheka kugleri	50.20	36.56	13.64	Globigerinatheka	Truncorotaloididae	M17-muricate, acarininiform	E1-With Symbionts
Globigerinatheka luterbacheri	50.20	30.28	19.92	Globigerinatheka	Truncorotaloididae	M17-muricate, acarininiform	E1-With Symbionts
Globigerinatheka mexicana	48.01	39.97	8.04	Globigerinatheka	Truncorotaloididae	M17-muricate, acarininiform	E1-With Symbionts
Globigerinatheka semiinvoluta	50.67	43.67	7.00	Globigerinatheka	Truncorotaloididae	M19-muricocarinate, anguloconical	E1-With Symbionts
Globigerinatheka subconglobata	49.39	43.31	6.08	Globigerinatheka	Truncorotaloididae	M17-muricate, acarininiform	E1-With Symbionts
Globigerinatheka tropicalis	50.20	43.54	6.66	Globigerinatheka	Truncorotaloididae	M17-muricate, acarininiform	E1-With Symbionts
Globigerinella adamsi	55.68	33.90	21.78	Globigerinella	Globigerinidae	M2-globular	E4-sub-thermocline
Globigerinella calida	42.36	40.14	2.22	Globigerinella	Globigerinidae	M4-spherical	E3-thermocline
Globigerinella obesa	39.07	34.03	5.04	Globigerinella	Globigerinidae	M3-globular with supplementary apertures	E3-thermocline
Globigerinella praesiphonifera	40.40	39.97	0.43	Globigerinella	Globigerinidae	M4-spherical	E3-thermocline
Globigerinella siphonifera	55.81	42.00	13.81	Globigerinella	Globigerinidae	M2-globular	E3-thermocline
Globigerinoides altiapertura	50.20	41.89	8.31	Globigerinoides	Truncorotaloididae	M17-muricate, acarininiform	E1-With Symbionts
Globigerinoides bisphericus	50.67	38.78	11.89	Globigerinoides	Truncorotaloididae	M17-muricate, acarininiform	E1-With Symbionts
Globigerinoides conglobatus	48.65	43.54	5.11	Globigerinoides	Globigerinidae	M2-globular	E1-With Symbionts
Globigerinoides diminutus	50.55	32.31	18.24	Globigerinoides	Globigerinidae	M2-globular	E1-With Symbionts
Globigerinoides extremus	48.31	40.65	7.66	Globigerinoides	Hedbergellidae	M7-globular	E1-With Symbionts
Globigerinoides fistulosus	51.79	50.79	1.00	Globigerinoides	Globigerinidae	M2-globular	E1-With Symbionts
Globigerinoides mitra	49.05	46.87	2.19	Globigerinoides	Truncorotaloididae	M11-keeled spines	E1-With Symbionts
Globigerinoides obliquus	47.31	39.27	8.04	Globigerinoides	Hedbergellidae	M9-planispiral	E1-With Symbionts
Globigerinoides parawoodi	50.20	48.01	2.19	Globigerinoides	Truncorotaloididae	M17-muricate, acarininiform	E1-With Symbionts
Globigerinoides primordius	48.65	37.99	10.66	Globigerinoides	Truncorotaloididae	M17-muricate, acarininiform	E1-With Symbionts
Globigerinoides ruber	47.41	41.89	5.52	Globigerinoides	Truncorotaloididae	M17-muricate, acarininiform	E1-With Symbionts
Globigerinoides sacculifer	47.41	34.29	13.12	Globigerinoides	Hantkeninidae	M6-planispiral	E1-With Symbionts
Globigerinoides seigliei	50.20	33.90	16.30	Globigerinoides	Globigerinidae	M2-globular	E1-With Symbionts
Globigerinoides subquadratus	47.41	42.67	4.74	Globigerinoides	Globigerinidae	M6-planispiral	E1-With Symbionts
Globigerinoides trilobus	46.92	40.40	6.52	Globigerinoides	Globigerinidae	M2-globular	E1-With Symbionts
Globoconella conoidea	5.81	0.00	5.81	Globoconella	Globigerinidae	M1-flat	E3-thermocline

Species				Genus	Family	Morphology	Ecology
Globoconella conomiozea	8.58	3.77	4.81	Globoconella	Globorotaliidae	M14-globorotaliform, keeled	E3-thermocline
Globoconella inflata	62.60	61.33	1.27	Globoconella	Truncorotaloididae	M18-muricocarinate, keeled	E3-thermocline
Globoconella miozea	6.03	3.85	2.18	Globoconella	Globorotaliidae	M14-globorotaliform, keeled	E3-thermocline
Globoconella pliozea	10.90	0.00	10.90	Globoconella	Globigerinidae	M3-globular with supplementary apertures	E3-thermocline
Globoconella puncticulata	62.60	62.08	0.52	Globoconella	Truncorotaloididae	M7-globular	E3-thermocline
Globoconella sphericomiozea	62.93	62.29	0.63	Globoconella	Globigerinidae	M2-globular	E3-thermocline
Globoconella terminalis	11.18	1.64	9.54	Globoconella	Globigerinidae	M2-globular	E3-thermocline
Globoquadrina conglomerata	62.29	61.33	0.96	Globoquadrina	Truncorotaloididae	M7-globular	E3-thermocline
Globoquadrina dehiscens	60.52	54.85	5.67	Globoquadrina	Truncorotaloididae	M17-muricate, acarininiform	E3-thermocline
Globorotalia flexuosa	8.90	1.98	6.92	Globorotalia	Globigerinidae	M3-globular with supplementary apertures	E3-thermocline
Globorotalia merotumida	6.61	3.66	2.95	Globorotalia	Pulleniatinidae	M7-globular	E3-thermocline
Globorotalia plesiotumida	6.24	1.86	4.39	Globorotalia	Pulleniatinidae	M7-globular	E3-thermocline
Globorotalia tumida	6.04	4.81	1.23	Globorotalia	Globorotaliidae	M14-globorotaliform, keeled	E3-thermocline
Globorotalia ungulata	6.21	0.00	6.21	Globorotalia	Globigerinidae	M3-globular with supplementary apertures	E3-thermocline
Globorotalia zealandica	14.76	8.83	5.93	Globorotalia	Globorotaliidae	M14-globorotaliform, keeled	E3-thermocline
Globorotaloides eovariabilis	43.54	36.37	7.17	Globorotaloides	Globigerinidae	M3-globular with supplementary apertures	E4-sub-thermocline
Globorotaloides hexagonus	43.85	36.08	7.77	Globorotaloides	Globigerinidae	M3-globular with supplementary apertures	E4-sub-thermocline
Globorotaloides quadrocameratus	43.77	35.67	8.11	Globorotaloides	Globigerinidae	M3-globular with supplementary apertures	E4-sub-thermocline
Globorotaloides testarugosa	44.08	40.06	4.02	Globorotaloides	Truncorotaloididae	M17-muricate, acarininiform	E4-sub-thermocline
Globorotaloides variabilis	44.03	43.89	0.14	Globorotaloides	Hantkeninidae	M6-planispiral	E4-sub-thermocline
Globoturborotalita anguliofficinalis	35.27	30.28	4.99	Globoturborotalita	Hedbergellidae	M7-globular	E2-Without Symbionts
Globoturborotalita apertura	35.52	30.28	5.24	Globoturborotalita	Globigerinidae	M2-globular	E2-Without Symbionts
Globoturborotalita bassriverensis	34.85	23.03	11.82	Globoturborotalita	Globigerinidae	M2-globular	E2-Without Symbionts
Globoturborotalita bollii	47.41	34.68	12.73	Globoturborotalita	Globigerinidae	M2-globular	E1-With Symbionts
Globoturborotalita brazieri	34.13	33.05	1.07	Globoturborotalita	Globoquadrinidae	M7-globular	E1-With Symbionts
Globoturborotalita connecta	34.16	4.81	29.34	Globoturborotalita	Globigerinidae	M2-globular	E1-With Symbionts
Globoturborotalita decoraperta	35.59	30.28	5.31	Globoturborotalita	Globigerinidae	M2-globular	E2-Without Symbionts
Globoturborotalita gnaucki	36.84	26.82	10.03	Globoturborotalita	Globoquadrinidae	M7-globular	E2-Without Symbionts
Globoturborotalita kennetti	50.44	37.99	12.45	Globoturborotalita	Globigerinidae	M2-globular	E1-With Symbionts
Globoturborotalita labiacrassata	34.42	32.74	1.68	Globoturborotalita	Globigerinidae	M2-globular	E2-Without Symbionts
Globoturborotalita martini	33.90	24.80	9.10	Globoturborotalita	Globoquadrinidae	M7-globular	E1-With Symbionts
Globoturborotalita nepenthes	36.46	33.90	2.56	Globoturborotalita	Hantkeninidae	M10-tubulospinate	E2-Without Symbionts
Globoturborotalita ouachitaensis	33.48	23.03	10.44	Globoturborotalita	Globoquadrinidae	M7-globular	E1-With Symbionts

Globoturborotalita rubescens	37.61	17.54	20.07	Globoturborotalita	Globigerinidae	M2-globular	E2-Without Symbionts
Globoturborotalita tenella	38.09	33.90	4.19	Globoturborotalita	Hantkeninidae	M10-tubulospinate	E2-Without Symbionts
Globoturborotalita woodi	32.10	3.30	28.80	Globoturborotalita	Globoquadrinidae	M7-globular	E1-With Symbionts
Guembelitrioides nuttalli	42.78	31.90	10.89	Guembelitrioides	Truncorotaloididae	M17-muricate, acarininiform	E3-thermocline
Hantkenina alabamensis	1.95	0.00	1.95	Hantkenina	Globorotaliidae	M15-globorotaliform, anguloconical	E2-Without Symbionts
Hantkenina australis	2.58	0.56	2.01	Hantkenina	Globigerinidae	M2-globular	E3-thermocline
Hantkenina compressa	1.91	0.38	1.53	Hantkenina	Globorotaliidae	M15-globorotaliform, anguloconical	E2-Without Symbionts
Hantkenina dumblei	2.48	0.00	2.48	Hantkenina	Globigerinidae	M2-globular	E3-thermocline
Hantkenina lehneri	2.67	0.00	2.67	Hantkenina	Globorotaliidae	M7-globular	E3-thermocline
Hantkenina liebusi	3.35	0.61	2.74	Hantkenina	Globorotaliidae	M15-globorotaliform, anguloconical	E4-sub-thermocline
Hantkenina mexicana	3.52	1.80	1.72	Hantkenina	Globorotaliidae	M14-globorotaliform, keeled	E4-sub-thermocline
Hantkenina nanggulanensis	2.00	0.00	2.00	Hantkenina	Globorotaliidae	M15-globorotaliform, anguloconical	E2-Without Symbionts
Hantkenina primitiva	2.09	0.00	2.09	Hantkenina	Globorotaliidae	M16-globorotaliform, non-keeled	E3-thermocline
Hantkenina singanoae	3.33	1.88	1.45	Hantkenina	Globigerinidae	M3-globular with supplementary apertures	E3-thermocline
Hedbergella [ancestor]	0.01	0.00	0.01	Hedbergella	Globigerinidae	M5-clavate	-
Hedbergella holmdelensis	62.29	60.42	1.87	Hedbergella	Truncorotaloididae	M18-muricocarinate, keeled	E3-thermocline
Hedbergella monmouthensis	62.45	60.52	1.93	Hedbergella	Hedbergellidae	M13-turborotaliform, non-keeled	E3-thermocline
Hirsutella bermudezi	15.16	9.25	5.90	Hirsutella	Globorotaliidae	M16-globorotaliform, non-keeled	E4-sub-thermocline
Hirsutella challengeri	14.79	0.00	14.79	Hirsutella	Globorotaliidae	M14-globorotaliform, keeled	E4-sub-thermocline
Hirsutella cibaoensis	14.94	0.00	14.94	Hirsutella	Globigerinidae	M4-spherical	E4-sub-thermocline
Hirsutella evoluta	15.73	12.40	3.33	Hirsutella	Globigerinidae	M5-clavate	E4-sub-thermocline
Hirsutella gigantea	9.44	4.49	4.95	Hirsutella	Globorotaliidae	M16-globorotaliform, non-keeled	E4-sub-thermocline
Hirsutella hirsuta	13.14	0.00	13.14	Hirsutella	Globorotaliidae	M14-globorotaliform, keeled	E4-sub-thermocline
Hirsutella juanai	15.10	0.00	15.10	Hirsutella	Globigerinidae	M3-globular with supplementary apertures	E4-sub-thermocline
Hirsutella margaritae	9.96	5.94	4.01	Hirsutella	Globorotaliidae	M14-globorotaliform, keeled	E4-sub-thermocline
Hirsutella praemargaritae	9.83	1.80	8.03	Hirsutella	Globorotaliidae	M7-globular	E4-sub-thermocline
Hirsutella praescitula	15.10	0.00	15.10	Hirsutella	Globigerinidae	M4-spherical	E4-sub-thermocline
Hirsutella primitiva	10.64	2.39	8.25	Hirsutella	Globorotaliidae	M14-globorotaliform, keeled	E4-sub-thermocline
Hirsutella scitula	9.24	5.32	3.92	Hirsutella	Globigerinidae	M3-globular with supplementary apertures	E4-sub-thermocline
Hirsutella theyeri	9.69	4.81	4.88	Hirsutella	Globorotaliidae	M16-globorotaliform, non-keeled	E4-sub-thermocline
Igorina albeari	3.60	0.00	3.60	Igorina	Globigerinidae	M2-globular	E1-With Symbionts
Igorina anapetes	56.82	50.20	6.61	Igorina	Truncorotaloididae	M17-muricate, acarininiform	E1-With Symbionts
Igorina broedermanni	56.53	54.61	1.92	Igorina	Hedbergellidae	M13-turborotaliform, non-keeled	E1-With Symbionts

Igorina lodoensis	56.53	45.72	10.81	Igorina	Truncorotaloididae	M17-muricate, acarininiform	E1-With Symbionts
Igorina pusilla	56.82	50.32	6.50	Igorina	Truncorotaloididae	M7-globular	E1-With Symbionts
Igorina tadjikistanensis	56.53	50.79	5.74	Igorina	Truncorotaloididae	M17-muricate, acarininiform	E1-With Symbionts
Menardella archeomenardii	7.17	0.00	7.17	Menardella	Globorotaliidae	M7-globular	E3-thermocline
Menardella exilis	7.37	2.30	5.07	Menardella	Globigerinidae	M7-globular	E3-thermocline
Menardella fimbriata	8.93	5.32	3.61	Menardella	Globigerinidae	M3-globular with supplementary apertures	E3-thermocline
Menardella limbata	5.83	0.00	5.83	Menardella	Globorotaliidae	M15-globorotaliform, anguloconical	E3-thermocline
Menardella menardii	5.72	5.02	0.70	Menardella	Globorotaliidae	M15-globorotaliform, anguloconical	E3-thermocline
Menardella miocenica	8.48	5.83	2.65	Menardella	Globorotaliidae	M14-globorotaliform, keeled	E3-thermocline
Menardella multicamerata	6.73	2.98	3.75	Menardella	Globorotaliidae	M14-globorotaliform, keeled	E3-thermocline
Menardella pertenuis	7.77	2.30	5.47	Menardella	Globorotaliidae	M14-globorotaliform, keeled	E3-thermocline
Menardella praemenardii	8.56	1.60	6.96	Menardella	Globorotaliidae	M7-globular	E3-thermocline
Menardella pseudomiocenica	6.14	5.59	0.55	Menardella	Globorotaliidae	M14-globorotaliform, keeled	E3-thermocline
Morozovella acuta	26.48	3.87	22.61	Morozovella	Globoquadrinidae	M7-globular	E1-With Symbionts
Morozovella acutispira	26.70	10.21	16.50	Morozovella	Globoquadrinidae	M7-globular	E1-With Symbionts
Morozovella aequa	24.86	0.00	24.86	Morozovella	Globigerinidae	M1-flat	E1-With Symbionts
Morozovella allisonensis	29.18	20.94	8.24	Morozovella	Globigerinidae	M2-globular	E1-With Symbionts
Morozovella angulata	27.68	10.46	17.22	Morozovella	Globigerinidae	M2-globular	E1-With Symbionts
Morozovella apanthesma	25.21	22.96	2.25	Morozovella	Globigerinidae	M6-planispiral	E1-With Symbionts
Morozovella aragonensis	29.91	23.55	6.36	Morozovella	Globoquadrinidae	M7-globular	E1-With Symbionts
Morozovella caucasica	30.28	10.46	19.82	Morozovella	Globigerinidae	M2-globular	E1-With Symbionts
Morozovella conicotruncata	27.26	16.98	10.28	Morozovella	Globigerinidae	M2-globular	E1-With Symbionts
Morozovella crater	29.18	10.46	18.72	Morozovella	Globigerinidae	M6-planispiral	E1-With Symbionts
Morozovella edgari	31.29	22.90	8.39	Morozovella	Globigerinidae	M2-globular	E1-With Symbionts
Morozovella formosa	30.68	26.93	3.75	Morozovella	Globigerinidae	M2-globular	E1-With Symbionts
Morozovella gracilis	25.91	22.96	2.95	Morozovella	Globigerinidae	M6-planispiral	E1-With Symbionts
Morozovella lensiformis	30.68	2.30	28.38	Morozovella	Globigerinidae	M2-globular	E1-With Symbionts
Morozovella marginodentata	26.02	19.30	6.72	Morozovella	Globigerinidae	M3-globular with supplementary apertures	E1-With Symbionts
Morozovella occlusa	25.91	2.09	23.82	Morozovella	Globigerinidae	M2-globular	E1-With Symbionts
Morozovella pasionensis	25.31	19.09	6.22	Morozovella	Globoquadrinidae	M7-globular	E1-With Symbionts
Morozovella praeangulata	29.17	4.20	24.97	Morozovella	Globigerinidae	M5-clavate	E1-With Symbionts
Morozovella subbotinae	25.21	22.69	2.52	Morozovella	Globigerinidae	M16-globorotaliform, non-keeled	E1-With Symbionts
Morozovella velascoensis	30.41	16.34	14.07	Morozovella	Globigerinidae	M2-globular	E1-With Symbionts

Morozovelloides bandyi	21.12	16.38	4.74	Morozovelloides	Globigerinidae	M3-globular with supplementary apertures	E1-With Symbionts
Morozovelloides coronatus	30.55	15.55	15.00	Morozovelloides	Globigerinidae	M2-globular	E1-With Symbionts
Morozovelloides crassatus	17.54	0.00	17.54	Morozovelloides	Globigerinidae	M2-globular	E1-With Symbionts
Morozovelloides lehneri	21.96	0.00	21.96	Morozovelloides	Globigerinidae	M3-globular with supplementary apertures	E1-With Symbionts
Neogloboquadrina acostaensis	61.33	57.56	3.77	Neogloboquadrina	Truncorotaloididae	M12-turborotaliform, keeled	E3-thermocline
Neogloboquadrina continuosa	60.73	57.10	3.63	Neogloboquadrina	Hedbergellidae	M12-turborotaliform, keeled	E3-thermocline
Neogloboquadrina dutertrei	61.33	55.20	6.13	Neogloboquadrina	Truncorotaloididae	M19-muricocarinate, anguloconical	E3-thermocline
Neogloboquadrina humerosa	61.54	55.49	6.05	Neogloboquadrina	Truncorotaloididae	M18-muricocarinate, keeled	E3-thermocline
Neogloboquadrina pachyderma	66.02	63.76	2.26	Neogloboquadrina	Hedbergellidae	M13-turborotaliform, non-keeled	E5-high-latitude
Orbulina suturalis	54.61	50.20	4.41	Orbulina	Truncorotaloididae	M17-muricate, acarininiform	E3-thermocline
Orbulina universa	54.61	50.44	4.18	Orbulina	Truncorotaloididae	M19-muricocarinate, anguloconical	E4-sub-thermocline
Orbulinoides beckmanni	54.61	50.20	4.41	Orbulinoides	Truncorotaloididae	M17-muricate, acarininiform	E1-With Symbionts
Paragloborotalia acrostoma	40.98	33.90	7.08	Paragloborotalia	Hantkeninidae	M10-tubulospinate	E3-thermocline
Paragloborotalia bella	42.09	35.89	6.20	Paragloborotalia	Truncorotaloididae	M17-muricate, acarininiform	E3-thermocline
Paragloborotalia griffinoides	43.70	39.67	4.02	Paragloborotalia	Hantkeninidae	M10-tubulospinate	E4-sub-thermocline
Paragloborotalia incognita	42.67	23.03	19.64	Paragloborotalia	Globigerinidae	M2-globular	E3-thermocline
Paragloborotalia kugleri	14.24	0.00	14.24	Paragloborotalia	Globigerinidae	M2-globular	E1-With Symbionts
Paragloborotalia mayeri	39.07	26.59	12.48	Paragloborotalia	Globigerinidae	M2-globular	E3-thermocline
Paragloborotalia nana	38.48	35.89	2.59	Paragloborotalia	Globigerinidae	M3-globular with supplementary apertures	E3-thermocline
Paragloborotalia opima	42.78	40.23	2.56	Paragloborotalia	Truncorotaloididae	M17-muricate, acarininiform	E3-thermocline
Paragloborotalia pseudokugleri	14.08	4.53	9.55	Paragloborotalia	Globigerinidae	M7-globular	E1-With Symbionts
Paragloborotalia semivera	39.17	30.28	8.89	Paragloborotalia	Hedbergellidae	M13-turborotaliform, non-keeled	E3-thermocline
Paragloborotalia siakensis	38.98	34.68	4.30	Paragloborotalia	Globigerinidae	M2-globular	E3-thermocline
Parasubbotina aff_pseudobulloides	46.32	40.40	5.92	Parasubbotina	Truncorotaloididae	M17-muricate, acarininiform	E4-sub-thermocline
Parasubbotina eoclava	46.72	42.90	3.82	Parasubbotina	Hantkeninidae	M6-planispiral	E6-upwelling/high
Parasubbotina griffinae	46.57	42.90	3.67	Parasubbotina	Hantkeninidae	M6-planispiral	E6-upwelling/high
Parasubbotina inaequispira	46.57	32.21	14.36	Parasubbotina	Globigerinidae	M2-globular	E6-upwelling/high
Parasubbotina prebetica	46.82	15.10	31.72	Parasubbotina	Globigerinidae	M2-globular	E6-upwelling/high
Parasubbotina pseudobulloides	45.72	41.89	3.83	Parasubbotina	Globigerinidae	M2-globular	E4-sub-thermocline
Parasubbotina pseudowilsoni	41.89	29.91	11.98	Parasubbotina	Globigerinidae	M2-globular	E3-thermocline
Parasubbotina varianta	38.58	34.03	4.55	Parasubbotina	Hedbergellidae	M12-turborotaliform, keeled	E3-thermocline
Parasubbotina variospira	43.46	38.98	4.49	Parasubbotina	Hantkeninidae	M10-tubulospinate	E3-thermocline
Planoglobanomalina pseudoalgeriana	70.92	66.02	4.90	Planoglobanomalina	Hedbergellidae	M7-globular	E2-Without Symbionts

Species				Genus	Family	Morphotype	Ecology
Planorotalites capdevilensis	22.96	21.12	1.84	Planorotalites	Globigerinidae	M16-globorotaliform, non-keeled	E2-Without Symbionts
Planorotalites pseudoscitula	22.96	15.10	7.86	Planorotalites	Globigerinidae	M2-globular	E2-Without Symbionts
Praemurica inconstans	57.79	50.67	7.12	Praemurica	Truncorotaloididae	M18-muricocarinate, keeled	E2-Without Symbionts
Praemurica lozanoi	57.10	45.72	11.38	Praemurica	Truncorotaloididae	M17-muricate, acarininiform	E2-Without Symbionts
Praemurica pseudoinconstans	57.79	55.78	2.01	Praemurica	Hedbergellidae	M13-turborotaliform, non-keeled	E2-Without Symbionts
Praemurica taurica	57.79	49.80	8.00	Praemurica	Truncorotaloididae	M17-muricate, acarininiform	E2-Without Symbionts
Praemurica uncinata	58.30	44.55	13.75	Praemurica	Globigerinidae	M2-globular	E2-Without Symbionts
Praeorbulina circularis	54.12	43.46	10.65	Praeorbulina	Truncorotaloididae	M19-muricocarinate, anguloconical	E1-With Symbionts
Praeorbulina curva	52.54	43.23	9.31	Praeorbulina	Truncorotaloididae	M19-muricocarinate, anguloconical	E1-With Symbionts
Praeorbulina glomerosa	53.82	46.32	7.50	Praeorbulina	Truncorotaloididae	M17-muricate, acarininiform	E1-With Symbionts
Praeorbulina sicanus	52.54	46.32	6.22	Praeorbulina	Truncorotaloididae	M17-muricate, acarininiform	E1-With Symbionts
Protentella nicobarensis	55.81	55.75	0.06	Protentella	Truncorotaloididae	M17-muricate, acarininiform	E6-upwelling/high
Protentella prolixa	55.96	55.75	0.21	Protentella	Truncorotaloididae	M18-muricocarinate, keeled	E6-upwelling/high
Protentelloides dalhousiei	56.25	53.03	3.21	Protentelloides	Globigerinidae	M2-globular	E6-upwelling/high
Protentelloides primitiva	56.25	42.78	13.46	Protentelloides	Globigerinidae	M2-globular	E6-upwelling/high
Pseudoglobigerinella bolivariana	55.96	44.78	11.18	Pseudoglobigerinella	Globigerinidae	M2-globular	E6-upwelling/high
Pseudohastigerina micra	66.03	65.77	0.26	Pseudohastigerina	Globigerinidae	M2-globular	E2-Without Symbionts
Pseudohastigerina naguewichiensis	71.75	70.14	1.61	Pseudohastigerina	Hedbergellidae	-	E2-Without Symbionts
Pseudohastigerina sharkriverensis	69.91	66.02	3.89	Pseudohastigerina	Hedbergellidae	M7-globular	E2-Without Symbionts
Pseudohastigerina wilcoxensis	66.04	64.58	1.46	Pseudohastigerina	Globigerinidae	M2-globular	E2-Without Symbionts
Pulleniatina finalis	62.67	55.89	6.78	Pulleniatina	Hedbergellidae	M13-turborotaliform, non-keeled	E3-thermocline
Pulleniatina obliquiloculata	61.97	60.12	1.85	Pulleniatina	Truncorotaloididae	M17-muricate, acarininiform	E3-thermocline
Pulleniatina praecursor	62.29	60.52	1.77	Pulleniatina	Globigerinidae	M2-globular	E3-thermocline
Pulleniatina praespectabilis	63.90	62.08	1.82	Pulleniatina	Hedbergellidae	M13-turborotaliform, non-keeled	E3-thermocline
Pulleniatina primalis	62.49	55.20	7.29	Pulleniatina	Globigerinidae	M2-globular	E3-thermocline
Pulleniatina spectabilis	66.02	63.93	2.09	Pulleniatina	Truncorotaloididae	M7-globular	E3-thermocline
Sphaeroidinella dehiscens	62.13	42.56	19.57	Sphaeroidinella	Truncorotaloididae	M7-globular	E3-thermocline
Sphaeroidinellopsis disjuncta	61.86	55.96	5.90	Sphaeroidinellopsis	Truncorotaloididae	M7-globular	E3-thermocline
Sphaeroidinellopsis kochi	61.13	54.31	6.82	Sphaeroidinellopsis	Hedbergellidae	M13-turborotaliform, non-keeled	E3-thermocline
Sphaeroidinellopsis paenedehiscens	62.29	59.81	2.48	Sphaeroidinellopsis	Truncorotaloididae	M18-muricocarinate, keeled	E3-thermocline
Sphaeroidinellopsis seminulina	60.73	57.79	2.94	Sphaeroidinellopsis	Truncorotaloididae	M18-muricocarinate, keeled	E3-thermocline
Subbotina angiporoides	40.31	34.68	5.63	Subbotina	Globigerinidae	M4-spherical	E3-thermocline
Subbotina cancellata	42.36	38.19	4.17	Subbotina	Truncorotaloididae	M17-muricate, acarininiform	E3-thermocline

Subbotina corpulenta	39.77	33.90	5.87	Subbotina	Hantkeninidae	M10-tubulospinate	E3-thermocline
Subbotina crociapertura	45.25	37.99	7.26	Subbotina	Truncorotaloididae	M17-muricate, acarininiform	E4-sub-thermocline
Subbotina eocaena	43.85	35.99	7.86	Subbotina	Globigerinidae	M1-flat	E4-sub-thermocline
Subbotina gortanii	43.94	43.85	0.09	Subbotina	Hantkeninidae	M10-tubulospinate	E4-sub-thermocline
Subbotina hagni	40.23	34.68	5.55	Subbotina	Globigerinidae	M3-globular with supplementary apertures	E3-thermocline
Subbotina hornibrooki	43.39	34.68	8.71	Subbotina	Globigerinidae	M3-globular with supplementary apertures	E3-thermocline
Subbotina jacksonensis	40.65	37.23	3.42	Subbotina	Hedbergellidae	M7-globular	E3-thermocline
Subbotina linaperta	38.98	26.59	12.38	Subbotina	Globoquadrinidae	M7-globular	E3-thermocline
Subbotina patagonica	43.86	43.39	0.47	Subbotina	Hantkeninidae	M10-tubulospinate	E4-sub-thermocline
Subbotina roesnaesensis	39.97	33.90	6.07	Subbotina	Hantkeninidae	M10-tubulospinate	E3-thermocline
Subbotina senni	46.54	42.27	4.27	Subbotina	Hantkeninidae	M6-planispiral	E5-high-latitude
Subbotina sp1	43.47	41.15	2.33	Subbotina	Hantkeninidae	M10-tubulospinate	E3-thermocline
Subbotina sp2	41.89	38.09	3.80	Subbotina	Hantkeninidae	M10-tubulospinate	E3-thermocline
Subbotina triangularis	36.08	21.66	14.42	Subbotina	Globigerinidae	M1-flat	E2-Without Symbionts
Subbotina triloculinoides	41.48	34.03	7.45	Subbotina	Hedbergellidae	M15-globorotaliform, anguloconical	E3-thermocline
Subbotina trivialis	43.12	22.96	20.16	Subbotina	Globigerinidae	M2-globular	E3-thermocline
Subbotina utilisindex	45.30	39.57	5.73	Subbotina	Globigerinidae	M3-globular with supplementary apertures	E4-sub-thermocline
Subbotina velascoensis	42.00	34.93	7.07	Subbotina	Hedbergellidae	M7-globular	E3-thermocline
Subbotina yeguaensis	43.85	39.77	4.08	Subbotina	Globigerinidae	M3-globular with supplementary apertures	E4-sub-thermocline
Truncorotalia cavernula	14.04	13.68	0.36	Truncorotalia	Globorotaliidae	M13-turborotaliform, non-keeled	E4-sub-thermocline
Truncorotalia crassaconica	14.08	13.13	0.95	Truncorotalia	Globorotaliidae	M14-globorotaliform, keeled	E4-sub-thermocline
Truncorotalia crassaformis	11.49	2.75	8.74	Truncorotalia	Globigerinidae	M2-globular	E4-sub-thermocline
Truncorotalia crassula	12.40	0.80	11.60	Truncorotalia	Globigerinidae	M5-clavate	E4-sub-thermocline
Truncorotalia excelsa	13.75	9.09	4.67	Truncorotalia	Globorotaliidae	M13-turborotaliform, non-keeled	E4-sub-thermocline
Truncorotalia hessi	13.84	13.56	0.27	Truncorotalia	Globorotaliidae	M12-turborotaliform, keeled	E4-sub-thermocline
Truncorotalia oceanica	11.63	4.37	7.26	Truncorotalia	Globigerinidae	M2-globular	E4-sub-thermocline
Truncorotalia pachytheca	13.79	6.96	6.83	Truncorotalia	Globorotaliidae	M13-turborotaliform, non-keeled	E4-sub-thermocline
Truncorotalia ronda	13.36	2.39	10.97	Truncorotalia	Globigerinidae	M3-globular with supplementary apertures	E4-sub-thermocline
Truncorotalia tenuitheca	13.64	11.79	1.85	Truncorotalia	Globorotaliidae	M12-turborotaliform, keeled	E4-sub-thermocline
Truncorotalia tosaensis	13.36	0.00	13.36	Truncorotalia	Globigerinidae	M6-planispiral	E4-sub-thermocline
Truncorotalia truncatulinoides	13.68	11.79	1.89	Truncorotalia	Globorotaliidae	M12-turborotaliform, keeled	E4-sub-thermocline
Truncorotalia viola	13.56	11.79	1.77	Truncorotalia	Globorotaliidae	M12-turborotaliform, keeled	E4-sub-thermocline
Turborotalia altispiroides	57.56	51.17	6.39	Turborotalia	Truncorotaloididae	M17-muricate, acarininiform	E2-Without Symbionts

Turborotalia ampliapertura	57.56	50.44	7.13	Turborotalia	Hedbergellidae	M13-turborotaliform, non-keeled	E2-Without Symbionts
Turborotalia cerroazulensis	10.80	0.00	10.80	Turborotalia	Globorotaliidae	M7-globular	E2-Without Symbionts
Turborotalia cocoaensis	3.77	2.39	1.38	Turborotalia	Globorotaliidae	M14-globorotaliform, keeled	E3-thermocline
Turborotalia cunialensis	3.73	1.47	2.27	Turborotalia	Globorotaliidae	M15-globorotaliform, anguloconical	E2-Without Symbionts
Turborotalia euapertura	65.96	62.56	3.39	Turborotalia	Globigerinidae	M2-globular	E4-sub-thermocline
Turborotalia frontosa	65.82	62.52	3.30	Turborotalia	Truncorotaloididae	M7-globular	E4-sub-thermocline
Turborotalia increbescens	4.45	2.09	2.36	Turborotalia	Globorotaliidae	M14-globorotaliform, keeled	E2-Without Symbionts
Turborotalia pomeroli	57.10	50.67	6.43	Turborotalia	Truncorotaloididae	M18-muricocarinate, keeled	E2-Without Symbionts
Turborotalia possagnoensis	57.79	48.31	9.48	Turborotalia	Truncorotaloididae	M17-muricate, acarininiform	E2-Without Symbionts
Turborotalita carcoselleensis	0.28	0.00	0.28	Turborotalita	Globigerinidae	M5-clavate	E2-Without Symbionts
Turborotalita clarkei	1.69	0.00	1.69	Turborotalita	Globigerinidae	M1-flat	E2-Without Symbionts
Turborotalita cristata	0.89	0.00	0.89	Turborotalita	Globorotaliidae	M15-globorotaliform, anguloconical	E2-Without Symbionts
Turborotalita humilis	0.40	0.06	0.34	Turborotalita	Globorotaliidae	M14-globorotaliform, keeled	E2-Without Symbionts
Turborotalita praequinqueloba	0.19	0.00	0.19	Turborotalita	Globorotaliidae	M14-globorotaliform, keeled	E2-Without Symbionts
Turborotalita quinqueloba	1.91	0.00	1.91	Turborotalita	Globorotaliidae	M15-globorotaliform, anguloconical	E5-high-latitude

Table A2 Morphogroups of morphospecies

	Morphogroup	Morphological Characteristics	Morphogroup Identifier	Morphospecies
Spinose	Morphogroup 1	flat	M1-flat	Turborotalita
	Morphogroup 2	globular	M2-globular	Subbotina, Globigerina, Globoturborotalita
	Morphogroup 3	globular with supplementary apertures	M3-globular with supplementary apertures	Globigerinoides, Globigerinatheka, Guembilitriodes
	Morphogroup 4	spherical	M4-spherical	Praeorbulina, Orbulina, Orbulinoides, Globigerinatheka
	Morphogroup 5	clavate	M5-clavate	Beella
	Morphogroup 6	planispiral	M6-planispiral	Globigerinella
Non-spinose	Morphogroup 7	globular	M7-globular	Globoquadrina
	Morphogroup 8	globular, keeled	M8-globular, keeled	Pulleniatina spectabilis
	Morphogroup 9	planispiral	M9-planispiral	Pseudohastigerina
	Morphogroup 10	tubulospinate	M10-tubulospinate	Hantkenina
	Morphogroup 11	keeled spines	M11-keeled spines	Astrorotalia
	Morphogroup 12	turborotaliform, keeled	M12-turborotaliform, keeled	Turborotalia,some Truncorotalia, Fohsella
	Morphogroup 13	turborotaliform, non-keeled	M13-turborotaliform, non-keeled	Hedbergella
	Morphogroup 14	globorotaliform, keeled	M14-globorotaliform, keeled	Menardella

	Morphogroup 15	globorotaliform, anguloconical	M15-globorotaliform, anguloconical	some Truncorotalia
	Morphogroup 16	globorotaliform, non-keeled	M16-globorotaliform, non-keeled	Hirsutella
	Morphogroup 17	muricate, acarininiform	M17-muricate, acarininiform	Acarinina
	Morphogroup 18	muricocarinate, keeled	M18-muricocarinate, keeled	some Morozovella, Morozovelloides
	Morphogroup 19	muricocarinate, anguloconical	M19-muricocarinate, anguloconical	some Morozovella, Morozovelloides

Table A3 Ecogroups of morphospecies

Ecogroup	Ecological Characteristics	Ecogorup Identifier	Signature
E1-With Symbionts	Open ocean mixed-layer tropical/ subtropical, with symbionts	E1-With Symbionts	Very heavy $\delta_{13}C$ and relatively light $\delta_{18}O$
E2-Without Symbionts	Open ocean mixed-layer tropical/ subtropical, without symbionts	E2-Without Symbionts	$\delta_{13}C$ lighter than species with symbionts; also with relatively light $\delta_{18}O$
E3-thermocline	Open ocean thermocline	E3-thermocline	Light $\delta_{13}C$ and relatively heavy $\delta_{18}O$
E4-sub-thermocline	Open ocean sub-thermocline	E4-sub-thermocline	Very light $\delta_{13}C$ and very heavy $\delta_{18}O$
E5-high-latitude	High-latitude	E5-high-latitude	Species that are only found in high-latitude sites
E6-upwelling/high	Upwelling/high	E6-upwelling/high	Species that are only found in sites of high productivity or upwelling

Table A4 Number of morphospecies and lifespan grouped by family

Family	# of Species	Start of Lifespan	End of Lifespan	Mean Lifespan
Hedbergellidae	29	71.750	30.219	5.381
Globigerinidae	140	66.040	0	9.619
Truncorotaloididae	69	66.020	30.280	5.863
Hantkeninidae	16	47.413	33.900	4.125
Globoquadrinidae	16	38.976	0	13.719
Globorotaliidae	64	22.440	0	3.957
Pulleniatinidae	6	6.608	0	2.701
	340	0	0	6.481

Table A5 Number of morphospecies and lifespan grouped by morphogroup

Morphogroup Identifier	# of Species	Start of Lifespan	End of Lifespan	Mean Lifespan
M1-flat	6	43.850	0	9.866
M2-globular	80	66.040	0	11.425
M3-globular with supplementary apertures	27	45.298	0	7.327
M4-spherical	9	42.359	0	5.390
M5-clavate	6	29.168	0	7.534
M6-planispiral	10	47.413	0	6.705
M7-globular	52	70.919	0	7.850
M8-globular, keeled	1	4.610	4.210	0.400
M9-planispiral	5	55.810	32.100	9.185
M10-tubulospinate	11	43.939	33.900	3.725
M11-keeled spines	0	49.053	46.866	2.187
M12-turborotaliform, keeled	8	61.330	11.790	2.265
M13-turborotaliform, non-keeled	16	66.020	6.960	4.712
M14-globorotaliform, keeled	24	16.690	0	4.515
M15-globorotaliform, anguloconical	17	41.476	0	2.883
M16-globorotaliform, non-keeled	9	25.210	0	3.267
M17-muricate, acarininiform	36	61.970	30.280	6.828
M18-muricocarinate, keeled	13	62.600	50.670	3.923
M19-muricocarinate, anguloconical	8	61.330	40.056	5.853

Table A6 Number of morphospecies and lifespan grouped by ecogroup

Ecogorup Identifier	# of Species	Start of Lifespan	End of Lifespan	Mean Lifespan
E1-With Symbionts	110	56.815	0	7.093
E2-Without Symbionts	42	71.750	0	7.085
E3-thermocline	107	66.020	0	6.782
E4-sub-thermocline	68	65.955	0	7.761
E5-high-latitude	3	66.020	0	16.033
E6-upwelling/high	9	56.245	15.100	9.033

Table A7 Comparison of morphospecies turnover with oxy-18 events

marine δ18O event	age (Ma)	eccentricity related (blue areas) (Ma)	obliquity- and eccentricity related (green areas) (Ma)	speciation age (Ma)	count.	prob.	extinction age (Ma)	count.	prob.	turnover age (Ma)	count.	prob.
							1.9-1.8	4	0.077	1.9-1.8	4	0.077
				2.0-1.9	4	0.077	2.0-1.9	1	0.020	2.0-1.9	5	0.097
				2.1-2.0	2	0.041	2.1-2.0	2	0.041	2.1-2.0	4	0.082
100/98 (37)	2.41-2.35	2.40-2.35					2.4-2.3	7	0.125	2.4-2.3	7	0.125
				2.5-2.4	1	0.018				2.5-2.4	1	0.018
G16-10 (38)	2.92-2.82	2.82-2.72	2.89-2.72							3.0-2.9	1	
M2/MG2 (39)	3.37-3.30		3.27-3.12	3.4-3.3	2	0.035	3.4-3.3	2	0.035	3.4-3.3	4	0.070
							3.6-3.5	2	0.035	3.6-3.5	2	0.035
Gi2/6 (39)	3.78-3.66			3.7-3.6	1	0.018	3.7-3.6	1	0.018	3.7-3.6	2	0.036
				3.8-3.7	2	0.036	3.8-3.7	2	0.036	3.8-3.7	4	0.073
							3.9-3.8	2	0.035	3.9-3.8	2	0.035
Gi16/18 (39)	4.06-4.00		4.12-3.91; 4.29-4.26									
		4.39-4.35		4.4-4.3	2	0.033	4.4-4.3	1	0.017	4.4-4.3	3	0.050
				4.6-4.5	1	0.017	4.6-4.5	2	0.034	4.6-4.5	3	0.051
				4.7-4.6	3	0.051				4.7-4.6	3	0.051
Si4/6 (38)	4.88-4.82	4.83-4.76										
				4.9-4.8	1	0.018	4.9-4.8	4	0.068	4.9-4.8	5	0.086
TG20/22 (39)	5.88-5.81		5.51-5.49; 5.59	5.5-5.4	1	0.017				5.5-5.4	1	0.017
				5.6-5.5	2	0.035	5.6-5.5	1	0.018	5.6-5.5	3	0.053
				5.7-5.6	1	0.018				5.7-5.6	1	0.018
				5.8-5.7	3	0.055				5.8-5.7	3	0.055
				5.9-5.8	2	0.038	5.9-5.8	2	0.038	5.9-5.8	4	0.077
			6.58-6.33	6.7-6.6	1	0.020				6.7-6.6	1	0.020
Tort./Mess. 1,2 (40)	7.3-7.2; 7.0-6.9	7.23-7.2		7.2-7.1	1	0.021				7.2-7.1	1	0.021
Late Tort. (41)	7.6	7.65-7.63	7.27-7.67; 8.08-7.95									
				7.8-7.7	1	0.022				7.8-7.7	1	0.022
				8.6-8.5	2	0.044				8.6-8.5	2	0.044
Mi7? (41)	8.8		8.95-8.74	8.9-8.8	1	0.023	8.9-8.8	1	0.023	8.9-8.8	2	0.047
				9.0-8.9	1	0.023				9.0-8.9	1	0.023
				9.3-9.2	1	0.023	9.3-9.2	1	0.023	9.3-9.2	2	0.047
Mi7? (41,42)	9.6-9.0	9.67-9.63; 9.31-9.27		9.7-9.6	1	0.024				9.7-9.6	1	0.024
				9.9-9.8	1	0.024	9.9-9.8	1	0.024	9.9-9.8	2	0.049

							10.3-10.2	2	0.048	10.3-10.2	2	0.048
Mi6 (41, 43, 44)	10.45-10.35						10.5-10.4	3	0.067	10.5-10.4	3	0.067
Mi5 (41, 43, 44)	11.8-11.7; 11.5-11.4			11.7-11.6	1	0.024				11.7-11.6	1	0.024
							11.8-11.7	3	0.068	11.8-11.7	3	0.068
		12.16-12.10										
		12.52-12.48	12.62-12.42	12.5-12.4	1	0.023	12.5-12.4	3	0.065	12.5-12.4	4	0.088
Mi4 (41, 43)	13.2 / 12.8			13.2-13.1	1	0.022	13.2-13.1	1	0.022	13.2-13.1	2	0.043
				13.7-13.6	2	0.044	13.7-13.6	1	0.023	13.7-13.6	3	0.067
				13.8-13.7	2	0.045	13.8-13.7	1	0.023	13.8-13.7	3	0.069
Mi3B (43, 45-47)	13.9-13.8		13.69-13.62	13.9-13.8	1	0.023	13.9-13.8	3	0.067	13.9-13.85	4	0.090
				14.1-14.0	3	0.067				14.1-14.0	3	0.067
				14.8-14.7	2	0.045	14.8-14.7	2	0.045	14.8-14.7	4	0.091
Mi3A (47)	14.2	14.16-14.10		14.3-14.2	1	0.024	14.3-14.2	1	0.024	14.3-14.2	2	0.024
			14.90-14.89; 15.02-14.93	15.2-15.1	3	0.070	15.2-15.1	2	0.048	15.2-15.1	5	0.117
Mi2 (43, 48)	15.9		16.07-16.00; 15.89-15.68	16.0-15.9	1	0.023	16.0-15.9	1	0.023	16.0-15.9	2	0.045
				16.4-16.3	3	0.073	16.4-16.3	6	0.136	16.4-16.3	9	0.210
M1b (42, 49)	17.4-17.3	19.98-16.94	17.44-17.25	17.3-17.2	2	0.045				17.3-17.2	2	0.045
				17.6-17.5	3	0.071	17.6-17.5	2	0.049	17.6-17.5	5	0.120
			18.30-18.26	18.3-18.2	1	0.025				18.3-18.2	1	0.025
		19.04-18.95		19.1-19.0	1	0.028	19.1-19.0	1	0.028	19.1-19.0	2	0.056
M1aa (48, 49)	19.4		19.47-19.42				19.4-19.3	2	0.053	19.4-19.3	2	0.053
M1a (42, 50)	21.15-21.05	21.06-21.00		21.2-21.1	2	0.053	21.2-21.1	1	0.027	21.2-21.1	3	0.080
		21.42-21.39										
			21.91-21.88	21.9-21.8	1	0.028	21.9-21.8	1	0.028	21.9-21.8	2	0.056
				22.5-22.4	4	0.028				22.5-22.4	4	0.028
Mi1 (43, 50)	23.1-23.0			23.0-22.9	3	0.100	23.0-22.9	4	0.129	23.0-22.9	7	0.229
		23.90-23.82										
			24.34-24.15									

Table A8 FAD, LAD, lifespan, family and groups of Planktonic Foraminifera lineages

Lineage Name	FAD	LAD	Lifespan	Morphogroup	Ecogroup
[Ancestor]: H. [ancestor]	71.750	70.140	1.610	-	-
N1-N3: H. holmdelensis > G. archeocompressa > G. planocompressa > G. compressa	70.919	62.672	8.247	M7-globular	E3-thermocline
N102-T100: A. subsphaerica > A. mckannai > A. soldadoensis	60.520	54.846	5.674	M17-muricate, acarininiform	E1-With Symbionts
N103-N109-N115-N117-T118: A. soldadoensis > A. esnehensis > A. angulosa > A. interposita > A. alticonica	57.445	48.310	9.135	M17-muricate, acarininiform	E1-With Symbionts
N104-T105: A. esnehensis	56.530	50.200	6.330	M17-muricate, acarininiform	E1-With Symbionts
N106-T107: A. sibaiyaensis	55.960	55.746	0.214	M17-muricate, acarininiform	E1-With Symbionts
N110-N112-T113: A. interposita > A. pentacamerata > A. aspensis > A. collactea > A. medizzai	53.181	30.280	22.901	M17-muricate, acarininiform	E1-With Symbionts
N119-T120: A. alticonica > A. pseudosubsphaerica	50.670	41.890	8.780	M17-muricate, acarininiform	E1-With Symbionts
N126-N127: A. coalingensis > A. primitiva	57.560	38.778	18.782	M17-muricate, acarininiform	E1-With Symbionts
N128-T129: A. esnaensis > A. wilcoxensis > A. pseudotopilensis	57.560	50.795	6.765	M17-muricate, acarininiform	E1-With Symbionts
N13-T14: G. australiformis	55.893	43.540	12.353	M13-turborotaliform, non-keeled	E3-thermocline
N130-N131-N136-N142-N144-T148: A. pseudotopilensis > A. quetra > A. boudreauxi > A. mcgowrani > A. bullbrooki > A. praetopilensis > M. bandyi > M. crassatus > M. coronatus > A. topilensis > A. rohri	55.276	39.970	15.306	M17-muricate, acarininiform	E1-With Symbionts
N133-T135: A. boudreauxi > A. bullbrooki > A. punctocarinata	46.567	40.400	6.167	M17-muricate, acarininiform	E1-With Symbionts
N137-N139-T143: M. bandyi > M. crassatus > M. coronatus > M. lehneri	44.408	37.990	6.418	M17-muricate, acarininiform	E1-With Symbionts
N145-T146: A. topilensis > A. rohri	41.393	40.228	1.165	M17-muricate, acarininiform	E1-With Symbionts
N149-N163: D. galavisi > D. pseudovenezuelana	38.976	34.764	4.212	M7-globular	E3-thermocline
N15-N17: T. frontosa > T. possagnoensis > T. pomeroli > T. cerroazulensis > T. altispiroides > T. increbescens > T. cocoaensis	48.310	37.322	10.988	M7-globular	E4-sub-thermocline
N150-N151-T153: P. pseudokugleri > P. kugleri	25.210	21.120	4.090	M16-globorotaliform, non-keeled	E1-With Symbionts
N152-T154: F. peripheroronda > F. birnageae > F. peripheroacuta > F. praefohsi > F. lenguaensis > F. paralenguaensis > F. fohsi > F. lobata > F. robusta	21.484	11.790	9.694	M13-turborotaliform, non-keeled	E3-thermocline
N165: D. galavisi > D. globularis > D. sp	34.764	33.900	0.864	M7-globular	E3-thermocline
N166-T167: D. tapuriensis > D. sellii	33.900	24.795	9.105	M7-globular	E4-sub-thermocline
N168: D. sellii > D. binaiensis	32.206	24.795	7.411	M7-globular	E4-sub-thermocline
N171: D. galavisi > D. globularis > D. sp > D. prasaepis > D. venezuelana	33.900	32.629	1.271	M7-globular	E3-thermocline
N172: D. prasaepis > D. venezuelana > D. rohri	32.629	29.302	3.327	M7-globular	E4-sub-thermocline
N175: D. galavisi > D. globularis > D. baroemoenensis	32.629	26.704	5.926	M7-globular	E3-thermocline
N177: D. galavisi > D. globularis > D. baroemoenensis	26.704	26.591	0.113	M7-globular	E3-thermocline
N179-T180: D. larmeui > G. dehiscens	26.704	10.208	16.496	M7-globular	E3-thermocline
N18-T19: T. pomeroli > T. cerroazulensis > T. cocoaensis	37.322	34.030	3.292	M7-globular	E2-Without Symbionts

N182-T183: P. aff_pseudobulloides > P. pseudobulloides > P. varianta	66.033	60.625	5.408	M2-globular	E4-sub-thermocline
N184-N186-N187-N188-T189: P. varianta > P. variospira > P. griffinoides > P. pseudowilsoni	63.394	40.400	22.994	M2-globular	E3-thermocline
N190-N199-T200: G. quadrocameratus > C. unicavus > G. eovariabilis	55.683	33.900	21.783	M2-globular	E4-sub-thermocline
N191-T192: P. griffinoides > P. nana	55.200	33.900	21.300	M2-globular	E4-sub-thermocline
N193-N195-T197: P. nana > P. opima > P. incognita	45.486	15.100	30.386	M2-globular	E3-thermocline
N201-N998-N295-N203: G. eovariabilis > G. testarugosa > G. hexagonus > G. variabilis	43.484	13.836	29.647	M2-globular	E4-sub-thermocline
N206-N210-N212-T213: C. unicavus > C. howei > C. globiformis > C. dissimilis	54.117	17.540	36.577	M2-globular	E4-sub-thermocline
N207-T208: C. howei > C. africanus	43.007	33.900	9.107	M2-globular	E4-sub-thermocline
N21-T24: T. increbescens > T. ampliapertura	37.322	30.280	7.042	M13-turborotaliform, non-keeled	E2-Without Symbionts
N215-N217-N231-N235-T236: P. inaequispira > P. prebetica > P. griffinae > P. bolivariana	55.960	44.783	11.177	M2-globular	E6-upwelling/high
N218-T219: P. eoclava	48.648	43.540	5.108	M2-globular	E6-upwelling/high
N220-N221-T362: C. eocanica > C. colombiana > C. jarvisi > C. akersi	47.413	34.290	13.123	M6-planispiral	E4-sub-thermocline
N223-N225-N227-T228: C. caucasica > H. singanoae > H. mexicana > H. liebusi > H. lehneri > H. dumblei > H. australis > H. compressa > H. primitiva > H. alabamensis > H. nanggulanensis	44.033	33.900	10.133	M10-tubulospinate	E4-sub-thermocline
N23-N156-N157-N160-T161: N. continuosa > N. acostaensis > N. humerosa > P. primalis > P. praecursor	22.440	1.804	20.636	M7-globular	E3-thermocline
N232-T233: P. griffinae > P. bolivariana	46.866	37.322	9.544	M2-globular	E6-upwelling/high
N237-T238: G. nuttalli > G. subconglobata > G. kugleri > G. mexicana > G. korotkovi > G. barri	45.720	41.890	3.830	M2-globular	E3-thermocline
N239-N240-N244-N246-T247: G. subconglobata > G. kugleri > G. mexicana > G. korotkovi > G. barri > G. curryi > G. index	43.501	35.667	7.835	M3-globular with supplementary apertures	E1-With Symbionts
N241-T242: G. mexicana > G. semiinvoluta	43.424	36.081	7.343	M3-globular with supplementary apertures	E1-With Symbionts
N248-T249: G. index	42.560	34.680	7.880	M3-globular with supplementary apertures	E1-With Symbionts
N25: H. praescitula > G. zealandica	18.260	16.690	1.570	M16-globorotaliform, non-keeled	E4-sub-thermocline
N251-T252: G. kugleri > G. curryi	43.463	39.770	3.692	M3-globular with supplementary apertures	E1-With Symbionts
N253-T254: G. curryi > G. euganea > O. beckmanni	43.346	39.970	3.376	M3-globular with supplementary apertures	E1-With Symbionts
N256-N2-N198-T67: H. monmouthensis	69.907	66.020	3.887	M7-globular	E3-thermocline
N257: E. eobulloides > E. edita > S. trivialis	66.040	65.603	0.438	M2-globular	E3-thermocline
N259-N261-N262-T263: S. trivialis > S. triloculinoides > S. triangularis	65.603	55.200	10.403	M2-globular	E3-thermocline
N26-N32: H. praescitula > G. zealandica > M. archeomenardii > H. scitula > H. gigantea	16.690	14.240	2.450	M16-globorotaliform, non-keeled	E4-sub-thermocline
N264-N265-N276-N278-N281-N283-T284: S. roesnaesensis > S. eocaena > S. senni > S. yeguaensis > G. officinalis > G. praebulloides > G. ciperoensis > G. obesa	56.245	22.960	33.285	M2-globular	E3-thermocline
N267: S. eocaena > S. hagni > S. corpulenta	49.053	45.064	3.989	M2-globular	E4-sub-thermocline
N269: S. eocaena > S. jacksonensis	45.064	42.359	2.705	M2-globular	E4-sub-thermocline
N27: G. miozea > G. conoidea > G. conomiozea > G. terminalis > G. sphericomiozea	16.690	5.321	11.369	M14-globorotaliform, keeled	E3-thermocline
N271-T272: S. eocaena > S. sp1 > S. sp2	42.359	32.312	10.047	M2-globular	E4-sub-thermocline

N273-T274: S. sp1 > S. sp2	33.582	32.735	0.847	M2-globular	E3-thermocline
N279-T280: G. ciperoensis > G. angulisuturalis	30.550	22.900	7.650	M2-globular	E2-Without Symbionts
N285-N286-T288: G. praebulloides > G. primordius > G. eamesi > G. falconensis > G. bulloides > G. umbilicata	28.574	0	28.574	M2-globular	E1-With Symbionts
N291-T372: G. eamesi	24.381	2.091	22.290	M2-globular	E1-With Symbionts
N292-T299: B. praedigitata > B. digitata	10.200	0	10.200	M5-clavate	E4-sub-thermocline
N30: M. archeomenardii	14.240	14.075	0.165	M14-globorotaliform, keeled	E3-thermocline
N301-T303: G. calida	3.800	0	3.800	M2-globular	E3-thermocline
N305: S. cancellata > S. velascoensis	62.889	60.014	2.874	M2-globular	E3-thermocline
N306-T307: S. velascoensis > S. hornibrooki	60.014	55.200	4.814	M2-globular	E3-thermocline
N308-T309: S. hornibrooki > G. bassriverensis	55.810	53.033	2.777	M2-globular	E3-thermocline
N310-T313: S. cancellata > S. patagonica > S. linaperta > S. angiporoides > S. utilisindex	60.014	30.280	29.734	M2-globular	E3-thermocline
N314-N318: G. bassriverensis > T. carcoselleensis > G. martini > G. ouachitaensis	55.200	42.002	13.198	M2-globular	E2-Without Symbionts
N315-T316: T. carcoselleensis > T. praequinqueloba > T. quinqueloba > T. humilis	43.656	0	43.656	M1-flat	E2-Without Symbionts
N319-T320: G. ouachitaensis > G. gnaucki	42.002	23.032	18.969	M2-globular	E1-With Symbionts
N322: G. martini > G. woodi > G. labiacrassata	42.002	30.280	11.722	M2-globular	E1-With Symbionts
N324-N336-N342-N344-N348-N352-N354-T356: G. woodi > G. connecta > G. trilobus > G. parawoodi > S. disjuncta > G. bollii > G. nepenthes > G. decoraperta > G. apertura	30.280	1.640	28.640	M2-globular	E1-With Symbionts
N325-T361: G. brazieri > G. subquadratus	22.960	15.100	7.860	M2-globular	E1-With Symbionts
N326-N332-N334-T360: G. subquadratus > G. altiapertura > G. obliquus > G. mitra > G. diminutus	22.042	11.540	10.502	M3-globular with supplementary apertures	E1-With Symbionts
N327-N329-T330: G. altiapertura > G. obliquus > G. extremus	20.789	1.300	19.489	M3-globular with supplementary apertures	E1-With Symbionts
N337-N339-T341: G. connecta > G. trilobus > G. bisphericus > G. sacculifer > G. fistulosus	21.882	0	21.882	M2-globular	E1-With Symbionts
N34-N40-T44: M. praemenardii > M. menardii > M. limbata > G. merotumida > M. fimbriata	14.075	0	14.075	M14-globorotaliform, keeled	E3-thermocline
N345-T347: S. disjuncta > S. seminulina > S. kochi > S. paenedehiscens > S. dehiscens	17.540	0	17.540	M7-globular	E3-thermocline
N349-T350: G. decoraperta > G. rubescens > G. tenella	10.790	0	10.790	M2-globular	E2-Without Symbionts
N35-N37-T39: M. limbata > M. pseudomiocenica > M. miocenica	10.300	2.300	8.000	M14-globorotaliform, keeled	E3-thermocline
N358-T229: H. alabamensis > H. nanggulanensis	37.513	33.900	3.613	M10-tubulospinate	E2-Without Symbionts
N364-T162: P. primalis > P. praecursor > P. obliquiloculata > P. finalis	5.700	0	5.700	M7-globular	E3-thermocline
N366-N298-N300-T304: G. obesa > G. praesiphonifera > G. siphonifera > B. praedigitata > G. calida	30.158	0	30.158	M2-globular	E3-thermocline
N4-T12: G. compressa > G. ehrenbergi > G. chapmani > G. pseudomenardii > G. planoconica > P. pseudoalgeriana	62.672	44.595	18.077	M13-turborotaliform, non-keeled	E3-thermocline
N42-T41: G. merotumida > G. plesiotumida	9.449	3.770	5.679	M14-globorotaliform, keeled	E3-thermocline
N45-T43: G. tumida > G. ungulata > G. flexuosa	5.720	0	5.720	M14-globorotaliform, keeled	E3-thermocline
N47: H. praescitula > H. scitula > H. gigantea	14.240	8.478	5.762	M14-globorotaliform, keeled	E4-sub-thermocline
N48-T50: H. praemargaritae > H. primitiva > H. margaritae > H. evoluta > H. hirsuta	8.478	0	8.478	M14-globorotaliform, keeled	E4-sub-thermocline

N5-N6-N8-T9: G. imitata > G. ovalis > G. luxorensis > P. wilcoxensis > P. micra > P. sharkriverensis	62.672	32.312	30.360	M13-turborotaliform, non-keeled	E3-thermocline
N51-N122-T123: H. scitula	8.478	0	8.478	M14-globorotaliform, keeled	E4-sub-thermocline
N52-N54-T53: H. cibaoensis > T. crassula	9.440	4.490	4.950	M16-globorotaliform, non-keeled	E4-sub-thermocline
N56-N58-N59-T61: T. crassaformis > T. oceanica > T. ronda > T. viola > T. hessi	5.828	0	5.828	M15-globorotaliform, anguloconical	E4-sub-thermocline
N62-T63: T. tenuitheca > T. tosaensis > T. truncatulinoides > T. excelsa > T. pachytheca	3.593	0.610	2.983	M15-globorotaliform, anguloconical	E4-sub-thermocline
N64-T66: T. truncatulinoides > T. excelsa > T. pachytheca > T. cavernula	1.465	0	1.465	M15-globorotaliform, anguloconical	E4-sub-thermocline
N68-N69-N70-N71: P. taurica > P. pseudoinconstans > P. inconstans > P. uncinata	66.020	62.077	3.943	M7-globular	E2-Without Symbionts
N72: I. pusilla > I. tadjikistanensis	62.290	61.330	0.960	M7-globular	E1-With Symbionts
N76-N101: M. praeangulata > M. angulata > M. conicotruncata	62.600	61.543	1.057	M18-muricocarinate, keeled	E1-With Symbionts
N77-T266: S. yeguaensis > S. crociapertura > S. gortanii	47.712	26.591	21.122	M2-globular	E4-sub-thermocline
N79: M. pasionensis > M. acutispira > M. occlusa	60.116	59.307	0.809	M18-muricocarinate, keeled	E1-With Symbionts
N80-N368-N370-T78: M. conicotruncata > M. velascoensis > M. pasionensis > M. acutispira > M. occlusa > M. acuta > M. edgari	61.543	55.200	6.343	M19-uricocarinate, anguloconical	E1-With Symbionts
N83-N84-T85: M. praeangulata > M. angulata > M. apanthesma > M. aequa > P. pseudoscitula	61.543	50.670	10.873	M18-muricocarinate, keeled	E1-With Symbionts
N86-T87: P. pseudoscitula > P. capdevilensis	56.958	36.558	20.399	M17-muricate, acarininiform	E2-Without Symbionts
N88-N89-N90-N93: M. subbotinae > M. marginodentata > M. gracilis	57.100	50.670	6.430	M18-muricocarinate, keeled	E1-With Symbionts
N94-T95: M. lensiformis > M. crater > M. aragonensis	54.610	43.230	11.380	M19-uricocarinate, anguloconical	E1-With Symbionts
N98-T96: M. crater > M. caucasica	52.786	43.463	9.324	M19-uricocarinate, anguloconical	E1-With Symbionts
N99-N125: A. strabocella > A. nitida > A. coalingensis	61.970	57.560	4.410	M17-muricate, acarininiform	E1-With Symbionts
T10: P. naguewichiensis	35.890	32.100	3.790	M9-planispiral	E2-Without Symbionts
T108: A. africana	55.810	55.746	0.064	M17-muricate, acarininiform	E1-With Symbionts
T11: G. pseudomenardii	60.709	57.100	3.609	M12-turborotaliform, keeled	E3-thermocline
T111: A. aspensis	49.053	48.011	1.041	M17-muricate, acarininiform	E1-With Symbionts
T114: A. medizzai	41.311	35.890	5.421	M17-muricate, acarininiform	E1-With Symbionts
T116: A. angulosa > A. cuneicamerata	51.667	43.540	8.127	M17-muricate, acarininiform	E1-With Symbionts
T121: A. echinata	42.783	31.898	10.886	M17-muricate, acarininiform	E1-With Symbionts
T124: H. bermudezi	2.091	0	2.091	M16-globorotaliform, non-keeled	E4-sub-thermocline
T132: A. quetra	53.821	50.200	3.621	M17-muricate, acarininiform	E1-With Symbionts
T134: A. punctocarinata	44.080	40.400	3.680	M17-muricate, acarininiform	E1-With Symbionts
T138: M. lehneri	43.939	40.056	3.883	M17-muricate, acarininiform	E1-With Symbionts
T140: A. mcgowrani	43.811	37.990	5.821	M17-muricate, acarininiform	E1-With Symbionts
T141: M. bandyi	43.540	41.890	1.650	M17-muricate, acarininiform	E1-With Symbionts
T147: A. rohri	40.814	38.187	2.627	M17-muricate, acarininiform	E1-With Symbionts
T155: F. lenguaensis > F. paralenguaensis	13.563	6.960	6.602	M13-turborotaliform, non-keeled	E3-thermocline
T158: N. humerosa > N. dutertrei	8.100	0	8.100	M7-globular	E3-thermocline
T159: N. pachyderma	10.800	0	10.800	M7-globular	E5-high-latitude

T16: T. altispiroides	39.970	37.226	2.744	M7-globular	E2-Without Symbionts
T164: D. pseudovenezuelana	34.764	26.817	7.947	M7-globular	E3-thermocline
T169: D. sellii	24.795	23.343	1.452	M7-globular	E4-sub-thermocline
T170: D. binaiensis	24.795	19.090	5.705	M7-globular	E4-sub-thermocline
T173: D. rohri	29.302	23.551	5.751	M7-globular	E4-sub-thermocline
T174: D. prasaepis > D. venezuelana > G. conglomerata	29.302	0	29.302	M7-globular	E4-sub-thermocline
T176: D. globularis > D. globosa > D. altispira	26.591	3.130	23.461	M7-globular	E3-thermocline
T178: D. baroemoenensis	26.591	3.300	23.291	M7-globular	E3-thermocline
T181: G. dehiscens	21.643	5.925	15.719	M7-globular	E3-thermocline
T185: P. variospira	61.863	60.520	1.343	M2-globular	E3-thermocline
T194: P. semivera > P. siakensis > P. mayeri > P. acrostoma > P. bella	30.550	10.460	20.090	M2-globular	E3-thermocline
T196: P. opima	29.669	26.930	2.739	M2-globular	E3-thermocline
T20: T. cocoaensis > T. cunialensis	34.848	34.030	0.818	M12-turborotaliform, keeled	E3-thermocline
T202: G. testarugosa	30.415	21.882	8.532	M2-globular	E4-sub-thermocline
T204: G. variabilis	13.836	4.813	9.023	M2-globular	E4-sub-thermocline
T205: G. hexagonus	13.836	0	13.836	M2-globular	E4-sub-thermocline
T209: C. africanus	37.895	34.680	3.215	M2-globular	E4-sub-thermocline
T211: C. globiformis	39.371	34.680	4.691	M4-spherical	E4-sub-thermocline
T214: C. stainforthi > C. parvulus	27.261	9.830	17.431	M2-globular	E4-sub-thermocline
T216: P. prebetica	51.543	50.795	0.748	M2-globular	E6-upwelling/high
T22: T. ampliapertura > T. euapertura	33.053	30.219	2.834	M7-globular	E2-Without Symbionts
T222: C. colombiana > C. jarvisi > C. akersi	46.517	42.270	4.247	M6-planispiral	E4-sub-thermocline
T224: H. lehneri	43.308	41.145	2.162	M10-tubulospinate	E3-thermocline
T226: H. australis	41.062	38.089	2.974	M10-tubulospinate	E3-thermocline
T230: H. nanggulanensis > C. inflata	36.463	33.900	2.563	M10-tubulospinate	E2-Without Symbionts
T234: P. bolivariana	44.642	42.672	1.970	M6-planispiral	E6-upwelling/high
T243: G. semiinvoluta	37.990	35.890	2.100	M3-globular with supplementary apertures	E1-With Symbionts
T245: G. barri	43.346	36.367	6.979	M3-globular with supplementary apertures	E1-With Symbionts
T250: G. tropicalis	39.074	34.030	5.044	M3-globular with supplementary apertures	E1-With Symbionts
T255: G. luterbacheri	40.228	34.680	5.548	M3-globular with supplementary apertures	E1-With Symbionts
T258: E. eobulloides > E. edita > E. spiralis	65.603	62.290	3.313	M2-globular	E3-thermocline
T260: S. triloculinoides	64.539	57.790	6.749	M2-globular	E3-thermocline
T268: S. hagni > S. corpulenta	45.064	32.206	12.858	M2-globular	E3-thermocline
T270: S. jacksonensis	42.359	33.900	8.459	M2-globular	E3-thermocline
T275: S. sp2	33.053	26.591	6.462	M2-globular	E3-thermocline
T277: S. senni	46.866	37.990	8.876	M2-globular	E5-high-latitude
T28: G. terminalis > G. pliozea	5.321	4.177	1.144	M15-globorotaliform, anguloconical	E3-thermocline
T282: G. angulisuturalis	27.344	20.940	6.404	M2-globular	E1-With Symbionts

T287: G. primordius	22.440	19.300	3.140	M3-globular with supplementary apertures	E1-With Symbionts
T29: G. sphericomiozea > G. puncticulata > G. inflata	5.321	0	5.321	M7-globular	E3-thermocline
T294: B. megastoma	0.282	0	0.282	M5-clavate	E4-sub-thermocline
T297: C. bermudezi	15.768	12.404	3.364	M5-clavate	E4-sub-thermocline
T302: G. adamsi	0.014	0	0.014	M5-clavate	E4-sub-thermocline
T31: M. archeomenardii	14.075	13.870	0.205	M14-globorotaliform, keeled	E3-thermocline
T317: T. humilis > T. cristata > T. clarkei	4.550	0	4.550	M1-flat	E2-Without Symbionts
T321: G. gnaucki > G. anguliofficinalis	34.848	23.032	11.815	M2-globular	E2-Without Symbionts
T323: G. labiacrassata	30.280	16.343	13.937	M2-globular	E2-Without Symbionts
T328: G. conglobatus	6.210	0	6.210	M3-globular with supplementary apertures	E1-With Symbionts
T33: H. challengeri > H. juanai	15.157	4.813	10.344	M16-globorotaliform, non-keeled	E4-sub-thermocline
T331: G. extremus	3.429	1.980	1.449	M3-globular with supplementary apertures	E1-With Symbionts
T333: G. mitra	17.757	12.404	5.353	M3-globular with supplementary apertures	E1-With Symbionts
T335: G. ruber > G. seigliei	15.100	0	15.100	M3-globular with supplementary apertures	E1-With Symbionts
T338: G. bisphericus > P. sicanus > P. curva > P. glomerosa > P. circularis > O. suturalis > O. universa	17.127	0	17.127	M3-globular with supplementary apertures	E1-With Symbionts
T340: G. fistulosus	3.300	1.880	1.420	M3-globular with supplementary apertures	E1-With Symbionts
T343: G. parawoodi	20.853	16.380	4.473	M3-globular with supplementary apertures	E1-With Symbionts
T346: S. kochi	10.814	4.530	6.284	M7-globular	E3-thermocline
T351: G. tenella	2.091	0	2.091	M2-globular	E2-Without Symbionts
T353: G. bollii > G. kennetti	12.404	2.390	10.014	M3-globular with supplementary apertures	E1-With Symbionts
T355: G. nepenthes	10.814	4.370	6.444	M2-globular	E2-Without Symbionts
T357: A. palmerae	49.053	46.866	2.187	M11-keeled spines	E1-With Symbionts
T359: S. angiporoides	38.483	29.913	8.569	M2-globular	E3-thermocline
T36: M. multicamerata	6.733	2.980	3.753	M14-globorotaliform, keeled	E3-thermocline
T363: S. crociapertura	44.736	39.970	4.766	M2-globular	E4-sub-thermocline
T365: P. praespectabilis > P. spectabilis	5.220	4.210	1.010	M7-globular	E3-thermocline
T367: P. prolixa > P. nicobarensis	29.180	4.202	24.978	M6-planispiral	E6-upwelling/high
T369: M. allisonensis	55.960	55.746	0.214	M18-muricocarinate, keeled	E1-With Symbionts
T371: M. edgari	55.200	54.610	0.590	M19-uricocarinate, anguloconical	E1-With Symbionts
T373: G. druryi	21.120	0.563	20.557	M2-globular	E1-With Symbionts
T38: M. exilis > M. pertenuis	4.450	1.804	2.646	M14-globorotaliform, keeled	E3-thermocline
T46: G. ungulata	3.278	0	3.278	M14-globorotaliform, keeled	E3-thermocline
T49: H. theyeri	4.610	0	4.610	M14-globorotaliform, keeled	E4-sub-thermocline
T55: T. crassula	5.591	0.893	4.698	M15-globorotaliform, anguloconical	E4-sub-thermocline
T57: T. crassaconica	4.430	3.732	0.698	M15-globorotaliform, anguloconical	E4-sub-thermocline
T60: T. hessi	1.007	0.375	0.631	M15-globorotaliform, anguloconical	E4-sub-thermocline

T65: T. cavernula	0.780	0	0.780	M15-globorotaliform, anguloconical	E4-sub-thermocline
T7: P. sharkriverensis	44.642	39.271	5.371	M9-planispiral	E2-Without Symbionts
T73: I. albeari	61.330	57.560	3.770	M12-turborotaliform, keeled	E1-With Symbionts
T74: I. tadjikistanensis > I. lodoensis > I. broedermanni > I. anapetes	61.330	43.230	18.100	M7-globular	E1-With Symbionts
T75: P. lozanoi	62.130	42.560	19.570	M7-globular	E2-Without Symbionts
T81: M. occlusa	59.307	55.200	4.107	M18-muricocarinate, keeled	E1-With Symbionts
T82: M. pasionensis > M. acutispira	59.307	55.200	4.107	M18-muricocarinate, keeled	E1-With Symbionts
T91: M. marginodentata	54.728	51.667	3.061	M18-muricocarinate, keeled	E1-With Symbionts
T92: M. gracilis > M. formosa	55.031	50.670	4.361	M18-muricocarinate, keeled	E1-With Symbionts
T97: M. caucasica	46.507	43.667	2.840	M19-uricocarinate, anguloconical	E1-With Symbionts
T999: P. primitiva > P. dalhousiei	25.909	22.960	2.949	M6-planispiral	E6-upwelling/high

Table A9 Number of lineages and lifespan grouped by morphogroup

Morphogroup	#	Start of Lifespan	End of Lifespan	Mean Lifespan
M1-flat	2	43.656	0	24.103
M2-globular	59	66.040	28.491	12.435
M3-globular with supplementary apertures	20	43.501	19.715	7.204
M4-spherical	1	39.371	34.680	4.691
M5-clavate	4	15.768	3.101	3.465
M6-planispiral	5	47.413	29.279	9.454
M7-globular	35	70.919	23.888	8.894
M8-globular, keeled	0	0	NA	NA
M9-planispiral	2	44.642	35.686	4.580
M10-tubulospinate	5	44.033	36.187	4.289
M11-keeled spines	1	49.053	46.866	2.187
M12-turborotaliform, keeled	3	61.330	49.563	2.732
M13-turborotaliform, non-keeled	6	62.672	28.246	14.022
M14-globorotaliform, keeled	14	16.690	3.757	5.873
M15-globorotaliform, anguloconical	8	5.828	1.223	2.279
M16-globorotaliform, non-keeled	6	25.210	10.226	4.249
M17-muricate, acarininiform	25	61.970	43.494	7.171
M18-muricocarinate, keeled	9	62.600	54.519	3.891
M19-uricocarinate, anguloconical	5	61.543	48.034	6.095

Table A10 Number of lineages and lifespan grouped by Ecogroup

Ecogroup	#	Start of Lifespan	End of Lifespan	Mean Lifespan
E1-With Symbionts	72	62.600	0	7.839
E2-Without Symbionts	20	66.020	0	9.465
E3-thermocline	61	70.919	0	9.273
E4-sub-thermocline	48	66.033	0	8.404
E5-high-latitude	2	46.866	0	9.838
E6-upwelling/high	7	55.960	4.202	8.068

Table A11 FAD, LAD, lifespan, family and genus of calcareous nannofossils

Nannos name	FAD	LAD	Lifespan	Family	Genus
Emiliania huxleyi	0.28	0.00	0.28	Noelaerhabdaceae	Emiliania
Gephyrocapsa oceanica (>5.5)	1.57	0.00	1.57	Noelaerhabdaceae	Gephyrocapsa
Gephyrocapsa oceanica (>4)	1.70	0.00	1.70	Noelaerhabdaceae	Gephyrocapsa
Ceratolithus rugosus	4.98	0.00	4.98	Ceratolithaceae	Ceratolithus
Ceratolithus cristatus	5.06	0.00	5.06	Ceratolithaceae	Ceratolithus
Helicosphaera carteri	26.15	0.00	26.15	Helicosphaeraceae	Helicosphaera
Gephyrocapsa omega (<4)	1.05	0.03	1.02	Noelaerhabdaceae	Gephyrocapsa
Gephyrocapsa caribbeanica (>4)	1.68	0.21	1.47	Noelaerhabdaceae	Gephyrocapsa
Pseudoemiliania lacunosa (delicate)	3.92	0.41	3.51	Noelaerhabdaceae	Pseudoemiliania
Pseudoemiliania lacunosa (subell/subcir)	3.92	0.44	3.48	Noelaerhabdaceae	Pseudoemiliania
Gephyrocapsa omega (>4)	0.96	0.58	0.38	Noelaerhabdaceae	Gephyrocapsa
Crenalithus japonicus	3.73	0.78	2.95	Noelaerhabdaceae	Crenalithus
Crenalithus asanoi	1.12	0.83	0.30	Noelaerhabdaceae	Crenalithus
Crenalithus doronicoides	6.31	0.91	5.40	Noelaerhabdaceae	Crenalithus
Gephyrocapsa caribbeanica (>6.5)	1.53	1.24	0.29	Noelaerhabdaceae	Gephyrocapsa
Helicosphaera sellii	5.26	1.25	4.01	Helicosphaeraceae	Helicosphaera
Helicosphaera sellii (lrg holes)	4.98	1.28	3.70	Helicosphaeraceae	Helicosphaera
Calcidiscus macintyrei	12.41	1.61	10.80	Calcidiscaceae	Calcidiscus
Ceratolithus separatus	3.65	1.86	1.79	Ceratolithaceae	Ceratolithus
Discoaster brouweri	11.02	1.90	9.12	Discoasteraceae	Discoaster
Discoaster asymmetricus	8.79	1.92	6.86	Discoasteraceae	Discoaster
Discoaster triradiatus	10.72	1.92	8.79	Discoasteraceae	Discoaster
Discoaster blackstockae	8.89	1.96	6.93	Discoasteraceae	Discoaster
Discoaster dennei	7.33	2.02	5.31	Discoasteraceae	Discoaster
Discoaster pentaradiatus	9.84	2.29	7.56	Discoasteraceae	Discoaster
Discoaster surculus	8.26	2.51	5.75	Discoasteraceae	Discoaster
Discoaster pliostellulus	3.71	2.63	1.07	Discoasteraceae	Discoaster
Discoaster tamalis	4.67	2.73	1.94	Discoasteraceae	Discoaster
Discoaster variabilis	21.22	2.92	18.30	Discoasteraceae	Discoaster
Sphenolithus neoabies	15.94	3.53	12.41	Sphenolithaceae	Sphenolithus
Sphenolithus moriformis	61.61	3.53	58.08	Sphenolithaceae	Sphenolithus

Species	Value 1	Value 2	Value 3	Family	Genus
Sphenolithus verensis	13.43	3.61	9.82	Sphenolithaceae	Sphenolithus
Pontosphaera multipora	55.96	3.63	52.33	Pontosphaeraceae	Pontosphaera
Sphenolithus abies	13.71	3.67	10.04	Sphenolithaceae	Sphenolithus
Discoaster decorus	13.42	3.75	9.67	Discoasteraceae	Discoaster
Reticulofenestra pseudoumbilicus	4.45	3.82	0.63	Noelaerhabdaceae	Reticulofenestra
Reticulofenestra gelida (>8)	18.51	3.86	14.65	Noelaerhabdaceae	Reticulofenestra
Amaurolithus delicatus	7.33	3.93	3.40	Ceratolithaceae	Amaurolithus
Reticulofenestra pseudoumbilicus (>10)	13.94	4.03	9.91	Noelaerhabdaceae	Reticulofenestra
Schyphosphaera globulata (GoM)	8.29	4.05	4.24	Pontosphaeraceae	Schyphosphaera
Helicosphaera zeta	32.02	4.07	27.95	Helicosphaeraceae	Helicosphaera
Discoaster toralus	8.29	4.09	4.21	Discoasteraceae	Discoaster
Dictyococcites antarcticus	33.89	4.09	29.81	Noelaerhabdaceae	Dictyococcites
Helicosphaera intermedia	36.97	4.10	32.87	Helicosphaeraceae	Helicosphaera
Discoaster pansulus (cf. pansus)	14.36	4.24	10.12	Discoasteraceae	Discoaster
Amaurolithus tricorniculatus	5.19	4.45	0.75	Ceratolithaceae	Amaurolithus
Amaurolithus brevigracilis	7.35	4.64	2.70	Ceratolithaceae	Amaurolithus
Cryptococcolithus mediaperforatus	17.14	4.64	12.49	Calcidiscaceae	Cryptococcolithus
Ceratolithus armatus	5.20	4.67	0.54	Ceratolithaceae	Ceratolithus
Amaurolithus bizarrus	5.27	4.67	0.60	Ceratolithaceae	Amaurolithus
Ceratolithus cornulum	5.31	4.67	0.64	Ceratolithaceae	Ceratolithus
Ceratolithus acutus	5.34	4.81	0.53	Ceratolithaceae	Ceratolithus
Amaurolithus ninae	7.37	4.99	2.38	Ceratolithaceae	Amaurolithus
Ceratolithus larrymayeri	5.34	5.08	0.27	Ceratolithaceae	Ceratolithus
Ceratolithus atlanticus	5.39	5.15	0.24	Ceratolithaceae	Ceratolithus
Ceratolithus apiculus	5.37	5.17	0.20	Ceratolithaceae	Ceratolithus
Triquetrorhabdulus rugosus	13.50	5.23	8.27	Ceratolithaceae	Triquetrorhabdulus
Amaurolithus primus	7.56	5.24	2.32	Ceratolithaceae	Amaurolithus
Triquetrorhabdulus finifer	6.91	5.27	1.64	Ceratolithaceae	Triquetrorhabdulus
Reticulofenestra rotaria (<5)	7.27	5.30	1.96	Noelaerhabdaceae	Reticulofenestra
Triquetrorhabdulus farnesworthii	12.42	5.34	7.08	Ceratolithaceae	Triquetrorhabdulus
Triquetrorhabdulus rio	17.73	5.36	12.37	Ceratolithaceae	Triquetrorhabdulus
Triquetrorhabdulus extensus	10.85	5.37	5.48	Ceratolithaceae	Triquetrorhabdulus
Discoaster quinqueramus	8.32	5.44	2.88	Discoasteraceae	Discoaster

Helicosphaera stalis	13.02	5.56	7.46	Helicosphaeraceae	Helicosphaera
Discoaster newellii	8.23	5.59	2.64	Discoasteraceae	Discoaster
Helicosphaera stalis ovata	13.24	5.66	7.58	Helicosphaeraceae	Helicosphaera
Discoaster berggrenii	8.32	5.68	2.64	Discoasteraceae	Discoaster
Discoaster quinqueramus (>15)	7.57	5.74	1.82	Discoasteraceae	Discoaster
Discoaster neorectus	9.69	5.93	3.76	Discoasteraceae	Discoaster
Dictyococcites filewiczii	6.93	5.98	0.95	Noelaerhabdaceae	Dictyococcites
Discoaster tetracladus	8.29	6.00	2.29	Discoasteraceae	Discoaster
Discoaster pseudovariabilis	7.87	6.04	1.83	Discoasteraceae	Discoaster
Discoaster vinsonii	8.29	6.10	2.20	Discoasteraceae	Discoaster
Discoaster compactus	8.26	6.23	2.03	Discoasteraceae	Discoaster
Reticulofenestra rotaria (>5)	7.16	6.34	0.82	Noelaerhabdaceae	Reticulofenestra
Helicosphaera pacifica	11.90	6.34	5.56	Helicosphaeraceae	Helicosphaera
Discoaster subsurculus	14.27	6.46	7.81	Discoasteraceae	Discoaster
Discoaster extensus	15.68	6.46	9.22	Discoasteraceae	Discoaster
Discoaster tristellifer	7.52	6.52	1.00	Discoasteraceae	Discoaster
Discoaster abrachiatus	7.98	6.71	1.27	Discoasteraceae	Discoaster
Discoaster icarus	8.79	6.76	2.03	Discoasteraceae	Discoaster
Discoaster bergenii	8.11	6.80	1.31	Discoasteraceae	Discoaster
Discoaster calcaris	10.51	6.80	3.71	Discoasteraceae	Discoaster
Discoaster loeblichii	8.74	6.82	1.92	Discoasteraceae	Discoaster
Discoaster neohamatus	10.80	7.09	3.71	Discoasteraceae	Discoaster
Discoaster prolixus	8.29	7.20	1.09	Discoasteraceae	Discoaster
Triquetrorhabdulus striatus	8.79	7.20	1.58	Ceratolithaceae	Triquetrorhabdulus
Minylitha convallis	9.75	7.27	2.48	-	Minylitha
Discoaster pachyloeblichii	8.74	7.33	1.41	Discoasteraceae	Discoaster
Discoaster breviloeblichii	8.67	7.37	1.30	Discoasteraceae	Discoaster
Discoaster hexaramus	8.11	7.44	0.67	Discoasteraceae	Discoaster
Catinaster mexicanus	8.20	7.57	0.64	Discoasteraceae	Catinaster
Helicosphaera orientalis	13.64	7.68	5.96	Helicosphaeraceae	Helicosphaera
Discoaster astellaris	11.58	7.91	3.66	Discoasteraceae	Discoaster
Discoaster gemmulatus	11.11	8.03	3.09	Discoasteraceae	Discoaster
Discoaster prepentaradiatus	10.28	8.11	2.17	Discoasteraceae	Discoaster

Discoaster bellus	11.49	8.34	3.15	Discoasteraceae	Discoaster
Discoaster prepentaradiatus plautus	10.20	8.54	1.66	Discoasteraceae	Discoaster
Discoaster styzenii	9.73	8.55	1.18	Discoasteraceae	Discoaster
Discoaster trifolius	9.76	8.90	0.86	Discoasteraceae	Discoaster
Discoaster prepentaradiatus	9.10	8.93	0.17	Discoasteraceae	Discoaster
Discoaster bollii	10.72	9.20	1.51	Discoasteraceae	Discoaster
Discoaster triuncinus	11.02	9.23	1.79	Discoasteraceae	Discoaster
Discoaster hamatus (<15)	11.51	9.23	2.28	Discoasteraceae	Discoaster
Minylitha cancellata	10.12	9.33	0.80	-	Minylitha
Discoaster pentabollii	10.20	9.38	0.82	Discoasteraceae	Discoaster
Discoaster caulifloris	15.94	9.54	6.40	Discoasteraceae	Discoaster
Discoaster tribollii	10.08	9.62	0.46	Discoasteraceae	Discoaster
Discoaster hamatus (>15)	10.96	9.62	1.35	Discoasteraceae	Discoaster
Catinaster calyculus	10.96	9.66	1.30	Discoasteraceae	Catinaster
Catinaster calyculus extensus	10.73	9.69	1.04	Discoasteraceae	Catinaster
Catinaster rotundus	10.89	9.69	1.20	Discoasteraceae	Catinaster
Catinaster coalitus extensus	11.00	9.78	1.22	Discoasteraceae	Catinaster
Catinaster coalitus	11.53	9.83	1.71	Discoasteraceae	Catinaster
Discoaster micros	13.07	10.08	2.99	Discoasteraceae	Discoaster
Discoaster transitus	11.59	10.38	1.21	Discoasteraceae	Discoaster
Catinaster coalitus (>10)	10.73	10.40	0.33	Discoasteraceae	Catinaster
Discoaster gozoensis	17.69	10.45	7.24	Discoasteraceae	Discoaster
Discoaster exilis	17.39	10.49	6.90	Discoasteraceae	Discoaster
Coccolithus pliopelagicus (>11)	65.40	10.80	54.60	Coccolithaceae	Coccolithus
Catinaster glenos	12.76	10.85	1.91	Discoasteraceae	Catinaster
Helicosphaera bownii	15.02	10.85	4.17	Helicosphaeraceae	Helicosphaera
Discoaster discissus	13.88	11.00	2.88	Discoasteraceae	Discoaster
Coccolithus miopelagicus (>14)	14.91	11.00	3.91	Coccolithaceae	Coccolithus
Discoaster cuspidatus	13.03	11.04	1.99	Discoasteraceae	Discoaster
Discoaster cuspidatus (knb)	13.22	11.04	2.18	Discoasteraceae	Discoaster
Discoaster ulnatus	17.73	11.04	6.69	Discoasteraceae	Discoaster
Discoaster emblematicus	19.00	11.04	7.96	Discoasteraceae	Discoaster
Discoaster hexapleuros (knb)	12.19	11.16	1.03	Discoasteraceae	Discoaster

Discoaster formosus	13.76	11.21	2.54	Discoasteraceae	Discoaster
Helicosphaera walbersdorfensis	16.98	11.35	5.63	Helicosphaeraceae	Helicosphaera
Discoaster gamberi	13.64	11.38	2.26	Discoasteraceae	Discoaster
Discoaster kugleri	11.91	11.51	0.40	Discoasteraceae	Discoaster
Discoaster catillomicros	12.82	11.51	1.31	Discoasteraceae	Discoaster
Discoaster stellimicros	13.35	11.51	1.84	Discoasteraceae	Discoaster
Discoaster patulus	17.35	11.51	5.84	Discoasteraceae	Discoaster
Discoaster hexapleuros	11.96	11.53	0.43	Discoasteraceae	Discoaster
Discoaster deflandrei	55.86	11.58	44.29	Discoasteraceae	Discoaster
Discoaster sanmiguelensis	15.62	11.85	3.77	Discoasteraceae	Discoaster
Cyclicargolithus floridanus (<6)	46.29	11.96	34.33	Noelaerhabdaceae	Cyclicargolithus
Discoaster virginianus	13.64	12.02	1.62	Discoasteraceae	Discoaster
Cyclicargolithus floridanus (6-9)	46.29	12.05	34.24	Noelaerhabdaceae	Cyclicargolithus
Discoaster carneyi	13.74	12.13	1.62	Discoasteraceae	Discoaster
Coronocyclus nitescens (<9)	46.29	12.13	34.17	Coccolithaceae	Coronocyclus
Triquetrorhabdulus millowii	22.09	12.22	9.87	Ceratolithaceae	Triquetrorhabdulus
Helicosphaera vedderi	22.23	12.22	10.00	Helicosphaeraceae	Helicosphaera
Calcidiscus premacintyrei	17.06	12.37	4.69	Calcidiscaceae	Calcidiscus
Coronocyclus mesostenos	47.84	12.47	35.38	Coccolithaceae	Coronocyclus
Helicosphaera elongata	27.53	12.58	14.95	Helicosphaeraceae	Helicosphaera
Discoaster catinatus	13.61	12.69	0.92	Discoasteraceae	Discoaster
Discoaster signus	15.58	12.79	2.79	Discoasteraceae	Discoaster
Helicosphaera rhomba	24.40	12.82	11.58	Helicosphaeraceae	Helicosphaera
Cyclicargolithus bukryi	17.16	12.99	4.17	Noelaerhabdaceae	Cyclicargolithus
Helicosphaera obliqua	26.59	13.02	13.57	Helicosphaeraceae	Helicosphaera
Helicosphaera theodoridisii	17.85	13.03	4.83	Helicosphaeraceae	Helicosphaera
Discoaster musicus	14.50	13.07	1.43	Discoasteraceae	Discoaster
Reticulofenestra kahniae (<8)	19.45	13.07	6.39	Noelaerhabdaceae	Reticulofenestra
Sphenolithus heteromorphus	17.79	13.41	4.38	Sphenolithaceae	Sphenolithus
Helicosphaera californiana	16.48	13.50	2.98	Helicosphaeraceae	Helicosphaera
Discoaster apetalus	15.82	13.50	2.32	Discoasteraceae	Discoaster
Discoaster petaliformis	15.78	13.64	2.14	Discoasteraceae	Discoaster
Discoaster druggii (<10)	23.16	13.86	9.30	Discoasteraceae	Discoaster

Reticulofenestra pospichalii	14.40	13.89	0.51	Noelaerhabdaceae	Reticulofenestra
Helicosphaera scissura	20.35	14.02	6.33	Helicosphaeraceae	Helicosphaera
Discoaster arneyi	15.86	14.09	1.77	Discoasteraceae	Discoaster
Discoaster premicros	15.50	14.19	1.31	Discoasteraceae	Discoaster
Helicosphaera perch-nielseniae	32.92	14.28	18.64	Helicosphaeraceae	Helicosphaera
Discoaster druggii (10-15)	23.04	14.32	8.72	Discoasteraceae	Discoaster
Helicosphaera ampliaperta	19.12	14.90	4.22	Helicosphaeraceae	Helicosphaera
Reticulofenestra kahniae (>8)	19.35	14.90	4.45	Noelaerhabdaceae	Reticulofenestra
Helicosphaera bipuncta	32.92	14.96	17.96	Helicosphaeraceae	Helicosphaera
Discoaster salomonii	33.89	15.10	18.79	Discoasteraceae	Discoaster
Helicosphaera lenticulata	28.93	15.36	13.57	Helicosphaeraceae	Helicosphaera
Discoaster leroyi	55.86	15.38	40.48	Discoasteraceae	Discoaster
Sphenolithus puniceus	36.97	15.50	21.47	Sphenolithaceae	Sphenolithus
Dictyococcites albitectus	40.40	15.66	24.74	Noelaerhabdaceae	Dictyococcites
Dictyococcites onustus	45.49	16.02	29.47	Noelaerhabdaceae	Dictyococcites
Coronocyclus nitescens (>9)	46.29	16.02	30.27	Coccolithaceae	Coronocyclus
Sphenolithus preasii	17.87	16.04	1.83	Sphenolithaceae	Sphenolithus
Sphenolithus milanetti	16.86	16.48	0.38	Sphenolithaceae	Sphenolithus
Helicosphaera magnifica	20.61	16.60	4.01	Helicosphaeraceae	Helicosphaera
Helicosphaera alata	20.09	16.76	3.34	Helicosphaeraceae	Helicosphaera
Helicosphaera ampliaperta (>12)	18.77	16.80	1.97	Helicosphaeraceae	Helicosphaera
Discoaster shumnykii	23.25	17.18	6.08	Discoasteraceae	Discoaster
Discoaster druggii (>15)	22.76	17.35	5.41	Discoasteraceae	Discoaster
Helicosphaera mediterranea	28.17	17.43	10.74	Helicosphaeraceae	Helicosphaera
Sphenolithus apoxis	54.17	17.43	36.75	Sphenolithaceae	Sphenolithus
Sphenolithus multispinatus	22.98	17.50	5.48	Sphenolithaceae	Sphenolithus
Sphenolithus bipedis	28.97	17.52	11.45	Sphenolithaceae	Sphenolithus
Sphenolithus cometa	21.74	17.59	4.15	Sphenolithaceae	Sphenolithus
Sphenolithus conicus (<7)	28.97	17.60	11.37	Sphenolithaceae	Sphenolithus
Sphenolithus tintinnabulum	21.04	17.61	3.43	Sphenolithaceae	Sphenolithus
Triquetrorhabdulus carinatus	26.84	17.65	9.19	Ceratolithaceae	Triquetrorhabdulus
Sphenolithus truaxii	40.40	17.79	22.61	Sphenolithaceae	Sphenolithus
Sphenolithus belemnos	19.41	17.83	1.58	Sphenolithaceae	Sphenolithus

Discoaster durioi	19.00	18.05	0.95	Discoasteraceae	Discoaster
Sphenolithus pseudoheteromorphus	19.39	18.07	1.32	Sphenolithaceae	Sphenolithus
Discoaster calculosus s.s.	24.41	18.13	6.28	Discoasteraceae	Discoaster
Sphenolithus paratintinnabulum	23.31	18.61	4.70	Sphenolithaceae	Sphenolithus
Sphenolithus procerus	27.81	18.61	9.20	Sphenolithaceae	Sphenolithus
Sphenolithus dissimilis	22.66	18.77	3.89	Sphenolithaceae	Sphenolithus
Sphenolithus disbelemnos	23.27	18.77	4.51	Sphenolithaceae	Sphenolithus
Discoaster saundersii	24.30	18.85	5.45	Discoasteraceae	Discoaster
Dictyococcites sp.	50.00	19.01	30.99	Noelaerhabdaceae	Dictyococcites
Sphenolithus calyculus	24.68	19.33	5.35	Sphenolithaceae	Sphenolithus
Triquetrorhabdulus auritus	20.97	19.37	1.60	Ceratolithaceae	Triquetrorhabdulus
Sphenolithus conicus (>7)	28.57	19.55	9.02	Sphenolithaceae	Sphenolithus
Helicosphaera euphratis	50.00	19.55	30.45	Helicosphaeraceae	Helicosphaera
Ilselithina fusa	33.89	19.71	14.18	-	Ilselithina
Triquetrorhabdulus challengeri	22.27	19.89	2.38	Ceratolithaceae	Triquetrorhabdulus
Helicosphaera recta	32.92	20.17	12.75	Helicosphaeraceae	Helicosphaera
Cyclicargolithus abisectus (>11)	50.00	20.35	29.65	Noelaerhabdaceae	Cyclicargolithus
Cyclicargolithus abisectus (>12)	50.00	20.55	29.45	Noelaerhabdaceae	Cyclicargolithus
Camuralithus pelliculathus	25.38	21.00	4.39	-	Camuralithus
Helicosphaera truncata	32.92	21.04	11.88	Helicosphaeraceae	Helicosphaera
Helicosphaera disrupta	29.62	21.16	8.46	Helicosphaeraceae	Helicosphaera
Clausicoccus fenestratus	53.70	21.16	32.54	Coccolithaceae	Clausicoccus
Sphenolithus spinula	25.10	21.30	3.80	Sphenolithaceae	Sphenolithus
Sphenolithus microdelphix	24.73	21.36	3.37	Sphenolithaceae	Sphenolithus
Helicosphaera truempyi	25.71	21.64	4.07	Helicosphaeraceae	Helicosphaera
Sphenolithus capricornutus s.s.	24.28	23.00	1.28	Sphenolithaceae	Sphenolithus
Sphenolithus delphix	24.66	23.07	1.59	Sphenolithaceae	Sphenolithus
Sphenolithus ciperoensis	29.17	24.22	4.96	Sphenolithaceae	Sphenolithus
Sphenolithus bulbulus	32.02	24.25	7.77	Sphenolithaceae	Sphenolithus
Sphenolithus patifunditus	28.66	24.30	4.35	Sphenolithaceae	Sphenolithus
Sphenolithus avis	32.00	24.41	7.59	Sphenolithaceae	Sphenolithus
Sphenolithus directus	28.57	24.63	3.95	Sphenolithaceae	Sphenolithus
Sphenolithus peartiae	32.02	24.68	7.34	Sphenolithaceae	Sphenolithus

Sphenolithus triangularis	32.02	24.70	7.32	Sphenolithaceae	Sphenolithus
Sphenolithus ciperoensis (>6)	28.68	24.80	3.88	Sphenolithaceae	Sphenolithus
Helicosphaera bramlettei	49.11	24.87	24.24	Helicosphaeraceae	Helicosphaera
Sphenolithus tawfikii	32.02	25.05	6.97	Sphenolithaceae	Sphenolithus
Helicosphaera wilcoxoni	40.40	25.06	15.34	Helicosphaeraceae	Helicosphaera
Sphenolithus distentus	32.02	26.13	5.89	Sphenolithaceae	Sphenolithus
Sphenolithus peartiae (>7)	32.02	27.22	4.80	Sphenolithaceae	Sphenolithus
Helicosphaera compacta	42.87	27.38	15.49	Helicosphaeraceae	Helicosphaera
Sphenolithus pseudoradians	46.29	28.09	18.20	Sphenolithaceae	Sphenolithus
Sphenolithus apoxis (>8)	54.17	28.09	26.08	Sphenolithaceae	Sphenolithus
Helicosphaera ethologa	32.02	28.45	3.57	Helicosphaeraceae	Helicosphaera
Sphenolithus akropodus (<8)	34.44	28.66	5.79	Sphenolithaceae	Sphenolithus
Sphenolithus akropodus (>8)	34.44	29.29	5.15	Sphenolithaceae	Sphenolithus
Dictyococcites gartneri	53.70	30.43	23.27	Noelaerhabdaceae	Dictyococcites

Table A12 Number of species and lifespan of nannofossils grouped by family

Family	# of Species	Mean Lifespan	Start of Lifespan	End of Lifespan
Ceratolithaceae	25	0.49	26.84	0.00
Discoasteraceae	95	0.47	55.86	1.90
Sphenolithaceae	42	1.38	61.61	3.53
Calcidiscaceae	3	4.16	17.14	1.61
Noelaerhabdaceae	31	1.11	53.70	0.00
Helicosphaeraceae	35	0.94	50.00	0.00
Coccolithaceae	6	9.10	65.40	10.80
Pontosphaeraceae	2	26.16	55.96	3.63

Table A13 Comparison of nannofossil turnover with Oxy-18 events

marine δ18O event	age (Ma)	eccentricity related (blue areas) (Ma)	obliquity- and eccentricity related (green areas) (Ma)	speciation age (Ma)	count.	prob.	extinction age (Ma)	count.	prob.	turnover age (Ma)	count.	prob.
				1.6-1.5	**2**	0.154				1.6-1.5	2	0.154
				1.7-1.6	2	0.182	1.7-1.6	1	0.100	1.7-1.6	3	0.282
							2.2-2.1	1	0.059	2.2-2.1	1	0.059
100/98 (37)	2.41-2.35	2.40-2.35										
G16-10 (38)	2.92-2.82	2.82-2.72	2.89-2.72				3.0-2.9	1	0.048	3.0-2.9	1	0.048
M2/MG2 (39)	3.37-3.30		3.27-3.12									
							3.6-3.5	2	0.087	3.6-3.5	2	0.087
Gi2/6 (39)	3.78-3.66			3.7-3.6	1	0.043	3.7-3.6	3	0.120	3.7-3.6	4	0.163
				3.8-3.7	2	0.080	3.8-3.7	1	0.042	3.8-3.7	3	0.122
							3.9-3.8	2	0.077	3.9-3.8	2	0.077
				4.0-3.9	2	0.077	4.0-3.9	1	0.040	4.0-3.9	3	0.117
							4.1-4.0	5	0.167	4.1-4.0	5	0.167
							4.2-4.1	1	0.032	4.2-4.1	1	0.032
Gi16/18 (39)	4.06-4.00		4.12-3.91; 4.29-4.26				4.3-4.2	1	0.031	4.3-4.2	1	0.031
		4.39-4.35										
				4.5-4.4	1	0.031	4.5-4.4	1	0.031	4.5-4.4	2	0.063
				4.6-4.5	1	0.031	4.6-4.5	5	0.139	4.6-4.5	6	0.170
Si4/6 (38)	4.88-4.82	4.83-4.76					4.9-4.8	1	0.027	4.9-4.8	1	0.027
				5.0-4.9	2	0.054	5.0-4.9	1	0.028	5.0-4.9	3	0.082
				5.2-5.1	1	0.028	5.2-5.1	2	0.054	5.2-5.1	3	0.082
				5.3-5.2	3	0.081	5.3-5.2	3	0.081	5.3-5.2	6	0.162
				5.4-5.3	5	0.135	5.4-5.3	4	0.111	5.4-5.3	9	0.246
TG20/22 (39)	5.88-5.81		5.51-5.49; 5.59				5.5-5.4	1	0.027	5.5-5.4	1	0.027
							5.6-5.5	2	0.051	5.6-5.5	2	0.051
							5.7-5.6	2	0.049	5.7-5.6	2	0.049
							6.0-5.9	2	0.045	6.0-5.9	2	0.045
							6.1-6.0	3	0.064	6.1-6.0	3	0.064
				6.4-6.3	1	0.021	6.4-6.3	2	0.041	6.4-6.3	3	0.062

			6.58-6.33				6.5-6.4	2	0.039	6.5-6.4	2	0.039
Tort./Mess. 1,2 (40)	7.3-7.2; 7.0-6.9	7.23-7.2		7.2-7.1	1	0.018				7.2-7.1	1	0.018
Late Tort. (41)	7.6	7.65-7.63	7.27-7.67; 8.08-7.95	7.3-7.2	1	0.018	7.3-7.2	3	0.053	7.3-7.2	4	0.071
				7.4-7.3	4	0.070	7.4-7.3	2	0.036	7.4-7.3	6	0.107
				7.6-7.5	3	0.054	7.6-7.5	1	0.019	7.6-7.5	4	0.072
				8.0-7.9	1	0.019	8.0-7.9	1	0.019	8.0-7.9	2	0.037
				8.2-8.1	2	0.036	8.2-8.1	1	0.019	8.2-8.1	3	0.055
				8.3-8.2	9	0.167				8.3-8.2	9	0.167
				8.4-8.3	2	0.044	8.4-8.3	1	0.023	8.4-8.3	3	0.067
							8.6-8.5	2	0.043	8.6-8.5	2	0.043
				8.8-8.7	5	0.111				8.8-8.7	5	0.111
Mi7? (41)	8.8		8.95-8.74	8.9-8.8	1	0.025				8.9-8.8	1	0.025
							9.0-8.9	2	0.049	9.0-8.9	2	0.049
				9.1-9.0	1	0.024				9.1-9.0	1	0.024
							9.3-9.2	3	0.070	9.3-9.2	3	0.070
Mi7? (41,42)	9.6-9.0	9.67-9.63; 9.31-9.27		9.7-9.6	1	0.022	9.7-9.6	5	0.100	9.7-9.6	6	0.122
				9.8-9.7	3	0.060	9.8-9.7	1	0.021	9.8-9.7	4	0.081
				10.3-10.2	3	0.064				10.3-10.2	3	0.064
Mi6 (41, 43, 44)	10.45-10.35						10.5-10.4	3	0.063	10.5-10.4	3	0.063
				10.8-10.7	4	0.085				10.8-10.7	4	0.085
				10.9-10.8	3	0.070	10.9-10.8	3	0.070	10.9-10.8	6	0.140
				11.0-10.9	3	0.070	11.0-10.9	2	0.048	11.0-10.9	5	0.117
				11.1-11.0	2	0.048	11.1-11.0	4	0.091	11.1-11.0	6	0.139
				11.6-11.5	4	0.087	11.6-11.5	6	0.125	11.6-11.5	10	0.212
Mi5 (41, 43, 44)	11.8-11.7; 11.5-11.4											
				12.0-11.9	3	0.061	12.0-11.9	1	0.021	12.0-11.9	4	0.083
							12.1-12.0	2	0.041	12.1-12.0	2	0.041
		12.16-12.10		12.2-12.1	1	0.020	12.2-12.1	2	0.040	12.2-12.1	3	0.060
		12.52-12.48	12.62-12.42	12.5-12.4	2	0.038	12.5-12.4	1	0.019	12.5-12.4	3	0.057
				13.1-13.0	3	0.055	13.1-13.0	4	0.071	13.1-13.0	7	0.126
Mi4 (41, 43)	13.2 / 12.8											
				13.5-13.4	3	0.057	13.5-13.4	3	0.057	13.5-13.4	6	0.113
				13.7-13.6	4	0.075	13.7-13.6	1	0.020	13.7-13.6	5	0.095
				13.8-13.7	3	0.060				13.8-13.7	3	0.060
Mi3B (43, 45-47)	13.9-13.8		13.69-13.62	13.9-13.8	1	0.021	13.9-13.8	2	0.042	13.9-13.85	3	0.063

Mi3A (47)	14.2	14.16-14.10		14.3-14.2	1	0.020	14.3-14.2	1	0.020	14.3-14.2	2	0.040
				14.4-14.3	2	0.040	14.4-14.3	1	0.020	14.4-14.3	3	0.060
							14.9-14.8	2	0.040	14.9-14.8	2	0.040
			14.90-14.89; 15.02-14.93	15.0-14.9	1	0.020	15.0-14.9	1	0.020	15.0-14.9	2	0.040
							15.4-15.3	2	0.038	15.4-15.3	2	0.038
				15.5-15.4	1	0.019	15.5-15.4	1	0.019	15.5-15.4	2	0.038
				15.7-15.6	2	0.039	15.7-15.6	1	0.020	15.7-15.6	3	0.059
Mi2 (43, 48)	15.9		16.07-16.00; 15.89-15.68	16.0-15.9	2	0.043				16.0-15.9	2	0.043
							16.1-16.0	3	0.063	16.1-16.0	3	0.063
				16.5-16.4	1	0.021	16.5-16.4	1	0.021	16.5-16.4	2	0.042
				17.2-17.1	2	0.042	17.2-17.1	1	0.021	17.2-17.1	3	0.063
M1b (42, 49)	17.4-17.3	19.98-16.94	17.44-17.25									
				17.4-17.3	2	0.043	17.4-17.3	1	0.022	17.4-17.3	3	0.064
							17.5-17.4	3	0.061	17.5-17.4	3	0.061
							17.6-17.5	2	0.039	17.6-17.5	2	0.039
				17.7-17.6	1	0.020	17.7-17.6	3	0.057	17.7-17.6	4	0.076
				17.8-17.7	3	0.057	17.8-17.7	1	0.020	17.8-17.7	4	0.076
				17.9-17.8	2	0.039	17.9-17.8	1	0.020	17.9-17.8	3	0.059
			18.30-18.26							18.3-18.2		
		19.04-18.95		19.1-19.0	2	0.036	19.1-19.0	1	0.018	19.1-19.0	3	0.054
M1aa (48, 49)	19.4		19.47-19.42	19.4-19.3	2	0.037	19.4-19.3	2	0.037	19.4-19.3	4	0.074
M1a (42, 50)	21.15-21.05	21.06-21.00					21.2-21.1	2	0.034	21.2-21.1	2	0.034
				21.3-21.2	1	0.017				21.3-21.2	1	0.017
		21.42-21.39										
				21.8-21.7	1	0.017				21.8-21.7	1	0.017
			21.91-21.88									
Mi1 (43, 50)	23.1-23.0			23.0-22.9	1	0.019	23.0-22.9	1	0.019	23.0-22.9	2	0.037
		23.90-23.82										

Table A14 Global and regional cultural turnover event count of past 2000 years (0-2Ka)

Period (Ka)	Cultural Turnover Event Count	Africa (ID:1)	Eastern Mediterranean (ID:2)	Middle East . To India (ID:3)	East Asia And Oceania (ID:4)	Europe (ID:5)	Arctic And Subarctic (ID:6)	Northwest And Canada (ID:7)	North America (ID:8)	Middle America (ID:9)	South America (ID:10)	Dominant Region ID
0.025	8	2	0	3	0	0	0	0	0	0	3	3
0.075	21	0	6	7	7	0	1	0	0	0	0	3
0.125	13	1	1	0	1	0	0	1	8	0	1	8
0.175	11	0	2	0	5	2	0	1	1	0	0	4
0.225	5	1	0	1	0	1	1	0	1	0	0	1
0.275	2	0	0	2	0	0	0	0	0	0	0	3
0.325	2	0	0	0	1	0	0	0	1	0	0	4
0.375	10	0	0	0	6	0	1	1	2	0	0	4
0.425	4	0	0	0	0	0	0	0	1	3	0	9
0.475	39	2	1	7	1	3	2	0	8	10	5	9
0.525	13	0	5	2	0	5	0	0	0	0	1	2
0.575	10	0	0	2	2	0	0	0	2	4	0	9
0.625	9	1	0	2	4	0	0	0	1	0	1	4
0.675	4	0	0	2	0	0	0	0	2	0	0	3
0.725	12	0	2	5	4	0	0	0	1	0	0	3
0.775	15	0	0	2	5	3	0	0	2	2	1	4
0.825	2	1	0	0	0	1	0	0	0	0	0	1
0.875	9	0	0	0	4	2	0	0	1	0	2	4
0.925	10	0	4	3	0	1	0	0	2	0	0	2
0.975	9	0	0	0	0	0	1	0	5	3	0	8
1.025	8	0	0	0	1	2	0	0	3	1	1	8
1.075	11	1	0	3	2	0	0	0	2	3	0	3
1.125	2	0	0	1	0	0	0	0	1	0	0	3
1.175	9	0	0	1	0	0	0	0	1	5	2	9
1.225	13	2	1	6	0	3	0	0	0	1	0	3
1.275	7	0	0	0	1	0	0	0	0	4	2	9
1.325	7	0	0	4	0	0	0	0	3	0	0	3
1.375	13	3	3	3	1	0	0	0	0	2	0	1
1.425	7	0	1	0	4	0	0	0	2	0	0	4

1.475	20	0	0	0	6	3	1	1	3	4	2	4
1.525	4	0	2	0	0	2	0	0	0	0	0	2
1.575	8	0	0	0	1	1	0	0	3	2	1	8
1.625	3	0	1	0	1	0	0	0	0	1	0	2
1.675	19	4	9	0	2	3	0	0	1	0	0	2
1.725	2	0	0	0	0	0	0	0	0	2	0	9
1.775	8	0	1	2	3	0	0	0	0	2	0	4
1.825	4	0	0	0	0	1	0	0	0	3	0	9
1.875	0	0	0	0	0	0	0	0	0	0	0	1
1.925	3	0	2	0	0	0	0	0	0	0	1	2
1.975	18	2	0	2	2	0	1	1	7	1	1	8

VITA

Abdullah Khan Zehady

PhD Student (Earth history).

Department of Earth, Atmospheric, and Planetary Sciences.

Purdue University; West Lafayette, IN 47907-1397.

Professional Preparation

Purdue University West Lafayette, Indiana, USA		Computer Science	M. S.	2016.
Osaka University Osaka, Japan		Mathematical Science	B. Eng.	2014.
Kagawa National College of Technology	Kagawa, Japan	Information Eng.	Ass. Eng.	2012.

Appointments

2019 Summer   Software Engineering internship at Cisco Systems, San Jose, USA.

2017-   Doctoral student transferred to EAPS dept., Purdue University (to complete Spring 2020).

2015 Spring- Research assistant developing and researching for Purdue *TimeScale Creator* software .

2014 – 2016   Doctoral student at CS, Purdue University (MS completion in Fall 2016).

2015 Fall/Spring, 2016 Fall/Spring, 2017 Fall/Spring 2018 Fall/Spring 2019 Fall/Spring 2020 Fall/Spring   Graduate mentor of undergraduate courses (VIP ECE 279,379,479 – Earth History Visualization) taught by Professor James Ogg.

2014 Fall   Teaching assistant in graduate course (CS501: Computing for Science & Engineering).

2014 Summer   Software Engineer at GREE Inc., Tokyo, Japan.

Related Products

2017- Ongoing Data Mining project with Purdue Time Scale Creator Datapacks for trend analysis, investigation of uncertain cause-effects (asteroid impacts, massive volcanic eruptions, mass extinctions, swings in global climate and sea-level, disruptions of the planetary carbon cycle, etc.)

2015-2017 Administration, development of Java client software, *TimeScale Creator* website (*https://timescalecreator.org*), web based datapack maker modules of Purdue TimeScale Creator visualization system for Earth history .

Synergistic Activities

2014 Online Introductory Linear Algebra Course: Created course contents on linear Algebra and also for http://shikkhok.com- an educational website which achieved **Google Rise Award** in 2013.

PROJECTS & PUBLICATIONS

Zehady, A.K., Goldwasser D., **2016**. Disambiguation to Wikipedia: Using techniques of deep neural network and applying word embedding models to improve wikification(link to Wikipedia page) task, *Purdue University Machine Learning Research Project*.

Zehady, A.K., Ribeiro, B., **2016**. User Identity detection, feature learning, Bitcoin financial network data analysis, trend prediction, *Data Mining Project.*

Zehady, A.K., Bagchi, S., Chatterji S., **2014-2015,** NISHPAKSH: Evaluation of assembly algorithms for different operating regions of read length, read coverage, and error rate, *Purdue University Bioinformatics Project.*

Pacheco, M.L., Lee, I.T., Zhang, X., **Zehady, A.K.**, Daga, P., Jin, D., Parolia, A., Goldwasser, D., 2016. Adapting event embedding for implicit discourse relation recognition, in: Proceedings of the 20th SIGNLL Conference on Computational Natural Language Learning: Shared Task, CoNLL 2016. https://doi.org/10.18653/v1/k16-2019.

Fordham, B.G., Aze, T., Haller, C., **Zehady, A.K.**, Pearson, P.N., Ogg, J.G., Wade, B.S., 2018. Future-proofing the Cenozoic macroperforate planktonic foraminifera phylogeny of Aze & others (2011). PLoS One, 13(10). https://doi.org/10.1371/journal.pone.0204625.

Zehady, A.K., Fordham, B.G., Ogg, J.G., 2019. Integrated species–phenon trees: visualizing infraspecific diversity within lineages. Scientific Reports, 9(1), 1-17. https://doi.org/10.1038/s41598-019-55435-w.